RECOGNITION AND REPRESENTATION OF CONTOURS IN THE MEASUREMENT OF SPHERIC AND ASPHERIC SURFACES

BY

HARISH CHANDER SHARMA, B.Sc., M. Sc

A THESIS PRESENTED IN PARTIAL FULFILMENT
OF THE REQUIREMENTS FOR THE DEGREE OF
DOCTOR OF PHILOSOPHY
OF THE
COUNCIL FOR NATIONAL ACADEMIC AWARDS

SPONSORING ESTABLISHMENT: LEICESTER POLYTECHNIC
SCHOOL OF ELECTRONIC
ENGINEERING
P.O. BOX 143
LEICESTER, LE1 9BH

COLLABORATING ESTABLISHMENT: RANK TAYLOR HOBSON
P O BOX 36
THURMASTON LANE
LEICESTER, LE4 7JQ

DECEMBER, 1986

A B S T R A C T

RECOGNITION AND REPRESENTATION OF CONTOURS IN THE MEASUREMENT OF SPHERIC AND ASPHERIC SURFACES

by H C Sharma

Many high performance optical components, by design, are complex in shape. The production of such optical components requires specialised machining operations. The errors generated due to noise and other faulty aspects of the machine, introduce small deviations in the required profile. Certain optical materials such as germanium are extremely expensive. Hence there is a need to detect those components which are likely to give poor optical performance at an early stage in the production cycle. This information can then be utilised to control the machining process for maximum accuracy. A method is therefore required to correlate the machining error with the optical performance of the lens.

The main aim of this research has been to establish a suitable correlation between the profile error and the optical performance. The work was conducted by studying the error profiles of 29 lenses together with their modulation transfer function (MTF) curves.

The first two chapters provide the background knowledge about aspherised lens elements, their manufacturing techniques and related measurement problems. Chapters III and IV are devoted to an explanation of some optical theory and its relevance to the problem in hand. Subsequent chapters trace the development of procedures to correlate optical performance to profile error. The design and implementation of a suitable predictor is discussed in Chapter IX. Main conclusions, overall discussions, and suggestions about future work follow in Chapter X.

C O N T E N T S

LIST OF FIGURES

CHAPTER I

INTRODUCTION

CHAPTER I

INTRODUCTION

The study of complex shapes and contours has been a challenging area for mathematicians and theoreticians for a long time (1). In practice, the design, production and manufacture of components with complex shapes are important activities in many facets of engineering. For example there exist a large variety of components whose shape, for best performance, should be spherical, e.g. crank shaft journals, ball bearings, etc. (see Fig. 1.1). The manufacturing process often introduces errors of form on essentially a round component (2). The deviation of the component from its true shape may have a marked effect on the performance of the component. It is therefore necessary to have quantitative estimate of "out of roundness". A considerable amount of work has been done in this field and many parameters have been invented which assist in the measurement of roundness (3, 4, 5). The parameters can be used for quality control check or as diagnostic aids for detecting problems arising in the manufacturing process. The problem of measurement becomes more difficult where only partial arcs are available for measurement, e.g. ball bearing races, tool -tips, and spindles with key ways, etc. (6, 7).

Since roundness is easily associated with rotation and movement of spindles, shafts, gears, etc., applications of spheric components are readily appreciated. The measurement

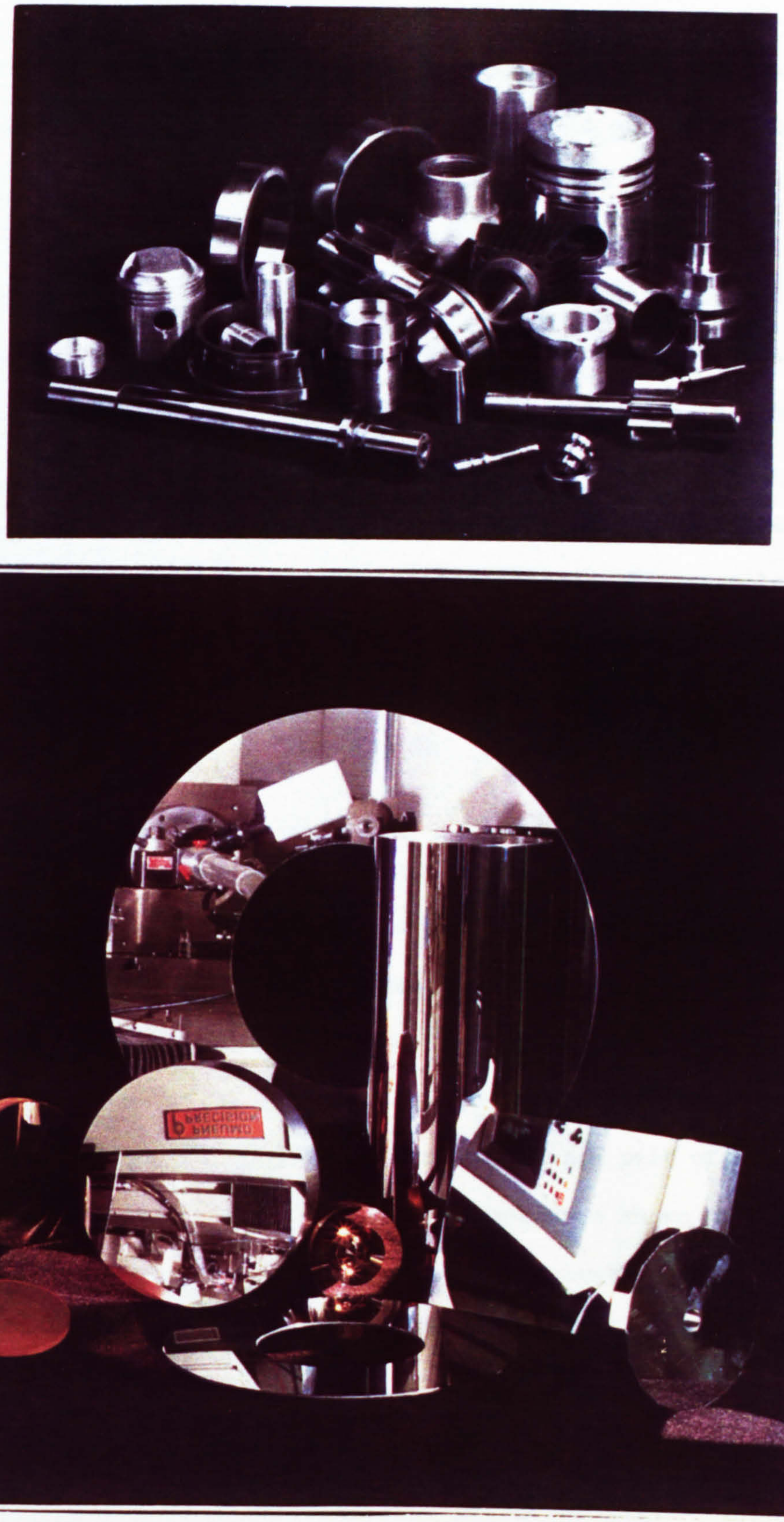

TYPICAL ENGINEERING COMPONENTS

FIGURE 1.1

of roundness of spheric components is hence an active part of measurement and inspection process in the field of engineering. Indeed many optical components are spheric (see Fig. 1.2).

At a first sight the design/manufacture of spheric/aspheric shapes appear to be highly specialised branches of mechanical engineering and hence of little interest to engineers in other discplines. However a closer examination reveals a heavy inter-dependance of traditional manufacturing and inspection with signal processing and pattern recognition. For example, machined surfaces give rise to a variety of signals which are used to determine statistical parameters as aids to measurement (8).

An extremely important role in measurement is played by optical technology which binds several engineering discplines together. Optical interference techniques are common in many areas of mechanical measurement (8). Man's interest in optical components is by no means recent. A picture painted by Tomasso de Modena in 1352 shows a man wearing a pair of spectacles (9). Ancient Egyptian lenses have known to be existed as early as A.D. 150. Modern day scientific applications dominated by data processing problems, rely heavily on optical technology (10, 11).

A significant part of important data is often visual.

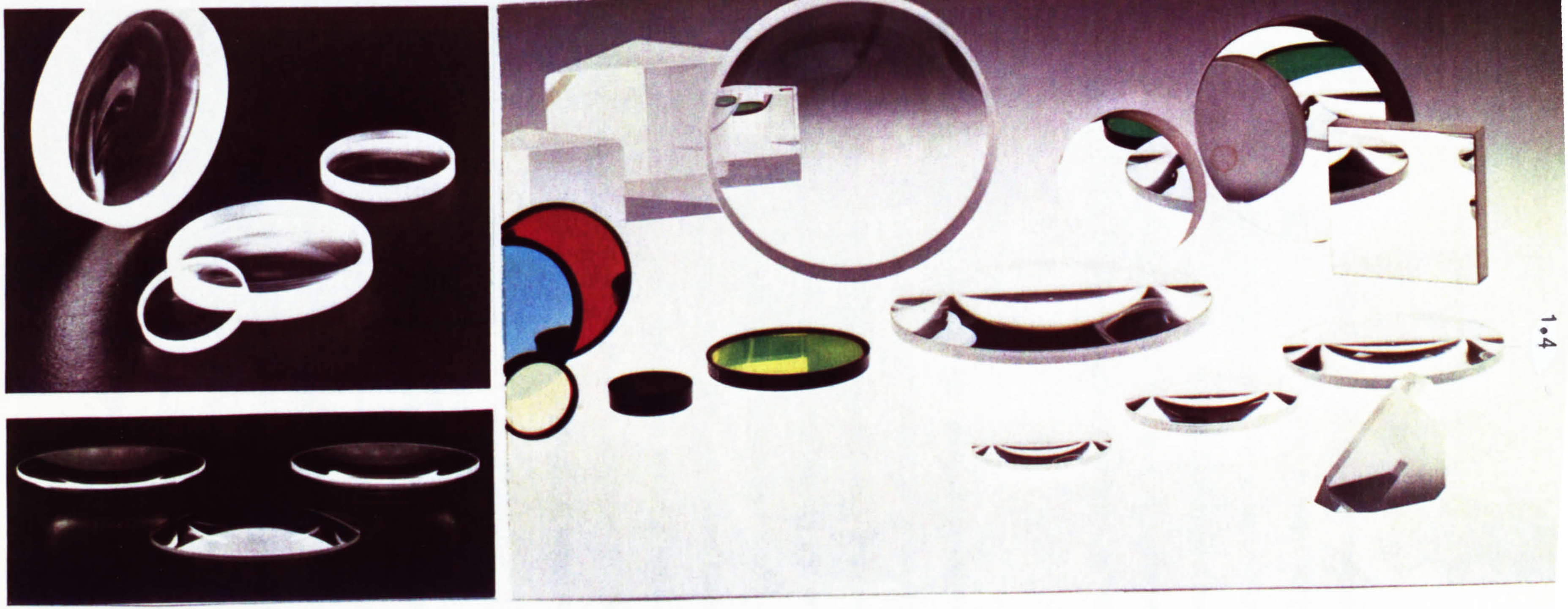

TYPICAL OPTICAL COMPONENTS

FIGURE 1.2

Collection, storage, transmission, and finally processing of such information must occupy a key place in many different spheres of research and development. For example "holographic interferometry" has been used to non-destructively test for hidden defects in car tyres, to study strain contours on jet turbine blades, and to study vibration patterns of musical instruments (6).

The recent development of faster and cheaper computers, smaller but high capacity storage media has acted as a catalyst to the growing interest in optical data processing. This combination provides us with a very powerful technology to solve engineering problems. Hence an individual researcher seeking to understand the process of manufacture and inspection of spherical and non-spherical components meets a bewildering range of techniques drawn from a wide spectrum of discplines. He, therefore has to be multi-discplinary in approach.

For example, one may come across integrated optical devices. These are of particular interest since they use parallel processing ability of light (12). A number of signal processing applications such as high speed A-D conversion and spectrum analysis have been realised (12). However, practical realisation of such devices require fabrication of lens elements which may be complicated in shape. Manufacture and test of such lenses hence requires good knowledge

of grinding, polishing, diamond turning, etc. (12). The relationship between the function of the device and its shape is hence of critical importance.

The diversity of usage of specially shaped lens elements can be illustrated by a further example found in laser plasma experiments. In one such case, six laser beams are focussed on to a microbaloon of .01 mm in diameter. The lenses have to be of special design and essentially non-spheric. They have to withstand power densities of $10^{10} W/cm^2$ (13).

The importance of manufacture of special optical shapes, is reflected by the arrival of highly sophisticated machine tools. For example Philips Research Laboratories have developed a high precision, single point, diamond tool, machining equipment (14). While the manufacture of non-spheric components has benefited from computer control of machine tools, the measurement of complex shapes is still lagging behind.

This research is concerned with the measurement of germanium lenses which are essentially non-spheric in shape. The main aim of the research is therefore, to device parameters or algorithms which allow prediction of optical performance from mechanical measurements taken during the manufacturing process.

However, before attempting to solve the measurement problem it is necessary to have a good appreciation of the factors which are inherently related to the manufacture/measurement of such lenses. The aspects which are worthy of consideration are as follows:

(a) The need to use non-spheric shapes

(b) The need to use germanium in the manufacture of optical components

(c) The method used to manufacture aspheric germanium lens elements

(d) Current procedures in error checking

(e) Early attempts to correlate error of form to optical performance

These points are discussed in Chapter II.

The main objective of Chapter III is to familiarise the reader with basic optical theory and to show how this theory is used in practice to measure optical performance. Chapter IV raises issues about linking errors in the profile to the optical performance. Since the problem in hand is multi-discplinary, a more detailed consideration is given to fundamentals in optics in Chapters III and IV, than would have been necessary otherwise. In addition an existing lens design software model is used to simulate profile errors, leading to important initial observations. An

instrument capable of measuring profile errors is discussed in Chapter V.

Subsequent chapters deal with analytical techniques applied to a specific batch of lenses which have been measured on the instrument previously described in Chapter V. Development of suitable parameters is traced and the results are supported by suitable theory and results where necessary. Chapters VIII and IX give details of a predictor which estimates the optical performance from errors found on the lens profile. Finally Chapter X is dedicated to overall conclusions. Ideas about extending the research are also discussed.

Matters which are closely associated with the research, but are not of direct relevance to the subject matter in Chapters I - X are provided in the appendicies.

The strength of this research lies in synthesising different discplines together and hence providing a unique solution to a difficult problem.

CHAPTER II

ASPHERICS

CHAPTER II

ASPHERICS

A contour which by design departs from a spheric shape is called an aspheric and the amount of asphericity encountered, varies from one design aim to another. On a simpler scale one may visualise the shape of moulds, used for casting plastic or glass equipment. Often an appreciable part of the effort to produce a mould, lies in producing the correct shape. This effort is reflected in the cost incurred to produce a particular mould. In practice a mould may be produced after several machining processes by skilled operators; the emphasis is generally on precision and accuracy. One factor in favour of production of moulds is that the quantity produced is likely to be small and hence care of individual components in machining and checking by experienced operatives is generally available (15). Never-the-less the final inspection of the product is mainly subjective. The curves described by the rotor blades of turbines are quite complex to measure. Currently holographic techniques for measurement are being developed at the Loughborough University. Engine pistons may not be round but often elliptical and in some cases the designed shape follows a fourth order polynomial. In such cases curve fitting exercises are relied on for measurement purposes. Certain types of cams may require a similar treatment (16).

2.1 Aspherics in Optical Components

A large variety of aspherics are produced in the area of

optical technology. Applications are found to range from small wavelengths ≈1.0 nm upto large wave lengths ≈ 5-10 μm, in both modes of reflection and refraction. For example x-ray instruments often use reflection techniques and the wave lengths of interest are 1.0 nm - 100 nm. To obtain acceptable quality of imagery, a design based on spherical mirrors would entail the use of too many elements adding complexity and possible cumulative losses from absorption and scatter. Many x-ray mirrors therefore need to be non-spherical, e.g. toroidal or conicoidal (17). Manufacture of such components is difficult since the low wave lengths impose high surface finish requirements while other optical criteria simultaneously demand high accuracy of the geometrical form. Aspheric mirrors are also used in telescopes.

In more common applications where generally glass materials are used for work in the visible range, spherical lens elements are used. Their manufacture and production is generally easier. Use of several lens elements provides the required quality, but at increased cost. This seems to be a reasonable compromise. Moreover in the visible range several types of modern glass are available, thus providing the designer with additional fle flexibility. For the purposes of inspection, several well established techniques suffice. For example "Newton Ring" method and many interferrometric methods are extensively used. Most standard texts in optics describe such methods.

Never-the-less examples of glass aspherics are found in specialised applications.

2.2

Infra Red Lenses

The situation is not quite the same when dealing with designs relating to infra red optics. This branch is important since infra red optics allows us to image in total darkness. In military applications where one has to image without being seen, infra red optics is heavily relied on. There are of course other situations, like imaging through smoke, plantations, and man made barriers, which require similar treatment. Study of wild life in their natural habitat, has been performed by the use of near infra red (1 μm) (18). The fact that infra red optics relies on detection of "heat waves", enhances the uses to which infra red optics can be put. For example, by thermal imaging of human body "hot spots" can be found. This information can be used by medical researchers to detect potential ailments. The patterns of heat radiation from plants are used in detecting diseased crop. In engineering studies of heat patterns on cutting tools, engines, etc., are of importance. Indeed, a known heat pattern may be imposed on a component and later detected in form of a "thermal signature". Such ideas may be of use in automation and robotics. High quality thermal imaging systems have resolution of $0.1^{o}c$. Resolutions of $1^{o} - 2^{o}$ may be more common place. Thus military,

medical, and industrial application of thermal imaging, promise an active interest for many researchers and instrument designers.

2.3

Use of Germanium for Infra Red (I R)

The first observation which has to be made in connection with I R optics is that ordinary glass does not transmit wave lengths much greater than 1 μm (near I R). Hence, while some fringe applications may be realised with glass, a vast proportion needs a different material which will transmit wave lengths $\approx$ 8 - 12 μm without significant loss. There are only a few high quality materials available to the optical designer in this spectral region. Although potential materials are being researched, the most widely used material is germanium (19, 20). Since germanium is manufac'ured in pure form for semi conductor industry, it has also become useful in the I R work. The second observation is that the high refractive index of germanium ($\approx$ 4 at 10 μm) is of notable contrast to indicies of 1.5 - 1.7, of typical glass materials in the visible range of frequencies. This is of a distinct advantage, since high refractive index allows shallower curves and hence lenses can be made thinner, reducing over all volume of the lens element. Other materials, with refractive index of $\approx$2.4 are available. These in combination with germanium (high refractive index) can help in colour correction. In

general, however germanium is very expensive. A very rough comparison between a germanium element and similar glass element may indicate the germanium elements to be some 30 - 40 times higher in cost than its glass counterpart. The cost of a 10" diameter, 1½" thick, blank germanium lens element has been estimated to be some £10,000. Even small lens elements 1" - 5" diameter could cost several hundred or even several thousand pounds. In addition, if only spherical lenses were employed, the manufacture would be easier but the number of lens elements would increase in order to meet performance criteria. This would add seriously to the overall cost, not only because of the additional cost of the elements, but also because of added mechanical complexity in assembly etc. Further such a system is likely to be bigger and bulkier. Germanium is twice as heavy as glass. There is, hence a strong motivation to reduce the number of lens elements in an infra red optics system (21).

2.4

Use of Aspherics in Germanium Elements

A significant saving in the number of elements used can be made by aspherising some of the lens elements. In certain optical systems, aspheric surface close to the pupil helps in correction of the main error - spherical aberration. In other cases, apart from correcting spherical aberration, uniform image quality is obtained. In wide angle lens systems aspheric

surface is also used to correct off-axis image errors (21). All these points have been dealt in greater detail by Paul Kuttner (21). However by the way of example, it may be valuable to re-emphasise a typical aspect of his report which will bring the aspheric and its use into a closer prospective.

For a single spherical germanium lens, the lateral aberration*, ΔY for an axial point may be plotted as a function of entrance height h. A familiar "square law" type of graph is obtained. The aberration in the vicinity of the origin being small ($\approx$10 μm) while at full entrance height reaching some 600 - 800 μm. This situation is depicted in Fig. 2.2. Figure 2.3 shows the same parameters when the entrance surface is aspherised. The maximum lateral aberration not exceeding 0.1 μm. An interesting observation is that in the corrected lens the lateral aberration does not maximise at the full entrance height. A rule of thumb suggests that in most systems a saving of one element may be made by aspherising methods. In some systems two or more elements may be saved.

Production of an aspheric

Since the required aspheric profile, is theoretically

*Here it will suffice to regard aberration as a measure of degradation in image quality

FOR MORE DETAILED DESCRIPTION SEE REF. (25)

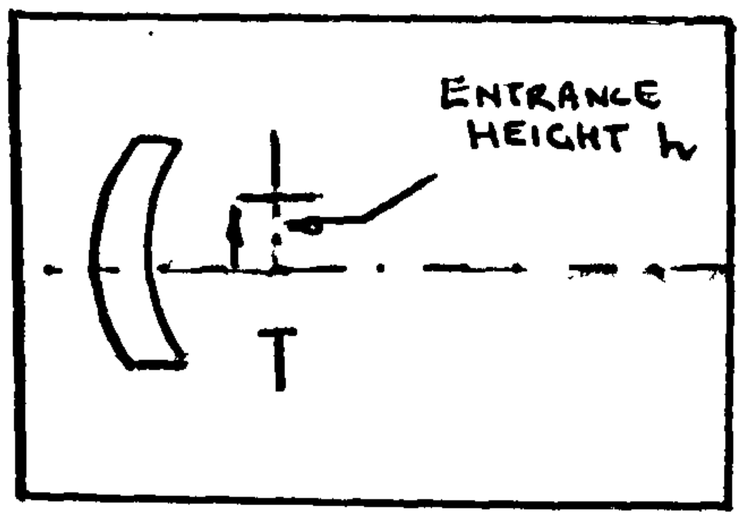

LATERAL ABERRATION AS FUNCTION OF ENTRANCE HEIGHT FOR SINGLE SPHERICAL GERMANIUM LENS

FIGURE 2.2

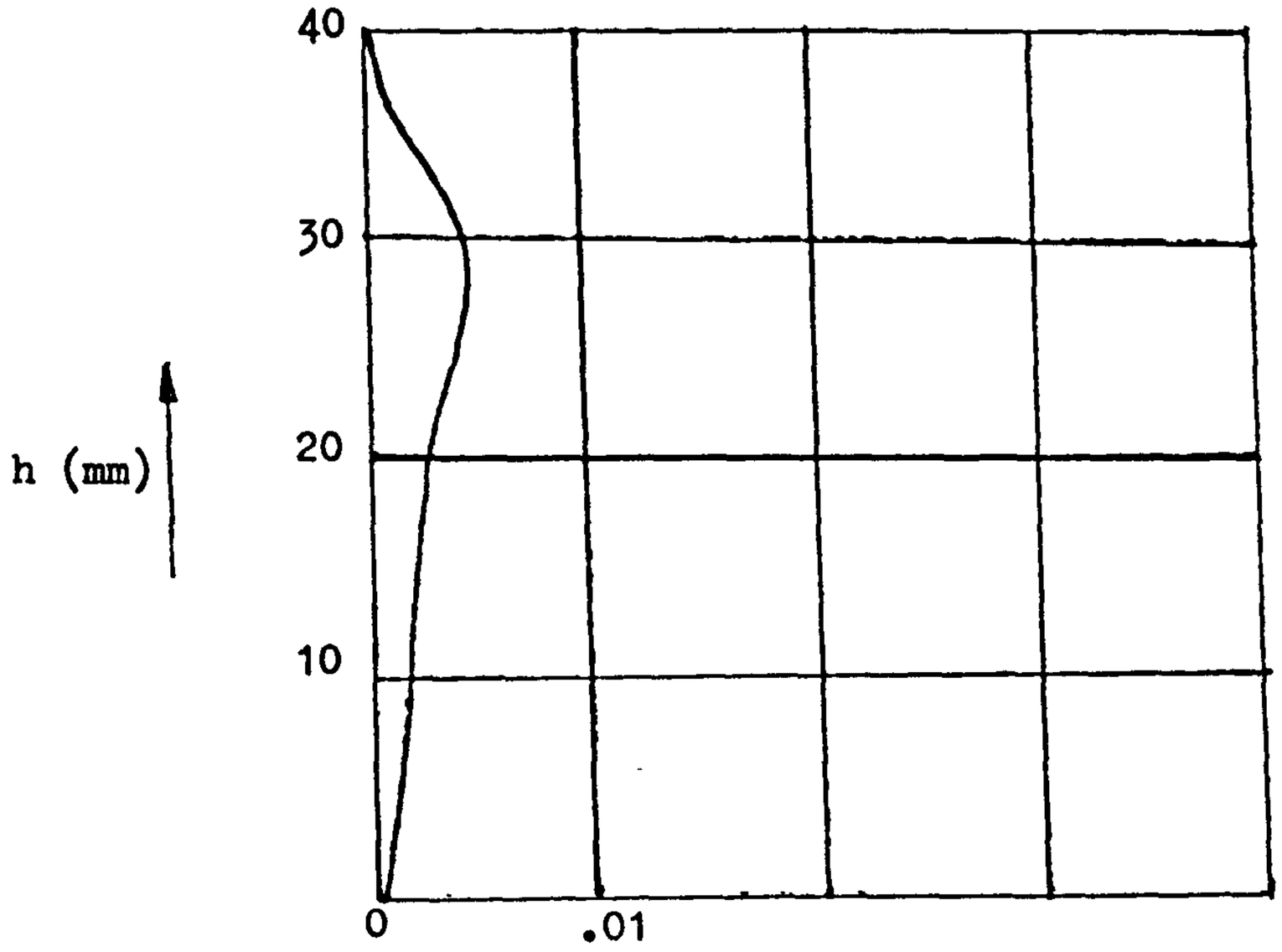

LATERAL ABERRATION AS FUNCTION OF HEIGHT FOR A SINGLE GERMANIUM LENS WITH ASPHERISED ENTERANCE HEIGHT

FIGURE 2.3

calculable, its specification is under the control of the designer. It can hence be quoted on a production drawing. The component is produced by almost standard machine tool procedure - the cutting tool being generally diamond material. The cutting sequence can be obtained from the original theoretical design and may be programmed into a computer which controls the machine tool. Figure 2.4 shows a schematic of such an arrangement. It is necessary to remember that a machine with extremely high mechanical stiffness with minimum of errors in gears, etc., is required. Upto fifth order polynomials are thus machined on materials like germanium.

A typical specification drawing for the manufacture of an aspheric lens element may be as shown in Fig. 2.5. A_2, A_4, A_6, etc., are the co-efficients of the polynomial in question. The term 'R' refers to a base radius from which various distances predicted by the polynomial are to be generated. For the particular example shown, R = plano i.e. a plane and hence represented by a straight line PQ. The aspherising distances are measured from this straight line. The equation defining the displacement in the X direction is:

$$X = A_2Y^2 + A_4Y^4 + A_6Y^6 + A_8Y^8 + A_{10}Y^{10}$$

where Y is the vertical distance, from the vertex of the lens.

Some idea of the distances involved may be obtained from the Table in Fig. 2.6.

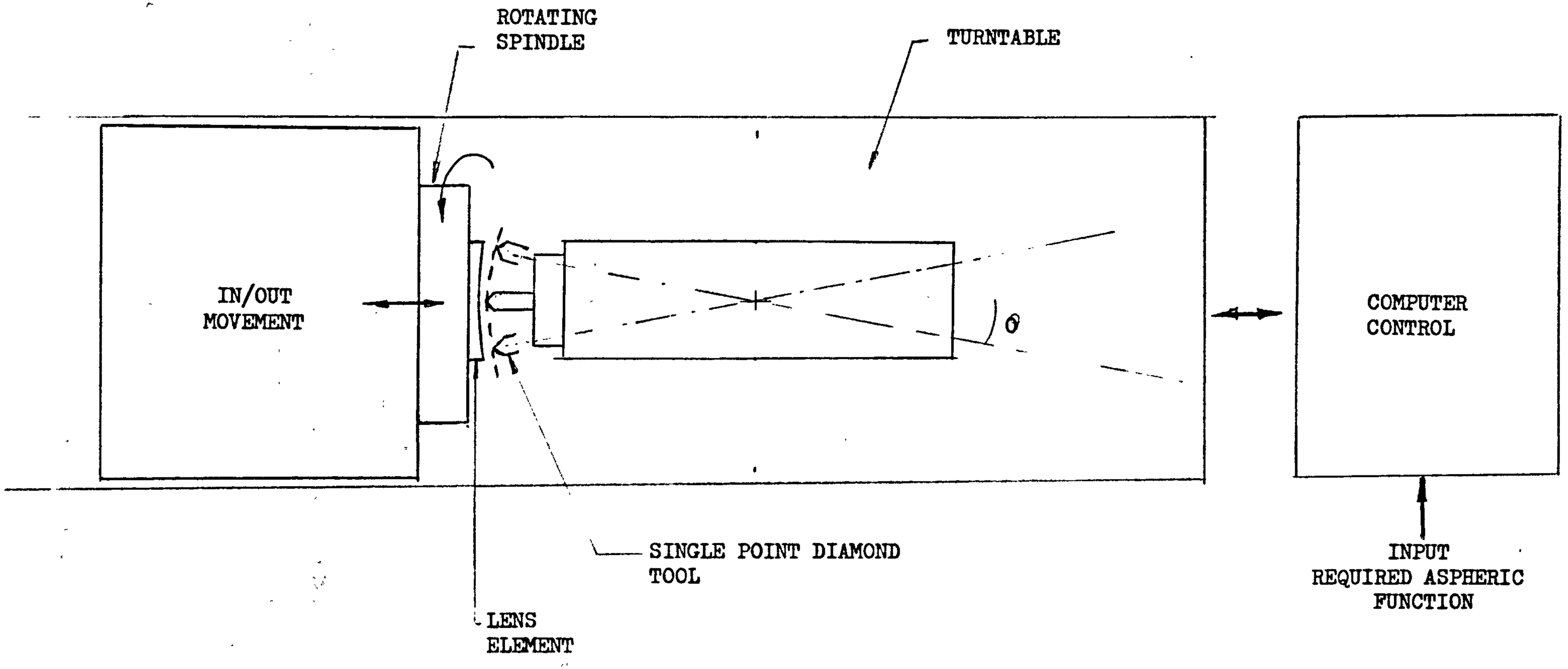

A SCHEMATIC OF ASPHERIC GENERATOR

FIGURE 2.4

2.10

MATERIAL MONOCRYSTALLINE GERMANIUM

FINISH Gr. B. POLISH

SCALE FULL SIZE

THIRD ANGLE PROJECTION

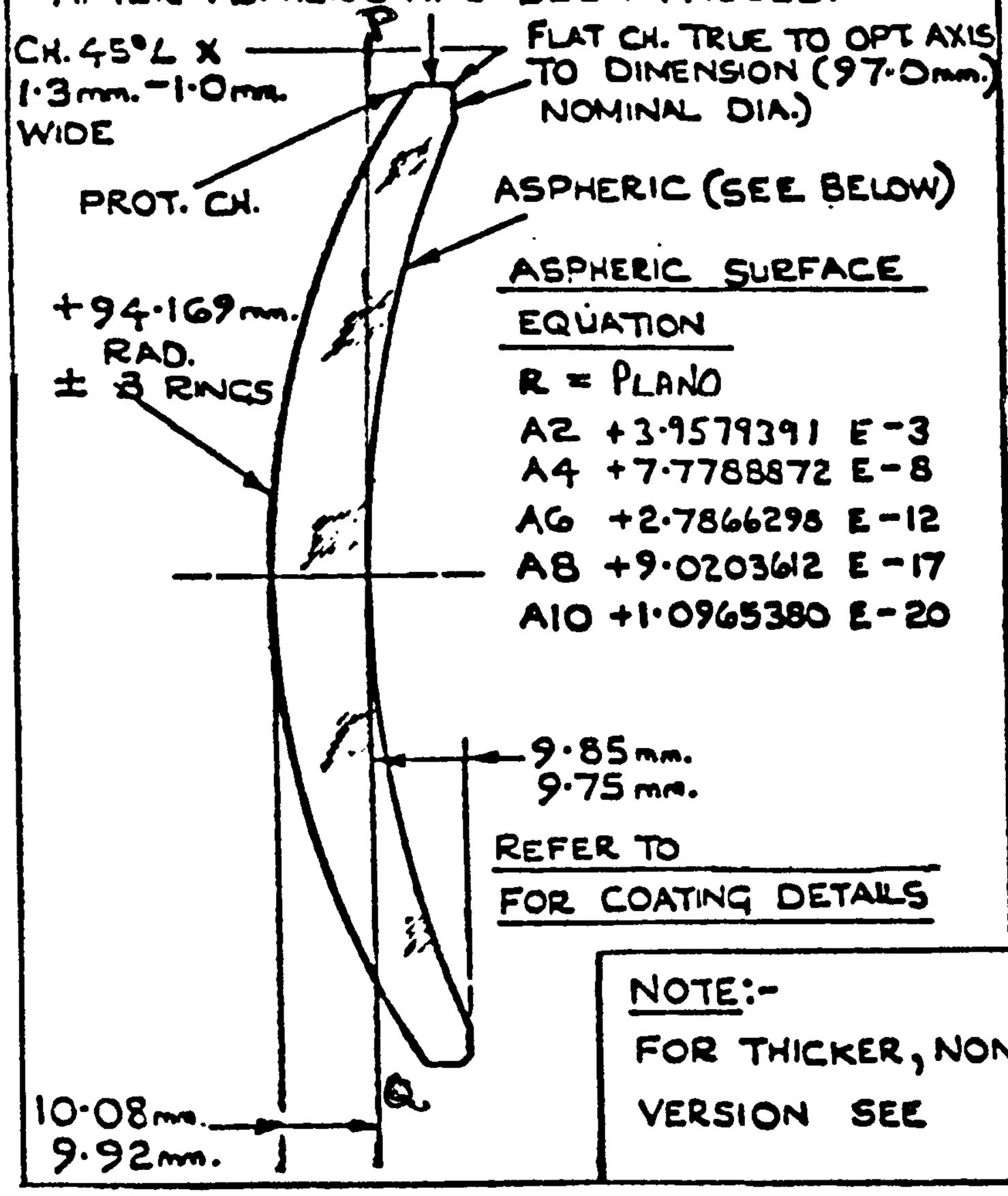

NOTE:-
FOR THICKER, NON STANDARD, VERSION SEE

DIMENSIONS PRIOR TO GENERATING ASPHERIC.

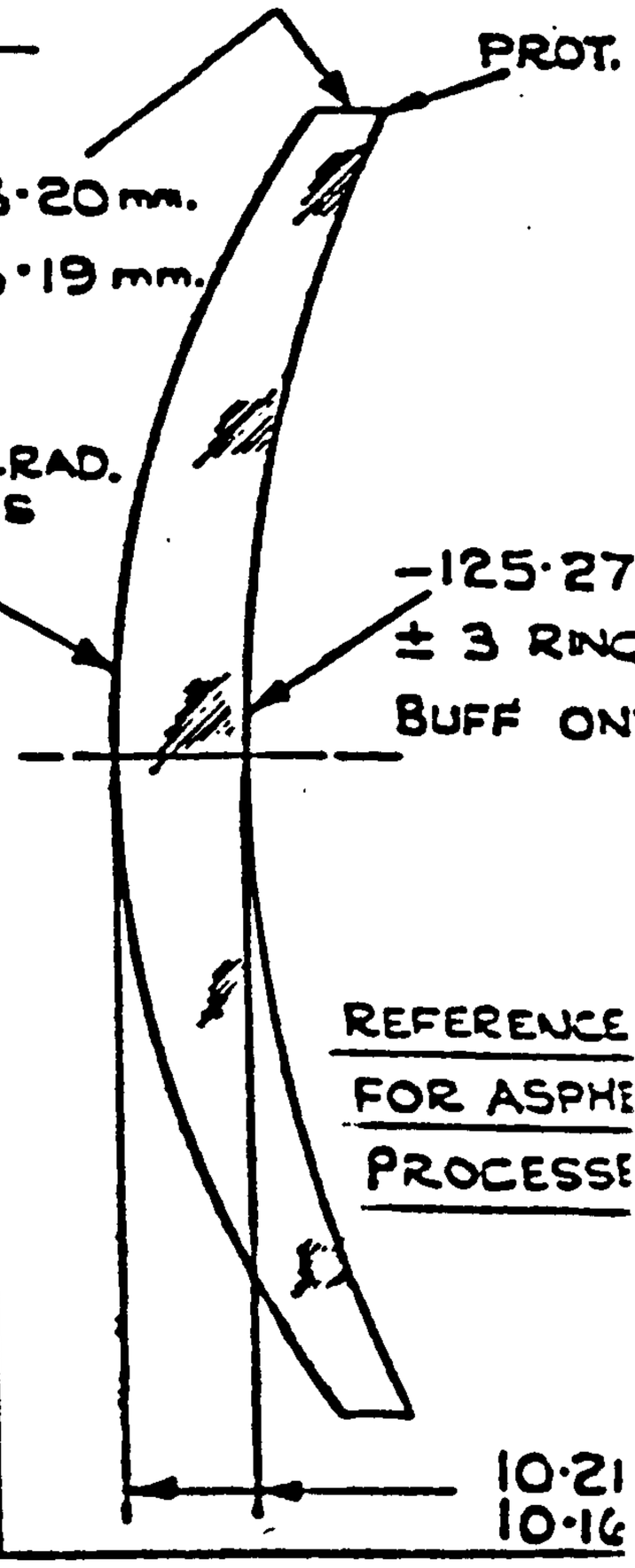

FIGURE 2.5

A TYPICAL ASPHERIC LENS ELEMENT

VERTICAL DISTANCE - Y (mm)	THEORETICAL ASPHERISING DISTANCE (x) Um
1 mm	3.95001689
2 mm	15.8330012
3 mm	35.6277548
4 mm	63.3469509
5 mm	98.9971391
6 mm	142.586752
7 mm	194.126115
8 mm	253.627458
9 mm	321.104925
10 mm	396.574594
20 mm	1.595802625 mm
40 mm	
50 mm	

FIGURE 2.6

THEORETICAL ASPHERISED DISTANCES

The very high initial cost of germanium coupled with expensive machining of several hours, requires that departures from design criteria to be kept to a minimum. Tool wear or breakage, machine vibration, poor setting up of the machine, etc., could lead to prohibitively expensive scrap material. A measurement/ inspection technique which is a part of production cycle may therefore be necessary.

2.6

Current Measurement Procedure by the Operators

An attempt in this direction is made where the aspheric generating machine itself is used for interim measurement. After the machining process is complete, the cutting tool is replaced with a Talysurf gauge. The original sequence is then re-run following the same traverse as the tool did. If the gauge shows no deflection then the design profile and the measured profile must be the same. Any deviation registered on a graph at a suitable magnification shows departure from the original profile (see Appendix A). This however, is a suspect procedure, since the machine errors encountered in cutting are likely to be repeated in the measurement also. Thus, little information about the true errors is available. This situation is improved by caliberating the machine by the use of a reference glass sphere, before making measurements. Again, the component has to be withdrawn from the machine and a whole operation of setting and re-setting embarked upon. This is bound to add

some uncertainty. Although as a guide in production this procedure appears to be valuable, it is not particularly desirable on three accounts:

(a) The philosophy of employing a production machine for measurement purposes, may not be attractive. Apart from the problem of machine errors etc., valuable production time is lost.

(b) A reasonably high degree of skill is required by the production operative to caliberate and measure components.

(c) While small quantities may be handled without too much trouble, large quantities, and wide range of products could make such measurement extremely difficult, if not impossible.

Despite such comments, practical shop floor experience suggests that the profile obtained after machining does not depart significantly from the design criteria. However, in addition to the correct profile shape, a good surface finish is also necessary. This is to improve transmission and also provide reliable surface on which thin film coatings can stick properly. In germanium elements, thin film coatings are absolutely essential. The lens element therefore, has to be polished. While polishing improves the surface finish to acceptable quality it may degrade the original profile. Hence

another measurement effort of the polished lens might be necessary. Such measurement may reveal a need for some re-machining. This in turn will require re-polishing. The final acceptable solution thus, is an iterative process, relying on a few experienced operatives and often open to fairly subjective judgements. Indeed, without a decisive measurement system, a suspect component will have other expensive processes done to it only to be later discovered as "not satisfactory". The absolute test being the operation of the actual final instrument system. If the instrument operates as expected all is well, otherwise suspect components may be replaced until a combination is found to perform well (22). However, this is rare.

2.7

Independent Measurement of Aspherics

There appears a need for an independent system, which although integrated into the production cycle does not occupy the production machine unnecessarily. The reasons as to why such a system is not already in use are complex. One of the main reasons being, that it is not quite clear as to what particular parameters are to be measured.

Ideally a measurement system should:

(a) provide quantitative answers for different aspects of the profile under consideration so that inspection could be done

without too stringent a requirement of skill;

(b) attempt to correlate the defect encountered with the faulty aspect of the machine. This is a very desirable feature since an immediate correction is then possible without waste of more material and time;

(c) be reasonably quick and lend itself to typical work shop environment.

The achievement of such a system is beset with some fundamental problems:

(a) While dimensional tolerancing is reasonably well understood, there does not exist a straight forward method for tolerancing contours, profiles, etc. This introduces subjective element in the measurement, as mentioned earlier.

(b) Tolerancing is often regarded synonymous with performance. In many engineering applications this may not be objectionable. However, in optical profiles, the actual mechanical out of tolerance does not bear a straight forward relationship to the performance of the lens. For example, it is possible that mechanical degradation of lens profile on one part of the lens is of less importance from optical point of view, and yet a similar defect on another part of the lens is totally unacceptable. Indeed a correction of one error might make another aspect unacceptable.

(c) The chain of operations, between the optical designer, the production operative, the inspector, and finally the user of the lens is often so long that correlating optical performance to mechanical/production tolerances in some useful way is an extremely cumbersome and difficult task.

In general, the machined component will have errors arising from different reasons, super imposed on each other. Irregularities which are caused by imperfections in the machine slide ways, or result from imperfect machine geometry such as squareness error between slideways may be classed as errors of form or shape. Irregularities resulting from machine vibration, or imperfections in tool setting may be classed as waviness or undulations. High frequency noise may be a function of cutting speed, feed rate, tool wear and the type of cutting fluid. Such noise forms surface texture (23).

Noise of higher frequency may not be seriously detrimental to the image, but is likely to reduce transmission to an unacceptable level. However, it has to be emphasised that the physical distances under discussion are relatively small. Consider, for example, an aluminium sphere of some 350 mm radius machined on a Pneumo Lathe (trade name). A part trace of this sphere is shown in Fig. 2.7. The trace represents the error between the best fit (least square) sphere and the actual sphere. A feature such as C - D represents an error

ALUMINIUM SPHERE

PROFILE

MEASURED RADIUS = 350.8 mm

SURFACE WAVINESS = 0.23 μm

V_V = 50 000 V_H = 10

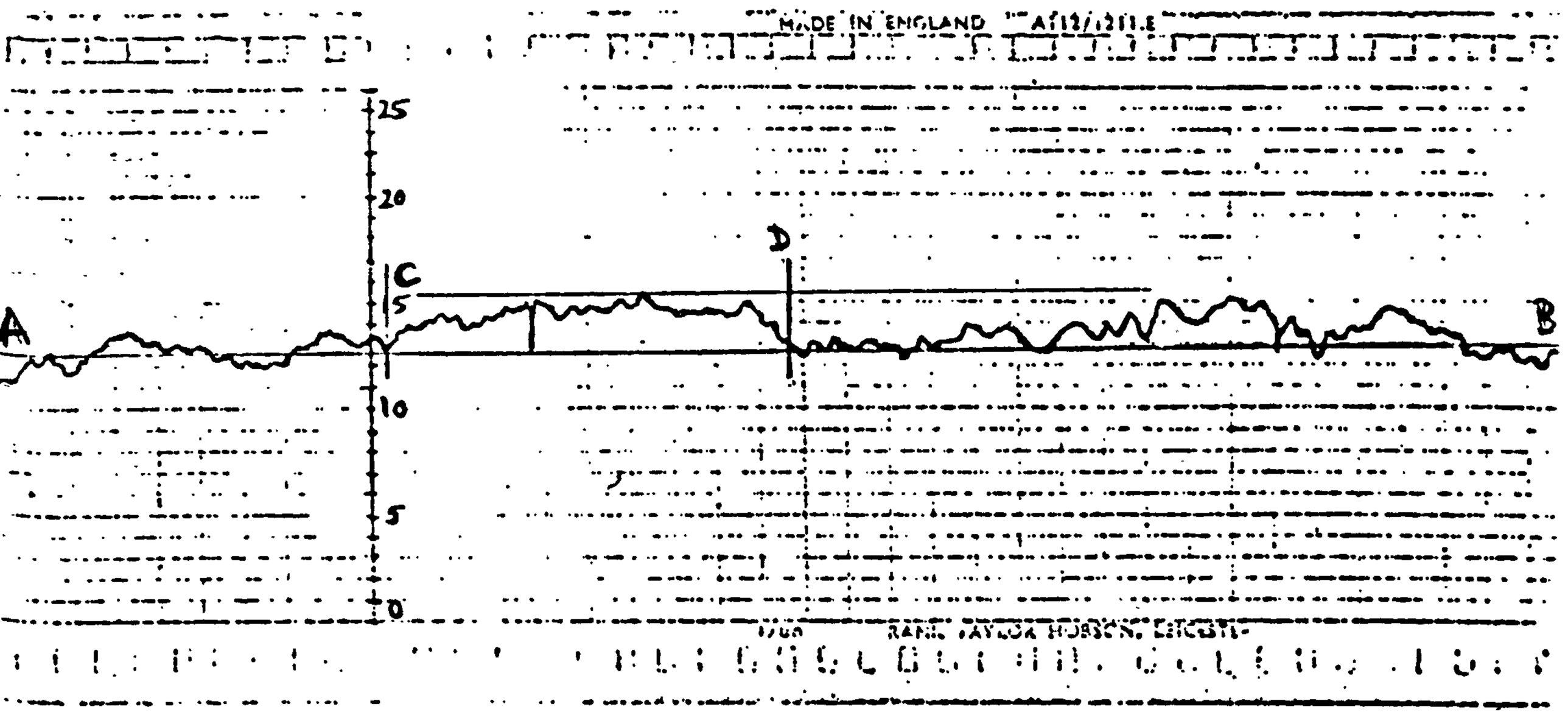

V_V - VERTICAL MAGNIFICATION

V_H - HORIZONTAL MAGNIFICATION

FIGURE 2.7

of about 0.1/0.2 μm. A similar trace for germanium sphere is shown in Fig. 2.8.

The observation of these traces raises the following issues:

(a) Can errors of such small amplitudes significantly affect the optical performance?

(b) Would one particular type of feature be more detrimental to the optical performance than another type of feature?

(c) Can the error forms and thus amplitudes be quantitatively related to the optical performance?

Some attempt to address these points has been made in the past. For example a parabolic mirror which gave poor optical performance was measured on a specially designed SIRA machine. However the mirror is relatively large. The base radius is some 452 mm. The measurement and its interpretation is discussed in Appendix B, since the optical performance of such large components is only of passing interest here.

This research is confined to the measurement of smaller germanium elements, where realistic production quantities are envisaged. However the lessons learned from the research may well be applicable to a variety of optical components.

GERMANIUM SPHERE

PROFILE

MEASURED RADIUS = 348.6 mm

SURFACE WAVINESS = 2.16 μm

V_V = 20 000 V_H = 10

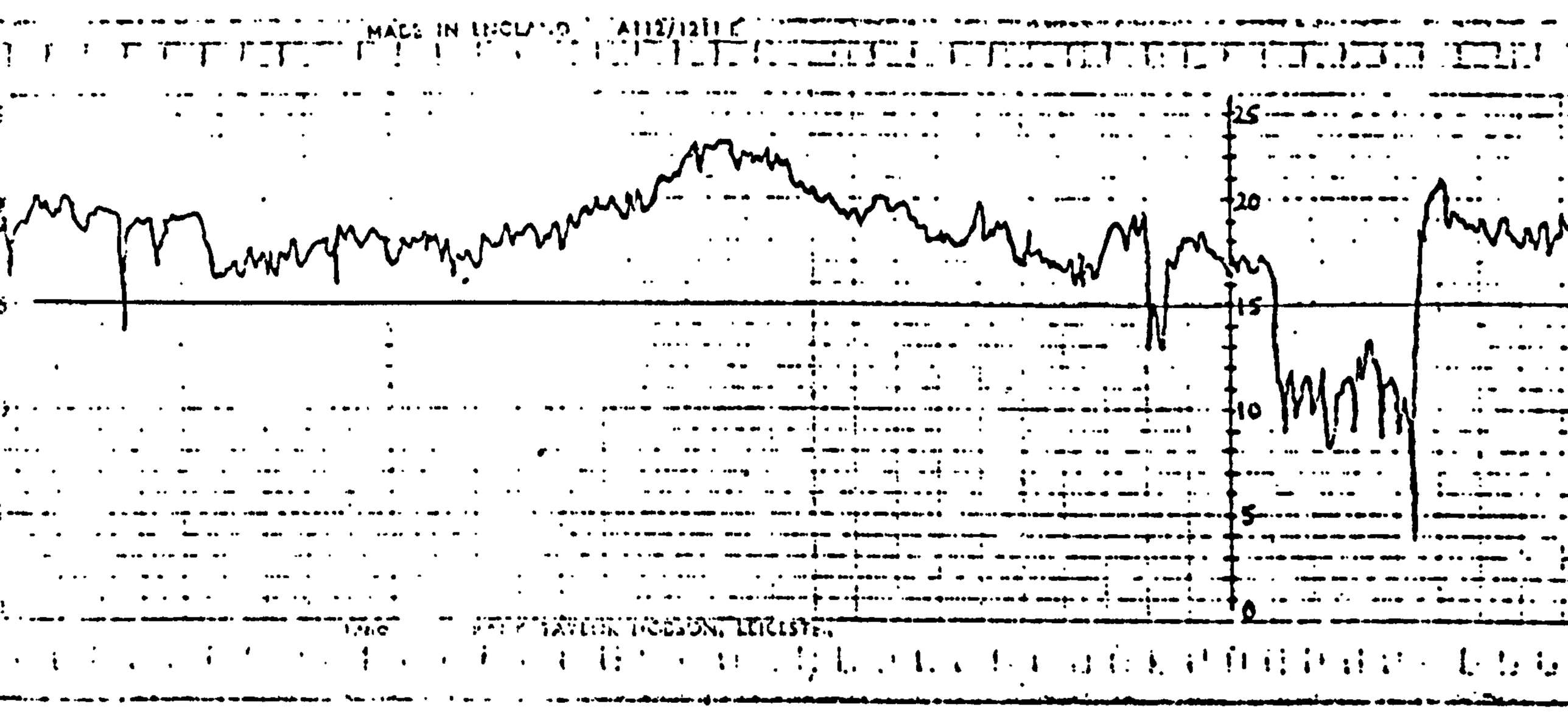

V_V - VERTICAL MAGNIFICATION

V_H - HORIZONTAL MAGNIFICATION

FIGURE 2.8

In order to conduct the research two sets of data would, hence be required:

(a) A set of error profiles pertaining to a batch of germanium lenses manufactured under normal production environment.

(b) The corresponding measures of optical performance.

At the time of starting the research the requirement (a) above could not be satisfactorily fulfilled. Firstly, sufficiently large quantity of lenses were not available, although the quantity was expected to rise quite rapidly. Secondly, an instrument which could provide the error profiles was in development stage. Hence the reliability of measurements made on this instrument could not be guaranteed.

It was therefore decided that a pilot study could be conducted using 6 lenses. The error profiles were obtained from the only development instrument available at that time. Some results and comments about this work are given in Appendix C. In addition a software lens design package was used to simulate some error forms in order to get an initial idea about the affect of such errors on optical performance. This aspect is discussed more fully in Chapter IV.

It must however, be emphasised that a set of results based on the measurement of some 29 lens elements was later made available.

As for the requirement (b), a clarification of exactly what is meant by "optical performance" is needed. A detailed discussion on this topic is available in the next chapter.

C H A P T E R I I I

OPTICAL SPECIFICATION

CHAPTER III

OPTICAL SPECIFICATION

In general only one surface of a lens is aspherised. The other surface of the lens may be flat or spherical in shape. The spherical shape is in general tested by using Newton's Ring method. High reliability of test is achievable, since the "rings" are in the visible region and hence of comparatively lower wave length than I R.

The aspheric side in general does not lend itself to Newton's Ring method. Apart from the method described earlier no other reliable mechanical test is done. The quality of the lens will hence be judged by the optical performance of the lens element.

3.1

What is Optical Performance

The function of an optical system is to produce the image of a given object as clearly as possible. This requirement immediately implies subjective judgement of an image and hence indicates the difficulty in quantitative measurement of image quality.

To complicate the matter further, the requirement from one image is not necessarily the same for another image; for example the features of an image which are of importance in military work may be relatively unimportant in another application area.

Despite diversities of this nature some form of standardised approach which defines optical performance, is required. Suitable instrumentation can then be designed to measure optical performance according to specification.

A logical approach is to consider the light from the object to be made up of a set of point sources. A perfect image would be produced if each object point produced an exactly similar point at the corresponding position in the image, with amplitude, size and phase adjusted to take into account the magnification if any.

In practice the image of a point is not a point. It is generally spread out. Further, the manner in which it is spread out may vary from one position to another in the object. Never-the-less, the intensity distribution of the image of a point source must reveal important facts about the imaging system.

Point Spread Function

Thus the intensity distribution function of a point source can be used as a basis of comparison between different systems. The intensity distribution of a point is called point spread function (PSF). The use of PSF as a basis for testing optical systems is attractive, because in practice, a "point"

source may be generated, and the intensity destribution i.e. PSF can be measured using suitable detectors. In geometric terms a "point" has to be infinitely small. When dealing with light sources, firstly generation of a perfect "point" is impossible. Secondly light consists of several frequencies and this fact may be of importance when testing an optical system. The property of a source which can be approximated to a "point" is called spatial coherence, while the possession of a single frequency is called "temporal coherence". Generally a thin laser beam meets both these requirements from practical point of view. Even so, in non-coherent systems, a point is regarded as a small circle:

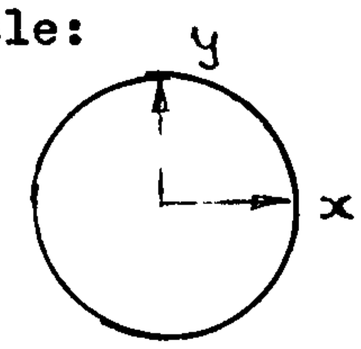

Thus the intensity distribution in the image may be measured in X or Y direction or any other direction given by the combination of X, Y directions.

3.3

Line Spread Function

To simplify matters, however, only one direction may be considered. An illuminated thin slit is hence used as a single dimensional object. The intensity distribution of the image when the object is a thin slit is called a line spread function (LSF) (see Fig. 3.1).

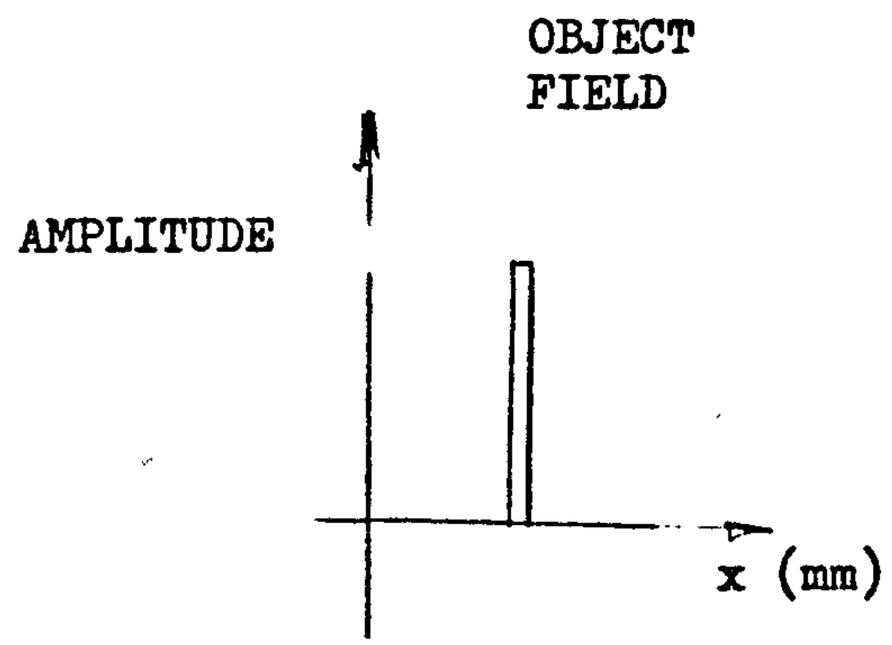

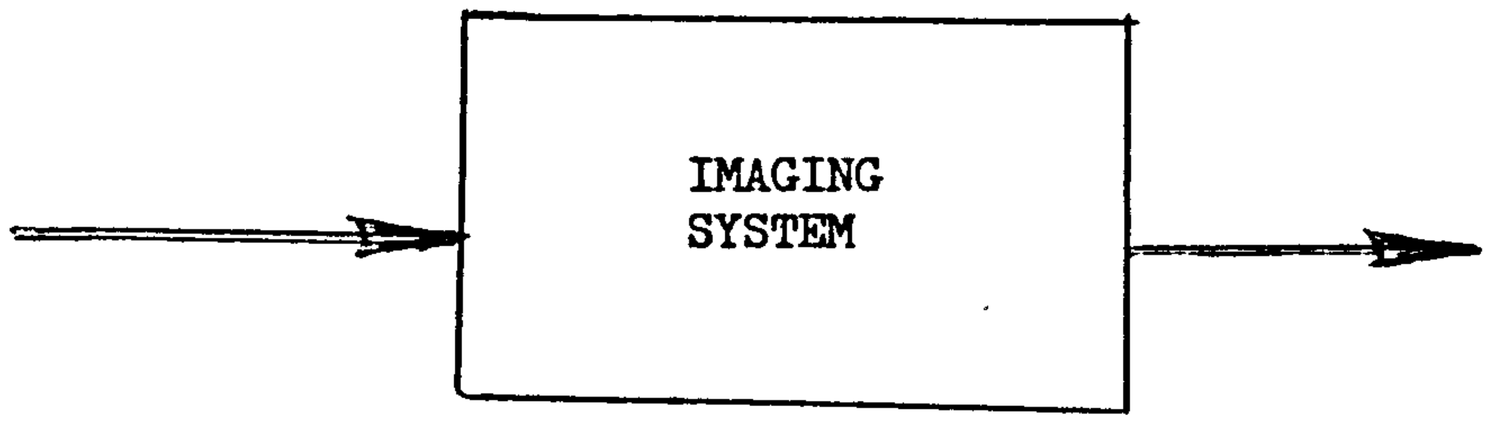

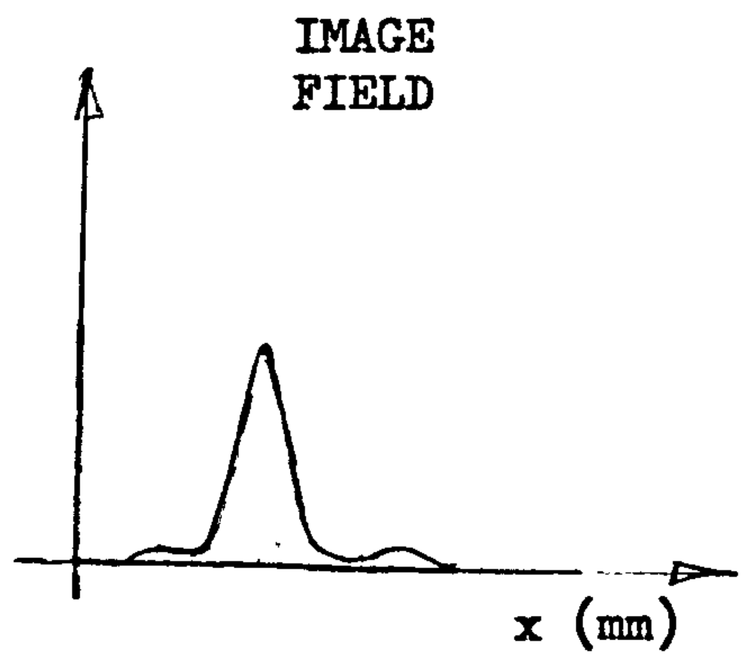

3.4

LINE SPREAD FUNCTION

FIGURE 3.1

The LSF consists of two effects:

(a) Diffraction effect due to the lens aperture which has nothing to do with the lens aberrations. Bigger the aperture, thinner is the LSF. For relatively large apertures, this effect is negligible. A system in which such an effect might play a prominent part is called, diffraction limited system.

(b) The LSF will be broadened by the aberrations of a lens. A lens which has no aberrations is only diffraction limited. In fact the normalised LSF may be regarded as an impulse response of the system. Thus if the impulse response of the system can be found by measurement, the output for any other input may be found by the convolution of LSF and the given input (see Fig. 3.2). An object may therefore be considered of several single dimensional sources of different amplitudes. The compsite output would then be convolution of inputs and the LSF. In practice, the detectors measure energy, hence it is important to differentiate between amplitude and (amptitude)^2, in mathematical expressions.

In general an impulse function is used to model a condition where a large amount of energy is associated with a very small duration of time. In optics, a very thin illuminated slit is associated with a large amount of energy concentrated in a very small space.

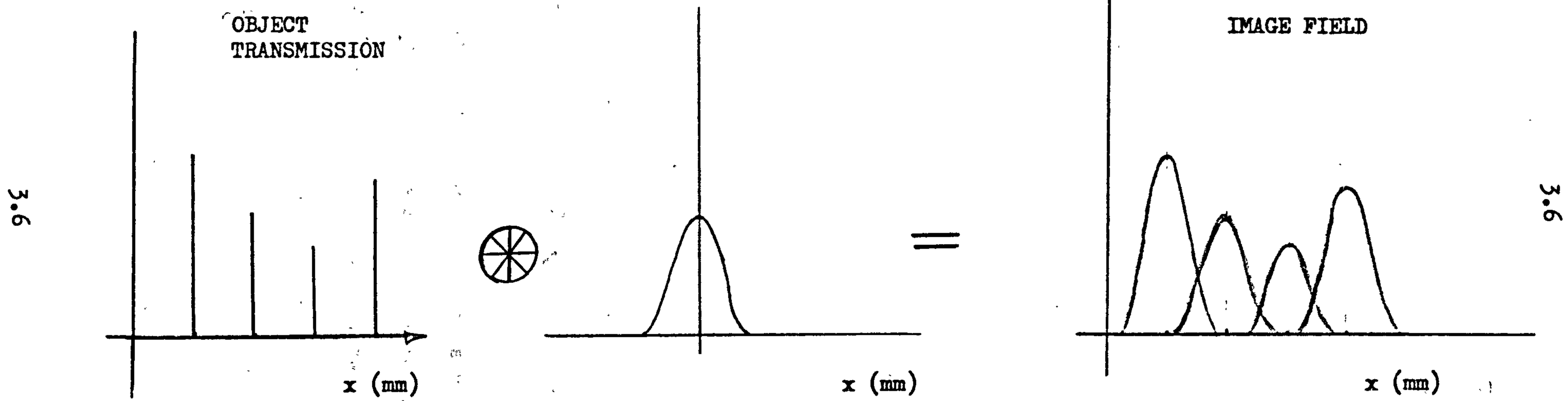

PRINCIPLE OF CONVOLUTION

FIGURE 3.2

Since the Fourier Transform (FT) of an impulse function leads to the concept of frequency in the time domain, the FT of LSF leads to the concept of spatial frequency. This fact is of great importance because:

(a) A lens (or optical system) test specification can be directly formulated in term of LSF (see example for Irtal 3, P 3.17 (trade name) system).

(b) The powerful analytical tool of Fast Fourier Transform (FFT) can be applied and concepts such as frequency response etc. can be practically realised.

3.4

Fourier Theory

A well known result of Fourier theory is that a signal f(t) can be considered as made up of several sine waves of different frequencies, which vary in phase and amplitude.

Similarly, a given distribution of intensity in the object plane of an optical system can be considered as arising from superimposed sine waves of different spatial frequencies. Thus a simplest object in optical terms would be a grating which produces a sinusoidal distribution of light. If we consider a one dimensional distribution of light f(u) where u has dimensions of distance. Mathematically, this can be

expressed as:

$$f(u) = \int_{-\infty}^{+\infty} F(s)e^{2\pi jsu}ds$$ where s is spatial frequency.

Notice the similarity with $f(t) = \frac{1}{2\pi}\int_{-\infty}^{+\infty} F(jw)e^{jwt}dw$

F(s) is a complex function of spatial frequency s.

The image is linearly related to the object. Hence a particular spatial frequency in the image is linearly related to the corresponding frequency component in the object. Thus, the distribution intensity $f^1(u)$ in the image can be built from sine waves and a function $F^1(s)$ also exists for the image. The linear relationship may then be expressed as follows:

$$F^1(s) = D(s)\ F(s)$$

where D(s) is a complex function of s and is independent of value of F(s)

Thus $D(s) = \frac{F^1(s)}{F(s)}$ $\frac{\text{output}}{\text{input}}$

3.5

OTF AND MTF

D(s) is hence a transfer function and appropriately called optical transfer function (OTF).

The OTF suitably normalised, is in fact the spatial frequency response of the system. Since OTF is a complex function, it has magnitude and phase. The magnitude (or modulus) is referred to as modulation transfer function (MTF) and the argument is called phase transfer function (PTF)

$$\text{Since } D(s) = \frac{F^1(s)}{F(s)} \quad \frac{\text{output}}{\text{input}}$$

an object f(u) could be chosen so that F(s) = 1; for such a condition:

$$D(s) = F^1(s)$$

What object should then be chosen such that F(s) = 1?

Thus

$$f(u) = \int_{-\infty}^{\infty} 1 \; e^{j2\pi su} ds.$$

From the distributing theory $f(u) = K \, \delta(u)$

Such an object is a very narrow bright line i.e. a slit and

its image $f^1(u)$, would hence be the LSF as mentioned earlier. Indeed, the OTF is equal to the Fourier transform of the normalised LSF (see Fig. 3.3). This relationship forms the basis for one of the most commonly used methods of measuring OTF, or MTF of an optical system.

3.6

Advantages of OTF

(a) The OTF of a system can be measured in an objective manner so that the results of measurements can form a basis of comparison between differing systems.

(b) Since the OTF in most cases can be theoretically prediticted from the design data a system can be designed to meet an image quality criterion specified in OTF terms.

(c) In practice, an optical system consists of several lenses and indeed several subsystems cascaded. The OTF of a complete incoherently coupled system can be calculated by cascading OTFs of the individual sub-units (see Fig. 3.4). Further, this cascading process can include transfer function of purely electronic units such as amplifiers, etc. provided suitable constant is applied to convert temperal frequencies to equivalent spatial frequencies. OTF, can also be obtained by doing the familiar frequency response test on a system.

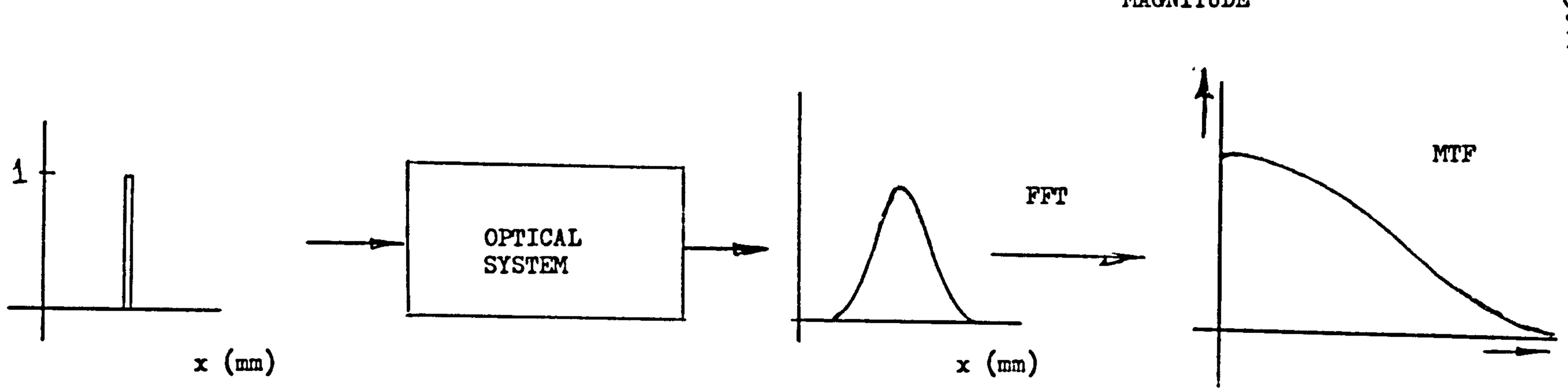

MODULATION TRANSFER FUNCTION

FIGURE 3.3

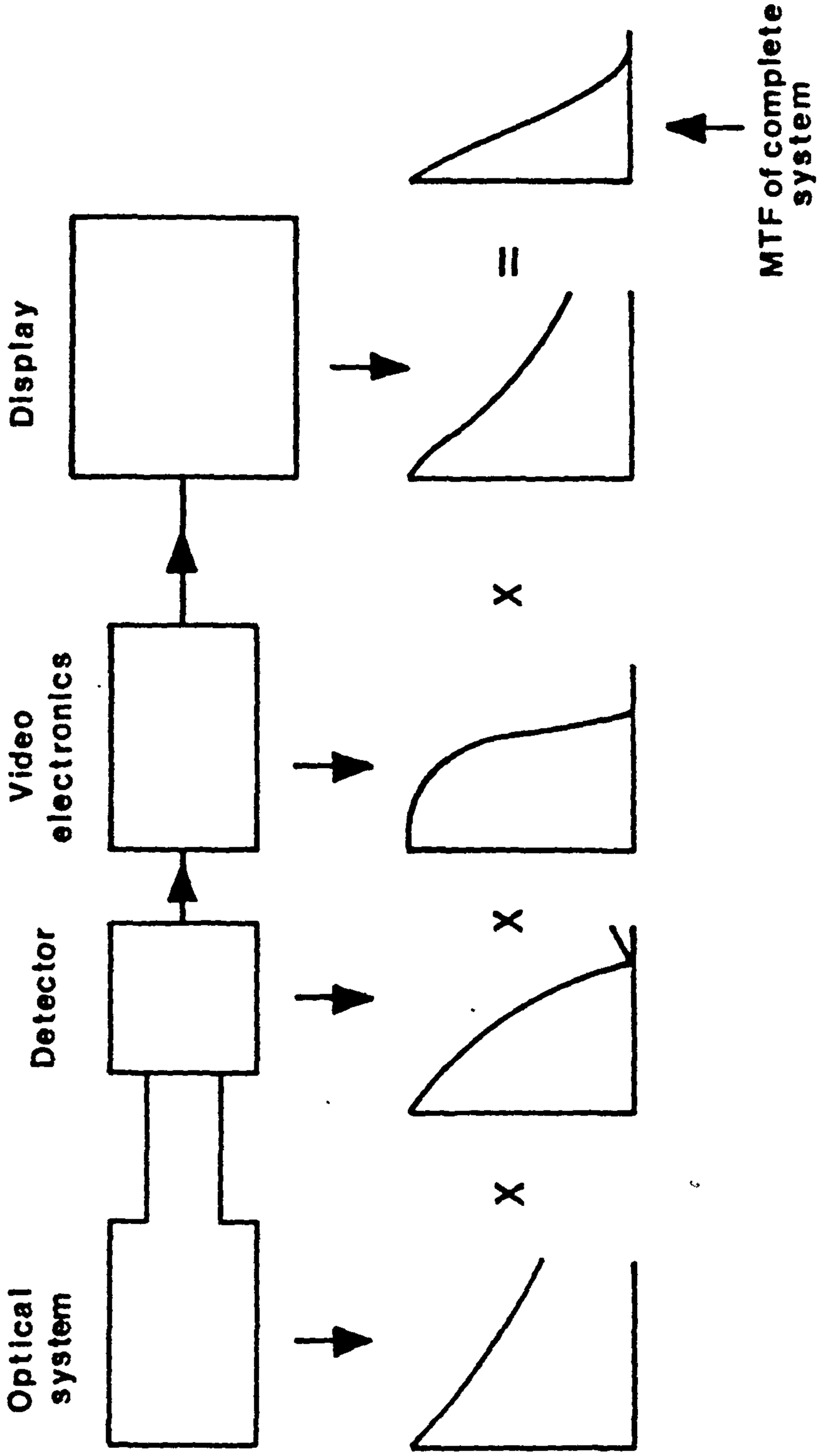
Optical system
Detector
Video electronics
Display
MTF curves
MTF of complete system
=
x
x
x

FIGURE 3.4

Hence the input has to be an object which has a single dimentional sine wave distribution of intensity, i.e. sinusoidal grating. Thus for spatial frequency 's:

the object $f(u) = A(1 + \alpha \sin(2\Pi su + \phi))$

and the image $f^1(u) = A^1 (1 + \alpha' \sin(2\Pi su + \phi^1))$

A and A^1 are functions of average intensities in the object and image plane. ϕ and ϕ^1 are the phase terms indicating the relative positions of the grating and its image respectively with respect to some fixed reference. It can be shown that MTF = $\frac{\alpha^1}{\alpha}$, where α is defined as

$$\text{contrast} = \frac{I_{max} - I_{min}}{I_{max} + I_{min}} \qquad (I - \text{intensity})$$

The term "modulation" hence becomes very much more appropriate. The PTF is given by $(\phi - \phi^1)$. Thus by using a range of sine wave gratings of different spatial frequencies and known contrasts several objects can be presented to the system under test. The output contrasts and phases can be measured. Thus the MTF and PTF can be obtained directly from the frequency response test as well.

A traditional optical bench is shown in the photograph of Fig. 3.5. A modern automatic optical test bench is shown in photograph of Fig. 3.6. In principle, the image of a thin slit is scanned by a suitable detector. The output of the detector can be converted directly to MTF or the LSF may be digitised and FFT found by using another computer.

The photographs of Figs. 3.7 and 3.8 show an Irtal 3 lens system and its specification curves. Figure 3.9 shows a typical measured LSF, while Fig. 3.10 shows typical MTF curves.

OTF TEST EQUIPMENT

FIGURE 3.5

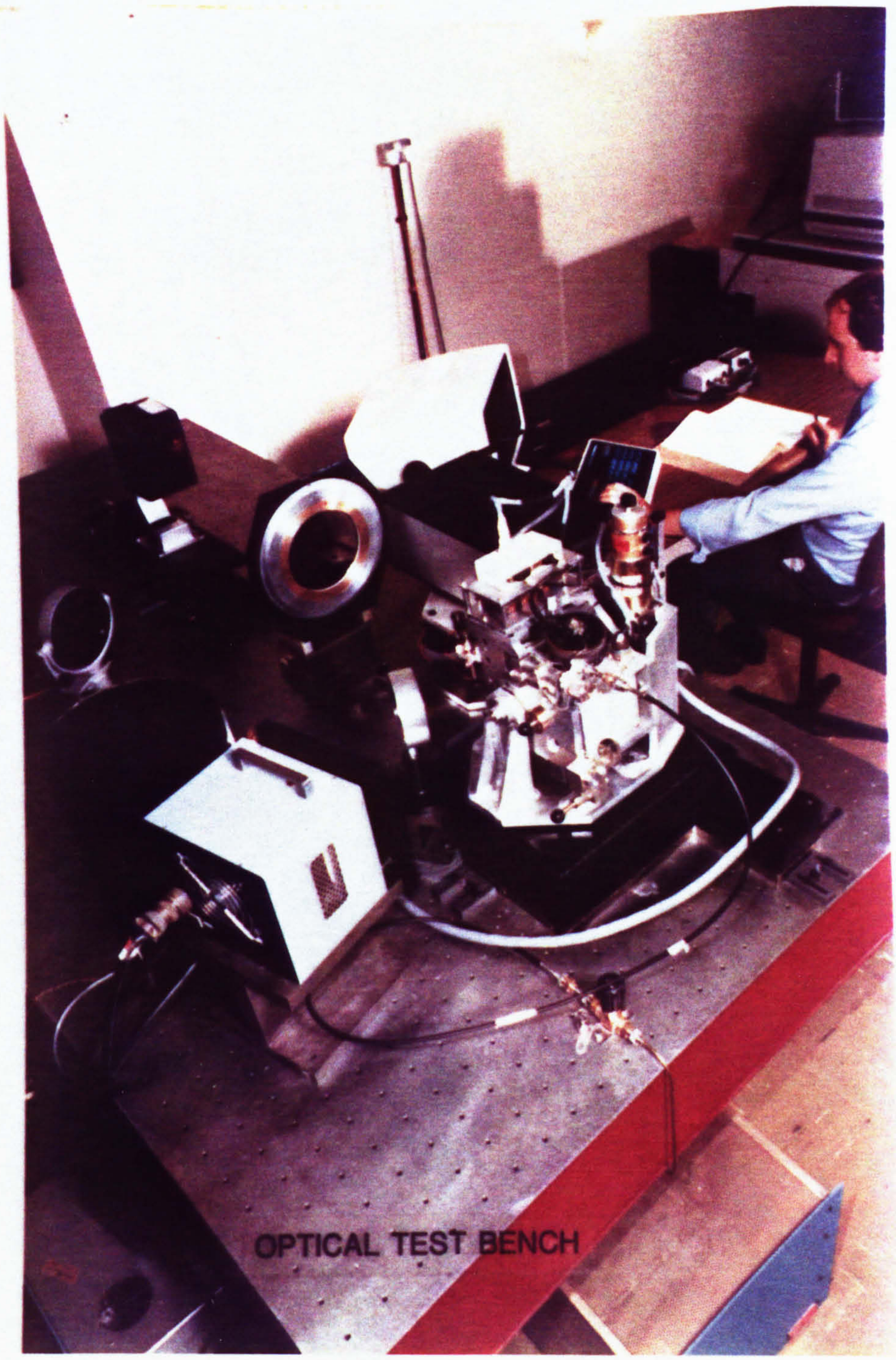

AUTOMATIC OTF TEST STATION

FIGURE 3.6

Irtal 3

Irtal 3 is a two element, two aspheric germanium lens.

Focal length: 100mm

Aperture: f/0·70

Waveband: 8–14 micron.

Back Focus: 49mm through 2mm germanium detector window.

Field coverage: Optimum performance over a flat field 18mm diameter. As performance versus field diagram shows, a lesser but useful performance may be expected over a 26mm diameter field.

Material: The germanium used in this lens is polycrystalline n-type, of resistivity 10 to 30 ohm-cm and is of optical quality. Single crystal material can be provided, at a premium price and possibly longer delivery.

Coatings: Single layer coatings are standard, multilayer coatings can be provided, at a economic price and possibly longer delivery.

Detector Window: Corrected for 2mm thick germanium detector window.

Minimum object distance: 1·5 metres (5 feet).

Mounting: Irtal 3 is mounted for laboratory use. The mount provides a rapid and sensitive focusing movement. An iris is provided with a range from f/0·70 to f/4·0. The lens body carries a mounting thread intended for use with mounting adaptors. Thread is 136·25mm diameter, 1mm pitch ISO metric form. Installation drawings are provided to allow design of adaptors. Alternatively Rank Optics would design and manufacture them.
Although it is not ruggedised to full military standards, steps have been taken to protect the germanium elements in case of an accident. The focus control has

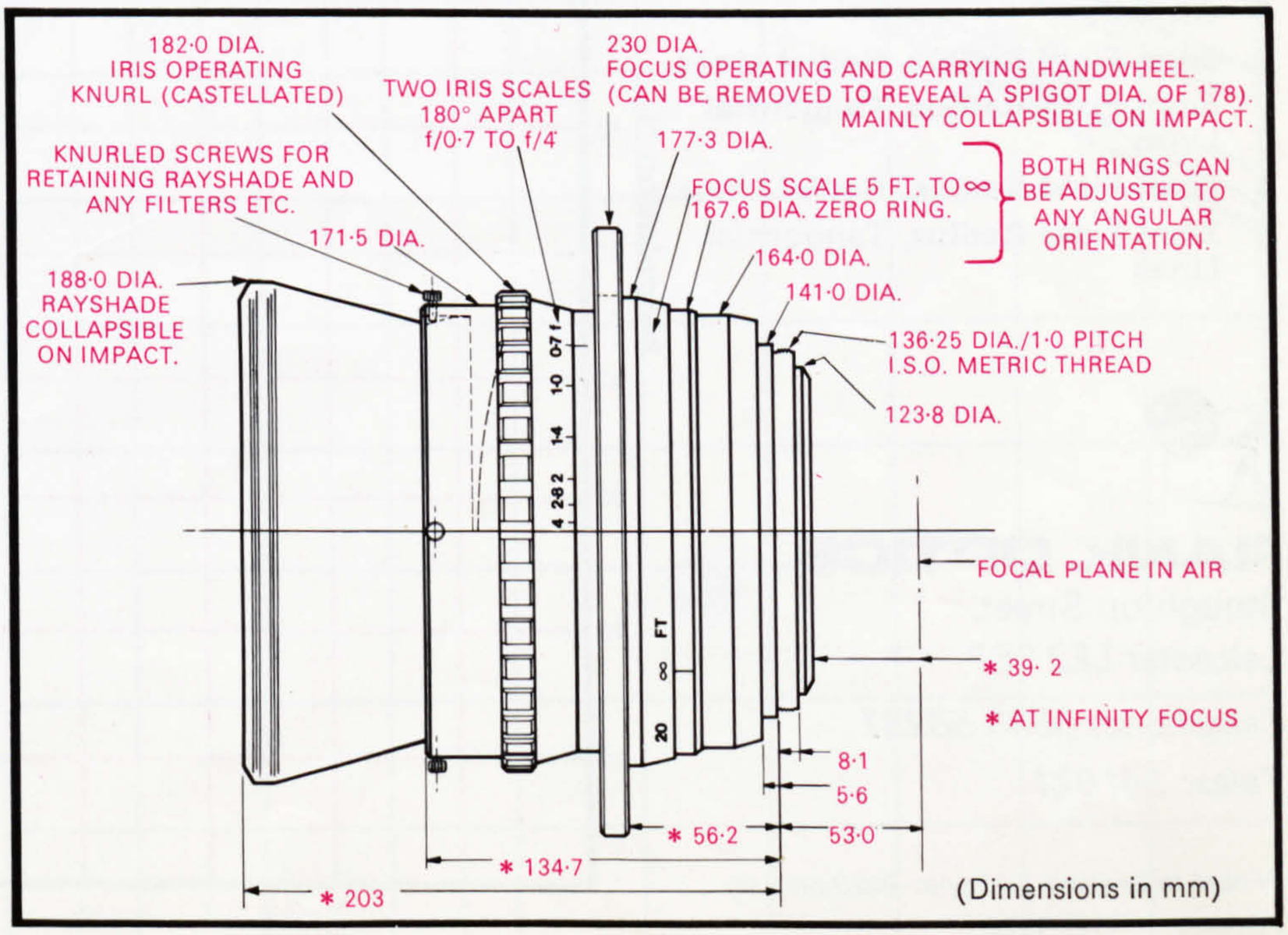

PAGE No. 3.17

Fig. 3.7

Quantity:

Though heavily aspherised, batch quantities can be supplied, because unique numerical control processes are used in their production. Unlike hand polished aspherics, price reductions can be offered for batch quantities.

been enlarged to steering wheel design. For most of its circumference there is then a finger space between the ring and the lens body. This reduces the char of impact shock being transmitted to the lens. The relieved portions act as shock absorbers, crumpling on impact.
The ray shade is also designed to collapse on impact, protecting the front element. The rear element is small and therefore less vulnerable, though it is also protected by the mounting adaptor.
The front filter holder is ruggedly designed and allows the lens to be attached an optical system by its front.
The focus scale may be adjusted for orientation and zeroed. This allows the sc to be made visible regardless of the lenses orientation on the camera. Similarl the f/no scale is duplicated on either side of the lens to improve visibility.
The focus handwheel is easily removed, allowing gears or belt drive focusing instead. The lens is black anodised with white lettering.

COMPUTED PERFORMANCE VERSUS FIELD RADIUS; MODULATION OF 5 c/mm. ;VIGNETTING (PERCENTAGE PUPIL AREA)

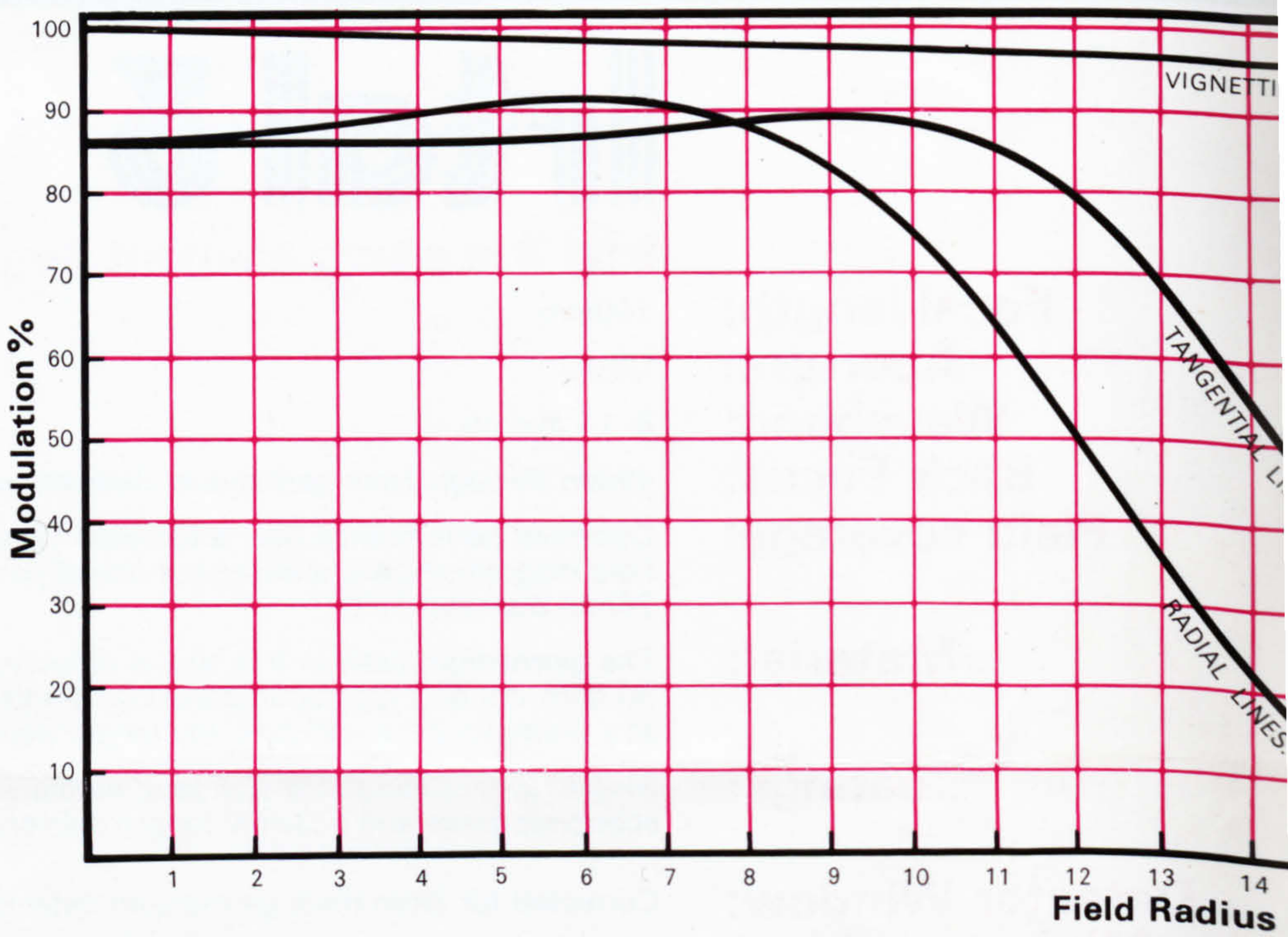

COMPUTED FREQUENCY RESPONSE CURVES POLYCHROMATIC M·T·F·, RELATIVE TO DIFFRACTION LIMIT OBJECT AT INFINITY

100mm focal length f/0·70

100%, Diffraction Limit

1 On Axis
2 5mm Field Radius, Radial Lines
3 5mm Field Radius, Tangential Lines
4 7mm Field Radius, Radial Lines
5 7mm Field Radius, Tangential Lines

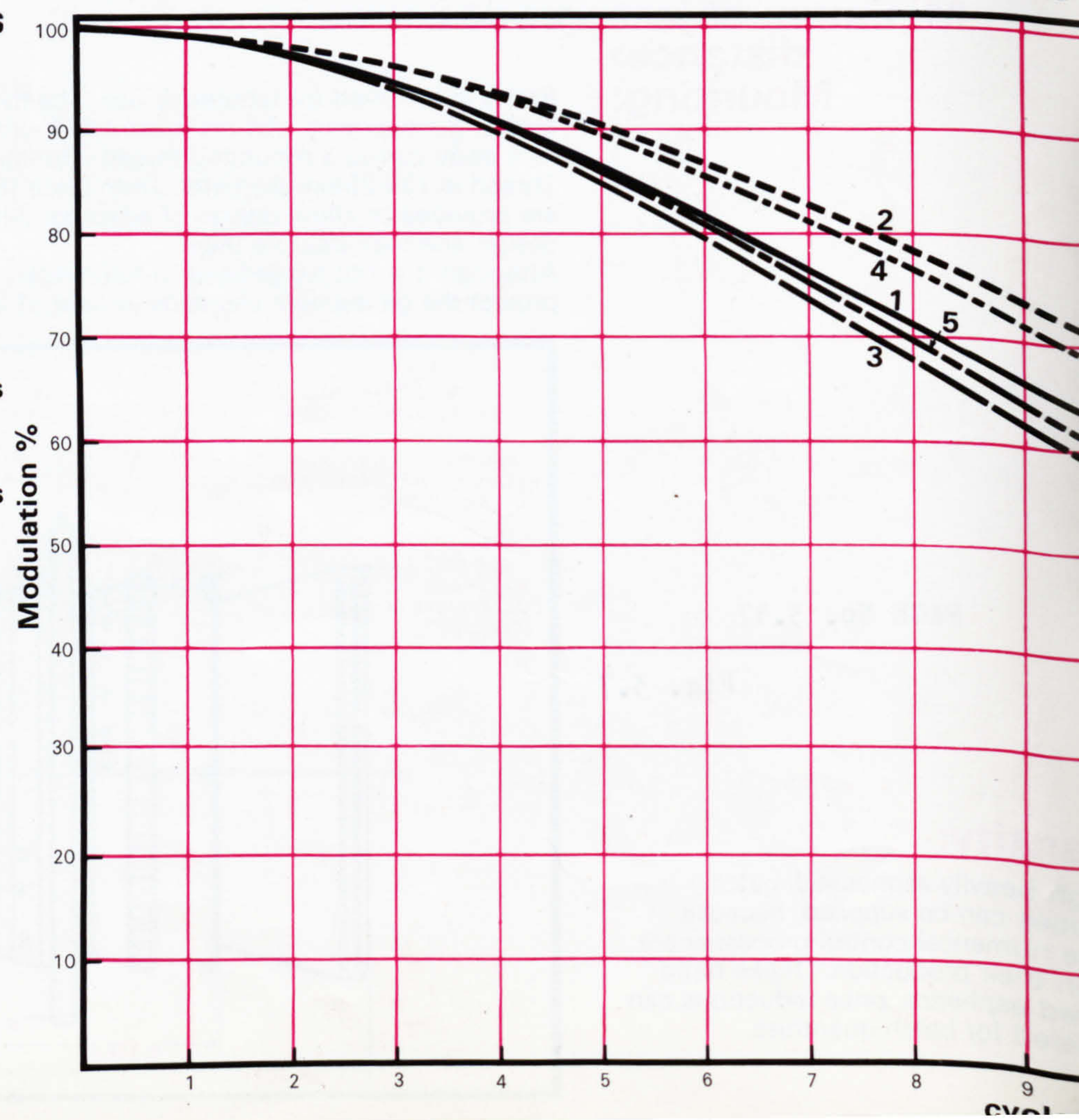

RANK OPTICS
Stoughton Street,
Leicester LE2 0SP
Telephone: 0533 58251
Telex: 341021

Printed in England by Taylor-Bloxham Ltd.
Leicester 2M/2/74

RANK TAYLOR HOBSON
P.O. Box 64, Stoughton Street, Leicester, LE2 0SP
England
Telephone : 0533 58251
Telex : 341021
Cables : Lenses Leicester

RANK PRECISION INDUSTRIES INC
411 Jarvis Avenue, Des Plaines, Illinois 60018, USA
Telephone : 312 297 7720
Telex : 726441

RANK PRECISION INDUSTRIES GMBH
6200 Wiesbaden, Gustav-Streseman-Ring 12-16
Postfach 4827, West Germany
Telephone: 010-49 6121 373051
Telex: 003 4186175

been enlarged to steering wheel design. For most of its circumference there is then a finger space between the ring and the lens body. This reduces the chances of impact shock being transmitted to the lens. The relieved portions act as shock absorbers, crumpling on impact.
The ray shade is also designed to collapse on impact, protecting the front element. The rear element is small and therefore less vulnerable, though it is also protected by the mounting adaptor.
The front filter holder is ruggedly designed and allows the lens to be attached to an optical system by its front.
The focus scale may be adjusted for orientation and zeroed. This allows the scale to be made visible regardless of the lenses orientation on the camera. Similarly the f/no scale is duplicated on either side of the lens to improve visibility.
The focus handwheel is easily removed, allowing gears or belt drive focusing instead. The lens is black anodised with white lettering.

**PERFORMANCE VERSUS FIELD RADIUS; MODULATION OF 5 c/mm.
;VIGNETTING (PERCENTAGE PUPIL AREA)**

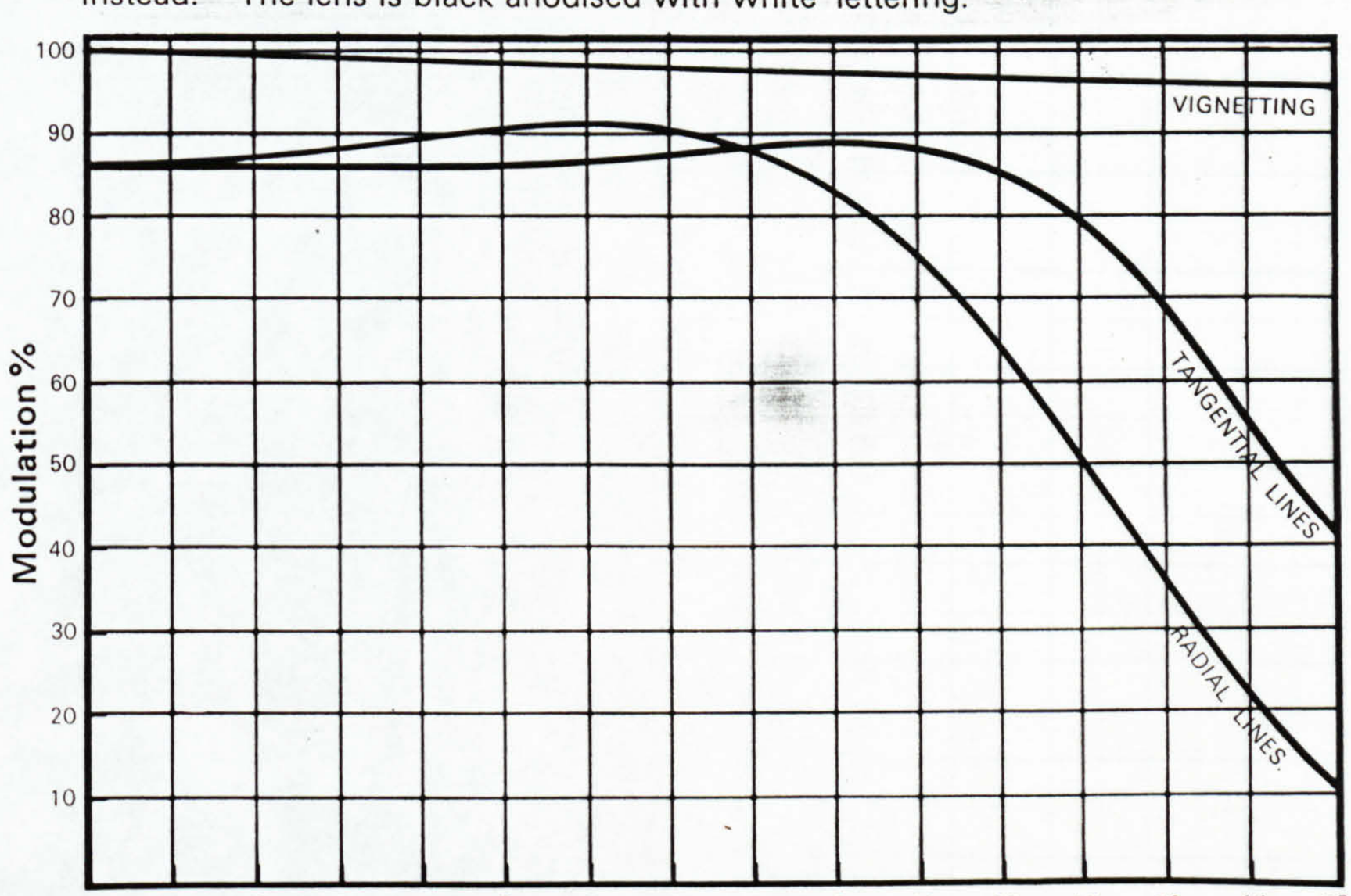

FREQUENCY RESPONSE CURVES POLYCHROMATIC M·T·F·, RELATIVE TO DIFFRACTION LIMIT OBJECT AT INFINITY

100mm focal length f/0·70

100%, Diffraction Limit

1 On Axis
2 5mm Field Radius, Radial Lines
3 5mm Field Radius, Tangential Lines
4 7mm Field Radius, Radial Lines
5 7mm Field Radius, Tangential Lines

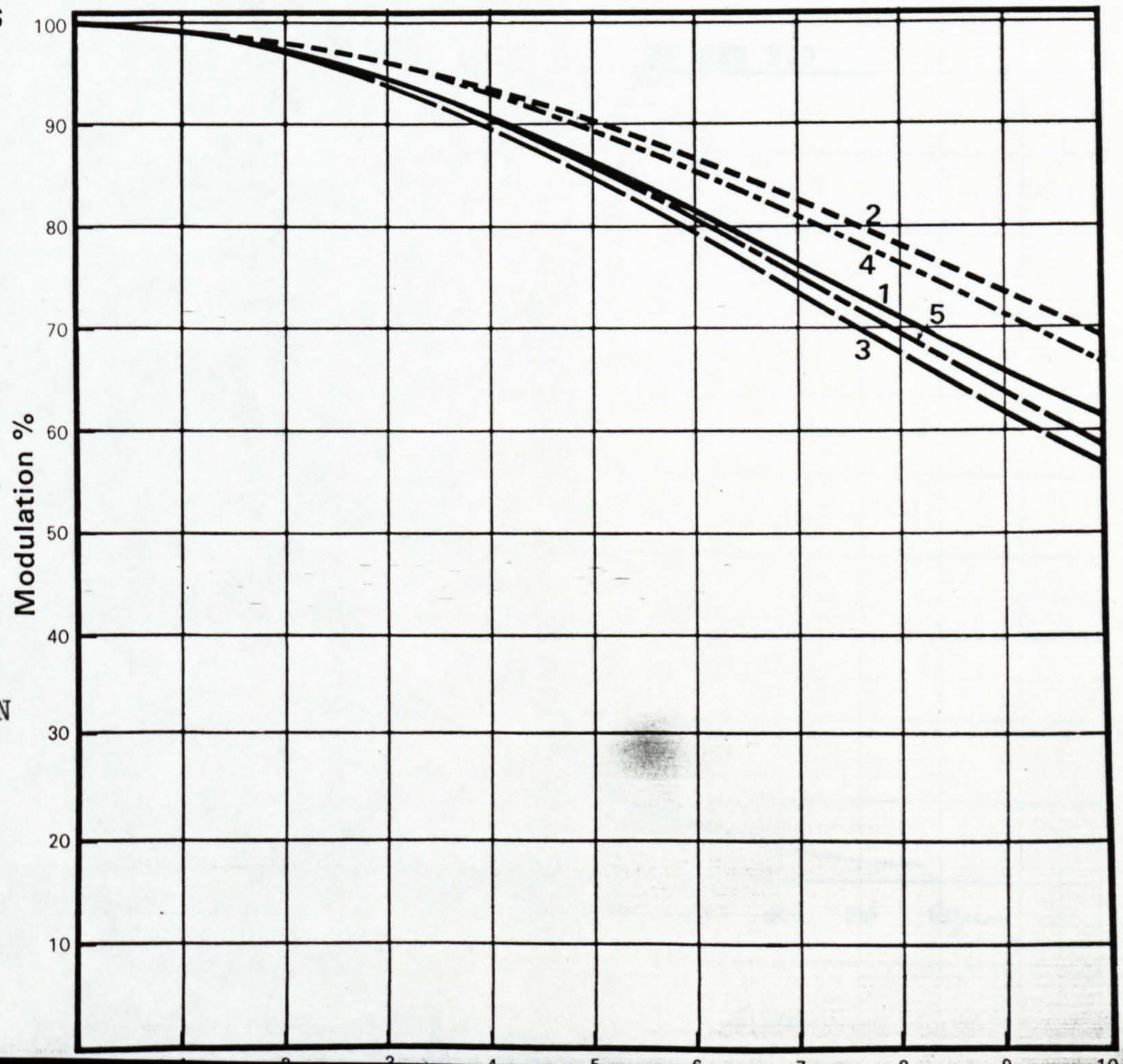

MTF SPECIFICATION CURVES

FIGURE 3.8

IRTHL 3 ELEMENTS IN BAe. MOUNT 102C044S04

LENS SET NO.. 2.

ON AXIS

OBJECT SLIT 1mm
IMAGE ANALYSER SLIT 12μm.

CONJUGATE ∞

AZIMUTH T

½ WIDTH ≡ 27.5μm

¼ WIDTH ≡ 40.5μm.

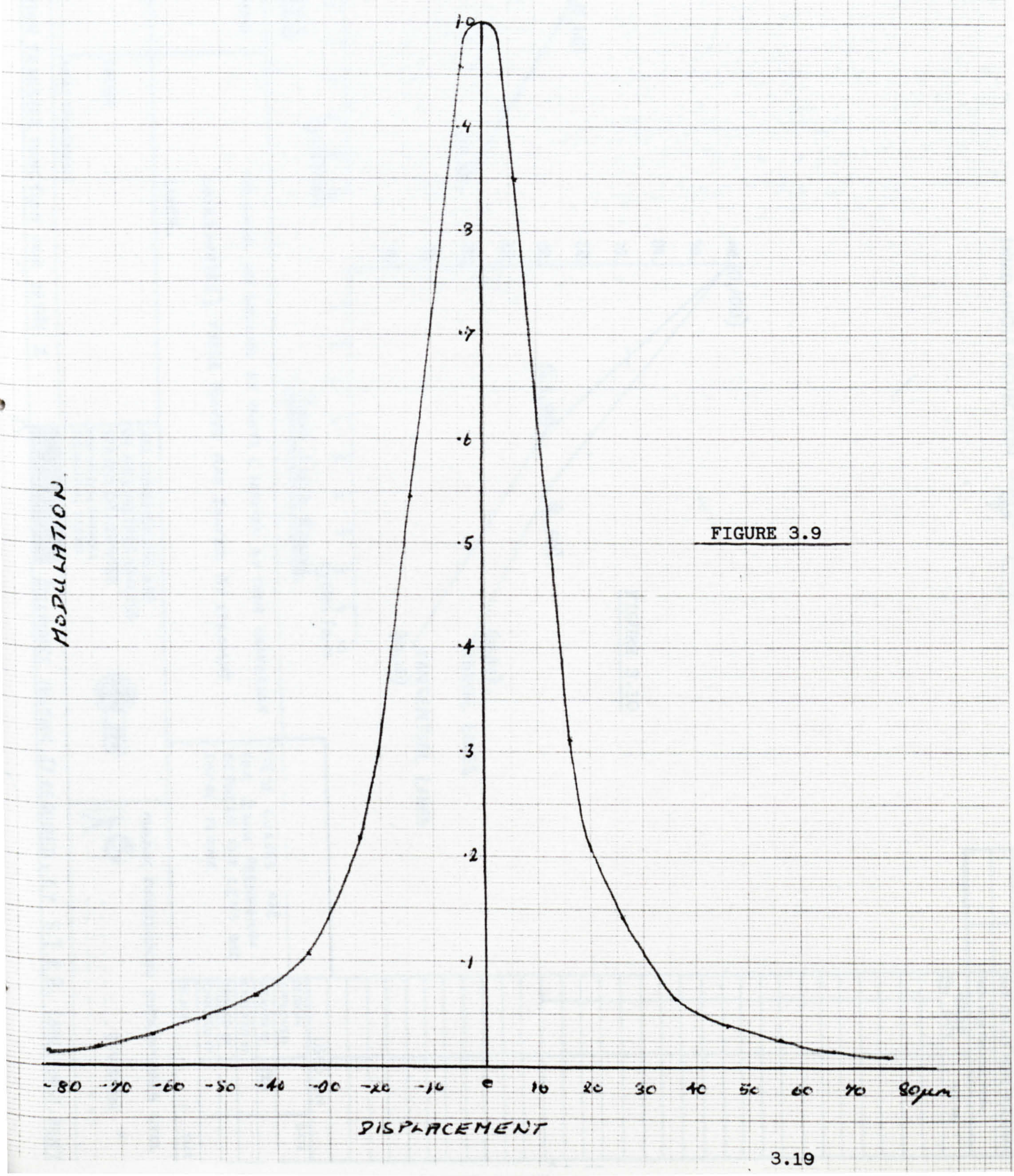

FIGURE 3.9

THIRD ANGLE PROJECTION

BY		
		NOT FOR PLANNING
		NOT ON ALT. NOTE PROCEDURE
		NOT FOR PRODUCTION

ISSUED No.	ISSUED DATE	ALT. No.

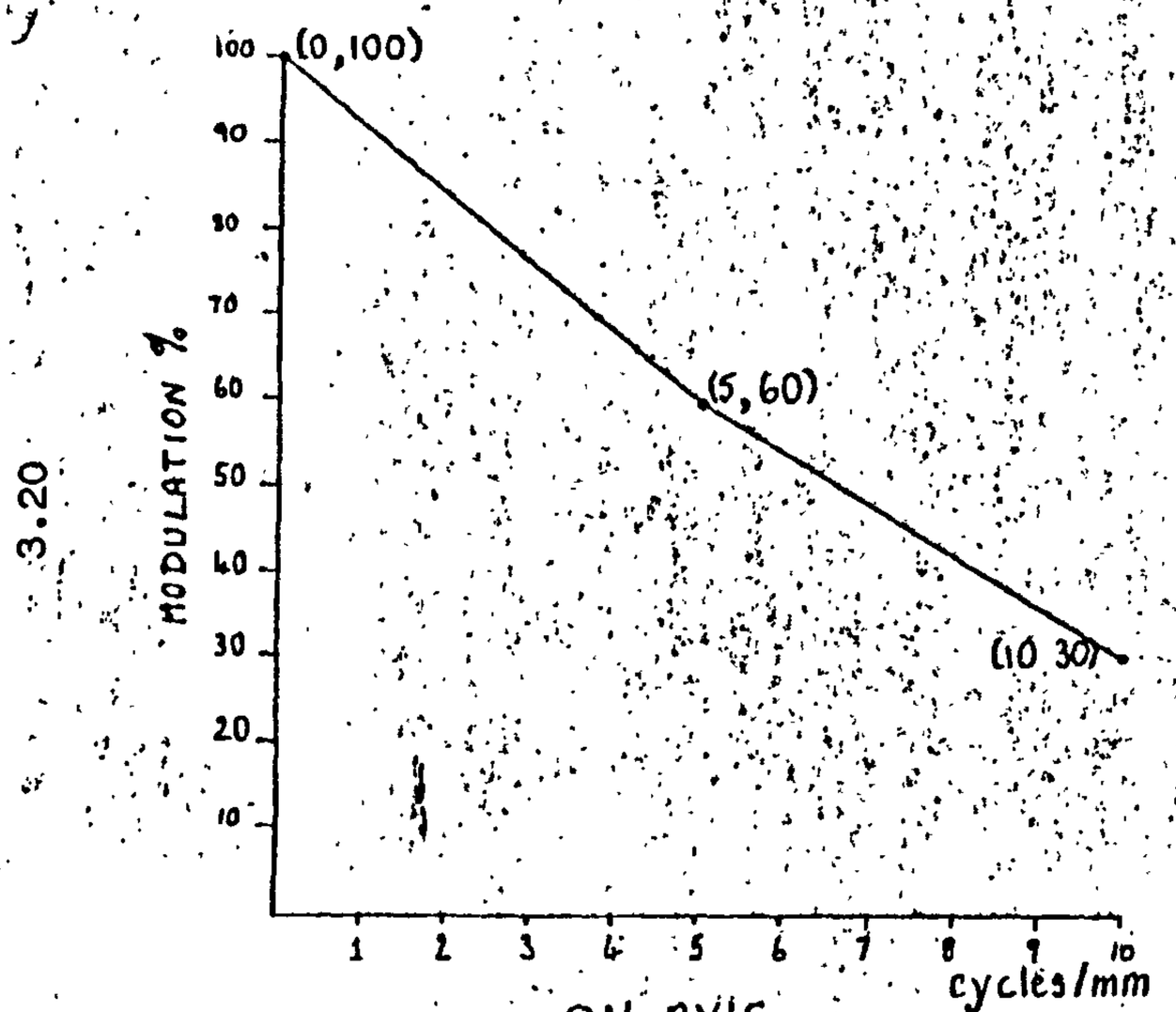

ON AXIS

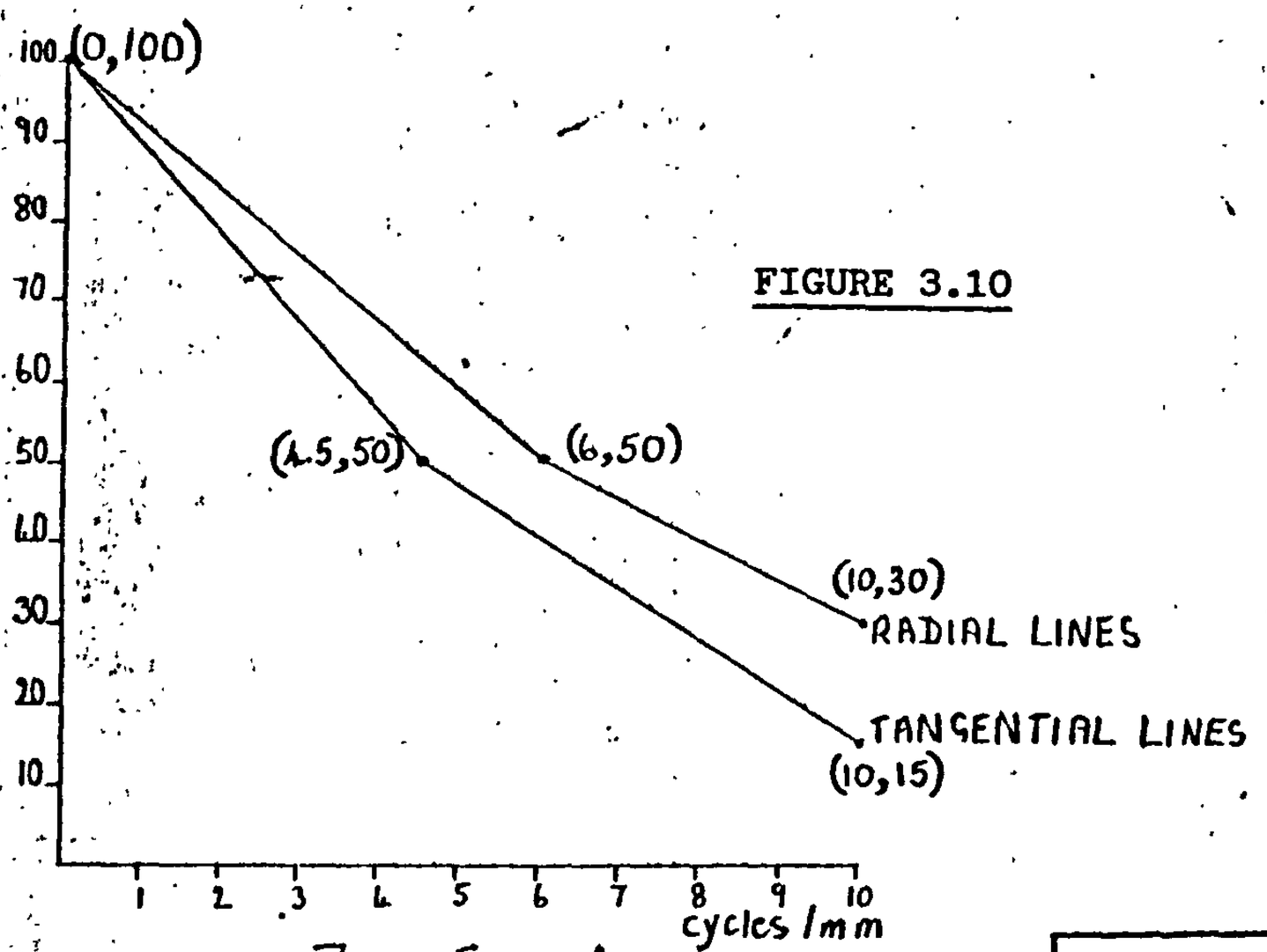

7mm FIELD RADIUS

FIGURE 3.10

WAVEBAND 8 to 11 MICROMETRE
APERTURE F/0.70
OBJECT INFINITY
ANALYZER 25Mm slit

THE CURVES ARE SPECIFIED BY POINTS (DENOTED BY THEIR CARTESIAN COORDINATES) THESE POINTS ARE JOINED BY STRAIGHT LINES.

THESE CURVES ARE FOR 2mm GERMANIUM BETWEEN THE LENS AND FOCAL PLANE

USED ON

		DATE
DESIGN APPROVED		
DRAWN BY	PRH	
CHECKED BY		
TRACED BY		
CHECKED BY		

SCALE.....SIZE

MATERIAL CODE.....

FINISH

HEAT TREATMENT

ALL DIMENSIONS ARE IN MILLIMETRES UNLESS STATED OTHERWISE
FOR SPECIAL SYMBOLS SEE MANUAL 2.1.0301

RANK PRECISION INDUSTRIES LTD.

DIVISION

TITLE MINIMUM MEASURED MODULATION TRANSFER FUNCTION FOR IRTAL 3

ACCEPTANCE TESTING, IF REQUIRED, BY S.I.R.A. CHISLEHURST. KENT

C H A P T E R I V

OPTICAL PERFORMANCE / PROFILE ERROR

CHAPTER IV

OPTICAL PERFORMANCE/PROFILE ERROR

From the preceding discussion two important questions arise:

(a) For two identical systems, if the MTF curves vary, which of the two curves signifies a "better" performance. For example the curves shown in the Fig. 4.1 could pertain to two similar systems. The first curve in general has higher modulation values for different spatial frequencies, but displays 0 modulation beyond spatial frequency 'a'. The second curve on the other hand, might in general have lower modulation for most spatial frequencies, but frequencies beyond 'a' display finite values of modulation.

Resolution and Contrast

If we consider 2 LSFs side by side as shown in Fig. 4.2 the distance 'd' is a measure of the resolution of system. If the two corresponding object slits were brought closer together, the images might merge and hence loss of resolution would occur. It follows therefore that for best resolution the LSF should be as "thin" as possible. Since the OTF is Fourier Transform of the LSF, reducing the width of the LSF introduces additional spatial frequency components in the corresponding OTF (see Fig. 4.3). Hence from resolution point of view the 2nd curve (MTF) may be classified as better. If this is done at the cost of the amplitude at various spatial

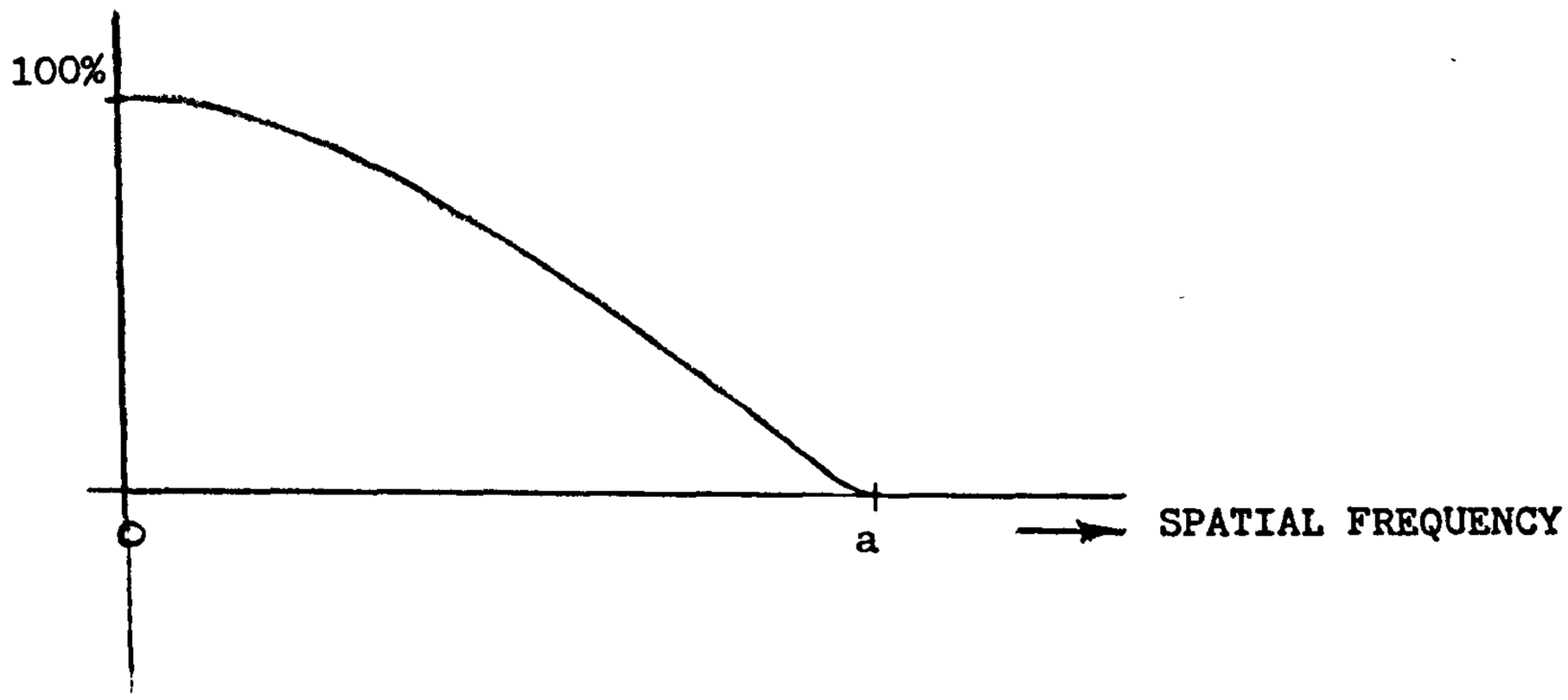

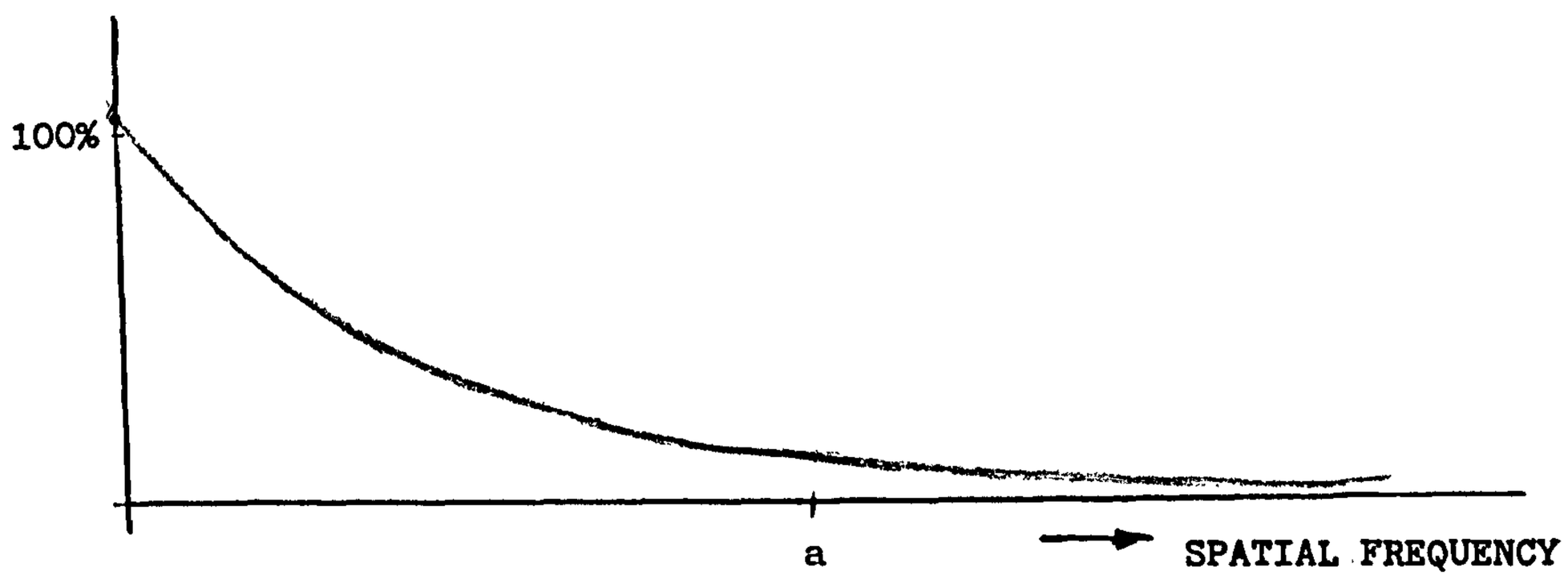

DIFFERENCE IN MTF CURVES

FIGURE 4.1 -

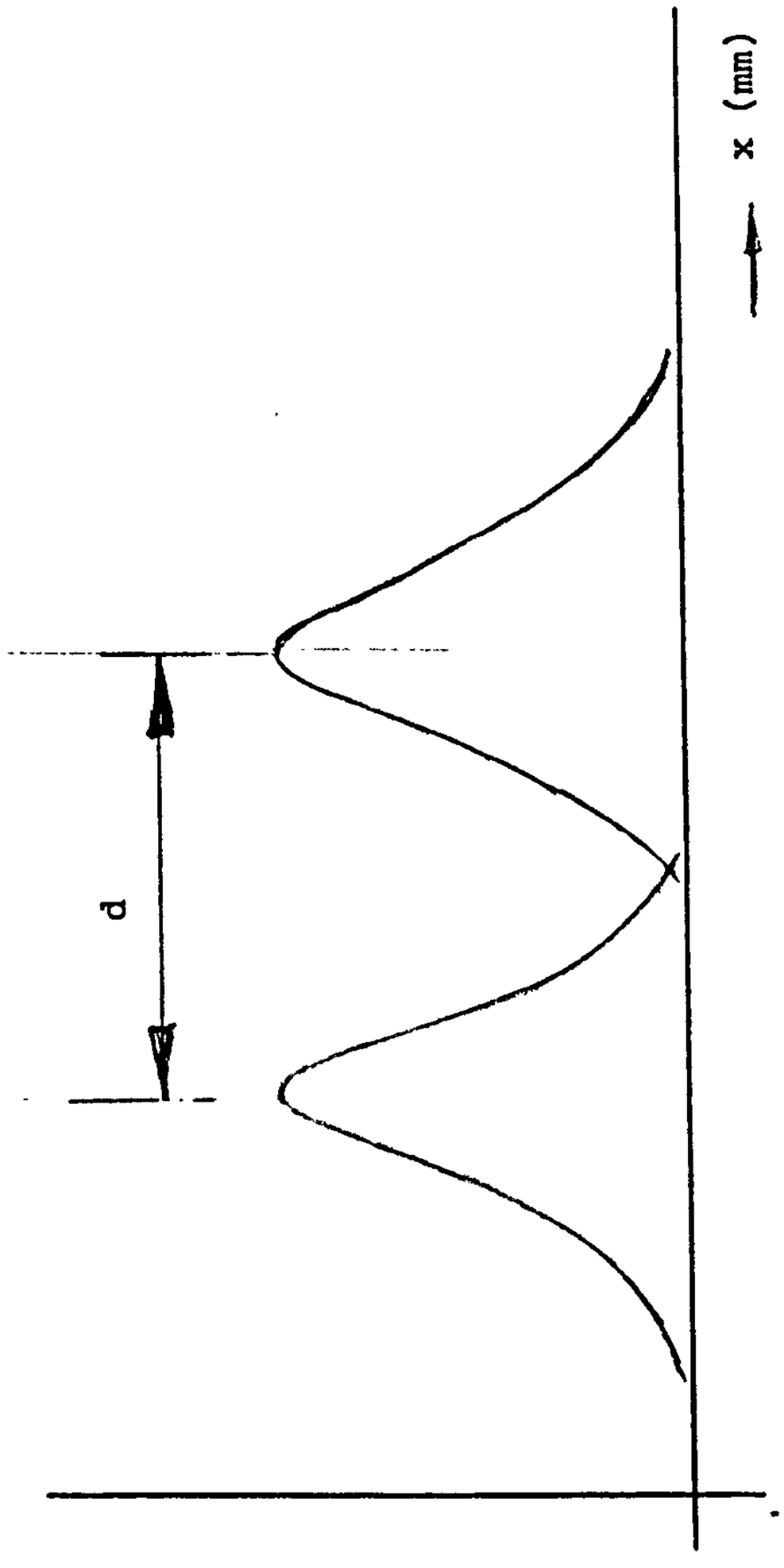

FIGURE 4.2

MEASURE OF RESOLUTION

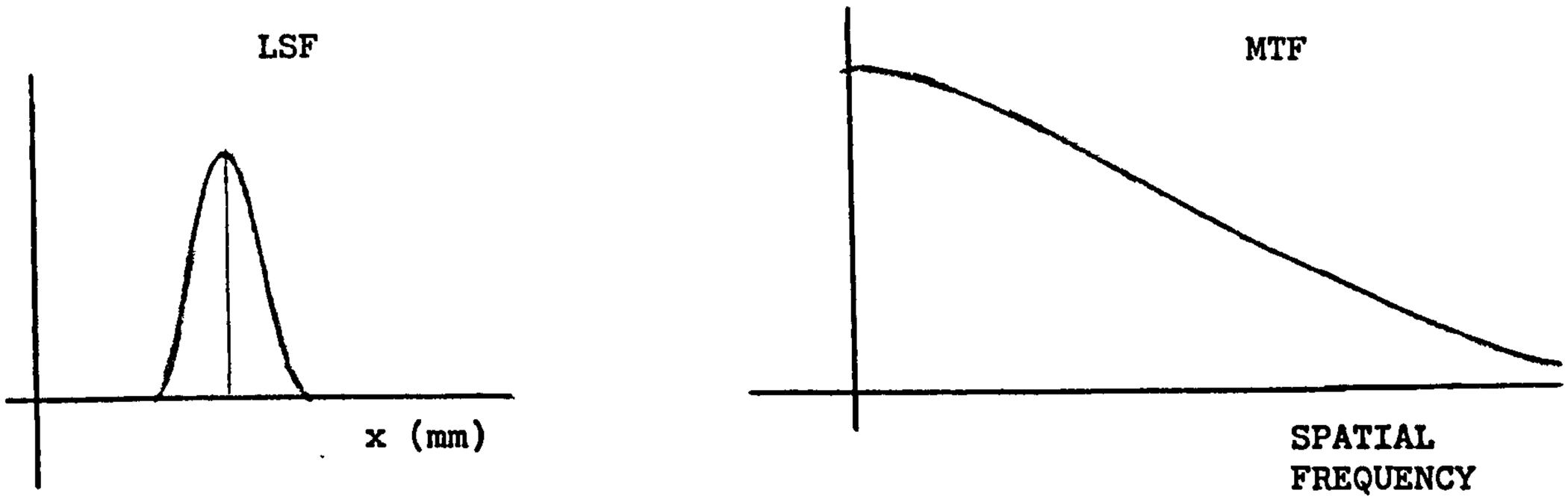

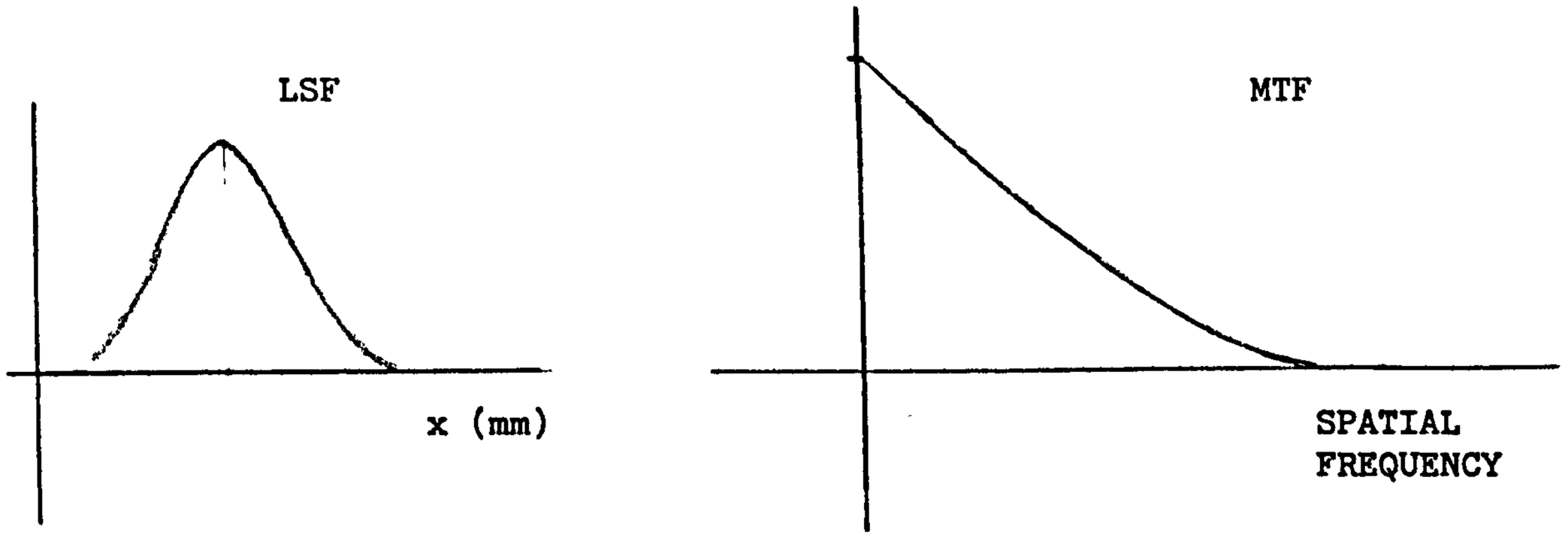

EFFECT OF LSF WIDTH ON MTF

FIGURE 4.3

frequencies, then a loss of contrast will occur. This is obvious from the fact that MTF is a "modulation", transfer function (see previous chapter) and reduction of modulation will result in loss of "sharpness" of the image. A higher resolution system which suffers from poor contrast, will allow detection of finer detail in the image, but the image will lack "sharpness". On the other hand a high contrast but poor resolution results in loss of finer detail, although the image may be "sharp".

Thus the MTF curve gives information about contrast and resolution. Further, by merely looking at the two curves of Fig. 4.1 it cannot be decided which is the better curve. The answer would depend on the application of the system.

The customer generally provides the value of modulation required at several points and hence the manufacturer has a specification MTF curve. For example a customer may specify 4 points of MTF. A lens designer can thus utilise this information to produce a "theoretical" model of the optical system on computer. In addition the MTF of the theoretical system may be computed and compared with the required MTF. The designer can thus "adjust" other physical parameters of the system (e.g. lens radii, etc.) until an acceptable MTF curve is obtained.

4.2

Software Design Model

One such program which has been used in the past at Rank Taylor Hobson to design Irtal 3 system is called GOTF (geometrical optical transfer function). In principle, for a given optical system the program traces a bundle of rays and generates the corresponding MTF. An initial study of an optical system may be therefore made without committing any hardware. Since, the geometry of lens elements and the corresponding required MTF of the system is known, the effect of introducing selected errors on chosen lens elements may be observed.

While the main advantage of this approach is obvious there are important limitations to be recognised:

(a) The type of errors which can be simulated with relative ease may or may not represent realistic machining error during production cycle.

(b) The simulation of very small errors may not be a sufficiently accurate procedure since the software model itself may rely on small approximations.

(c) The observations may/may not apply to systems in general.

However, in order to get an estimate of sensitivity between

the profile error of a specific lens element and the corresponding MTF, the GOTF software can be useful. As an example, for a given system the optimum design may be represented by the MTF curve of Fig. 4.4*. If then any of the aspheric terms on a given lens are changed, the corresponding effect on the MTF may be observed. If then any of the aspheric terms on a given lens are changed, the corresponding effect on the MTF may be observed.

4.3

Introducing Errors

The machining errors during the production cycle would result in the modification of the coefficients A_2, A_4, A_6, etc. in the equation, $X = A_2Y^2 + A_4Y^4 + A_6Y^6 + A_8Y^8 + A_{10}Y^{10}$. Since the machining of the lens is inherently a symmetrical process, the coefficients arising from any non symmetry can be regarded as small and hence negligable. In any event, to introduce odd terms in the above expression would demand major changes to the software model.

To get an initial "feel" of the model, the simplest step would be to modify one of the coefficients, say A_2 by a small amount say 10% and examine the corresponding MTF.

*For simplicity only axial image is considered

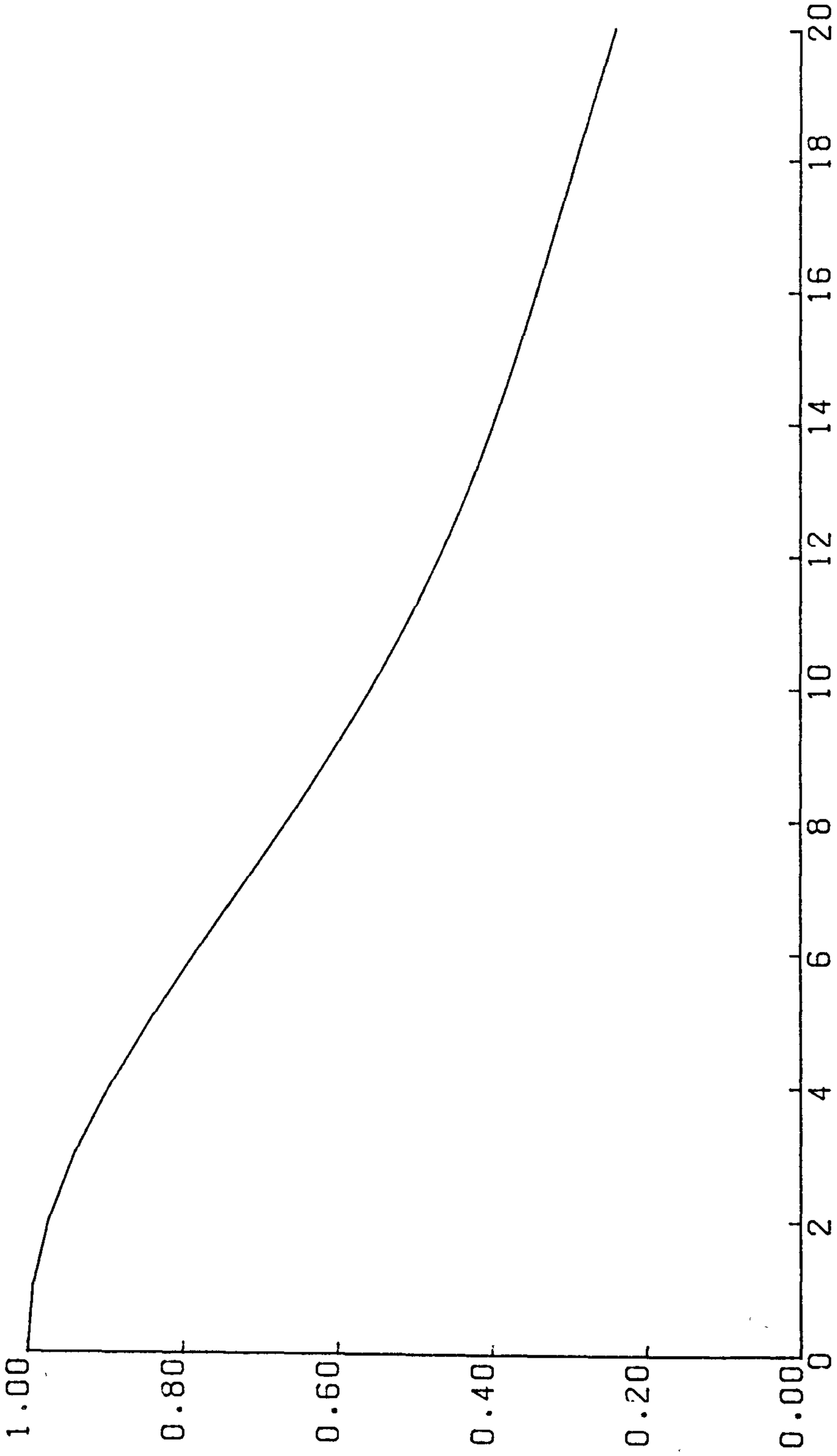
MTF vs Spatial Frequency For an Optimised Design
MTF
1.00
0.80
0.60
0.40
0.20
0.00
0
2
4
6
8
10
12
14
16
18
20
Spatial Frequency : Lines/mm

FIGURE 4.4

Figure 4.4 shows the MTF for normal unaltered system while Fig. 4.5 and Fig. 4.6 show the MTF with the A_2 and A_4 term modified respectively only by 10%. The serious degradation in the MTF which results by only a relatively small change in the aspheric equation illustrates the accuracy required in machining the required surface. Changes of a similar magnitude in the other coefficients produce equally devastating results.

Apart from illustrating the importance of accuracy, this approach has little to offer. The actual machining process is unlikely to introduce errors which modify only one term.

4.4

Expected Errors

The axis of rotation of the machine is generally the reference axis. Hence before actual cutting of the material commences, the centre of the lens element has to lie on the axis of rotation. This is a fairly skilled operation.

One would hence expect minimum errors in the centre region of the lens. In addition, the rays of light deflect the least in the centre of the lens and a small error in this region might be tolerable. The stiffness of the machine is likely to be higher towards the middle of the chuck. Hence as the machining proceed towards the periphery of lens, bigger errors in profile are expected. This situation is illustrated in Fig. 4.7.

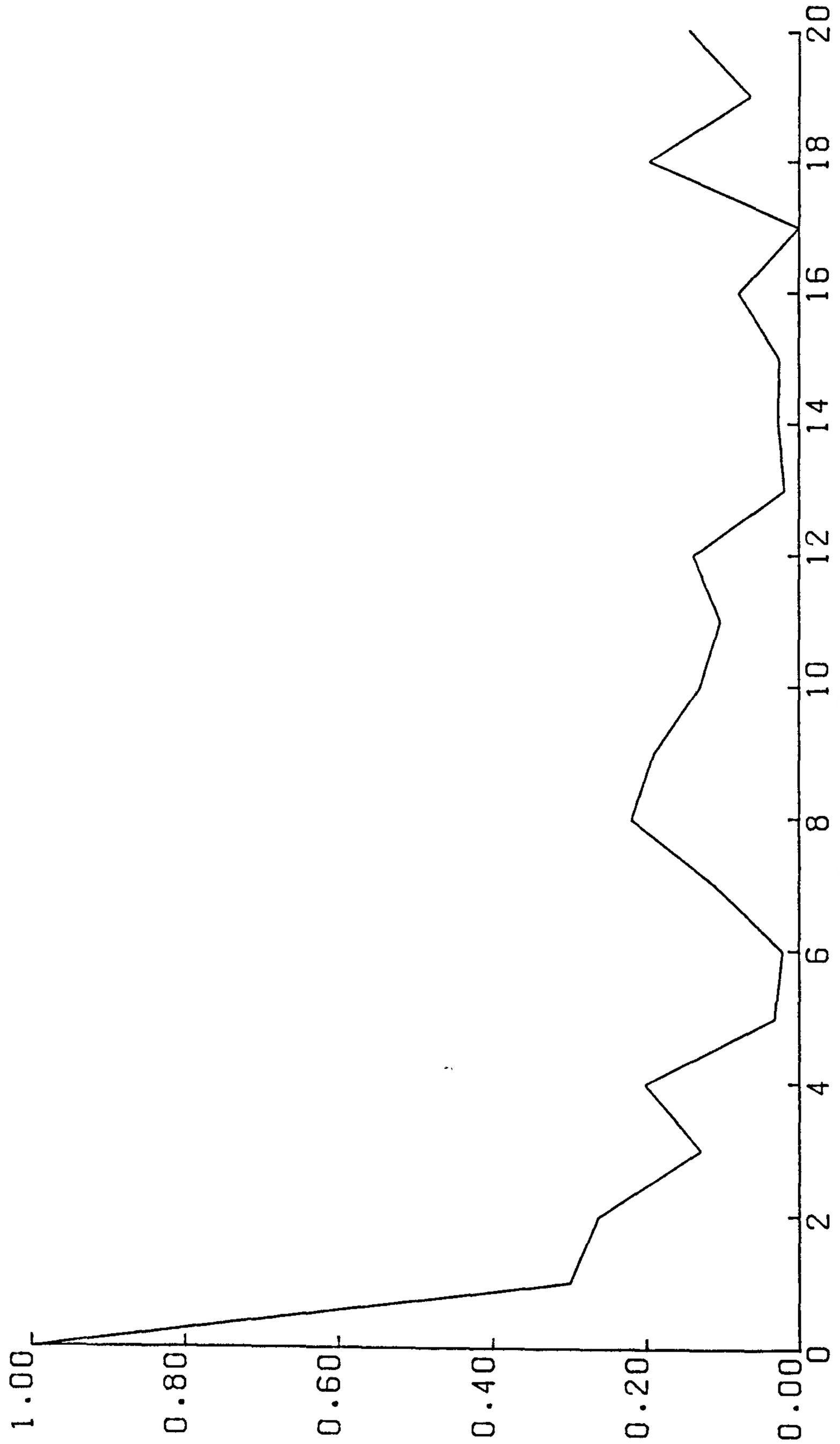
MTF vs Spatial Frequency
(A2 term changed by 10%)
Spatial Frequency : Lines/mm
MTF
1.00
0.80
0.60
0.40
0.20
0.00
0
2
4
6
8
10
12
14
16
18
20

FIGURE 4.5

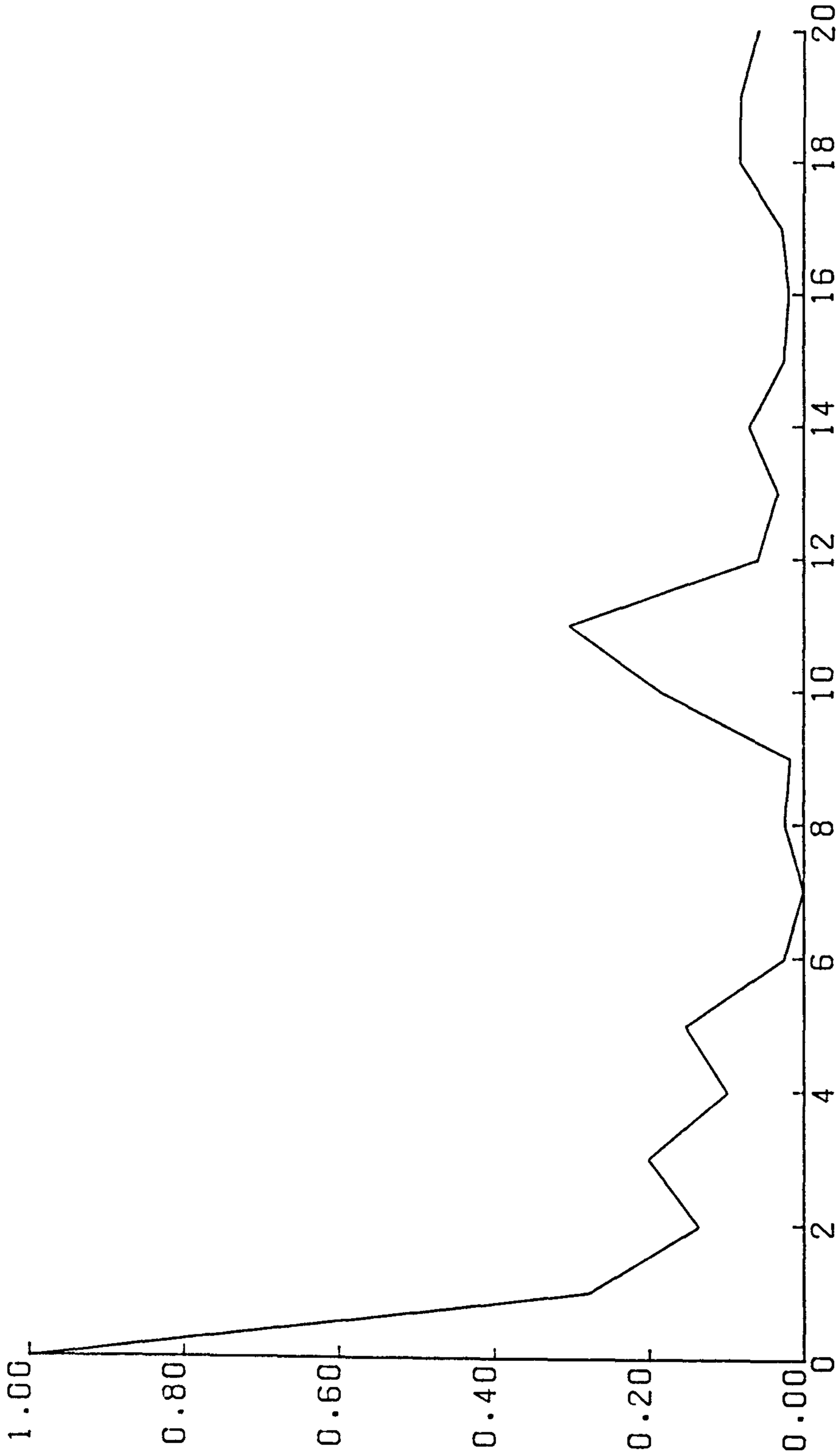
MTF
1.00
0.80
0.60
0.40
0.20
0.00
0
2
4
6
8
10
12
14
16
18
20
Spatial Frequency : Lines/mm
MTF vs Spatial Frequency
(A4 term changed by 10%)

FIGURE 4.6

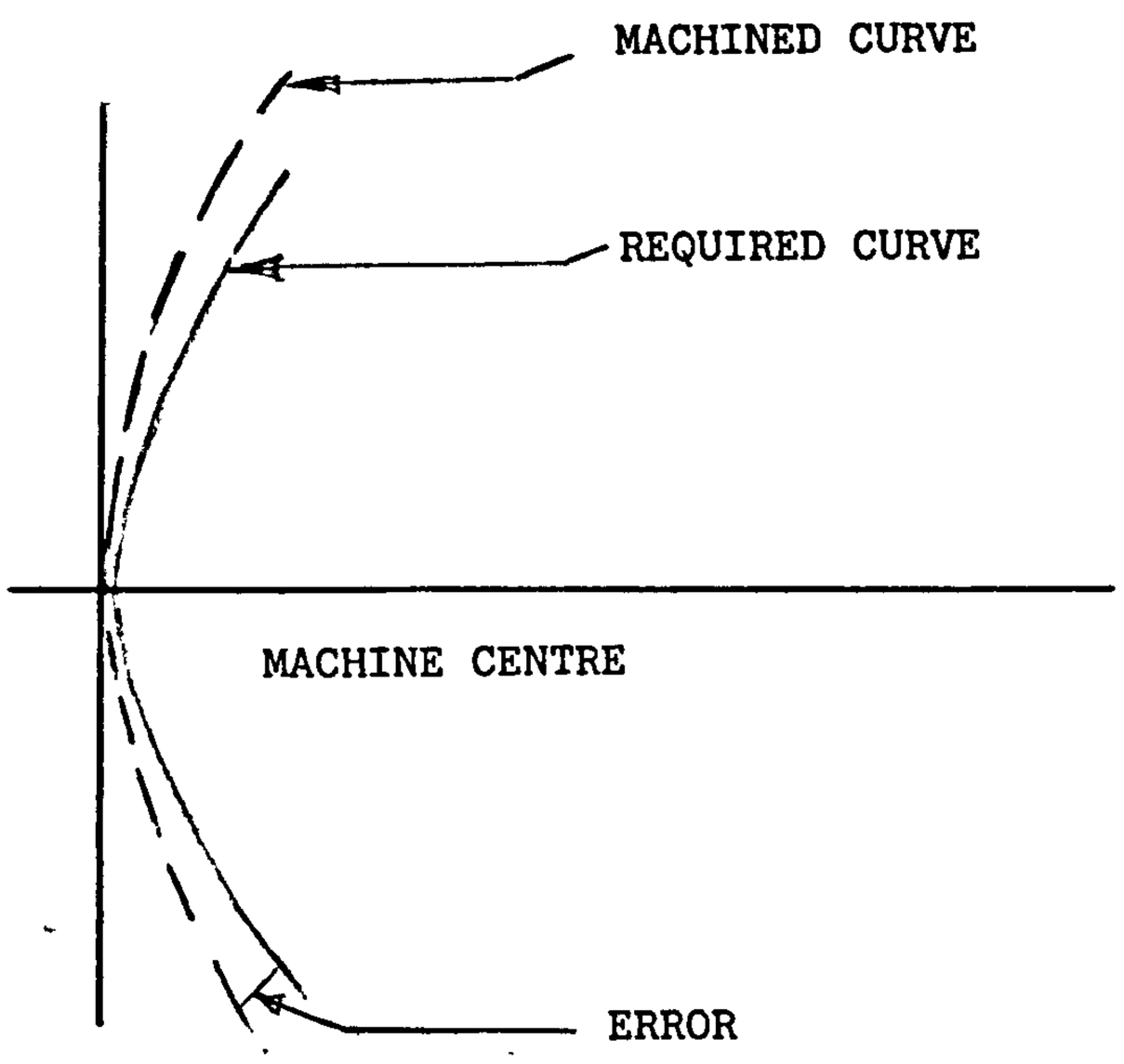

POSSIBLE ERRORS IN MACHINING

FIGURE 4.7

A second source of error might result due to machine vibration or small amount of wear in machine slides. This situation is illustrated in Fig. 4.8.

Such errors may even be introduced later on during the polishing phase of the lens element.

4.5

Using Chebychev Polynomials

A relatively straight forward method is required such that the errors described in the above section can be modelled without significantly changing the aspheric equation.

A set of chebychev polynomials may be utilised to represent approximate forms of the desired error curves. A generalised chebychev polynomial could be represented, as follows:

$$X = C_2S^2 + C_4S^4 + C_6S^6 + C_8S^8 + C_{10}S^{10}$$

where $C_2 \ldots C_{10}$ represent the coefficients. Fig. 4.9 shows a set of 4 normalised curves, which can be represented by suitable choice of the coefficients. The values of the coefficients which correspond to the normalised curves, which can be represented by suitable choice of the coefficients. The values of the coefficients which correspond to the normalised curves is shown in the Table of Fig. 4.10.

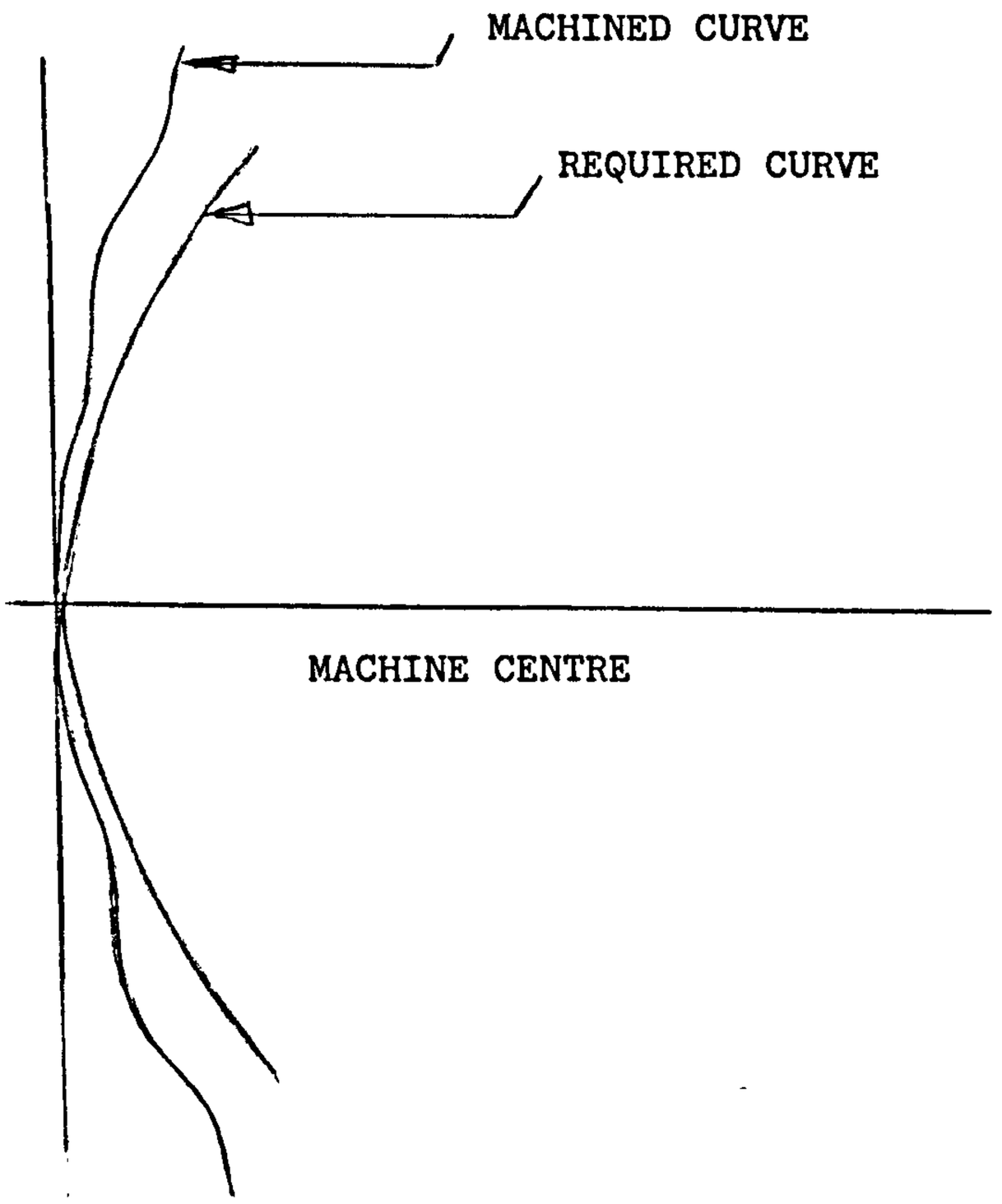

POSSIBLE EFFECTS OF VIBRATION

FIGURE 4.8

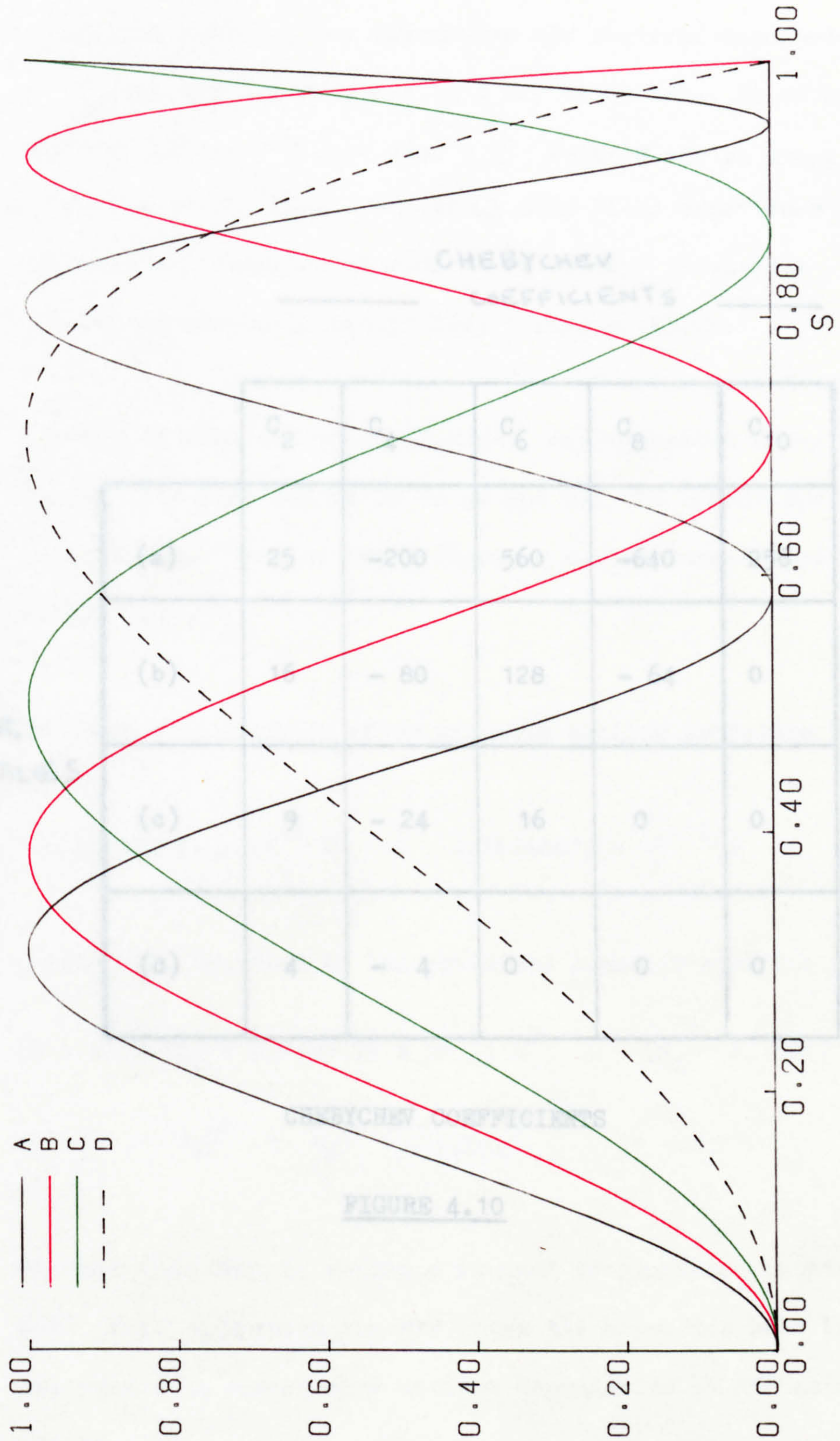

SIMULATION OF ERROR USING CHEBYCHEV POLYNOMIALS

FIGURE 4.9

CHEBYCHEV COEFFICIENTS

ERROR PROFILES

	C_2	C_4	C_6	C_8	C_{10}
(a)	25	-200	560	-640	256
(b)	16	- 80	128	- 64	0
(c)	9	- 24	16	0	0
(d)	4	- 4	0	0	0

CHEBYCHEV COEFFICIENTS

FIGURE 4.10

By suitable scaling, one may choose the required magnitude of the error. Any error type A to D may be chosen. As an example consider the curve D from Fig. 4.9. Point O may be considered the centre of the lens. Practical shop floor experience suggests that working tolerance of some 3 - 5 "rings" in visible spectrum is generally acceptable, 1 ring = .25 μm.

An error of some ten rings (2.5 um), may represent a realistic figure. The lens radius is 70 mm and all the dimensions are quoted in mm. Thus an error function can be represented as in Fig. 4.11.

The resulting equation after suitable scaling procedure is:

$$e = 2.0420495 \times 10^{-6} S^2 - 4.16744803 \times 10^{-10} S^4$$

adding this equation to the optimised aspheric equation yields

$$(X + e) = (A_2 + 2.0420495 \times 10^{-6}) S^2 + (A_4 - 4.16744803 \times 10^{-10}) S^4 + A_6 S^6 + A_8 S^8 + A_{10} S^{10}$$

The modified form of aspheric is used to generate the corresponding MTF. Fig. 4.12 shows the MTF after the error has been introduced. The resulting curves show serious degradation of MTF at mid spatial frequencies.

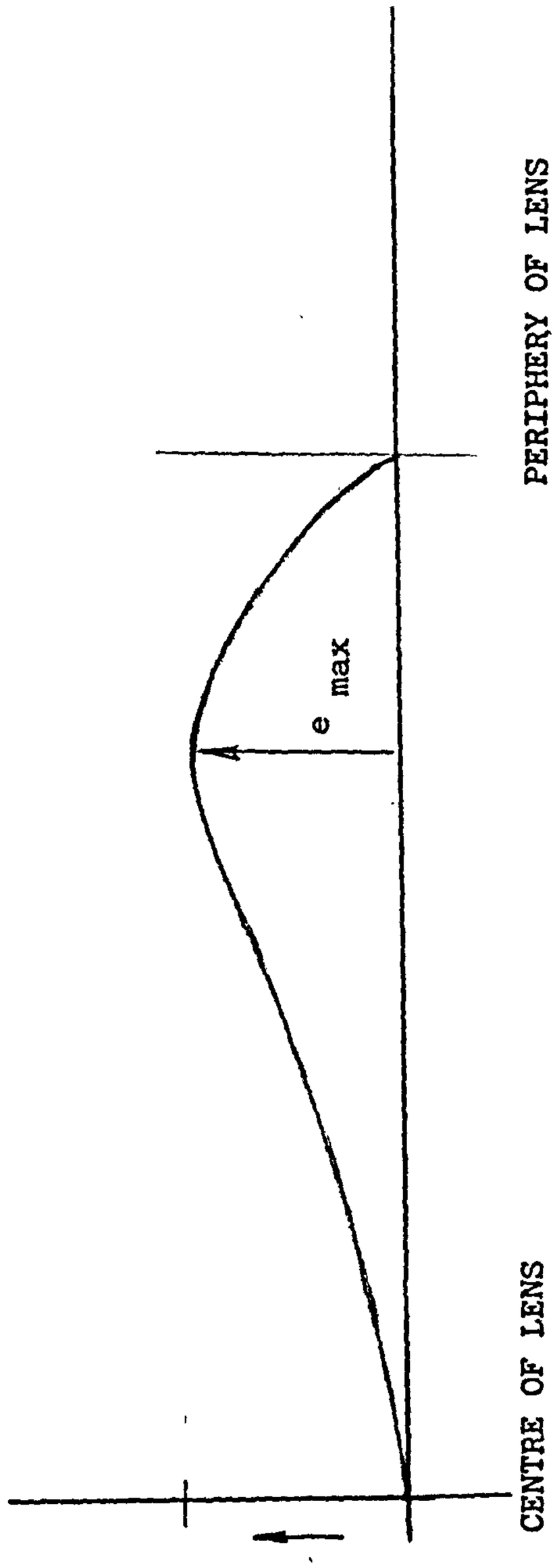

SINGLE BOW ERROR

FIGURE 4.11

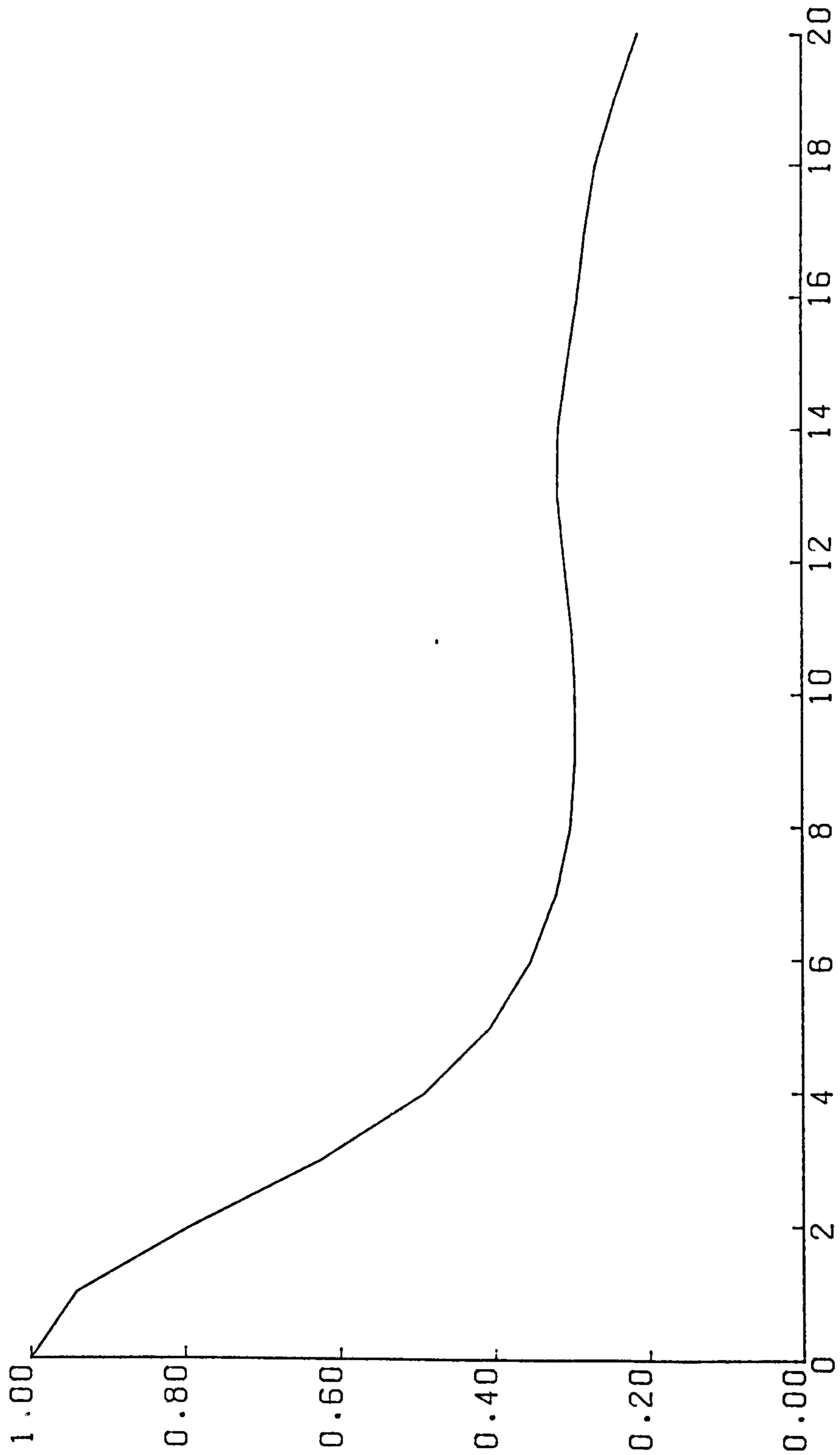
MTF vs Spatial Frequency
(Single Bow Fault - error 10 rings)
Spatial Frequency : Lines/mm
MTF
1.00
0.80
0.60
0.40
0.20
0.00
0
2
4
6
8
10
12
14
16
18
20

FIGURE 4.12

Several different error forms are simulated in this way, keeping the maximum error at 10 rings (2.5 μm). A particularly noteworthy case is of error form type C (see Fig. 4.13). The resulting degradation in the MTF appears to be particularly severe.

The shop floor practical experience suggests that a working accuracy of some 3 rings usually results in acceptable optical performance. The maximum error is hence reduced to 3 rings and the experiments repeated. In fact the MTFs thus obtained do not appear to deviate too far from the optimised curves (see Fig. 4.14, 4.15).

At this stage a more rigorous analysis of the results might be possible. However, such analysis is not particularly valuable from practical point of view.

The inference from the preceding text may be summarised by the following points:

Errors of the order of 10 rings (2.5 um) have a noticeably serious effect on the MTF.

(a) In general errors of type "single bow" have less severe effect on the MTF when compared with errors of type "double bow".

(b) Errors with maximum magnitude of 10 rings (2.5 um) have a serious noticeable effect on the MTF curves.

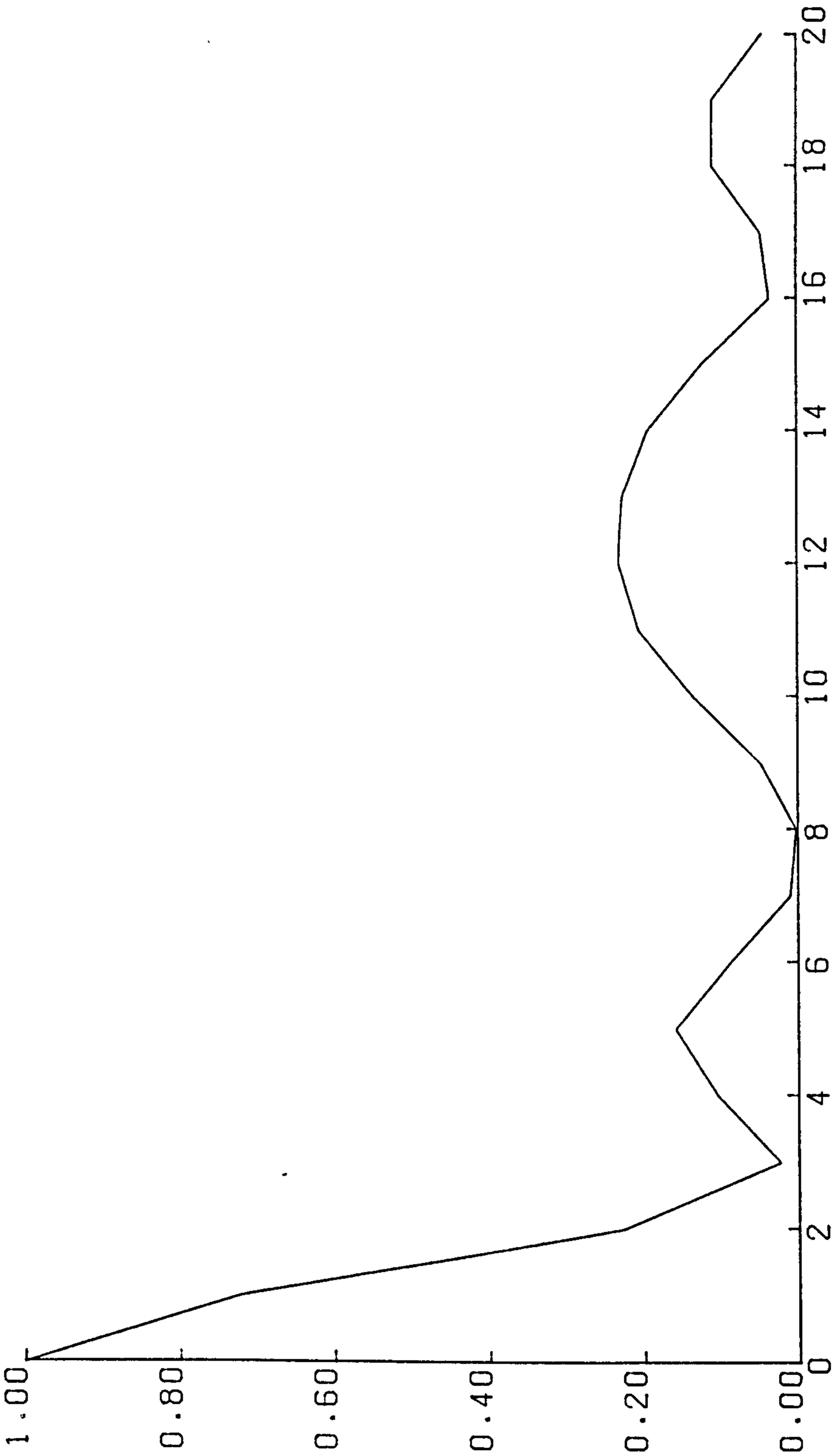
MTF vs Spatial Frequency
(Double Bow Fault - error 10 rings)
Spatial Frequency : Lines/mm
MTF
1.00
0.80
0.60
0.40
0.20
0.00
0
2
4
6
8
10
12
14
16
18
20

FIGURE 4.13

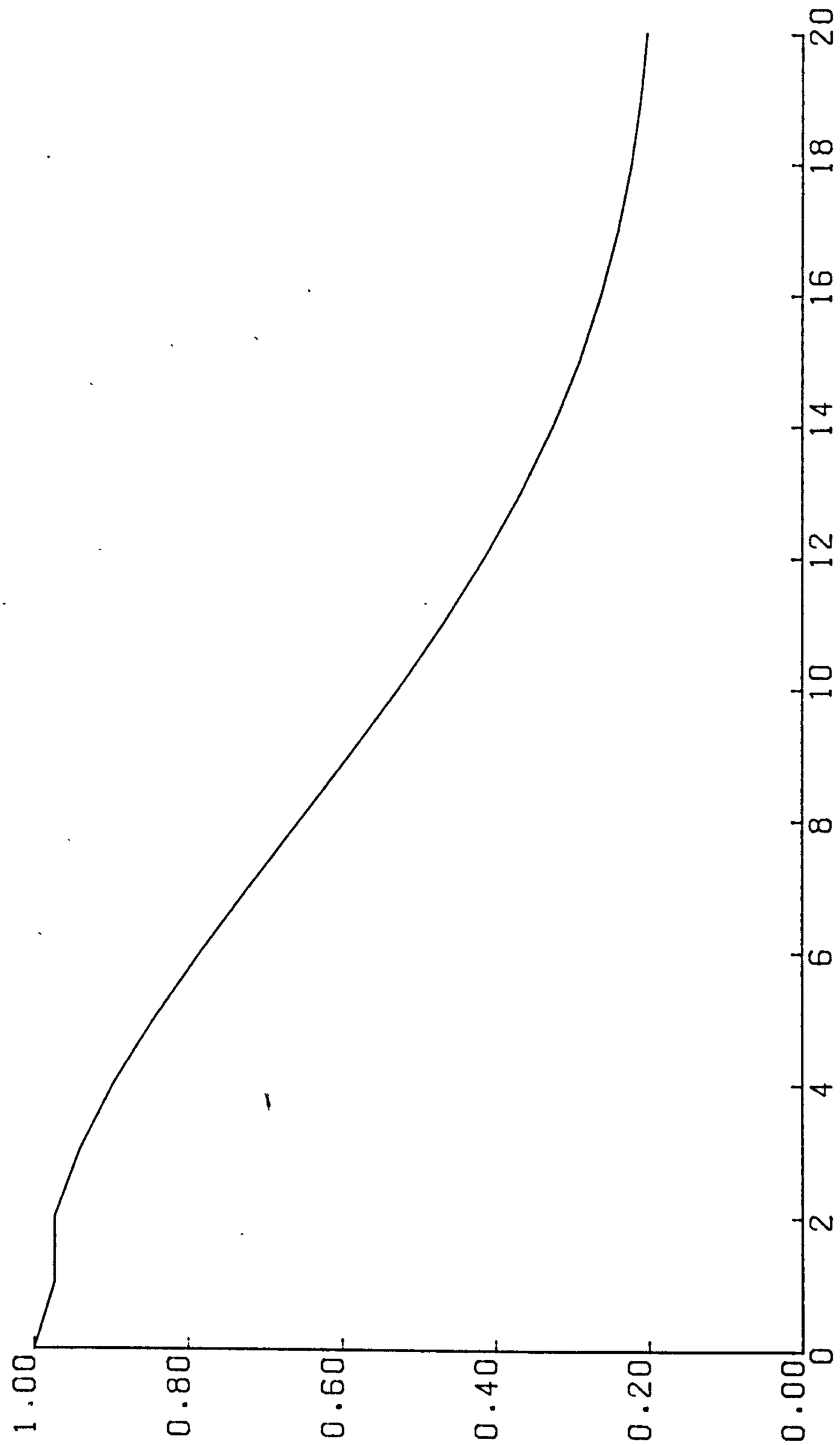
MTF vs Spatial Frequency
(Single Bow Fault - type 2 - error 3 rings)
MTF
1.00
0.80
0.60
0.40
0.20
0.00
0
2
4
6
8
10
12
14
16
18
20
Spatial Frequency : Lines/mm

FIGURE 4.14

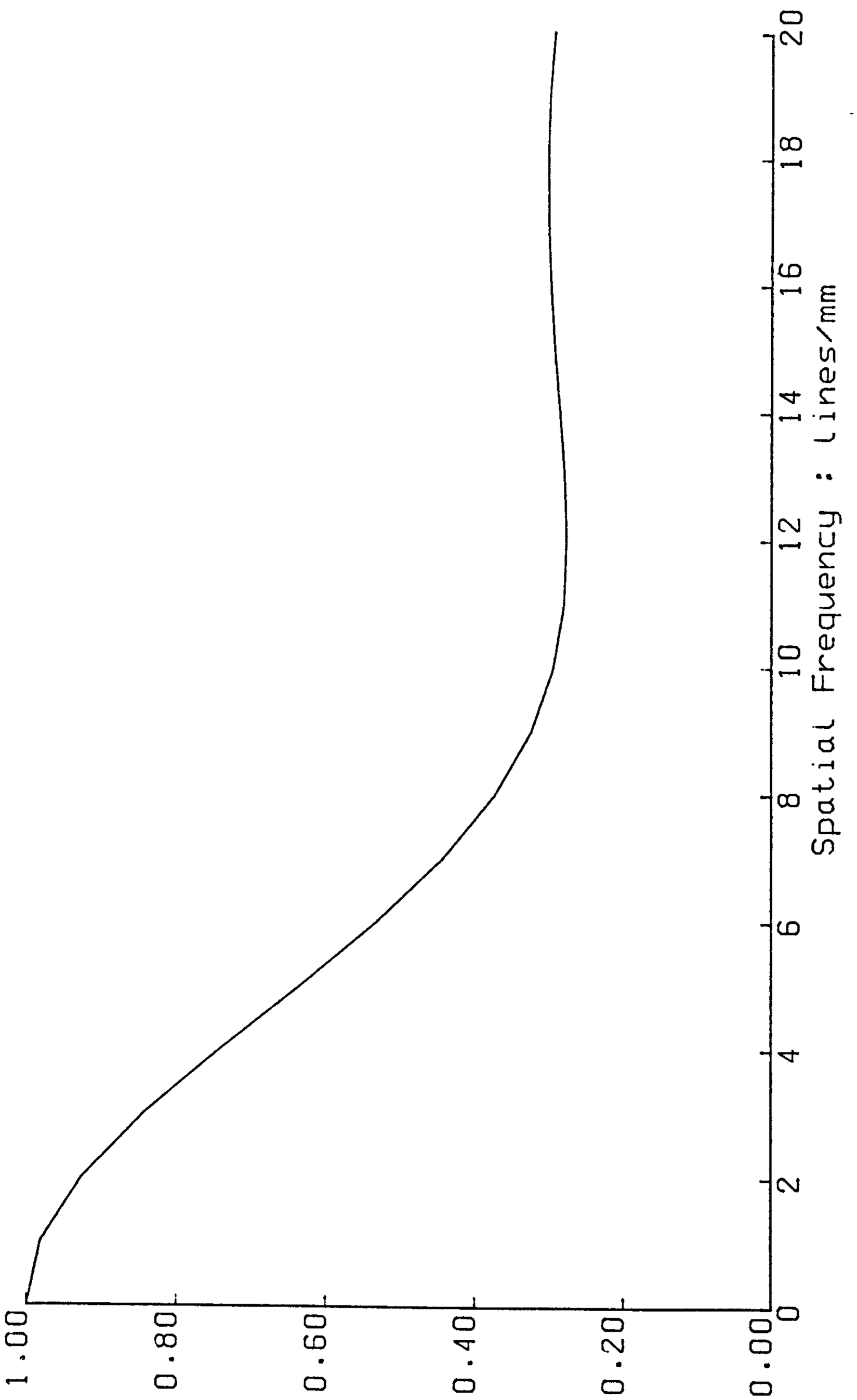
MTF vs Spatial Frequency
(Double Bow Fault - error 3 rings)
MTF
1.00
0.80
0.60
0.40
0.20
0.00
0
2
4
6
8
10
12
14
16
18
20
Spatial Frequency : Lines/mm

FIGURE 4.15

(c) Errors with maximum magnitude of 3 rings (.75 μm) are tolerable.

4.6

MTF (energy)

In addition it is obvious that the degradation of the MTF curve invariably reduces the area under the curve. Since the MTF is the Fourier Transform of the LSF, this area represents energy. Thus the best focus condition for a lens under optical test must correspond to maximum energy. The area under the curve, therefore, provides us with a very convenient, single quantity measure of optical performance.

In subsequent chapters the optical performance will be taken to mean the area under the MTF curve and will be denoted as MTF (energy).

C H A P T E R V

PRACTICAL MEASUREMENT OF ERROR PROFILE

CHAPTER V

PRACTICAL MEASUREMENT OF THE ERROR PROFILE

In order to mechanically measure the error profile, an instrument is required which is capable of:

(a) Storing the required profile

(b) Measuring the actual lens profile

(c) Computing the difference

(d) Displaying the error profile on a chart, etc.

In principle these tasks appear straight forward, but the practical realisation of them is by no means simple. Distances of some 3 rings (or less) were mentioned in the previous chapter. For a given lens the distance between the apex and the periphery could be several millimeters. Hence the transducer and the instrumentation must maintain a very high resolution. In addition a suitable arrangement to scan the surface of the lens with the transducer is needed. This in turn may introduce other errors.

5.1

Form Talysurf Measurement System

The detailed description of an instrument which gives us the required data is not of direct relevance. However, since such an instrument is novel and without it the research would be impossible, the principle of operation is described here. A schematic of the measuring system is shown in Fig. 5.1

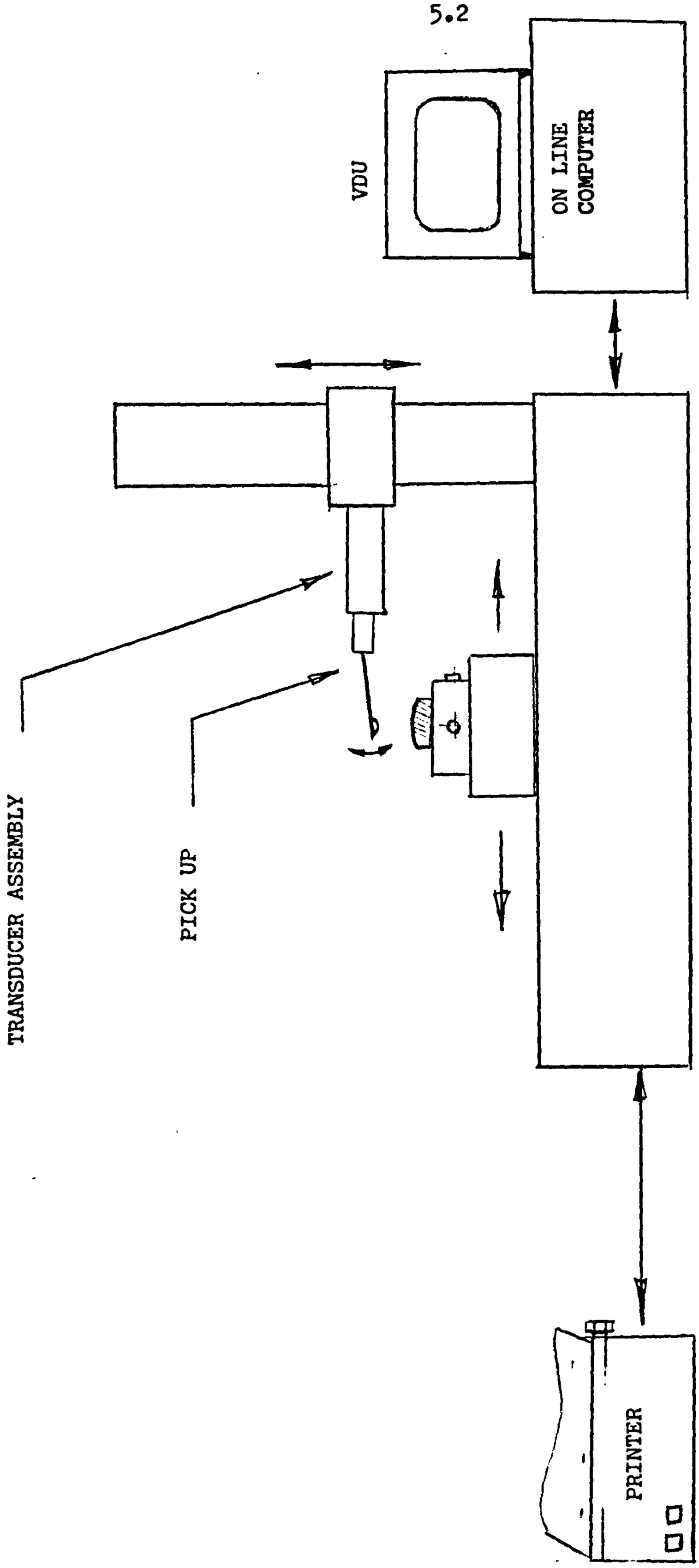

FORM TALYSURF INSTRUMENT

FIGURE 5.1

(also see Appendix D). The stylus consists of a pivoted pick-up arm, suitably attached at the other end to an interferometric transducer. The output of the transducer is suitably processed to yield a digital signal.

When a lens element is placed on the table to be measured, the axes of the component do not exactly coincide with the axes of the machine (see Fig. 5.2). Some set up error is taken out by mechanical adjustment, but small amounts of residual errors have to be taken out by suitable data processing. In principle the following steps are taken:

(a) A data file of some 1000 coordinate points is made by traversing the table so that the transducer scans the full test surface. A suitable correction is applied to this data to account for the geometry of the pick-up assembly.

(b) The specified asphere is then fitted to the data. An estimate of the angle of tilt and the X and Y coordinates is obtained. This correction is applied to the measured data.

(c) The specified asphere is then subtracted from the measured data and an error profile is generated.

5.2

Error Profiles of a Production Batch of Lenses

A batch of 30 lenses manufactured under normal production

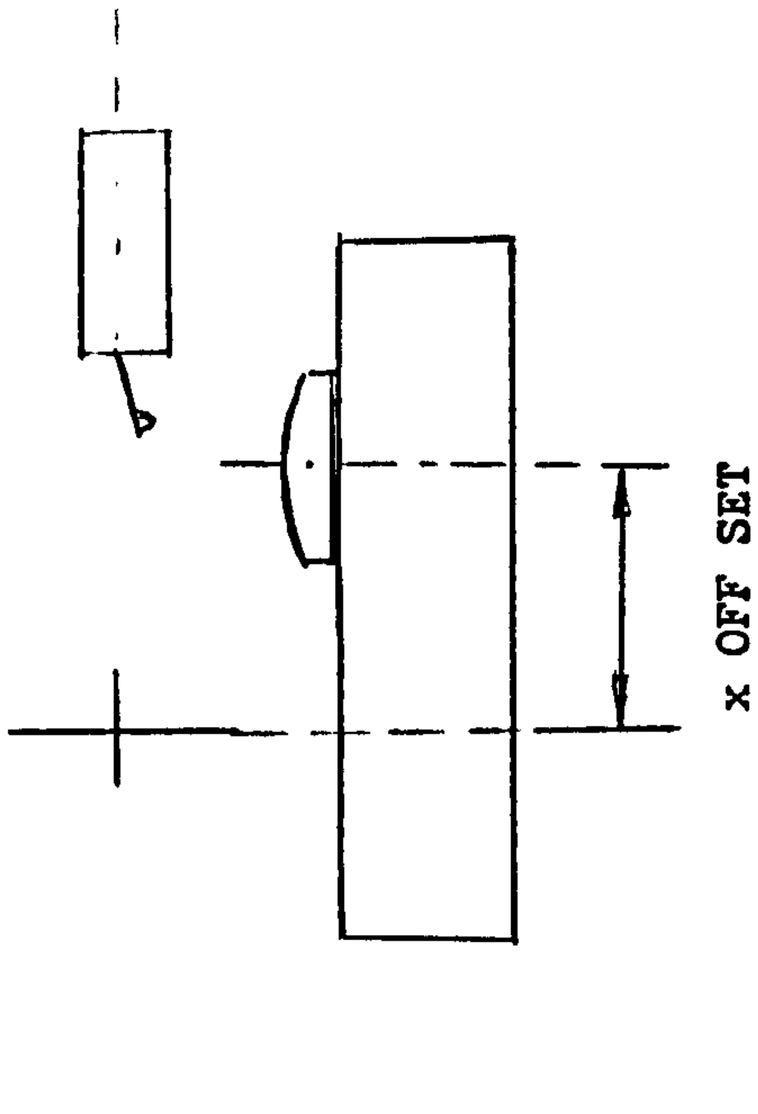

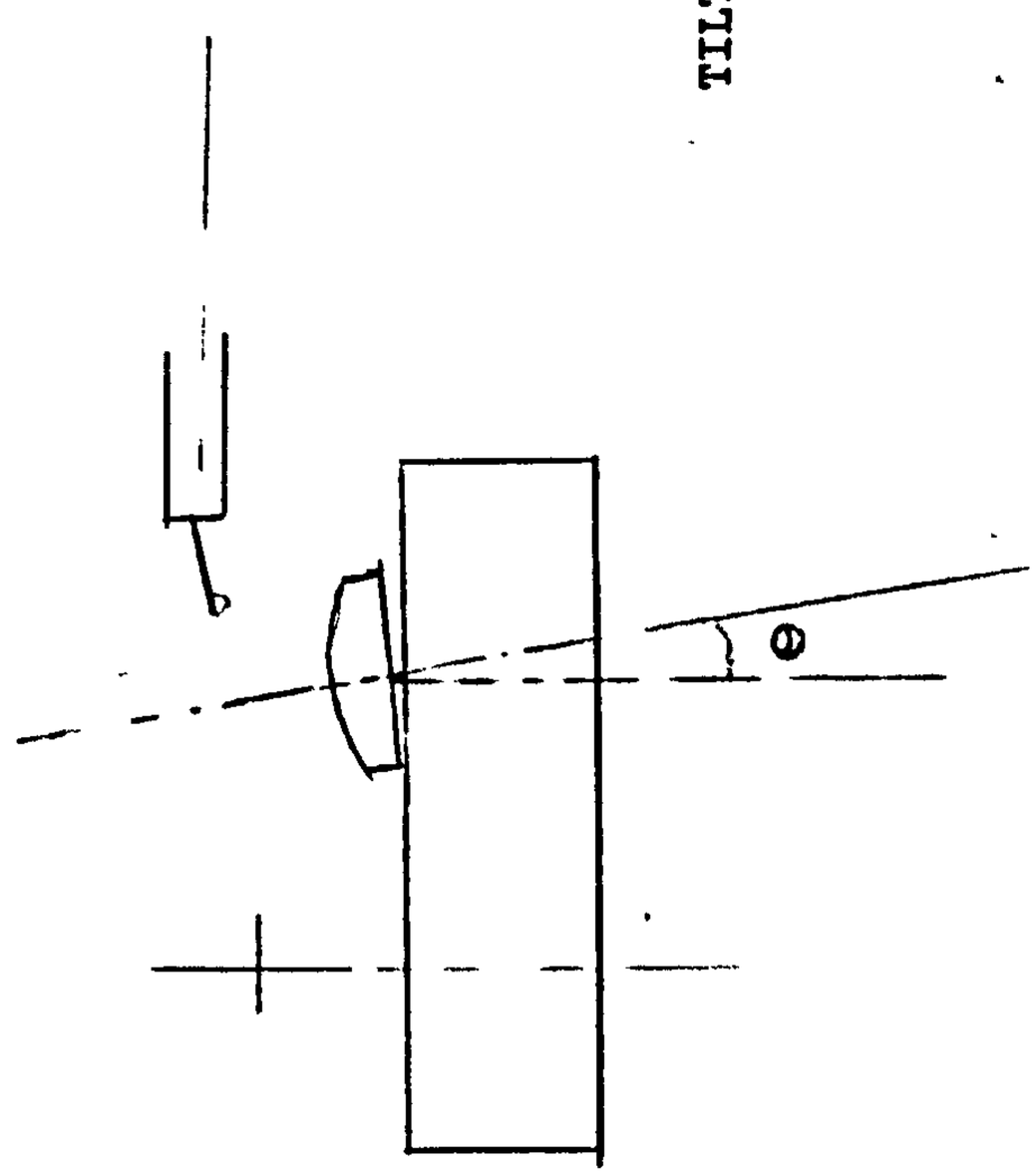

MEASUREMENT ON FORM TALYSURF

FIGURE 5.2

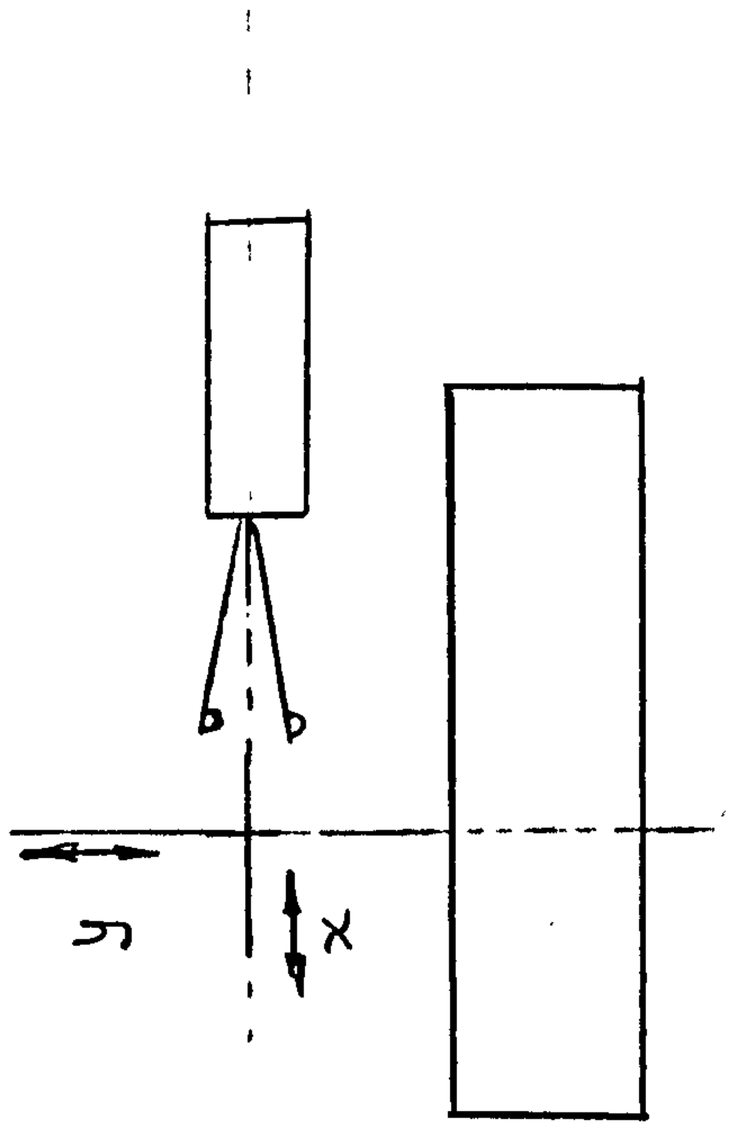

MACHINE AXES

conditions was chosen to provide the error profiles. The convex side of the lens is aspherised while the concave side is spherical. The approximate dimensions of the lens are shown in Fig. 5.3. For each lens there are three sets of measurement. Traces T_1 and T_2 are taken at mutually right angles to each other on the aspheric side. They are expected to be identical. However, there may be small variations. T_1 and T_2 are hence averaged to reduce experimental errors to a minimum. Since the errors on the spherical side will also affect the optical performance, a trace of the spherical side T_3 is taken as well. Thus for each lens there are 3 files. The errors on the spherical side are added to the aspheric side to generate a composite error profile for each lens.

Some typical examples of T_1, T_2, and T_3 are shown in Figs. 5.4 to 5.11. For each of these four lenses the results of the optical test in form of MTF curve is also available as shown in Figs. 5.12 to 5.15.

However, it should be pointed out that the MTF curve infact, represents the test of a system in which the lens is the test element. To arrive at a true MTF curve various corrections would have to be applied. Fortunately, this is not necessary since all the lenses are measured by the smae process and it is the relative performance of the lenses which is important rather than the absolute performance.

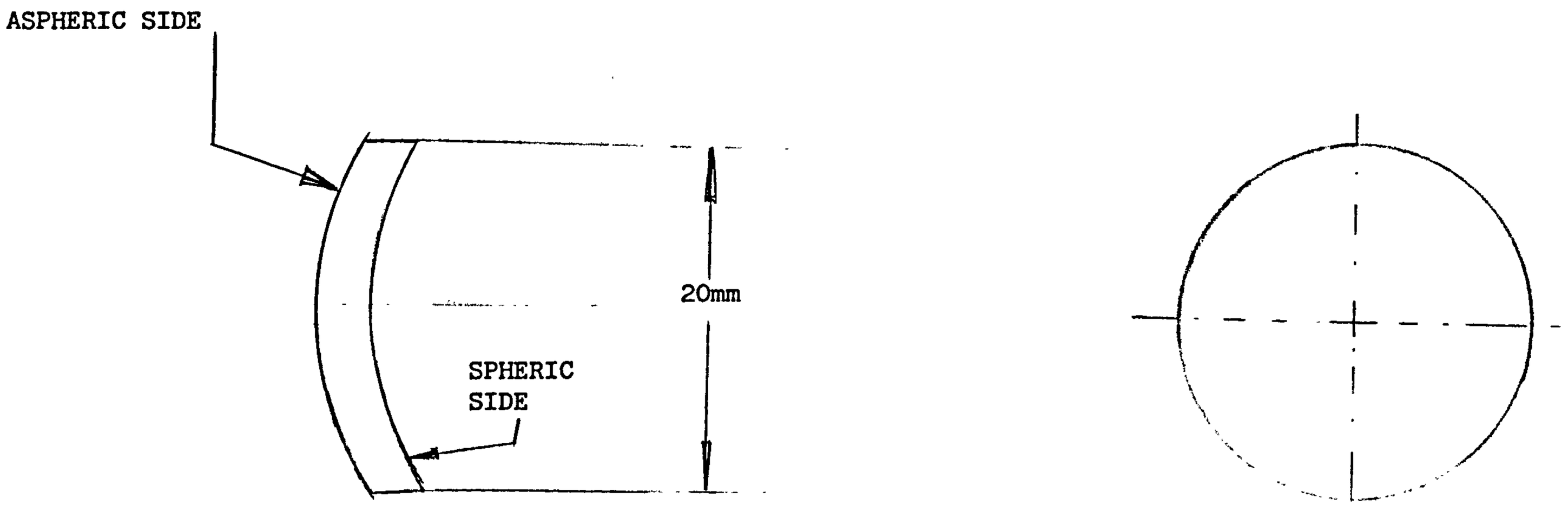

LENS GEOMETRY

FIGURE 5.3

5.6

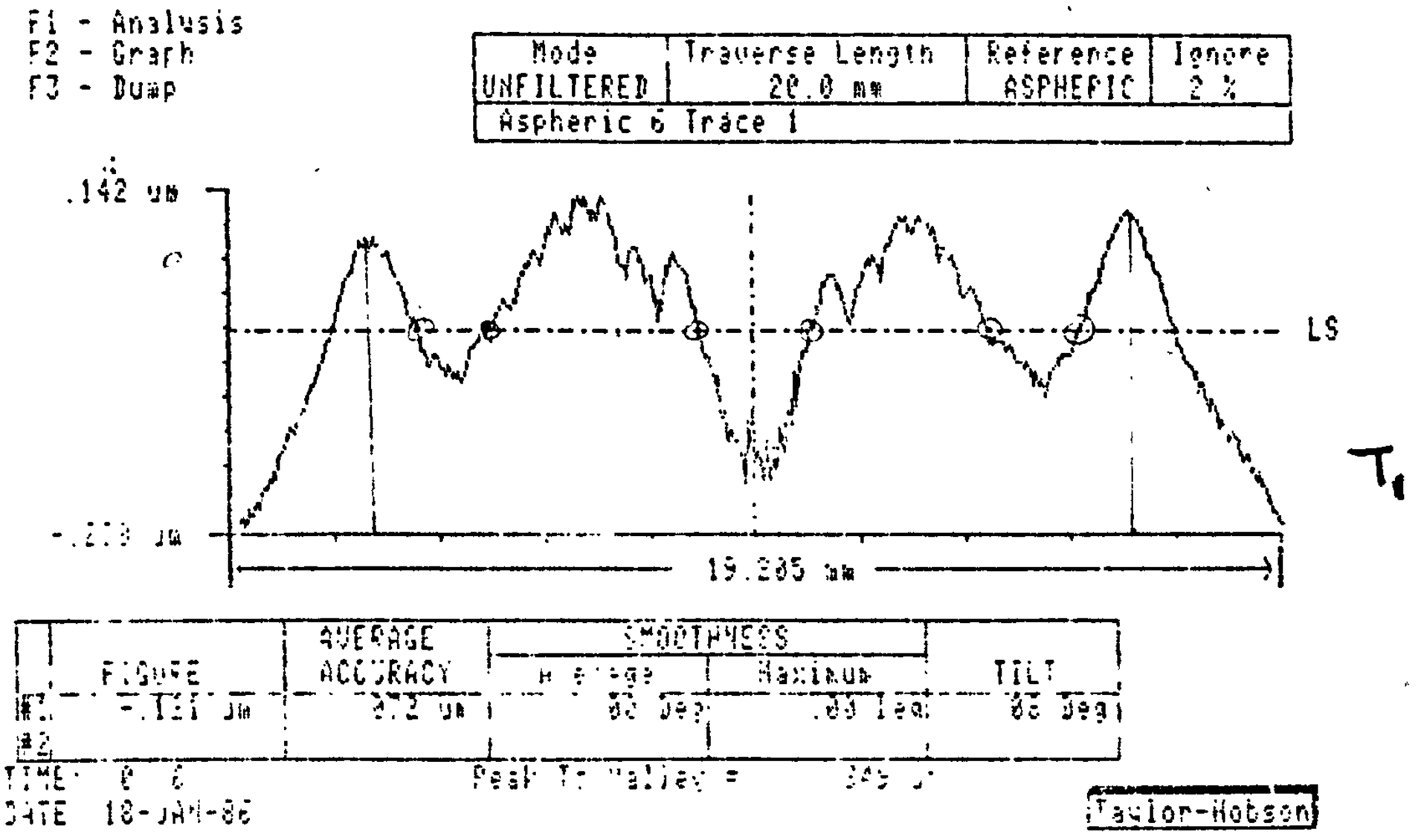
F1 - Analysis
F2 - Graph
F3 - Dump
Mode
UNFILTERED
Traverse Length
20.0 mm
Reference
ASPHERIC
Ignore
2 %
Aspheric 6 Trace 1
.142 um
-.213 um
LS
19.205 mm
T1
FIGURE
AVERAGE ACCURACY
SMOOTHNESS
Average
Maximum
TILT
#1
-.121 um
.072 um
.00 Deg
.03 Deg
.00 Deg
#2
TIME: 8 6
DATE 18-JAN-86
Peak To Valley = .343 um
Taylor-Hobson

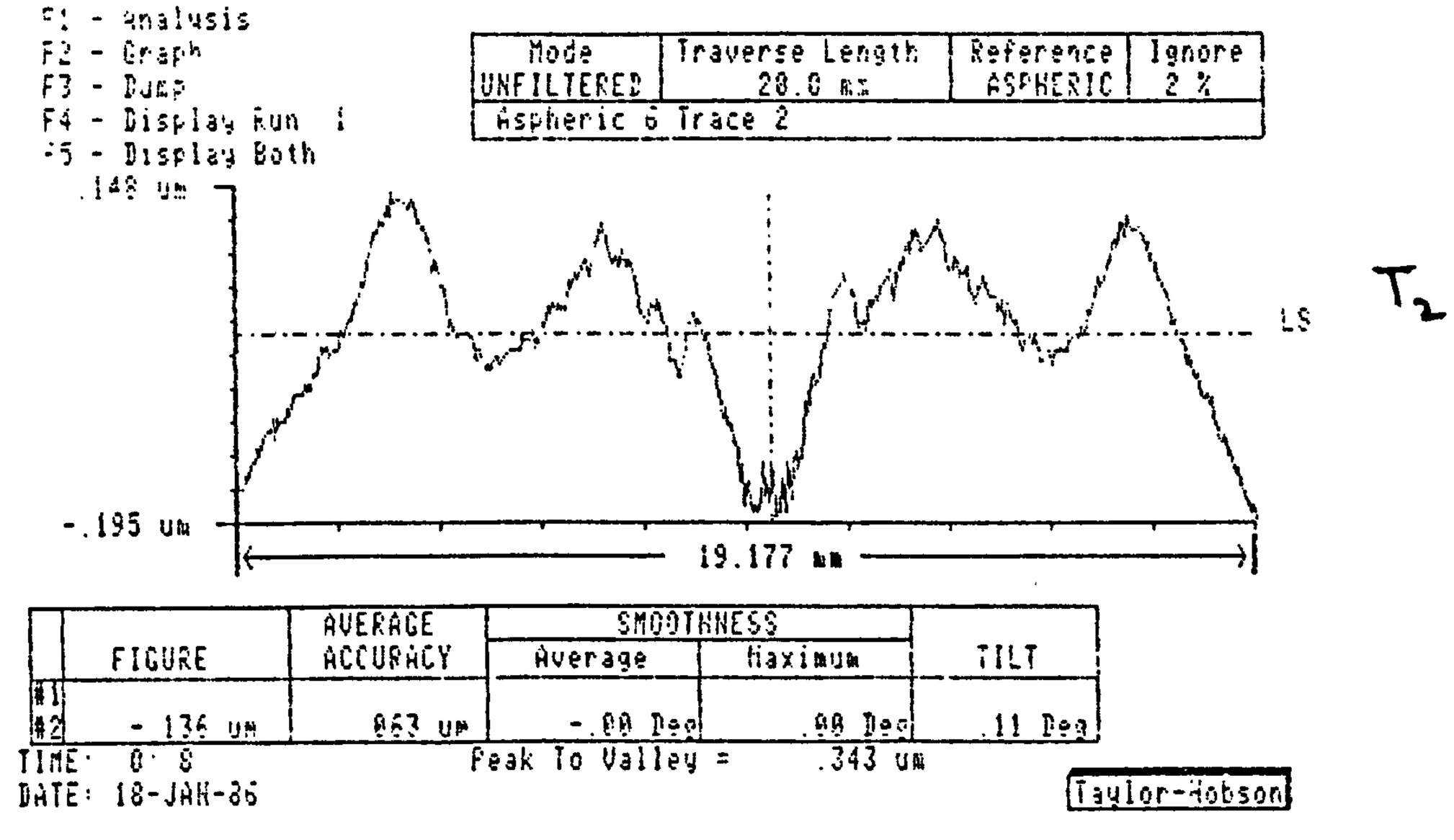
F1 - Analysis
F2 - Graph
F3 - Dump
F4 - Display Run 1
F5 - Display Both
Mode
UNFILTERED
Traverse Length
20.0 mm
Reference
ASPHERIC
Ignore
2 %
Aspheric 6 Trace 2
.148 um
-.195 um
LS
19.177 mm
T2
FIGURE
AVERAGE ACCURACY
SMOOTHNESS
Average
Maximum
TILT
#1
#2
- 136 um
063 um
-.00 Deg
.00 Deg
.11 Deg
TIME: 8: 8
DATE: 18-JAN-86
Peak To Valley = .343 um
Taylor-Hobson

FIGURE 5.4

F1 - Analysis
F2 - Graph
F3 - Dump
F4 - Expand
F5 - Exclude

Mode	Traverse Length	Reference	Ignore
UNFILTERED	20.0 mm	CONCAVE	0 %
Spheric 6 Trace 3			

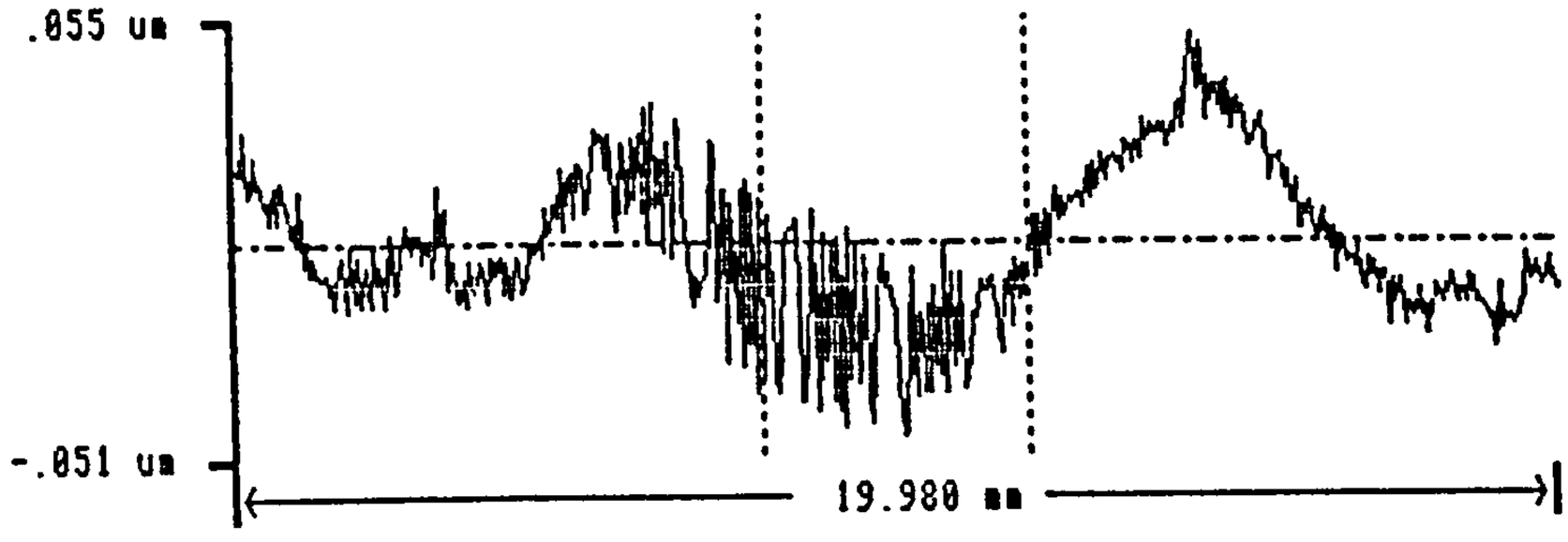

T3

Peak To Valley = .106 um

TIME: 10:49
DATE: 11-AUG-85

Taylor-Hobson

F1 - Analysis

Mode	Traverse Length	Reference	Ignore
UNFILTERED	20.0 mm	CONCAVE	0 %
Spheric 6 Trace 3			

RADIUS =	186.389 mm	PRa =	.015 um
		PRq =	.019 um
Lo =	19.980 mm	PRsk =	.1
PRp =	.055 um	PRku =	2.8
PRv =	.051 um	PDelq =	.04 Deg
PRt =	.106 um	PLamq =	182.684 um
		PS =	45.700 um
		PSm =	245.582 um
		PRz =	.099 um

FIGURE 5.5

TIME: 10:49
DATE: 11-AUG-85

Taylor-Hobson

F1 - Analysis
F2 - Graph
F3 - Dump

Mode	Traverse Length	Reference	Ignore
UNFILTERED	20.0 mm	ASPHERIC	2 %
Aspheric 27 Trace 1			

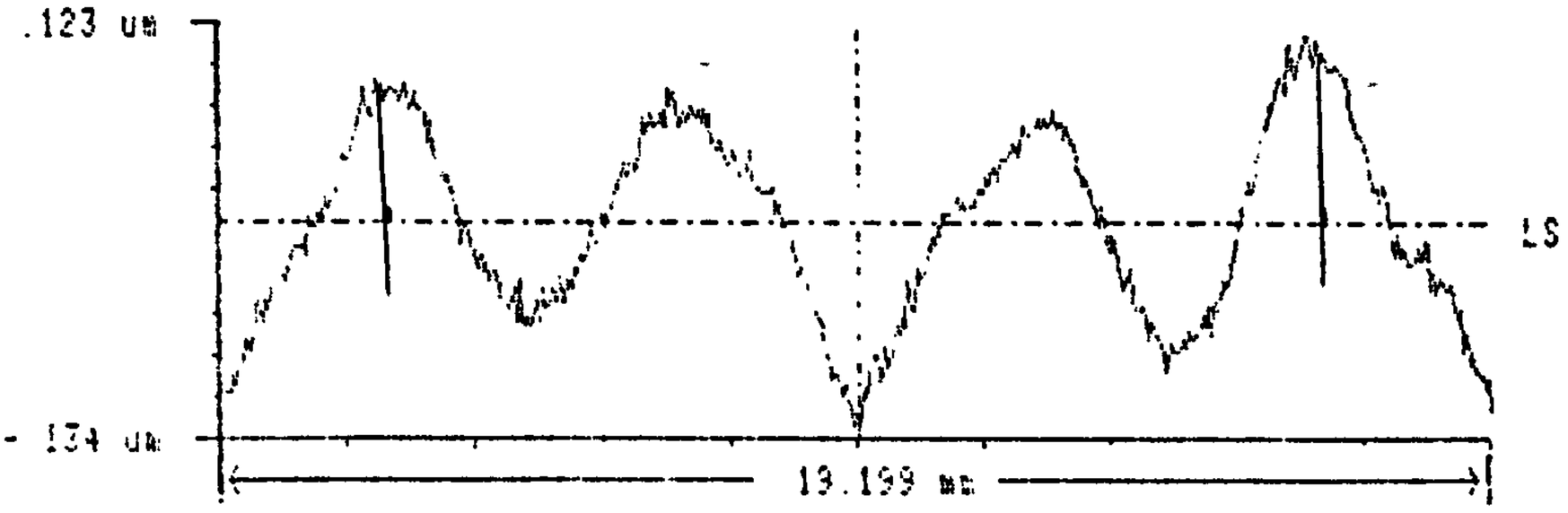

T_1

	FIGURE	AVERAGE ACCURACY	SMOOTHNESS Average	SMOOTHNESS Maximum	TILT
#1 #2	-.124 um	.249 um	.00 Deg	.00 Deg	.15 Deg

TIME: 0:26 Peak To Valley = 256 um
DATE: 21-JAN-86

Taylor-Hobson

F1 - Analysis
F2 - Graph
F3 - Dump

Mode	Traverse Length	Reference	Ignore
UNFILTERED	29.0 mm	ASPHERIC	2 %
Aspheric 27 Trace 2			

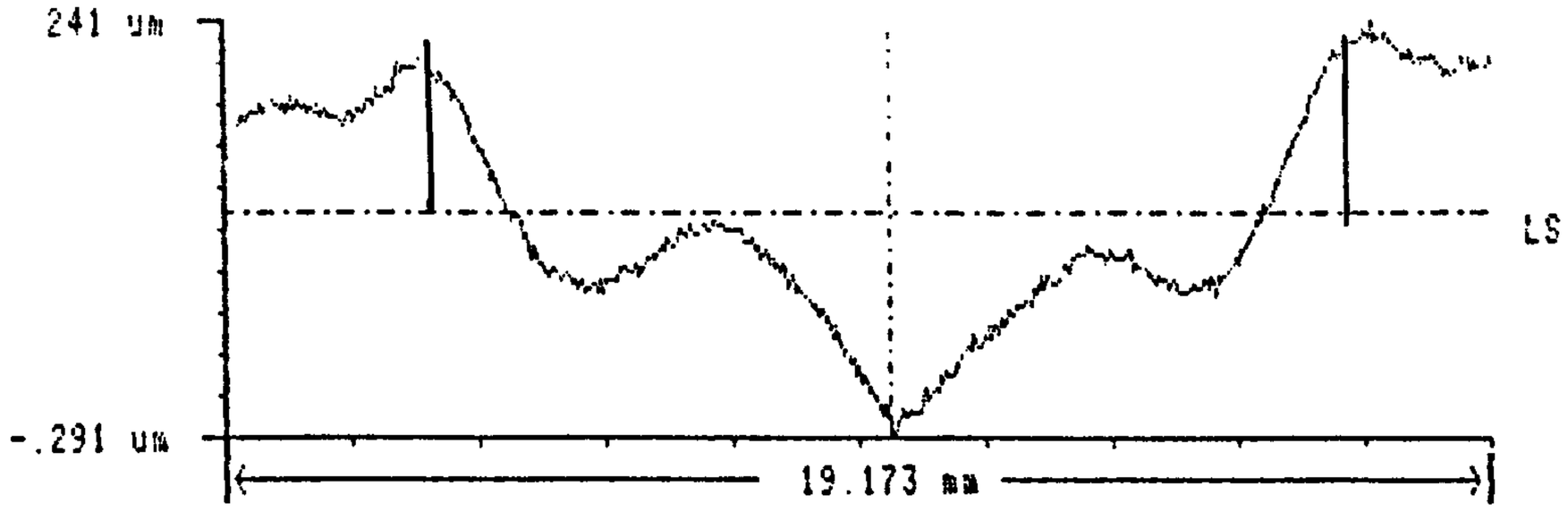

T_2

	FIGURE	AVERAGE ACCURACY	SMOOTHNESS Average	SMOOTHNESS Maximum	TILT
#1 #2	-.281 um	.128 um	.00 Deg	.00 Deg	.14 Deg

TIME: 0:27 Peak To Valley = 532 um
DATE: 21-JAN-86

Taylor-Hobson

FIGURE 5.6

F1 - Analysis
F2 - Graph
F3 - Dump
F4 - Expand
F5 - Exclude

Mode	Traverse Length	Reference	Ignore
UNFILTERED	20.0 mm	CONCAVE	0 %
Spheric 27 Trace 3			

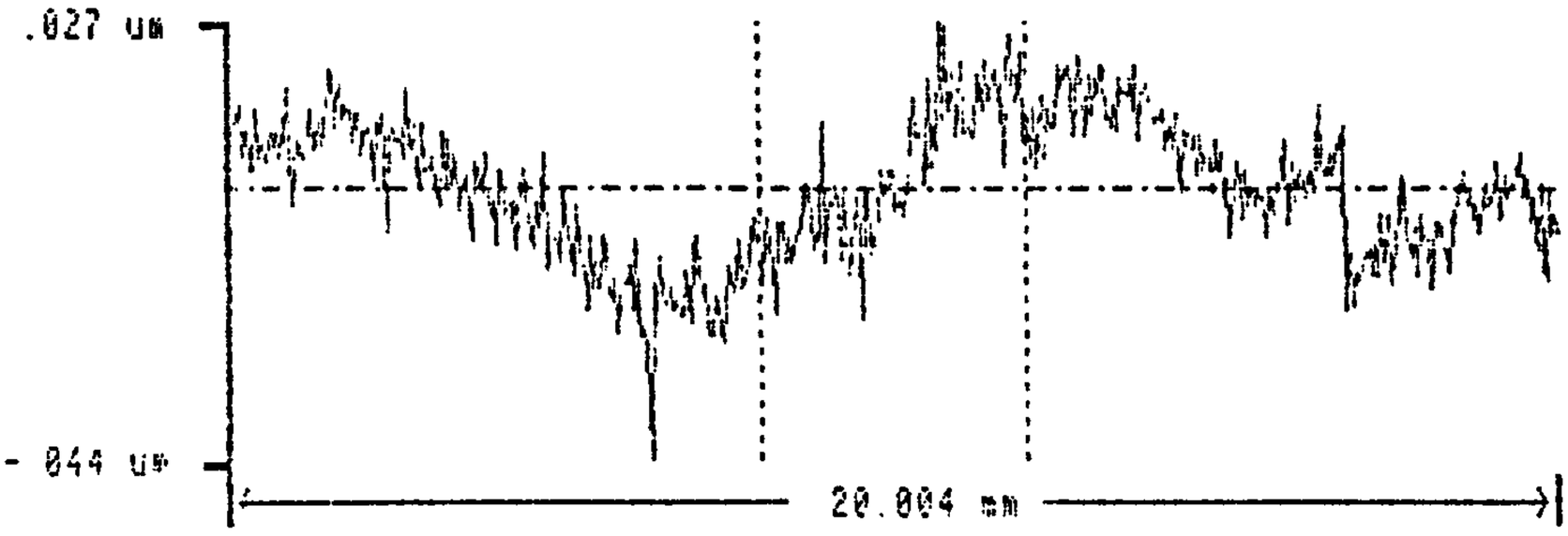

Peak To Valley = .071 um

TIME: 10:33
DATE: 1-NOV-85

Taylor-Hobson

F1 - Analysis

Mode	Traverse Length	Reference	Ignore
UNFILTERED	20.0 mm	CONCAVE	0 %
Spheric 27 Trace 3			

RADIUS =	186.476 mm	PRa =	.009 um
		PRq =	.011 um
Lo =	20.004 mm	PRsk =	-.2
PRp =	.027 um	PRku =	2.5
PRv =	.044 um	PDelq =	.02 Deg
PRt =	.071 um	PLamq =	203.066 um
		PS =	43.874 um
		PSm =	195.725 um
		PRz =	.056 um

TIME: 10:33
DATE: 1-NOV-85

Taylor-Hobson

FIGURE 5.7

F1 - Analysis
F2 - Graph
*F3 - Dump

Mode	Traverse Length	Reference	Ignore
UNFILTERED	20.0 mm	ASPHERIC	2 %
Aspheric 30 Trace 1			

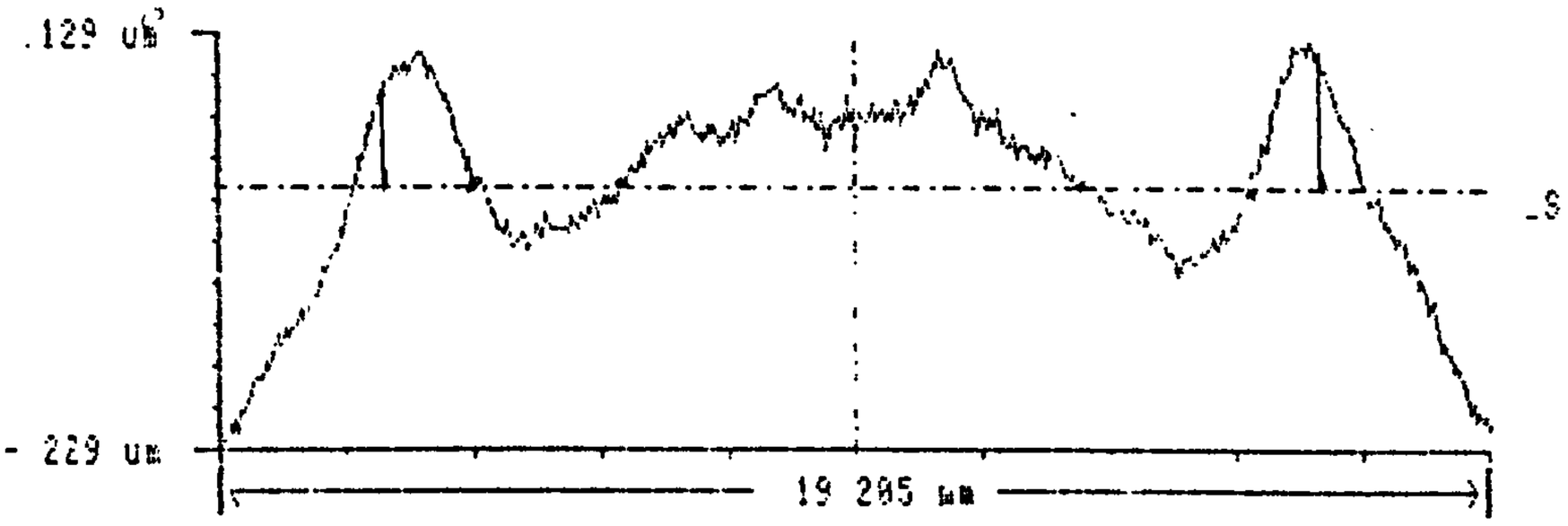

	FIGURE	AVERAGE ACCURACY	SMOOTHNESS Average	SMOOTHNESS Maximum	TILT
#1 #2	.050 um	.064 um	00 Deg	.00 Deg	00 Deg

TIME: 8:41 Peak To Valley = 358 um
DATE 21-JAN-86

Taylor-Hobson

T_1

F1 - Analysis
F2 - Graph
F3 - Dump

Mode	Traverse Length	Reference	Ignore
UNFILTERED	20.0 mm	ASPHERIC	2 %
Aspheric 30 Trace 2			

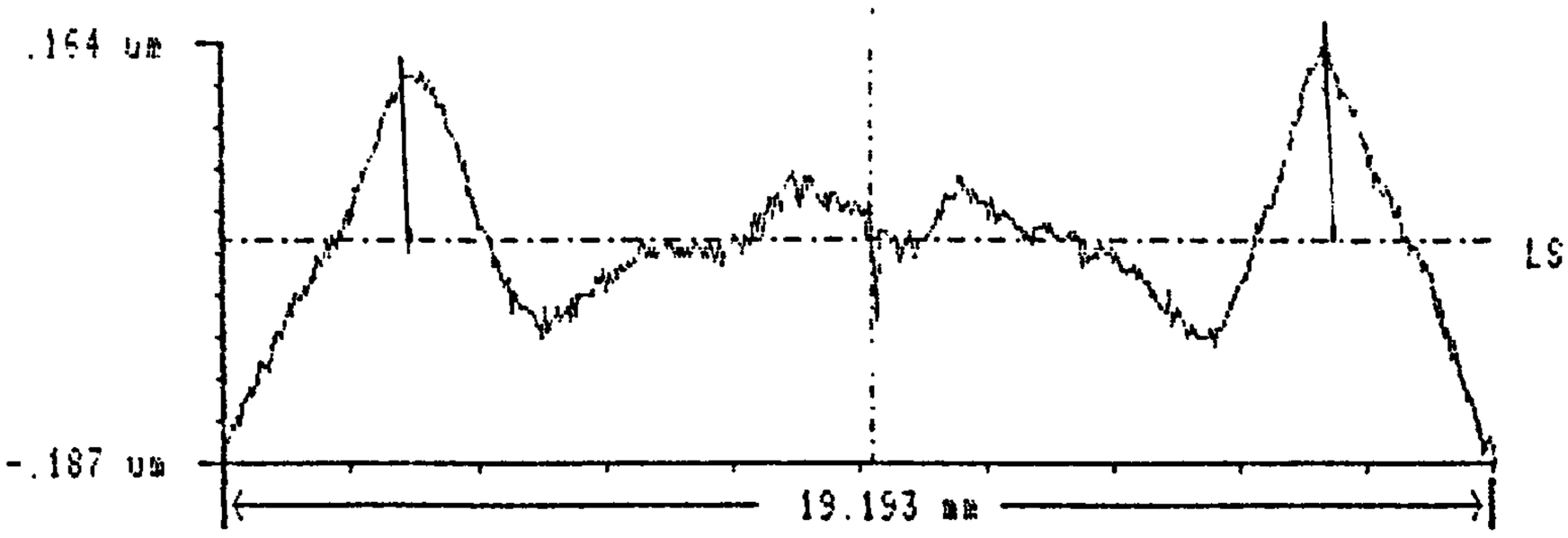

	FIGURE	AVERAGE ACCURACY	SMOOTHNESS Average	SMOOTHNESS Maximum	TILT
#1 #2	-.003 um	.050 um	-.00 Deg	.00 Deg	.01 Deg

TIME: 8:43 Peak To Valley = .350 um
DATE: 21-JAN-86

Taylor-Hobson

T_2

FIGURE 5.8

F1 - Analysis
F2 - Graph
F7 - Dump
F4 - E-pand
F5 - Exclude

Mode	Traverse Length	Reference	Ignore
UNFILTERED	20.0 mm	CONCAVE	0 %
Spheric 30 Trace 3			

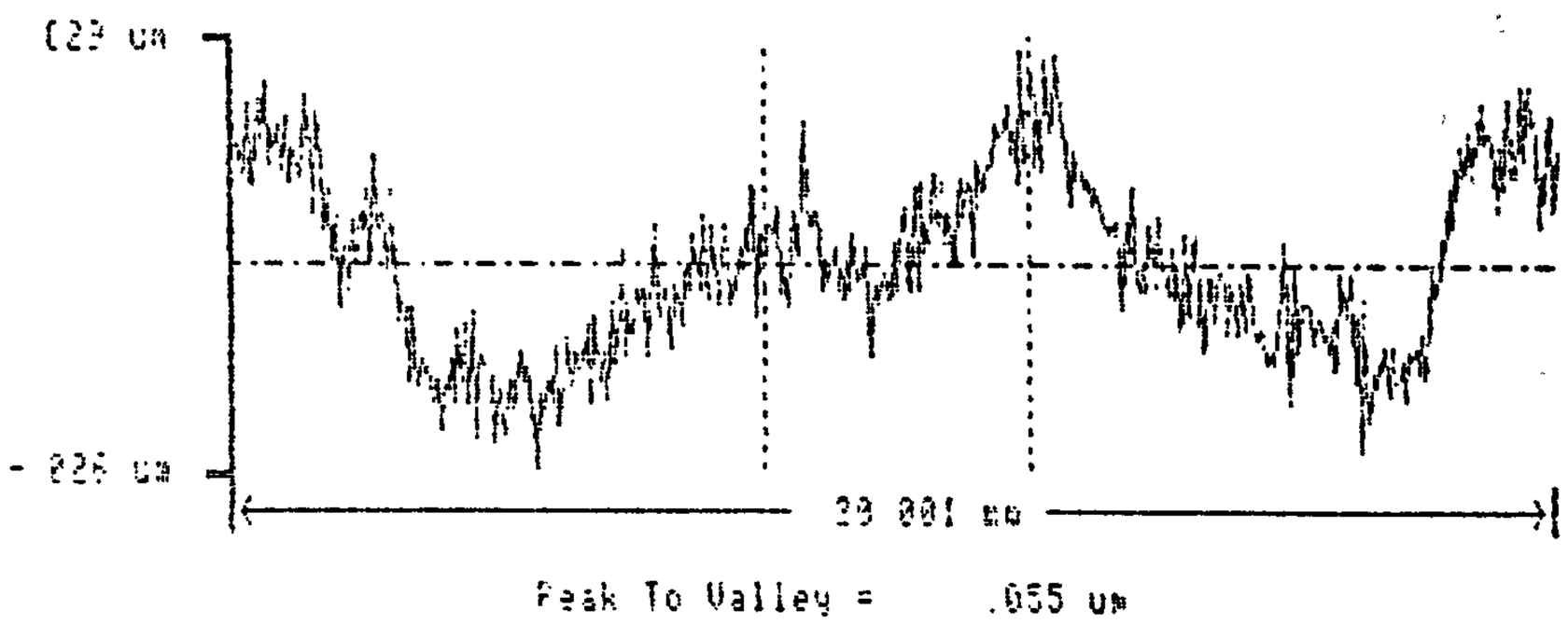

TIME: 16 54
DATE: 31-OCT-85

Taylor-Hobson

FIGURE 5.9

F1 - Analysis
F2 - Graph
F3 - Dump

Mode	Traverse Length	Reference	Ignore
UNFILTERED	20.0 mm	ASPHERIC	2 %
Aspheric 33 Trace 1			

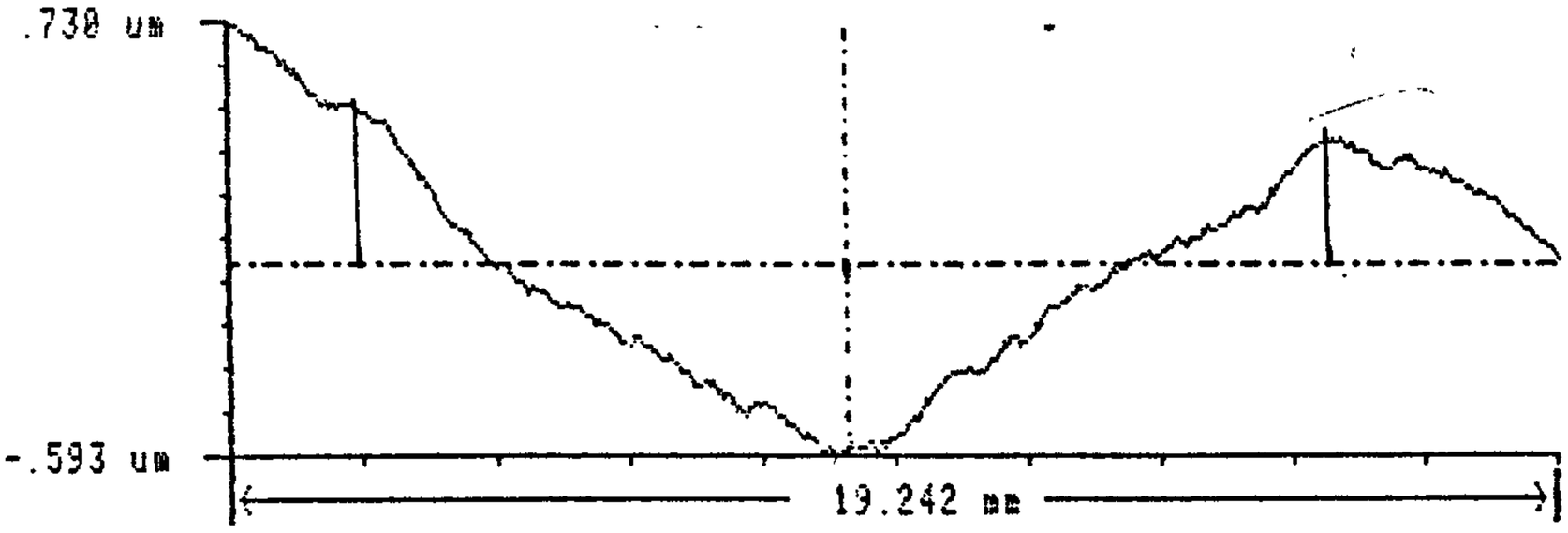

T1

	FIGURE	AVERAGE ACCURACY	SMOOTHNESS Average	SMOOTHNESS Maximum	TILT
#1 #2	-.552 um	.287 um	-.00 Deg	.00 Deg	.21 Deg

TIME: 8:50 Peak To Valley = 1.324 um
DATE: 21-JAN-86 -5- Taylor-Hobson

77·578

59·489

F1 - Analysis
F2 - Graph
F3 - Dump

Mode	Traverse Length	Reference	Ignore
UNFILTERED	22.0 mm	ASPHERIC	2 %
Aspheric 33 Trace 2			

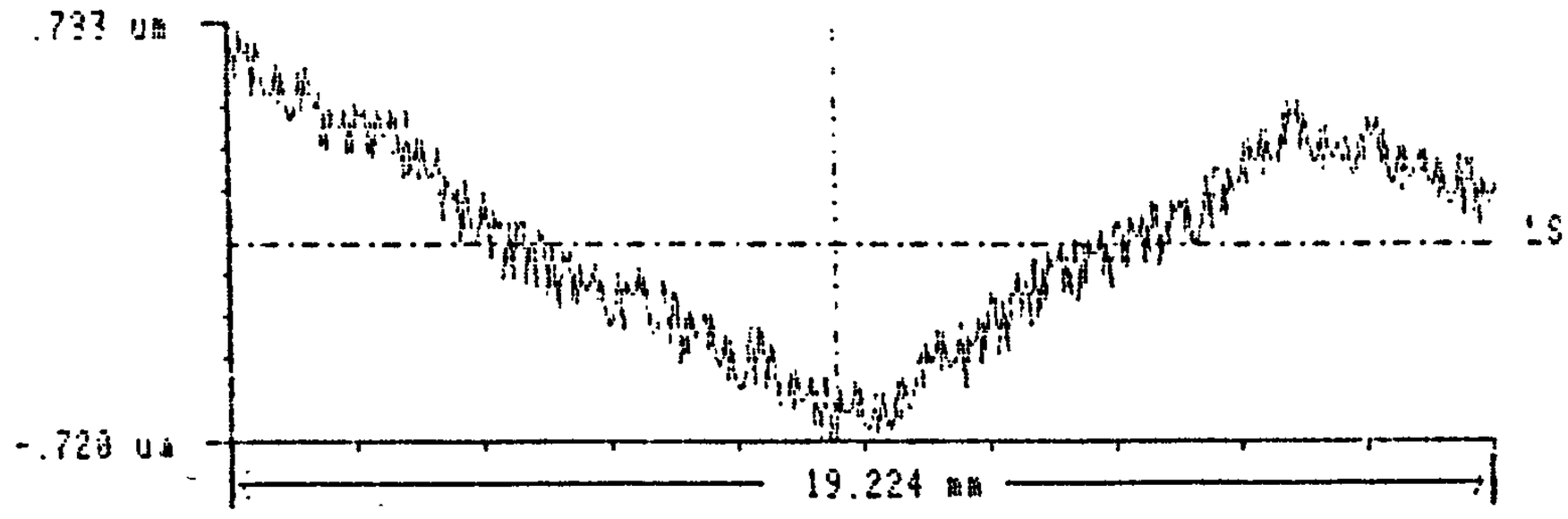

T2

	FIGURE	AVERAGE ACCURACY	SMOOTHNESS Average	SMOOTHNESS Maximum	TILT
#1 #2	-.524 um	398 um	-.00 Deg	.02 Deg	.20 Deg

TIME: 8:52 Peak To Valley = 1.503 um
DATE: 21-JAN-86 -5- Taylor-Hobson

FIGURE 5.10

F1 - Analysis
F2 - Graph
F3 - Dump
F4 - Expand
F5 - Exclude

Mode	Traverse Length	Reference	Ignore
UNFILTERED	20.0 mm	CONCAVE	0 %
Spheric 33 Trace 3			

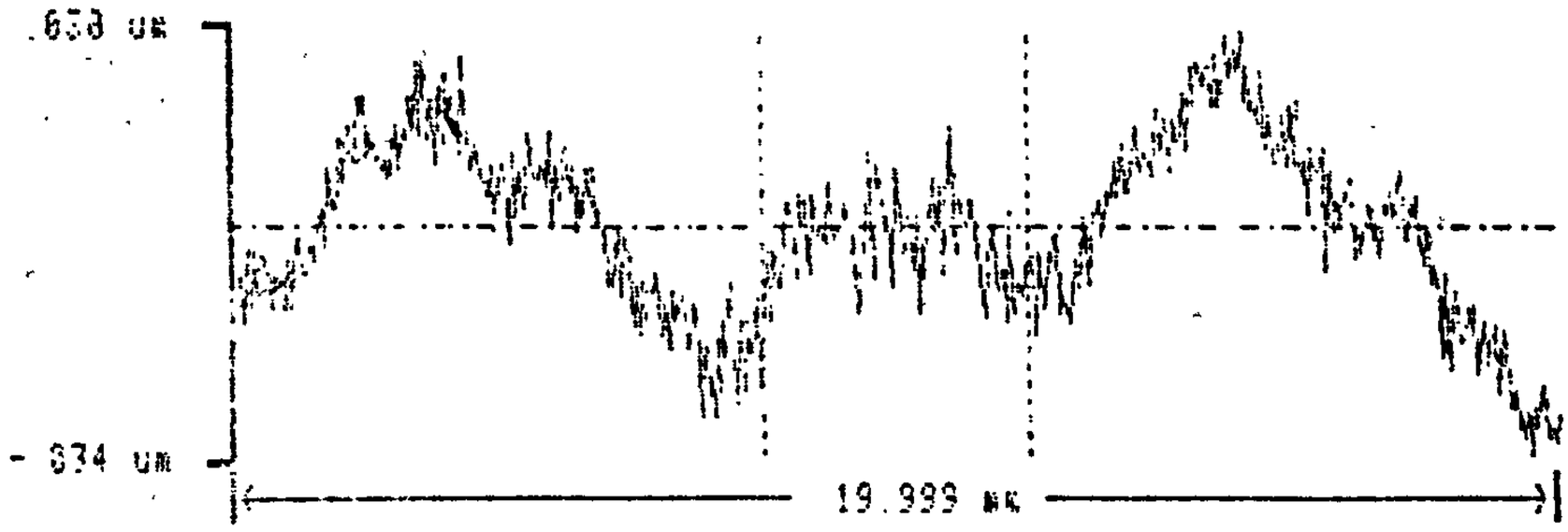

T3

Peak To Valley = 864 um

TIME: 15:49
DATE: 31-OCT-85

Taylor-Hobson

FIGURE 5.11

FIGURE 5.12

AREA UNDER CURVE (FROM 0 TO .4 CYCLES/MR) = 0. 1773
VALUE @ 0.2 CYCLES/MR = 076 %
VALUE @ 0.3 CYCLES/MR = 059 %

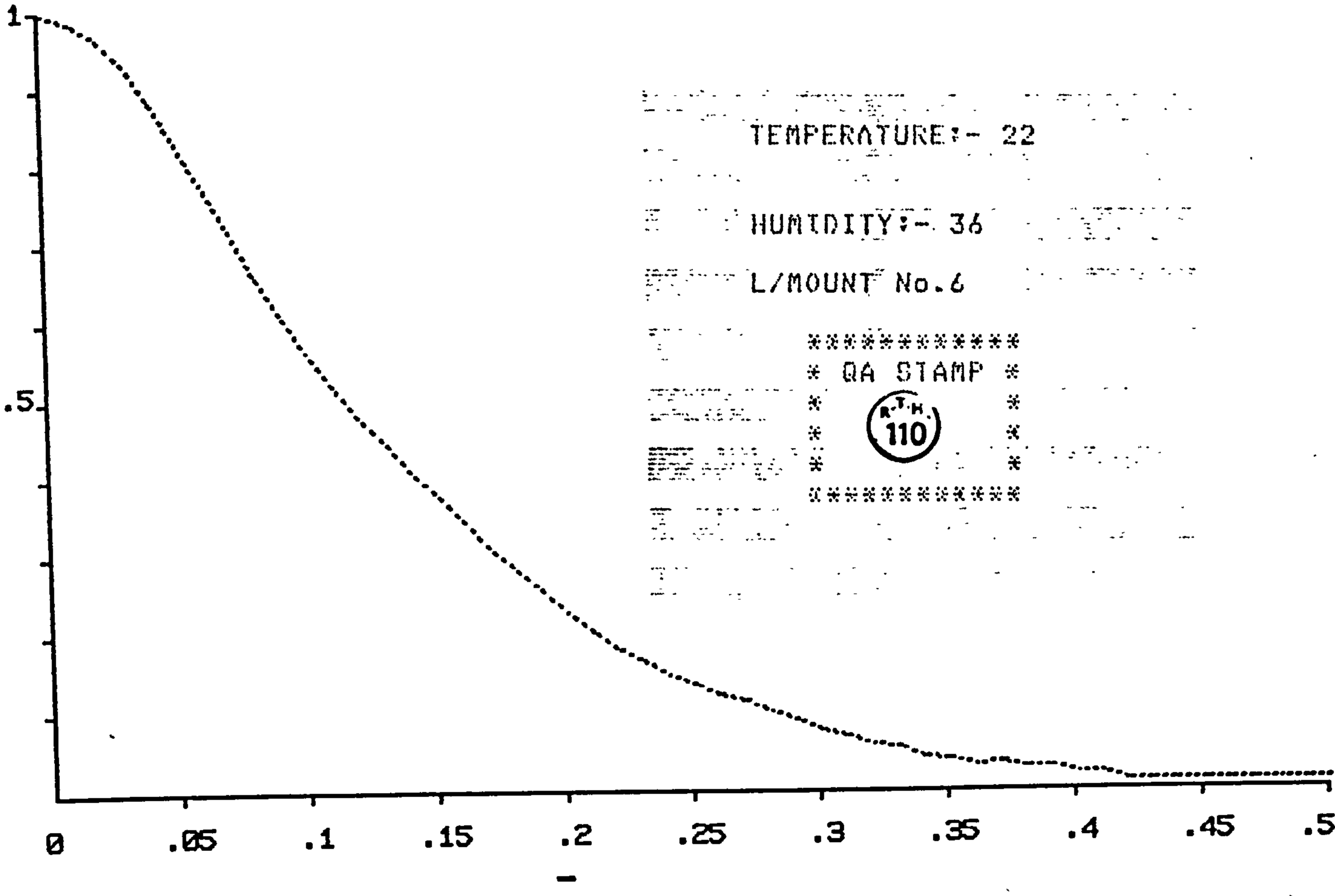

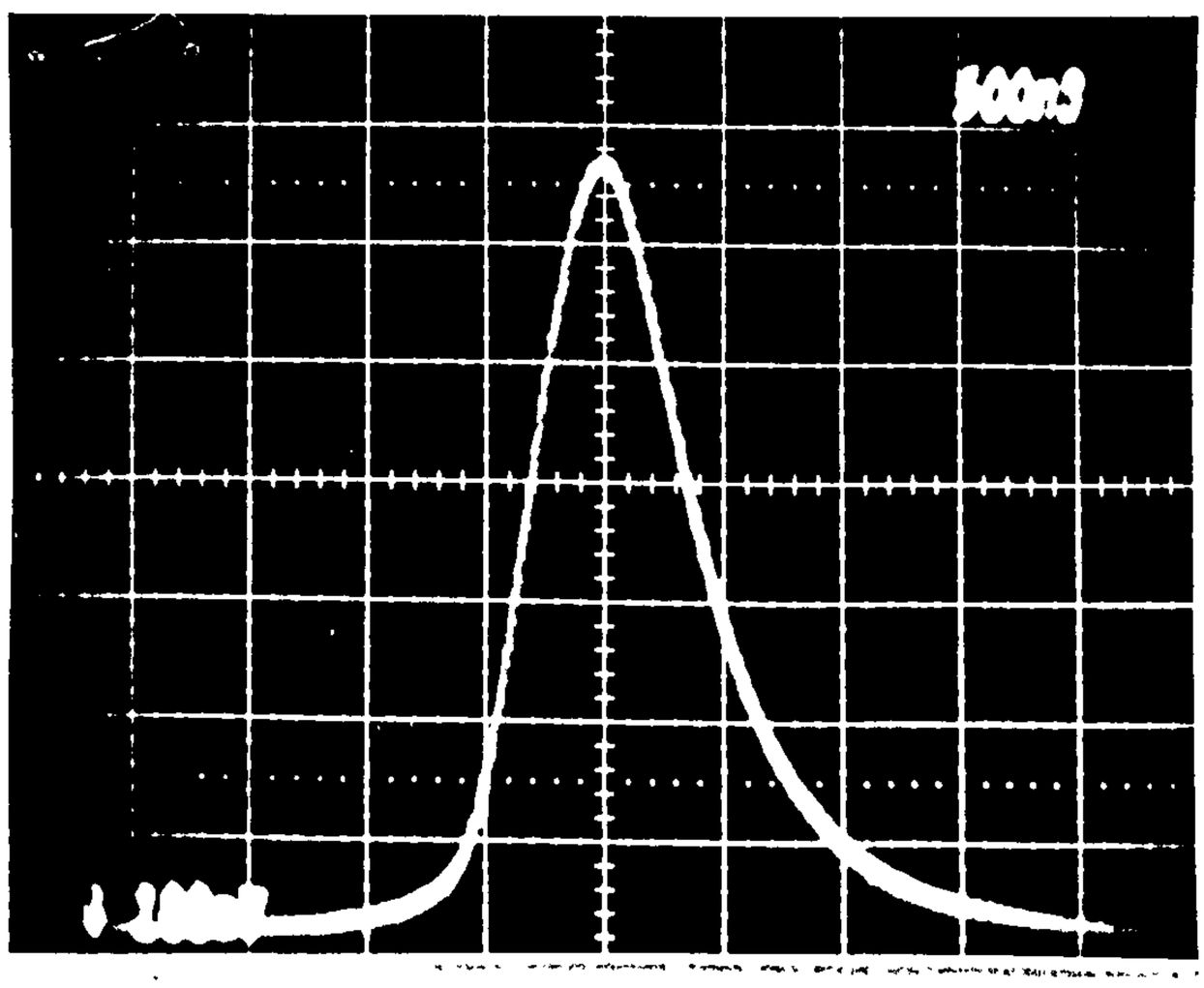

LSF

FIGURE 5.13

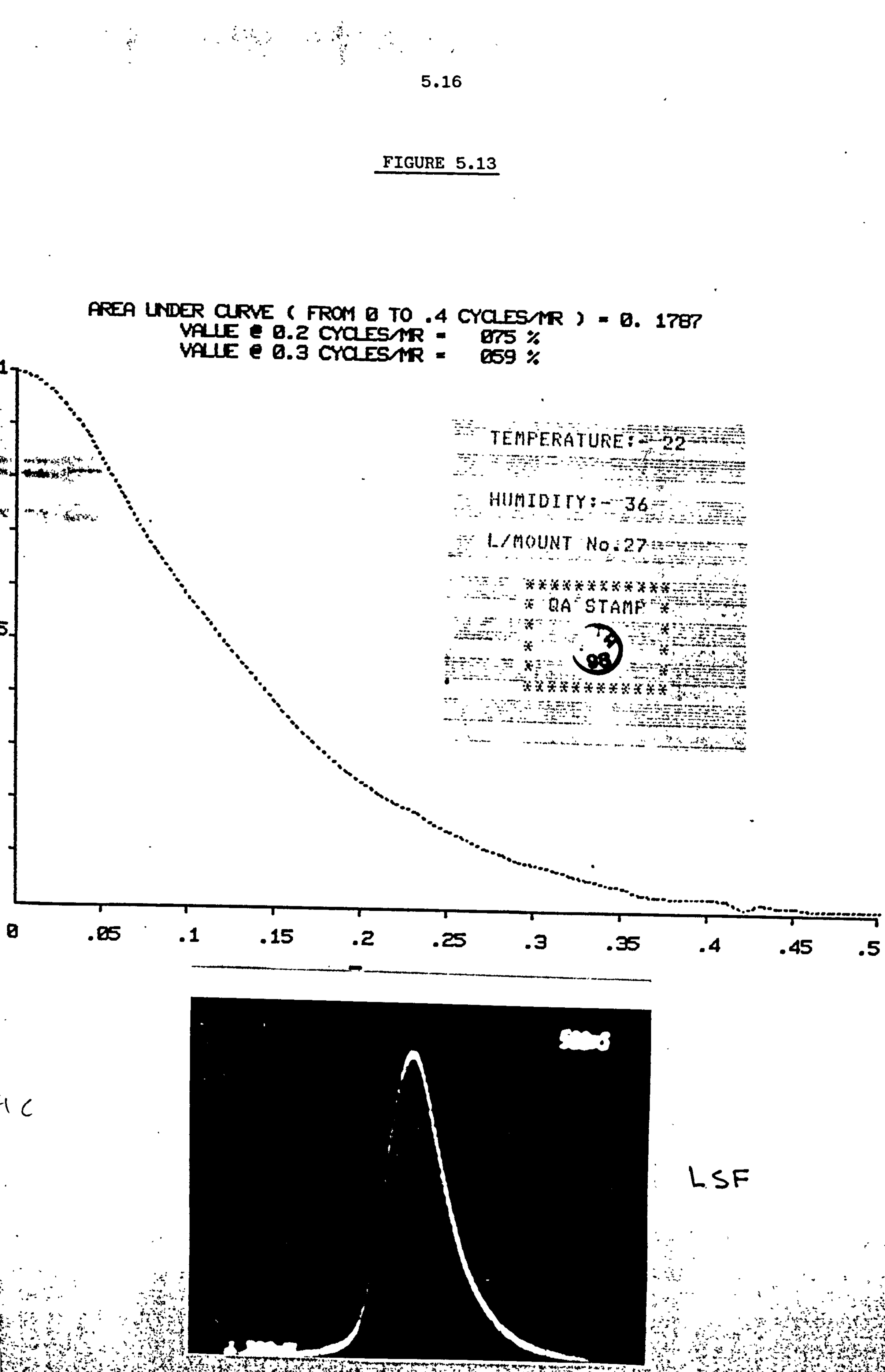
AREA UNDER CURVE (FROM 0 TO .4 CYCLES/MR) = 0. 1787
VALUE @ 0.2 CYCLES/MR = 075 %
VALUE @ 0.3 CYCLES/MR = 059 %
TEMPERATURE: 22
HUMIDITY: 36
L/MOUNT No:27
* QA STAMP *
0
.05
.1
.15
.2
.25
.3
.35
.4
.45
.5

FIGURE 5.14

AREA UNDER CURVE (FROM 0 TO .4 CYCLES/MR) = 0. 1791
VALUE @ 0.2 CYCLES/MR = 075 %
VALUE @ 0.3 CYCLES/MR = 052 %

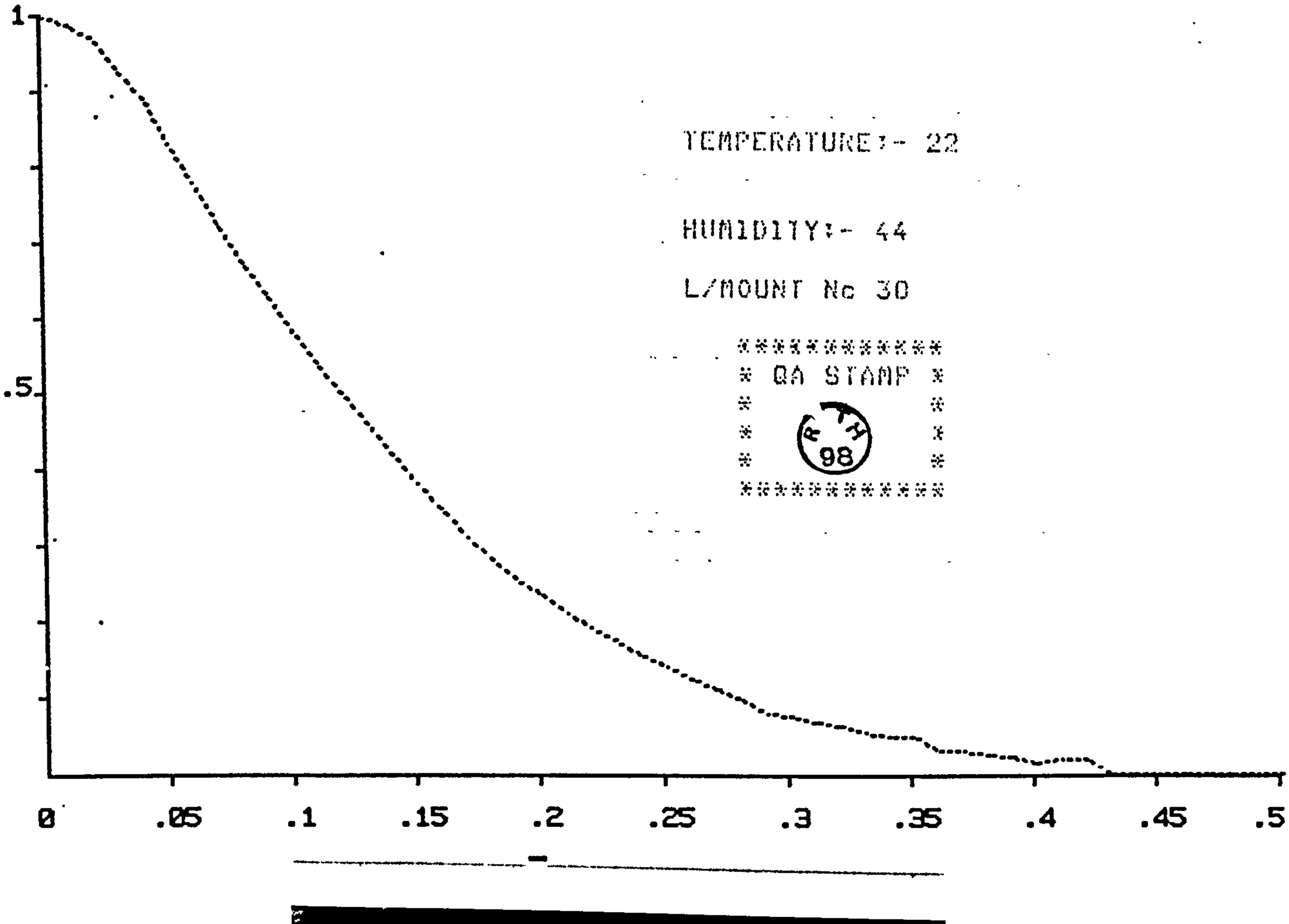

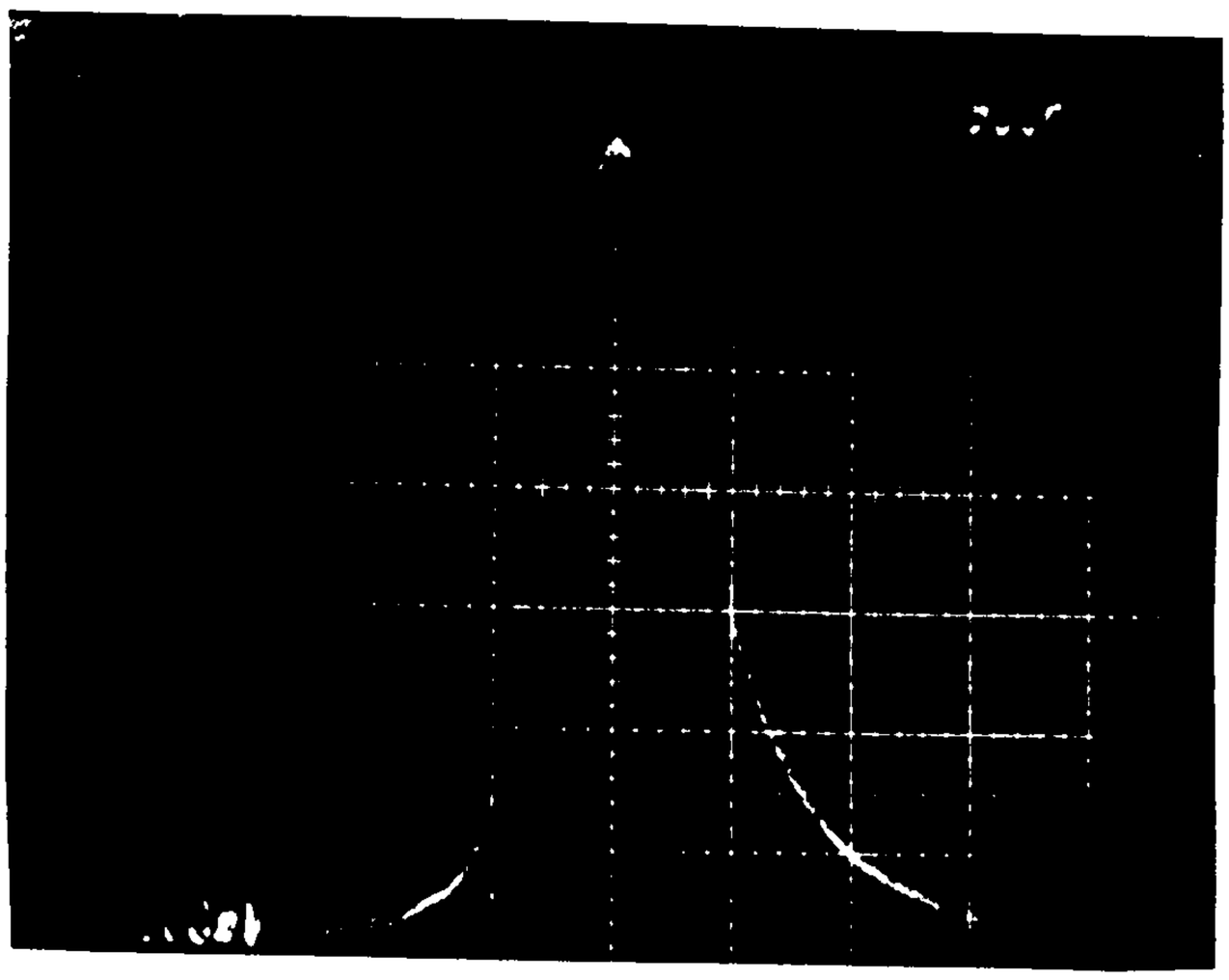

LSF

FIGURE 5.15

AREA UNDER CURVE (FROM 0 TO .4 CYCLES/MR) = 0. 1813
VALUE @ 0.2 CYCLES/MR = 077 %
VALUE @ 0.3 CYCLES/MR = 059 %

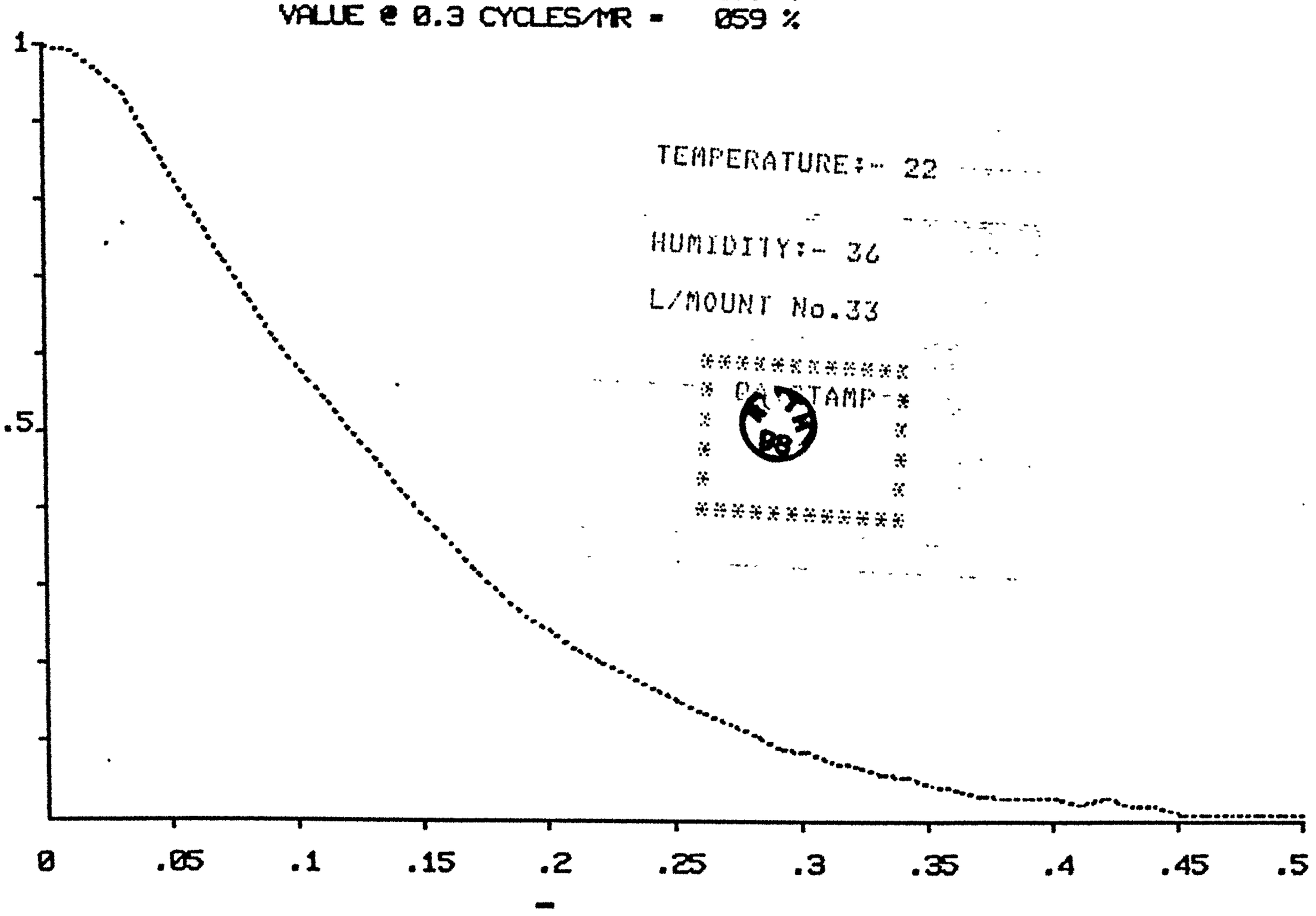

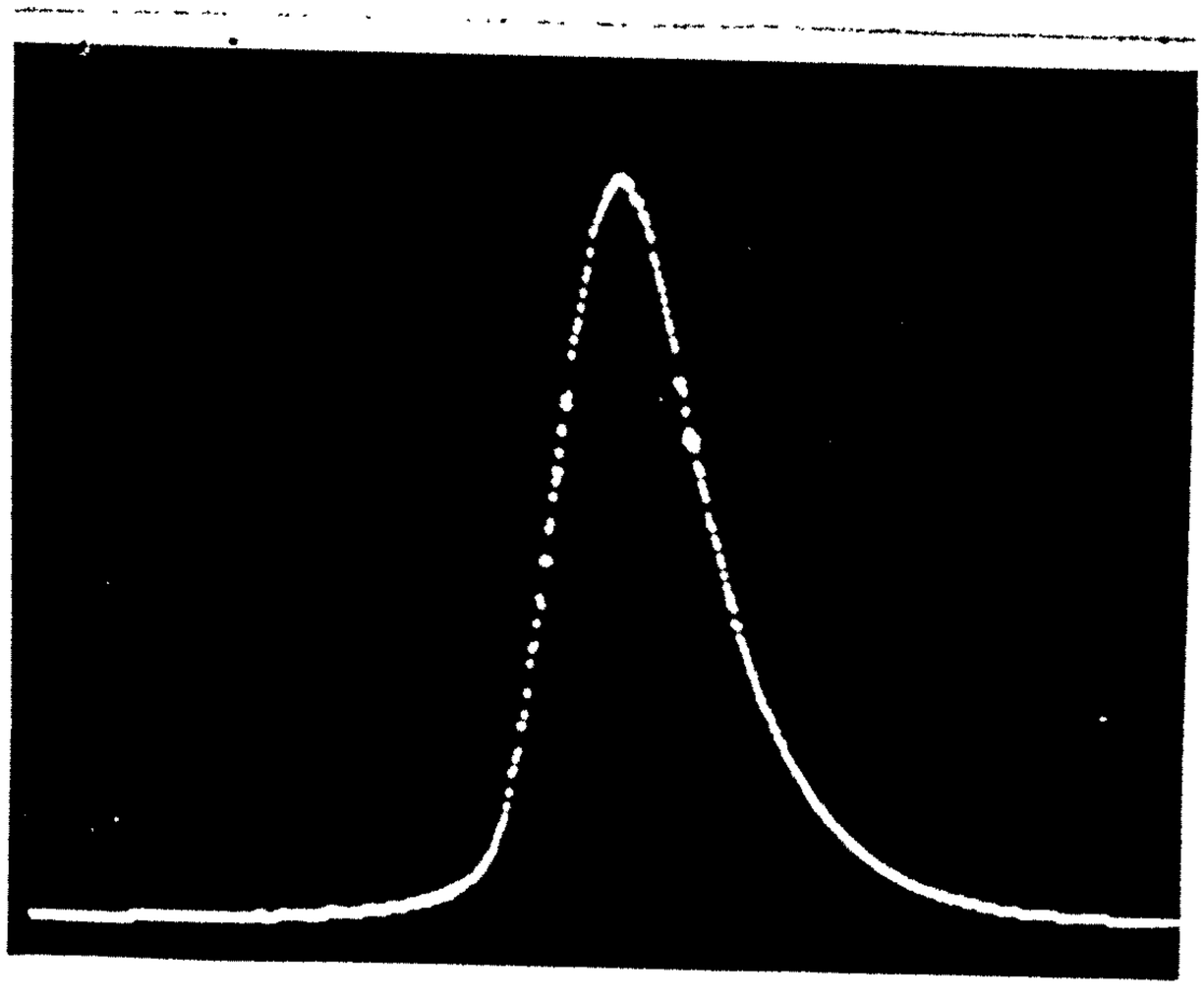

LSF

The area under the curve MTF (energy) for each of the lenses is also available. In order to utilise these results effectively a suitable strategy to handle the error profiles is needed. This aspect is investigated in the next chapter.

C H A P T E R V I

DATA ANALYSIS

CHAPTER VI

DATA ANALYSIS

6.1

Qualitative Observation of the Data

The first noteworthy point is that none of the lenses are infact rejects because of poor optical performance. Secondly, the error on the spherical side is much smaller than the aspheric side. Judging the optical performance on the "area" criterion, the optical performance varies only by a small amount. We are therefore, looking for a mechanism to correlate optical performance as characterised by area under the curve with some parameter derived from the composite error curve.

In chapter IV certain types of "artificial error" forms were modelled on the Ray Tracing MTF programme to study the effect on the resulting MTF. Since we now have "real errors", one logical approach would be to impose these errors on the software and examine the output MTF.

Another approach is to generate various parameters from the profile error and attempt to establish correlation between such parameters and the MTF (energy).

6.2

Mathematical Representation

In either of these cases a mathematical representation of

the error profile would be required. With this view in mind "Nag Routines" supported on the Burroughs machine were used to fit suitable polynomials to the error profile. The lens design software could only cope with polynomials upto 10th order. Upto 10th order polynomials were fitted to some profiles. A few profiles together with their respective least square errors are shown in Figs. 6.1 to 6.3. Inspection reveals that even the 10th order fit is inadequate for the worst of the cases. In order to reduce the least square error significantly and to maintain the "character" of the profile, higher orders were tried. Typically a polynomial of some 30th order is needed to at least visually resemble the original error profile (see Figs. 6.4 - 6.6). Such high orders make it impractical to simulate the error profile on the Ray Tracing/Lens design Rank Taylor Hobson programs.

Never-the-less the polynomial representation of the profile error does allow us to generate the "slope" related parameters. The process of analytical differentiation using the fitted polynomials represents a fairly straight forward task. Initially, several parameters were derived. The most straight forward one is the average error. In response to the belief that it is the slope of the error profile which is critical to lens performance average slope of the profile was also derived. However, none of these parameters revealed much correlation with the MTF (area under curve). It is hence concluded that there is little this approach has to offer.

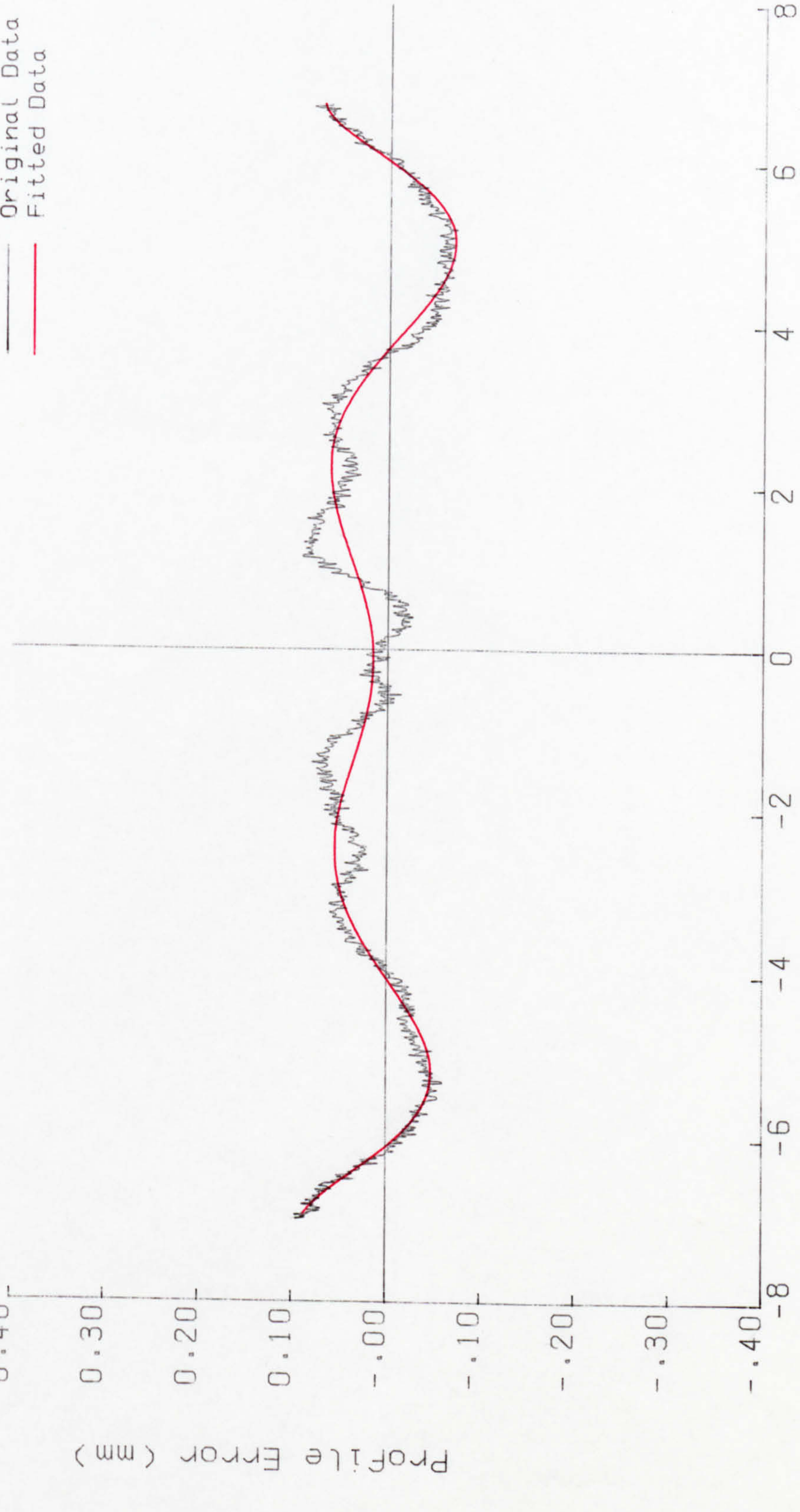
Original Data
Fitted Data
Lense Radius (mm)
8
6
4
2
0
-2
-4
-6
-8
Lens A14 - 10th order polynomial Fit
Least Square Error = .1621E-4
Profile Error (mm)
X10-3
0.40
0.30
0.20
0.10
.00
-.10
-.20
-.30
-.40

FIGURE 6.1

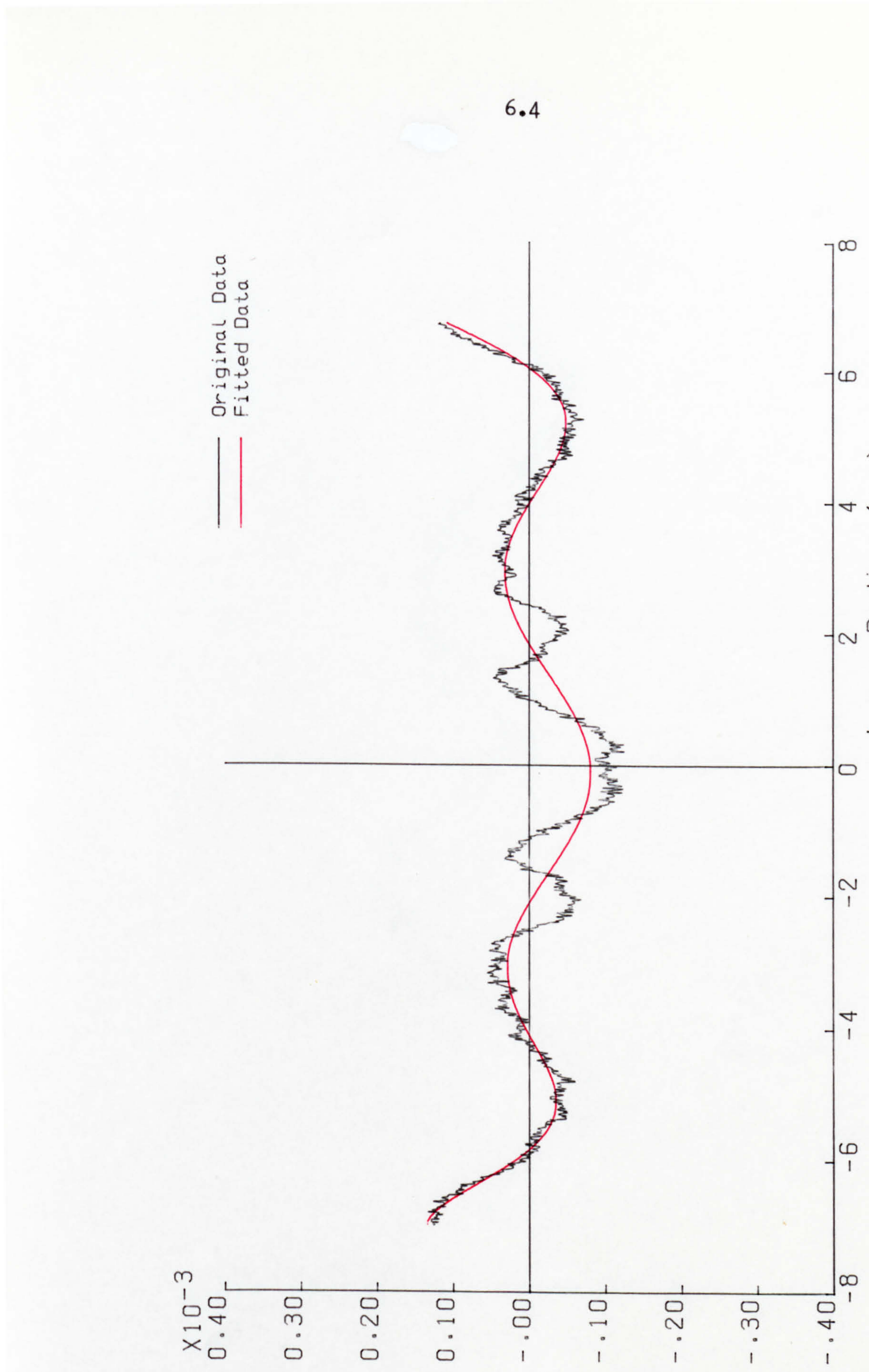
Original Data
Fitted Data
Lense Radius (mm)
8
6
4
2
0
-2
-4
-6
-8
Lens A17 - 10th order polynomial Fit
Least Square Error = .2589E-4
Profile Error (mm)
X10⁻³
0.40
0.30
0.20
0.10
.00
-.10
-.20
-.30
-.40

FIGURE 6.2

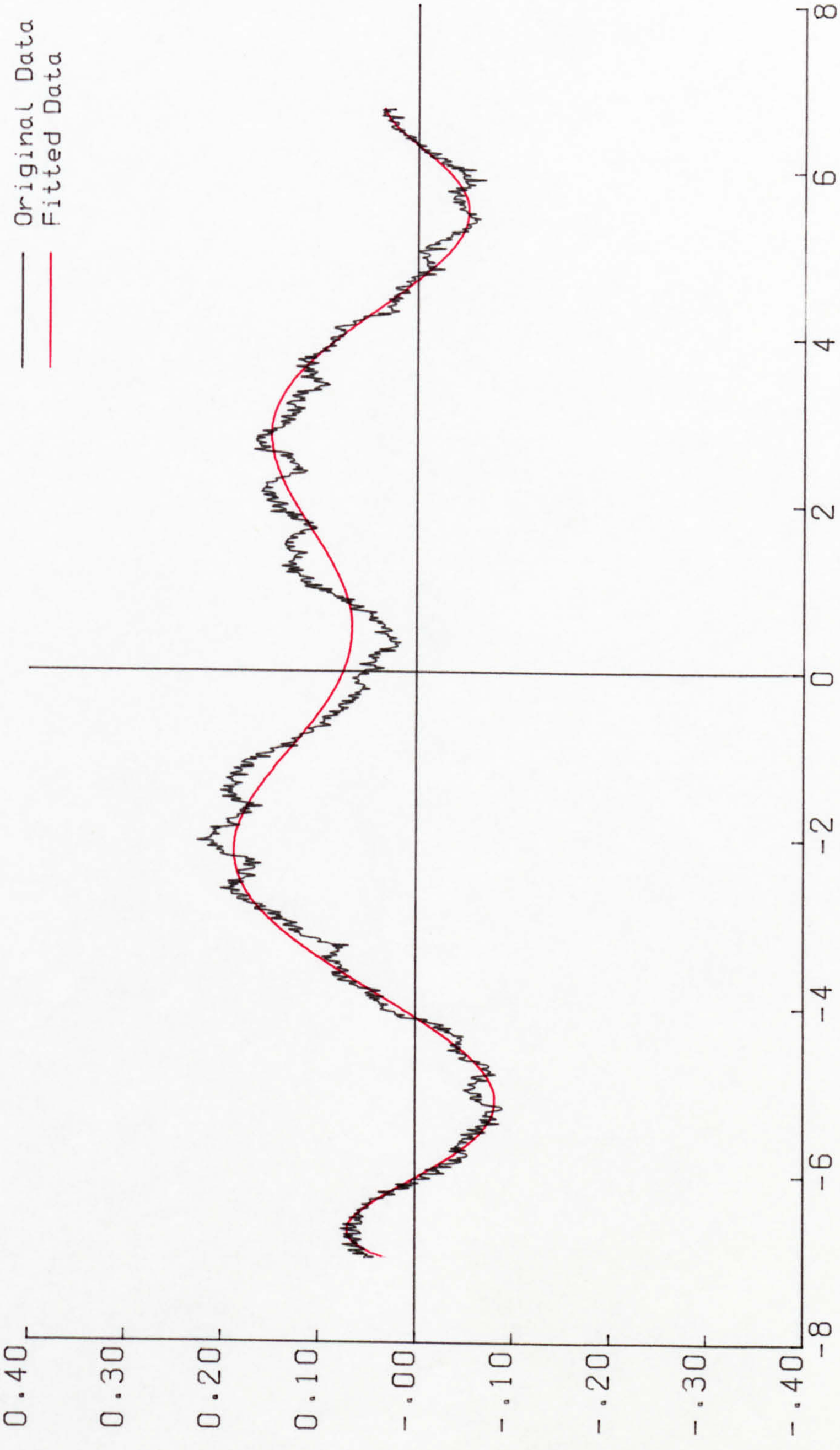
Original Data
Fitted Data
Lense Radius (mm)
8
6
4
2
0
-2
-4
-6
-8
Lens A15 - 10th order polynomial Fit
Least Square Error = .1791E-4
Profile Error (mm)
X10-3
0.40
0.30
0.20
0.10
.00
-.10
-.20
-.30
-.40

FIGURE 6.3

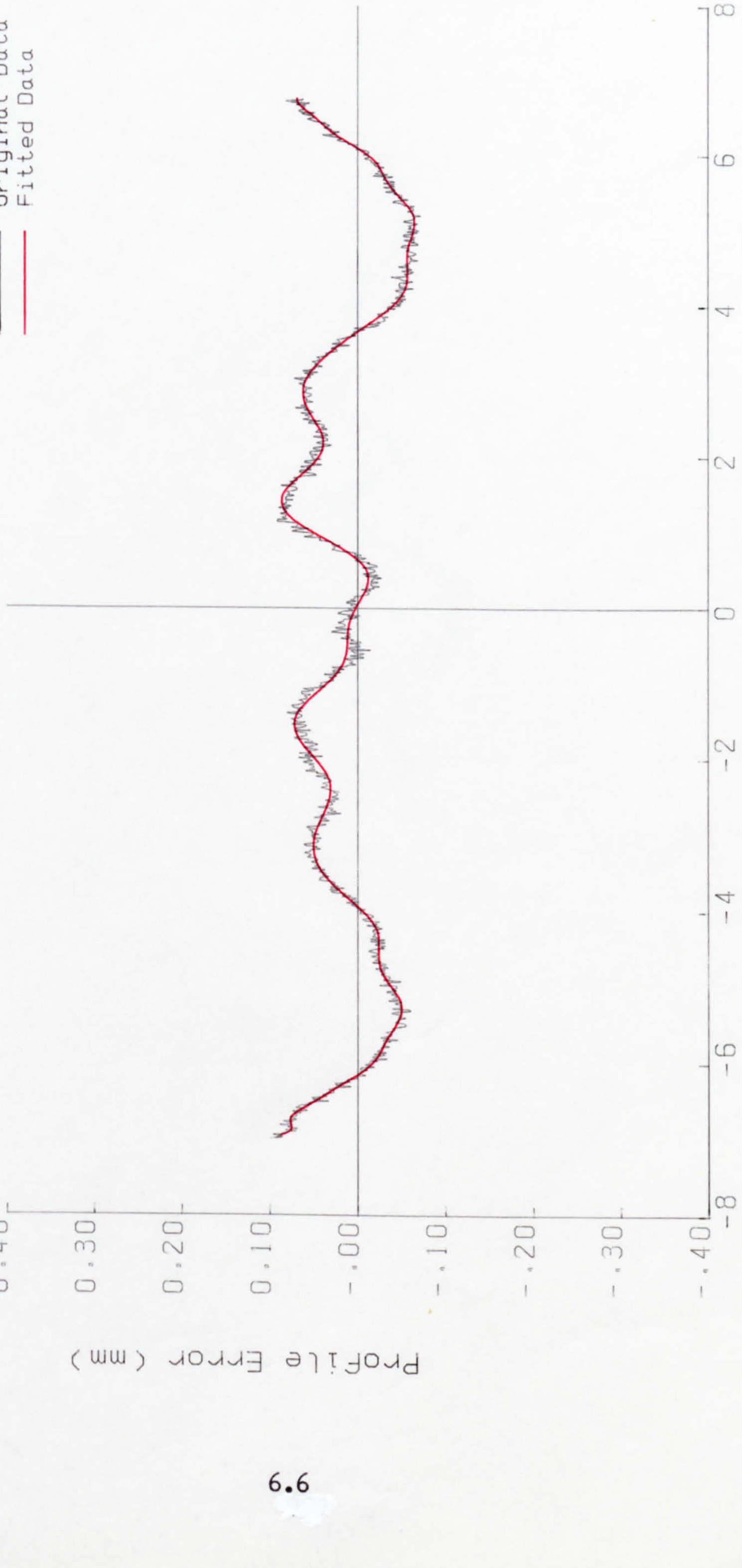
Original Data
Fitted Data
Lense Radius (mm)
8
6
4
2
0
-2
-4
-6
-8
Lens A14 - 35th order polynomial Fit
Least Square Error = .7244E-5
Profile Error (mm)
X10-3
0.40
0.30
0.20
0.10
.00
-.10
-.20
-.30
-.40

FIGURE 6.4

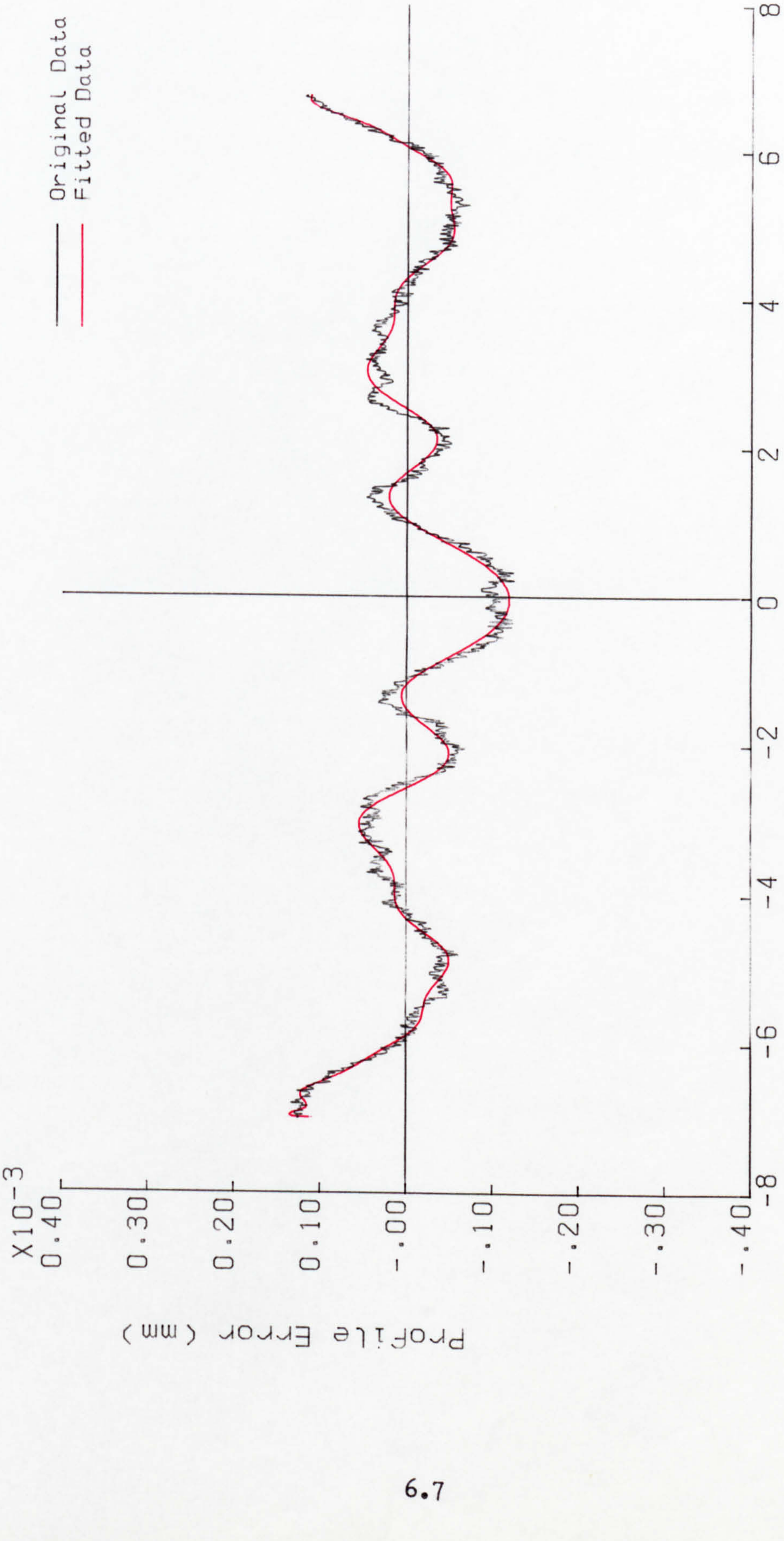
Original Data
Fitted Data
Lense Radius (mm)
8
6
4
2
0
-2
-4
-6
-8
Lens A17 - 32nd order polynomial Fit
Least Square Error = .1152E-4
Profile Error (mm)
X10-3
0.40
0.30
0.20
0.10
-.00
-.10
-.20
-.30
-.40

FIGURE 6.5

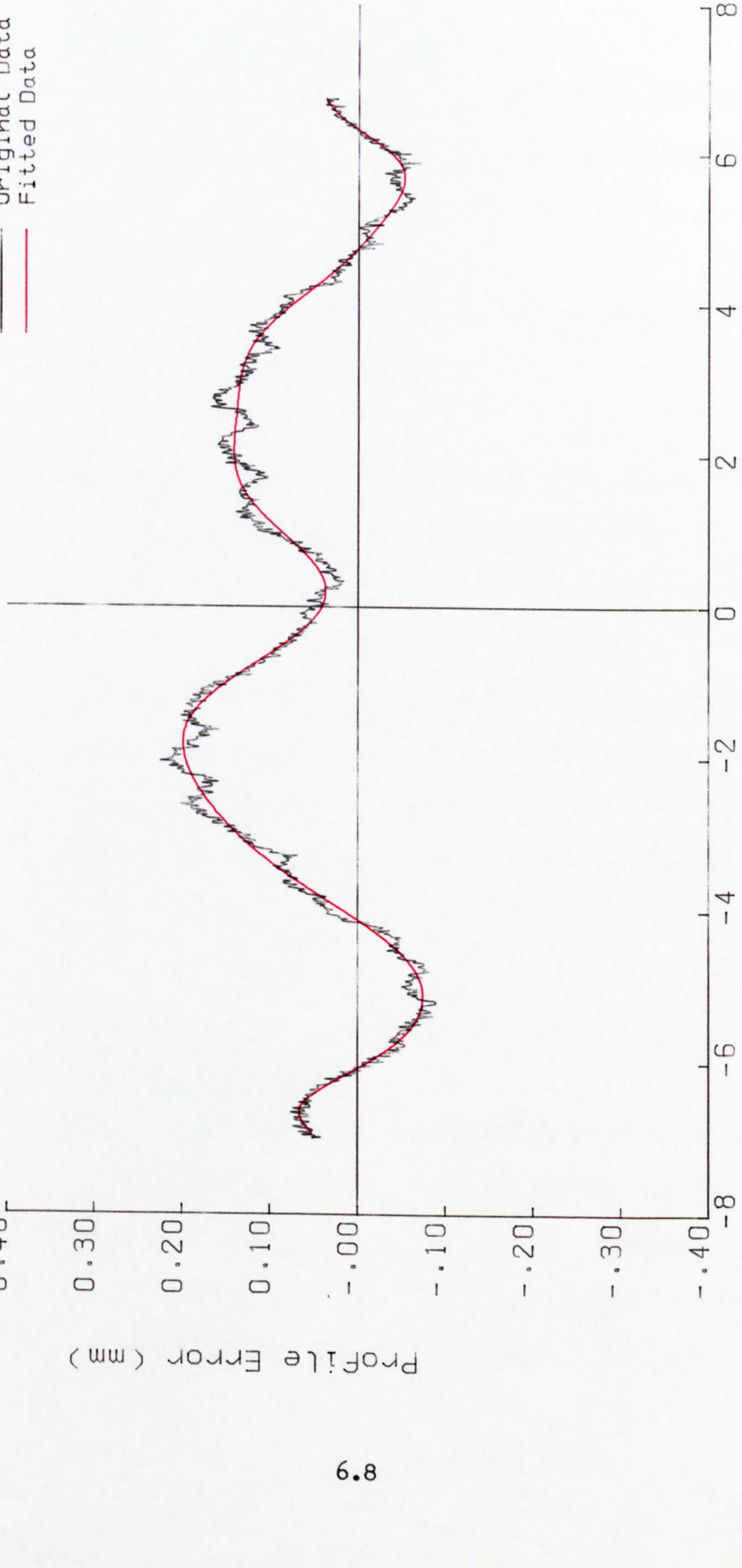
Original Data
Fitted Data
Lense Radius (mm)
8
6
4
2
0
-2
-4
-6
-8
Lens A15 - 23rd order polynomial Fit
Least Square Error = .1192E-4
Profile Error (mm)
X10-3
0.40
0.30
0.20
0.10
-.00
-.10
-.20
-.30
-.40

FIGURE 6.6

6.3

Harmonic Content of the Signal

Thus, it became necessary to examine other ways of representing the error profile. Typically the error profile consists of:

(a) Slow variation

(b) Localised features e.g. peaks, troughs, etc.

(c) High frequency noise

Each error profile may be regarded as a signal. The signal can be unambiguously represented by its frequency content, which is bound to take into account the features mentioned in (a), (b) and (c) above. The availability of Fast Fourier Transform (FFT) software makes this task relatively easy. Since there are about a 1000 data points per error profile, we can go up to 512 harmonics. Whether all the 512 harmonics need to be considered raises an issue for further investigation.

6.4

Information Content

In principle the variation of MTF (energy) from one lens to another must be due to the corresponding variation in the characteristics of the error profile. Further, the variations in the error profile must be characterised by the variation in the harmonic content of the signal. Thus, for a given set of

profiles the harmonics displaying maximum variation must be the ones containing the maximum information. The harmonics which show very little variation can therefore be discarded without a serious loss of information. These facts provide us with a simple yet effective method to perform data compression on the error profiles.

The harmonic content of each error profile is obtained by using the FFT program. The variance (or standard deviation) for each harmonic was then found. A set of such results are shown in the Table of Fig. 6.7. A sort program is used to arrange the standard deviation in descending order of magnitude (see Table of Fig. 6.8). The same result is depicted in a graphical form in Fig. 6.9. Thus, it may be deduced, that each error profile could be represented without significant loss of information by utilising the first few harmonics. This is a satisfying result, since the experience of optical engineers suggests that very high frequency components on the surface of the lens do not contribute to the image distortion. The high frequency noise merely reduces transmission.

6.5 Validation

In order to validate the preceding discussion, the error profile for each lens was first re-constructed using only

LENS	HARMONIC NUMBER 1	2	3	4	5	6	7	8	9	10
A 3	0.47029E-04	0.62860E-04	0.10502E-04	0.13877E-04	0.56251E-05	0.76944E-05	0.36888E-05	0.41926E-05	0.42090E-05	0.35471E-05
A 4	0.33803E-04	0.44033E-04	0.67472E-05	0.52835E-05	0.76114E-05	0.25660E-05	0.39940E-05	0.19960E-05	0.37688E-05	0.33444E-05
A 5	0.74726E-04	0.55184E-05	0.75350E-05	0.12041E-04	0.22384E-04	0.10772E-04	0.43324E-05	0.57443E-05	0.28753E-05	0.22265E-05
A 6	0.96596E-05	0.25126E-04	0.36156E-04	0.98040E-05	0.12255E-04	0.37484E-05	0.79223E-05	0.19878E-05	0.13038E-05	0.20208E-05
A 7	0.78710E-04	0.53591E-05	0.31423E-04	0.77458E-05	0.14939E-04	0.33604E-05	0.66645E-05	0.69624E-06	0.35040E-05	0.37167E-05
A 8	0.14265E-04	0.23091E-04	0.13708E-04	0.36922E-05	0.66875E-05	0.34666E-05	0.23122E-05	0.87994E-06	0.39581E-05	0.48157E-05
A 9	0.25025E-04	0.27951E-04	0.25271E-04	0.63128E-05	0.58254E-05	0.16161E-05	0.66148E-05	0.17202E-05	0.26108E-05	0.24242E-05
A10	0.80829E-04	0.13226E-04	0.19155E-04	0.76773E-05	0.49250E-05	0.68958E-05	0.39615E-05	0.42613E-05	0.27169E-05	0.22571E-05
A11	0.99086E-04	0.37191E-05	0.19836E-04	0.53465E-05	0.82798E-05	0.35744E-05	0.57386E-05	0.28414E-05	0.93799E-06	0.40796E-05
A12	0.17235E-04	0.75931E-05	0.91368E-05	0.15581E-04	0.11631E-05	0.27010E-05	0.82672E-05	0.62528E-05	0.19568E-06	0.46978E-05
A13	0.69681E-04	0.14979E-04	0.28470E-04	0.11555E-04	0.16028E-04	0.58799E-05	0.51619E-05	0.22406E-05	0.44359E-05	0.37555E-05
A14	0.11827E-04	0.56212E-05	0.24299E-04	0.74654E-05	0.70123E-05	0.26262E-05	0.52427E-05	0.29277E-05	0.46376E-05	0.23059E-05
A15	0.39164E-04	0.15511E-04	0.34675E-04	0.58601E-05	0.93562E-05	0.14104E-05	0.20596E-05	0.12417E-05	0.10975E-05	0.41798E-06
A16	0.36084E-04	0.19397E-04	0.23324E-04	0.69734E-05	0.10137E-04	0.97982E-06	0.74087E-05	0.19617E-05	0.17279-05	0.26706E-05
A17	0.18568E-04	0.43747E-05	0.24318E-04	0.13339E-04	0.13104E-04	0.69346E-05	0.94426E-05	0.22505E-05	0.19590E-05	0.61252E-05

HARMONIC CONTENT OF EACH PROFILE

FIGURE 6.7

....Continued

	HARMONIC NUMBER (continuation)									
LENS	1	2	3	4	5	6	7	8	9	10
A18	0.17265E-03	0.16985E-04	0.32396E-04	0.10149E-04	0.11719E-04	0.15581E-05	0.45717E-05	0.38709E-06	0.44453E-05	0.27570E-05
A19	0.98195E-04	0.17331E-04	0.32130E-04	0.61205E-05	0.10139E-04	0.37562E-05	0.28559E-05	0.23578E-05	0.11486E-05	0.15951E-05
A20	0.67381E-05	0.26651E-04	0.23525E-04	0.27987E-05	0.92761E-05	0.26874E-05	o.74222E-05	0.13983E-05	0.47079E-06	0.26203E-05
A21	0.84397E-04	o.58460E-04	0.37058E-04	0.37624E-05	0.11760E-05	0.41949E-05	0.39607E-05	o.20009E-05	0.13177E-05	0.29006E-05
A22	0.46341E-04	0.20218E-04	0.30225E-04	0.58523E-05	0.62620E-05	0.23846E-05	0.29872E-05	0.30587E-05	0.11324E-05	0.17819E-05
A23	0.23114E-04	0.36637E-04	0.24491E-04	0.67954E-05	0.89774E-05	0.48852E-05	0.46993E-05	0.41592E-05	0.21687E-05	0.26586E-05
A24	0.29108E-04	0.35043E-05	0.25719E-04	0.14967E-04	0.84193E-05	0.19600E-05	0.37188E-05	0.28004E-06	0.10255E-05	0.16238E-05
A25	0.21216E-04	0.10652E-04	0.24897E-04	0.93219E-05	0.61577E-05	0.16462E-05	0.21005E-05	0.22346E-05	0.10486E-05	0.15571E-05
A26	0.22651E-04	0.1175E-04	0.30733E-04	0.45219E-05	0.84522E-04	0.45412E-05	0.39721E-04	0.28074E-05	0.15583E-05	0.50148E.06
A27	0.88745E-05	0.45790E-05	0.37100E-04	0.68553E-05	0.46543E-05	0.37672E.05	0.36349E-05	0.20848E-05	0.69469E-06	0.21235E-06
A28	0.70258E-04	0.80590E-04	0.56894E-04	0.10818E-04	0.28297E-05	0.92073E-06	0.16242E-05	0.12078E-05	0.13574E-05	0.62500E-06
A29	0.98582E-04	0.29295E-04	0.28523E-04	0.11806E-04	0.28545E-05	0.43731E-04	0.10780E-05	0.32699E-05	0.16635E-05	0.13762E-05
A30	0.12352E-04	0.21821E-04	0.21947E-04	0.92110E-05	0.67141E-05	0.22992E-05	0.17160E-05	0.21170E-05	0.29051E-05	0.13135E-04
A31	0.11505E-03	0.19465E-04	0.40462E-04	0.92721E-05	0.12440E-04	0.11086E-05	0.77850E-05	0.18048E-05	0.18000E-05	0.38969E-05
A32	0.10955E-03	0.35378E-04	0.38605E-04	0.10541E-04	0.10338E-04	0.15809E-05	0.60133E-05	0.12323E-05	0.18020E-05	0.10378E-05
A33	0.19690E-03	0.10401E-04	0.35056E-04	0.12881E-04	0.15735E-04	0.24883E-05	0.87741E-05	0.17525E-05	0.12496E-05	0.43329E-05
A34	0.24029E-04	0.47284E-04	0.41896E-04	0.13454E-04	0.67931E-05	0.28242E-05	0.48859E-05	0.11406E-05	0.21805E-06	0.64849E-06
STD. DEV.	0.47754E-04	0.19389E-04	0.10871E-04	0.35133E-05	0.45574E-05	0.22050E-05	0.22677E-05	0.13926E-05	0.13136E-05	0.14485E-05

ORDER	HARMONIC No.	STANDARD DEVIATION	PERCENTAGE
1	1	0.47754E-04	100.00%
2	2	0.19389E-04	40.60%
3	3	0.10871E-04	22.76%
4	5	0.45574E-05	9.54%
5	4	0.35133E-05	7.36%
6	7	0.22677E-05	4.75%
7	6	0.22050E-05	4.62%
8	11	0.16576E-05	3.47%
9	10	0.14485E-05	3.03%
10	8	0.13926E-05	2.92%
11	20	0.13781-05	2.89%
12	13	0.13481E-05	2.82%
13	9	0.13136E-05	2.75%
14	12	0.11818E-05	2.47%
15	108	0.11756E-05	2.46%
16	418	0.11477E-05	2.40%
17	21	0.11309E-05	2.37%
18	22	0.11136E-05	2.33%
19	286	0.10788E-05	2.26%
20	249	0.10702E-05	2.24%

SORTED STANDARD DEVIATIONS

FIGURE 6.8

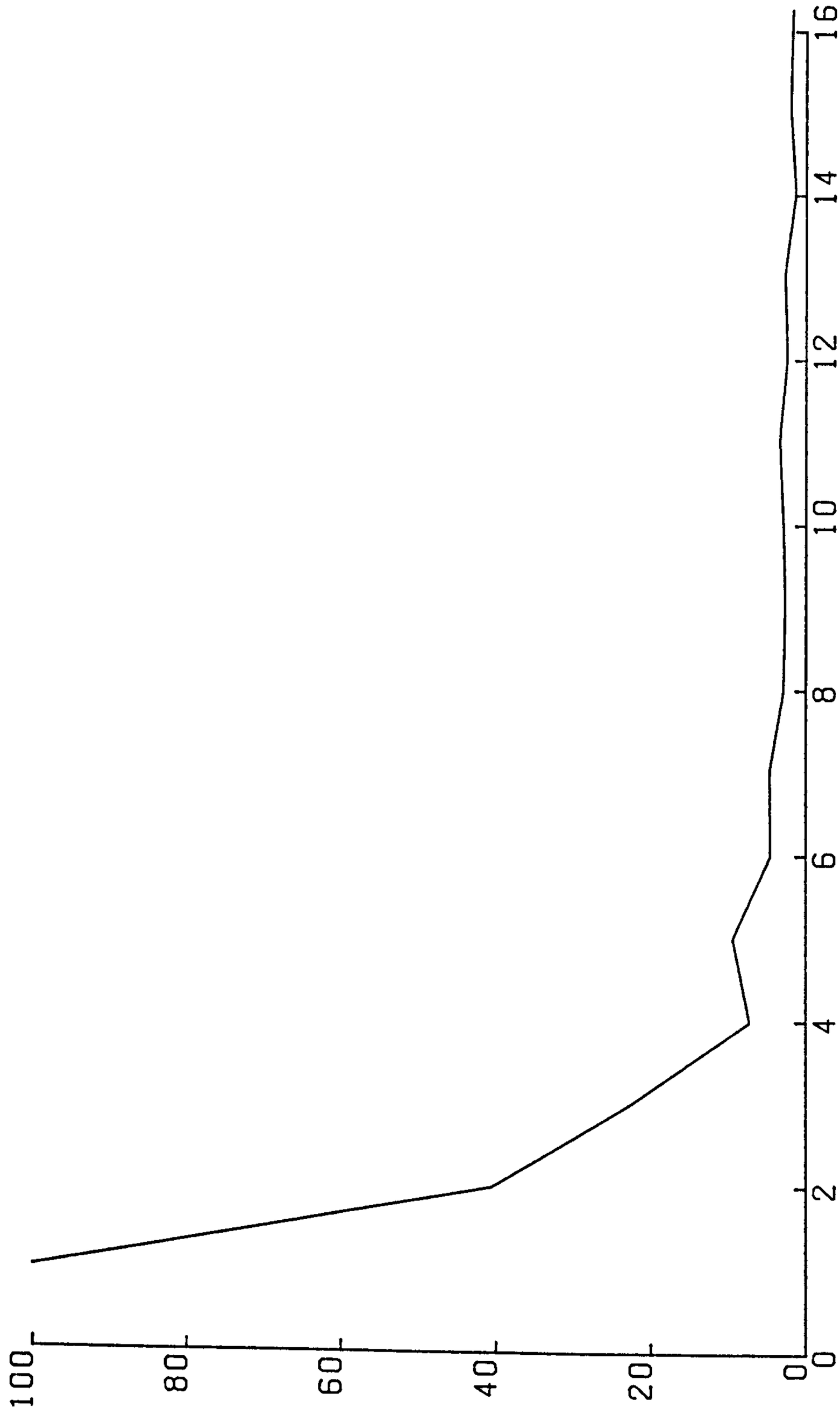
Normalised Std. Dev.
0
20
40
60
80
100
Standard Deviations as a Relative Measure
2
4
6
8
10
12
14
16
Harmonic Number

FIGURE 6.9

the 1st harmonic. The least square error from the original profile was computed. This procedure was repeated by increasing the number of harmonics by one. A set of typical results is shown in tabular and in graphical form in Figs. 6.10 to 6.15. A typical set of reconstructed error profiles using first 10 harmonics, are also shown in Figs. 6.16 to 6.18. This representation hence appears to be fairly satisfactory.

The reduction of optical energy i.e. area under the MTF curve is due to the error profile. It is therefore best to consider the energy content of each harmonic rather than its amplitude. There is a further advantage; the full description of a signal consists of not only the amplitude but also phase. By using energy the need to deal with the phase is eliminated.

The total energy $\propto a_1^2 + a_2^2 + a_3^2 + \ldots a_n^2$

where a_1 a_2 . . . a_n are the amplitude values. From the previous discussion if the first 10 harmonics are considered to contribute the total energy then the penalty in terms of accuracy is small. The energy in each harmonic can then be represented as percentage of the total. By the way of example a section of such results is shown in the table of Fig.6.19. Since the dominating harmonics are the first 2 or 3 harmonics, one might expect some correlation between the lower order

No. OF HARMONICS	LEAST SQUARE ERROR
1	0.147603E+05
1 to 2	0.400547E+04
1 to 3	0.694581E+03
1 to 4	0.870661E+02
1 to 5	0.854211E+01
1 to 6	0.687414E+00
1 to 7	0.455526E-01
1 to 8	0.301798E-02
1 to 9	0.270886E-03
1 to10	0.722102E-04

REDUCTION IN LEAST SQUARE ERROR WITH INCREASING HARMONICS - LENS A7

FIGURE 6.10

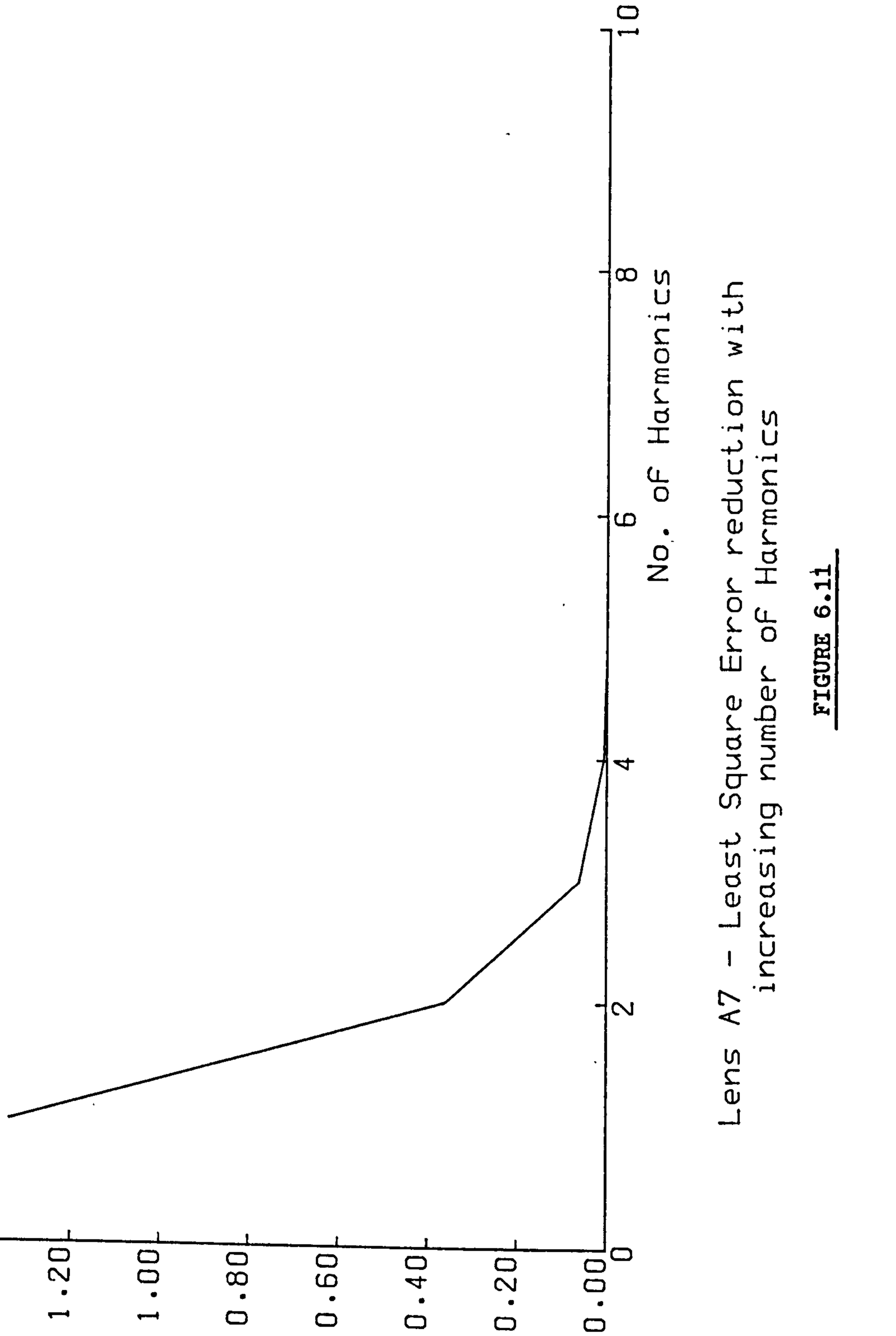
Lens A7 - Least Square Error reduction with increasing number of Harmonics
Least Sq. Error
X10^5
1.60
1.40
1.20
1.00
0.80
0.60
0.40
0.20
0.00
0
2
4
6
8
10
No. of Harmonics

FIGURE 6.11

No. OF HARMONICS	LEAST SQUARE ERROR
1	0.623514E+05
1 to 2	0.169200E+05
1 to 3	0.293411E+04
1 to 4	0.367754E+03
1 to 5	0.361053E+02
1 to 6	0.289066E+01
1 to 7	0.197002E+00
1 to 8	0.111603E-01
1 to 9	0.679774E-03
1 to10	0.124284E-04

REDUCTION IN LEAST SQUARE ERROR WITH INCREASING HARMONICS - LENS A9

FIGURE 6.12

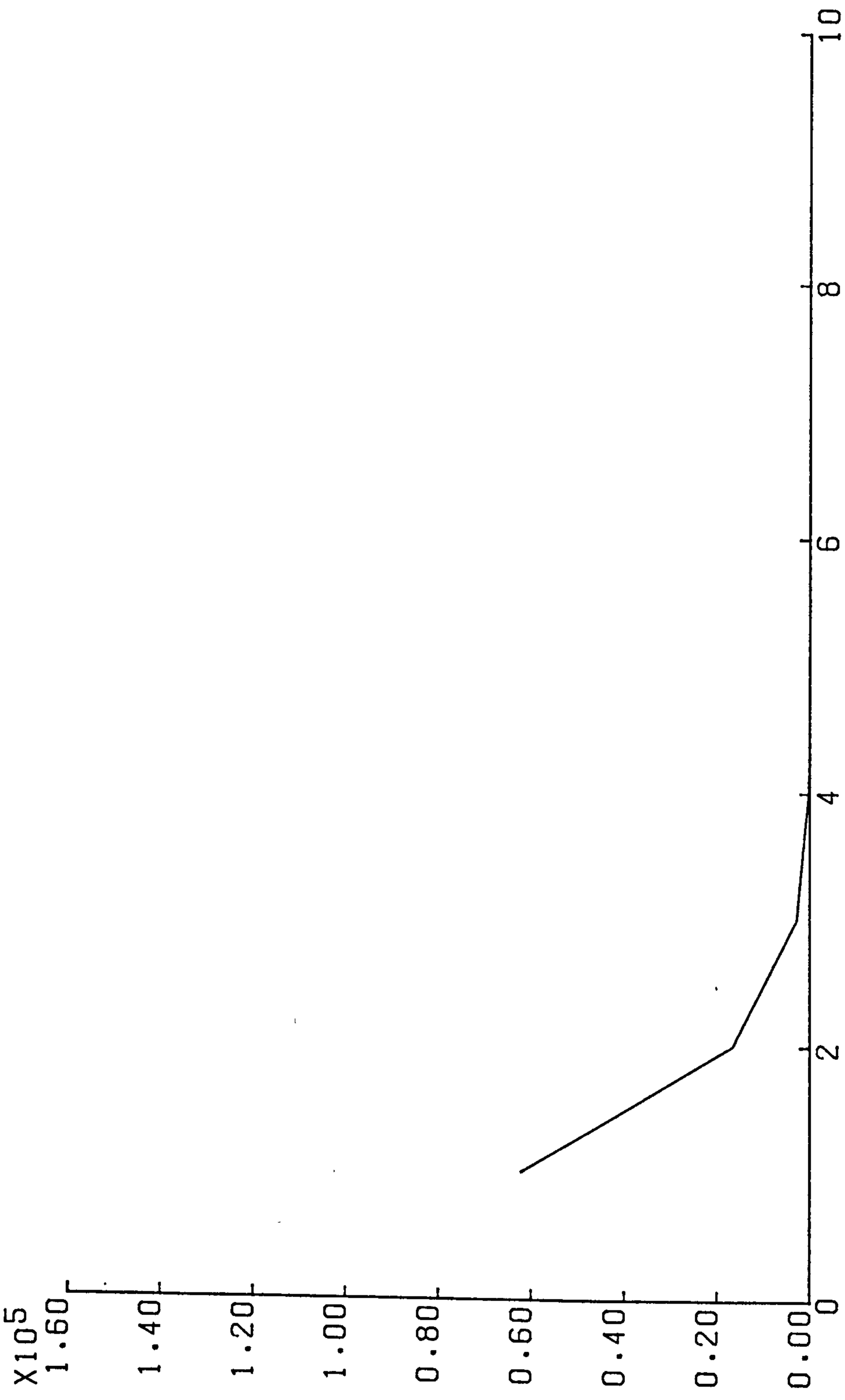
Lens A9 - Least Square Error reduction with increasing number of Harmonics
Least Sq. Error
X10^5
1.60
1.40
1.20
1.00
0.80
0.60
0.40
0.20
0.00
0
2
4
6
8
10
No. of Harmonics

FIGURE 6.13

No. OF HARMONICS	LEAST SQUARE ERROR
1	0.142364E+06
1 to 2	0.386325E+04
1 to 3	0.669932E+04
1 to 4	0.839675E+03
1 to 5	0.824360E+02
1 to 6	0.660095E+01
1 to 7	0.449448E+00
1 to 8	0.255392-01
1 to 9	0.151487E-02
1 to10	0.948492E-05

REDUCTION IN LEAST SQUARE ERROR WITH INCREASING HARMONICS - LENS A11

FIGURE 6.14

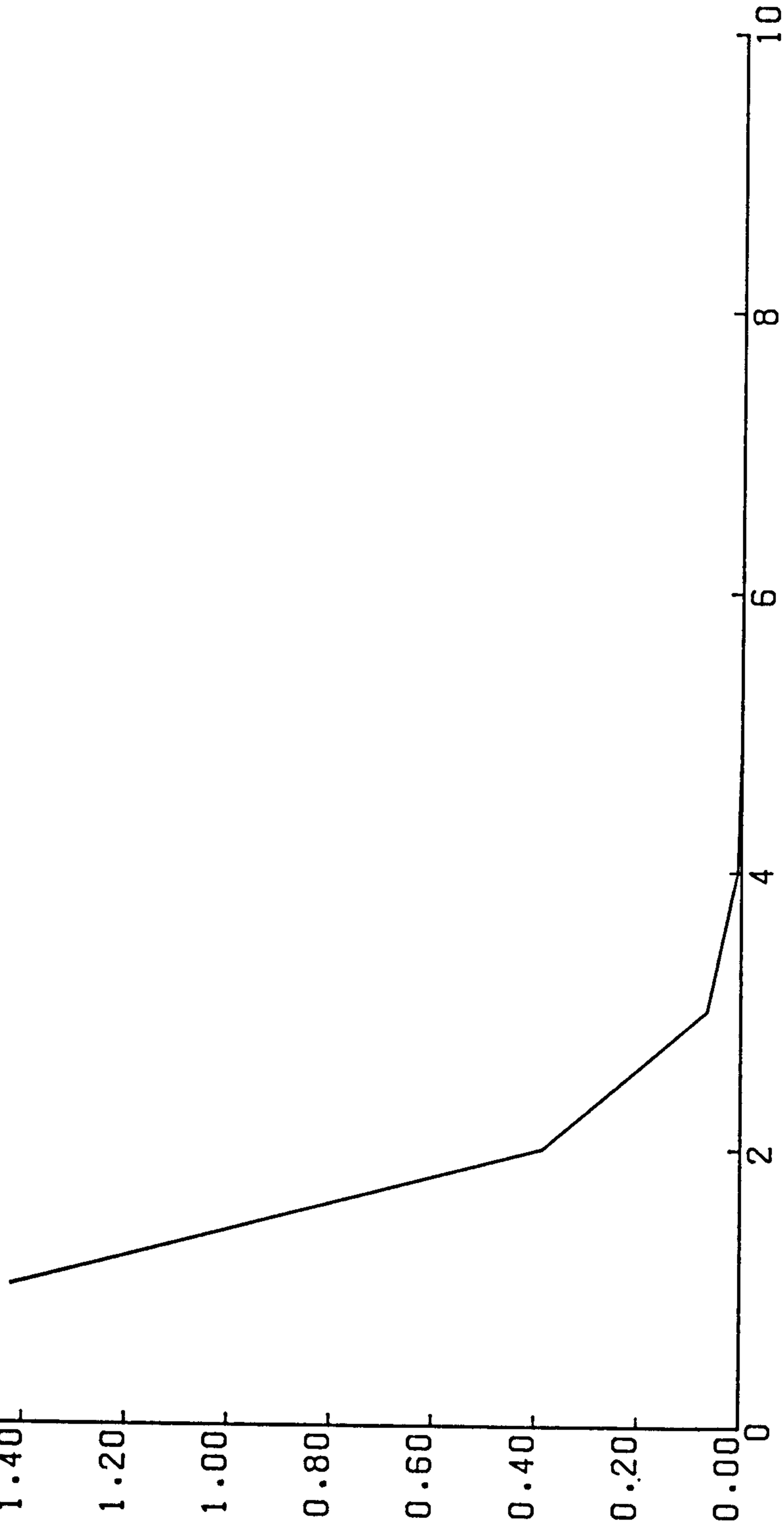
Lens A11 - Least Square Error reduction with increasing number of Harmonics
Least Sq. Error
X10^5
1.60
1.40
1.20
1.00
0.80
0.60
0.40
0.20
0.00
0
2
4
6
8
10
No. of Harmonics

FIGURE 6.15

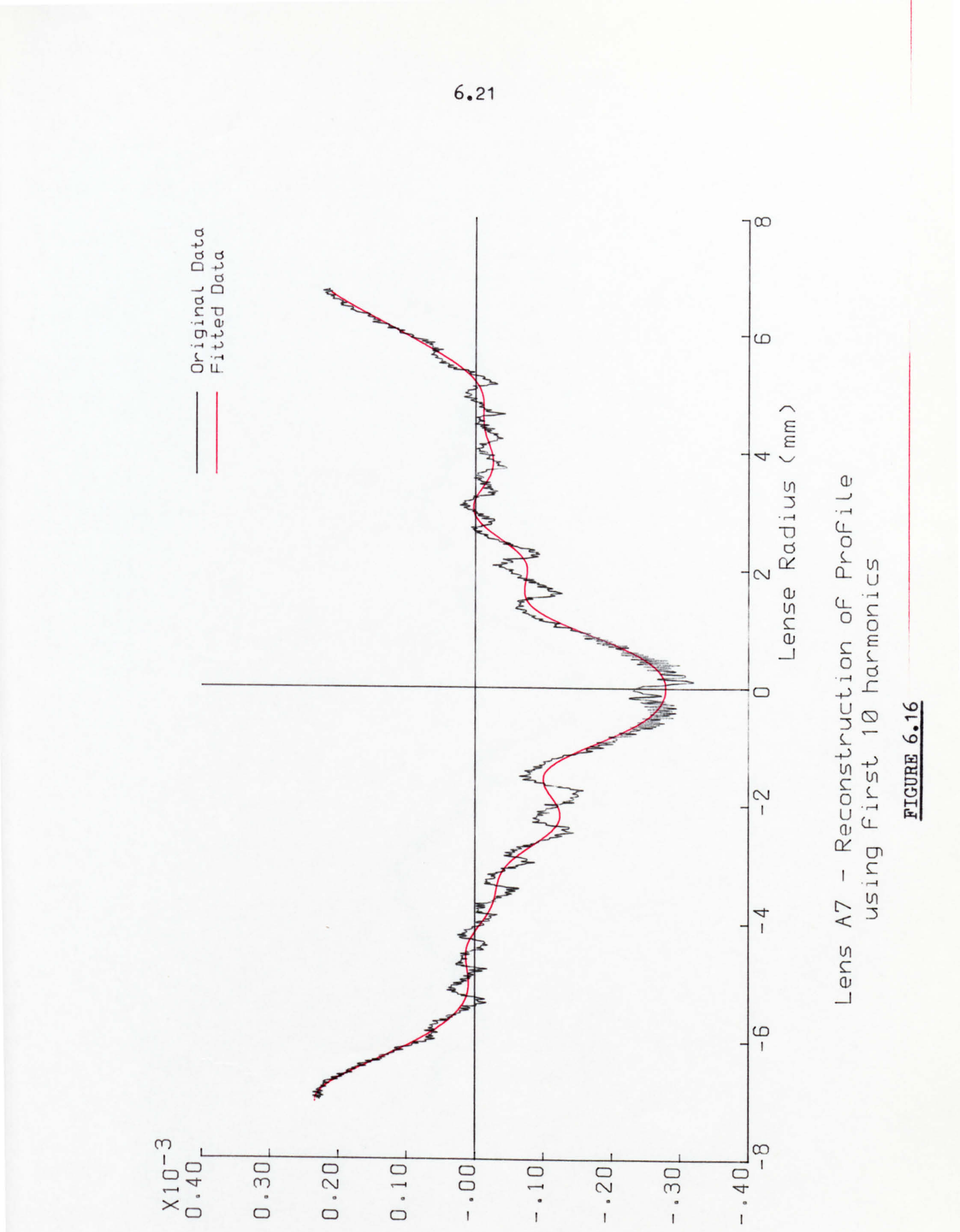

Lens A7 - Reconstruction of Profile
using First 10 harmonics

FIGURE 6.16

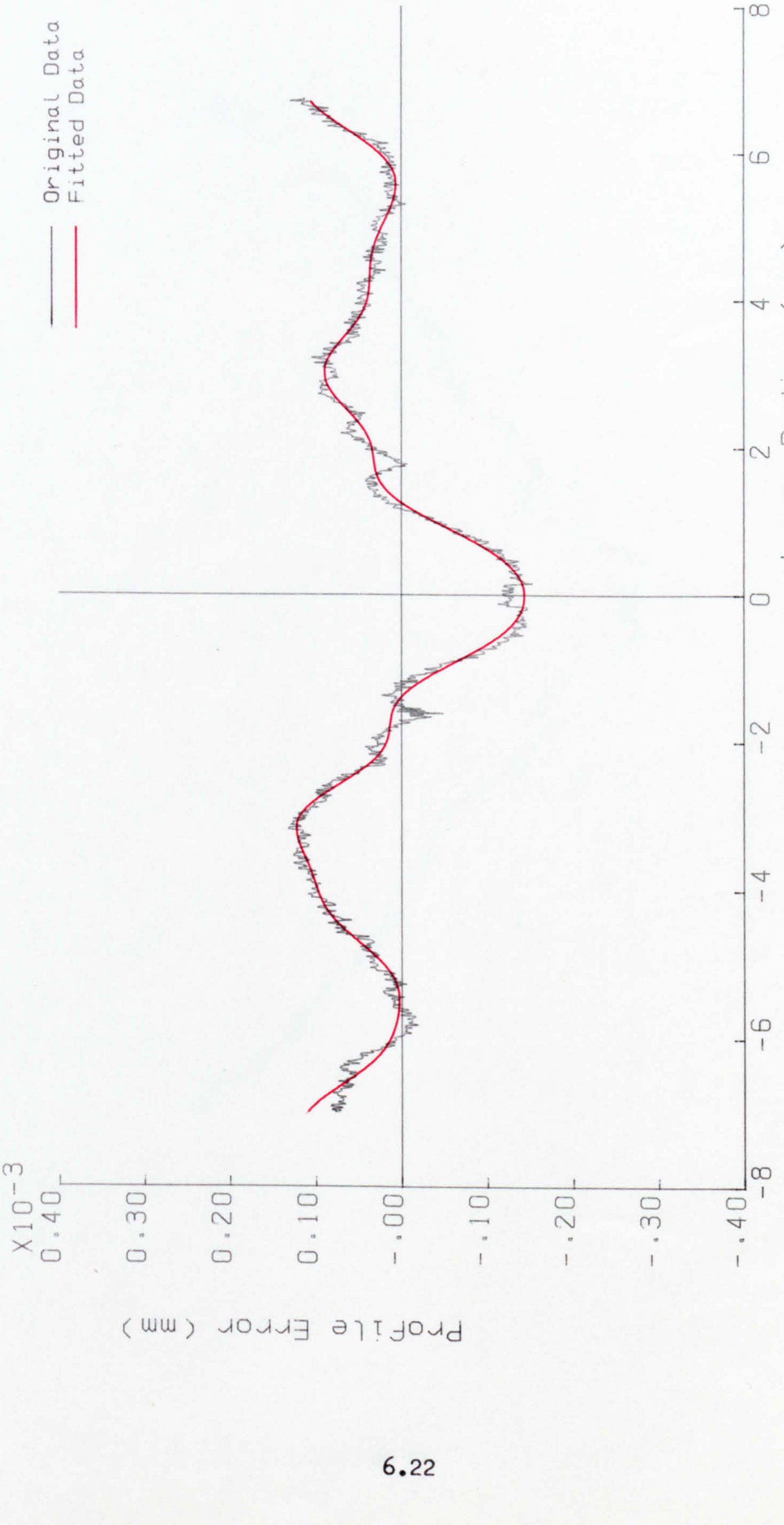

Lens A9 - Reconstruction of Profile
using First 10 harmonics

FIGURE 6.17

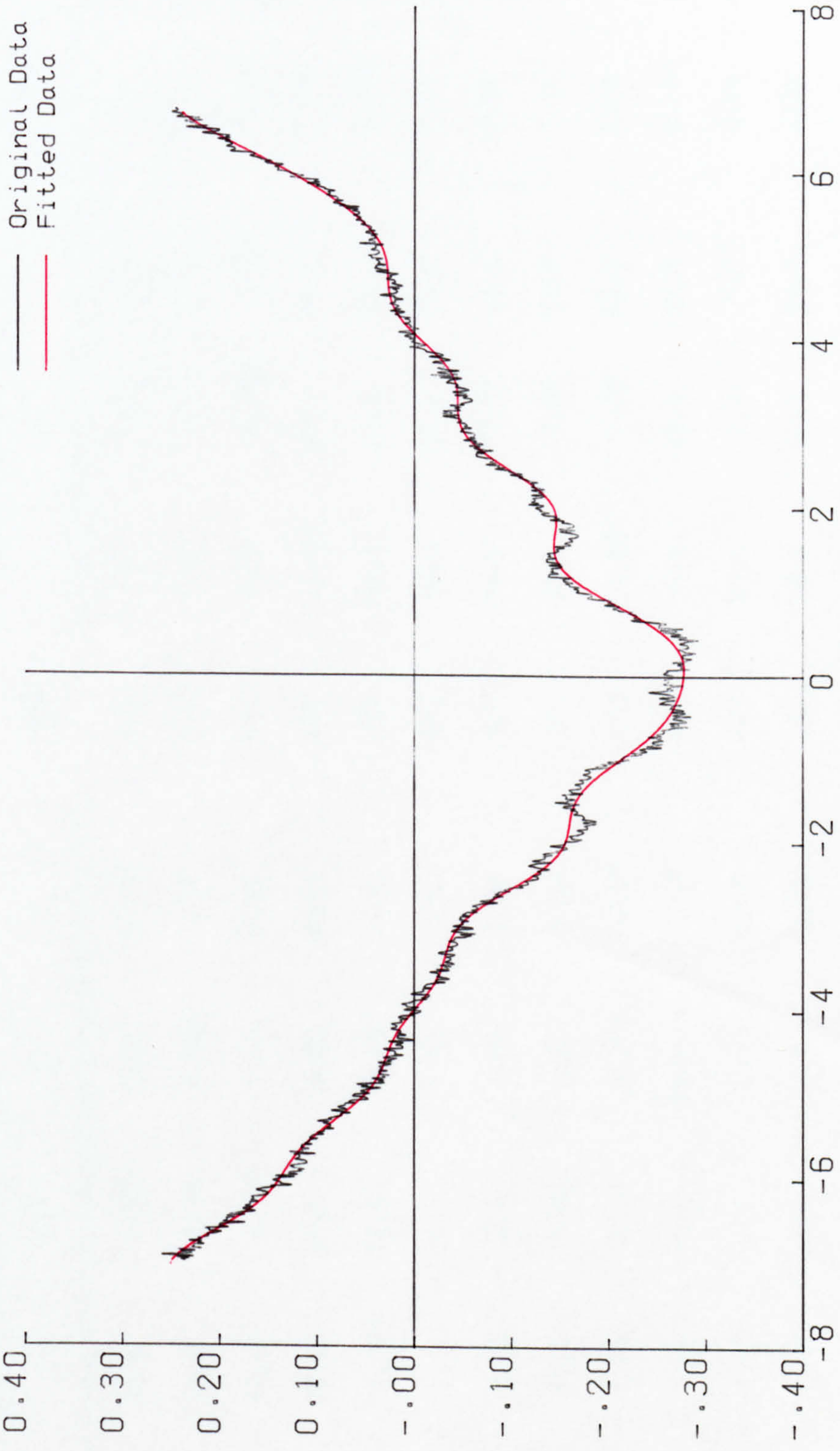

Lens A11 - Reconstruction of Profile
using First 10 harmonics

FIGURE 6.18

LENS	ENERGY % IN HARMONIC					LENS	ENERGY % IN HARMONIC				
	1	2	3	4	5		1	2	3	4	5
A 3	33.4	59.6	1.79	2.91	0.477	A16	7.7	13.8	30.4	1.78	3.76
A 4	35.0	59.4	1.39	0.849	1.77	A17	23.2	1.29	39.7	12.0	11.5
A 5	58.7	32.0	0.597	1.52	5.27	A18	94.8	0.918	3.34	0.328	0.437
A 6	3.95	26.7	55.3	4.06	6.35	A20	3.08	48.2	37.5	0.531	5.84
A 7	81.8	0.379	13.0	0.792	2.95	A22	60.1	11.4	25.6	0.959	1.06
A 8	19.6	51.3	18.1	1.31	4.30	A23	19.9	50.1	22.4	1.72	3.01
A 9	74.1	3.50	16.3	1.02	3.76	A25	34.0	8.57	46.8	6.56	2.86
A10	90.1	2.41	5.06	0.813	0.334	A26	29.8	7.26	54.9	1.19	4.15
A11	94.5	0.133	3.79	0.275	0.660	A27	4.99	1.33	87.3	2.98	1.37
A12	36.3	7.04	10.2	29.6	0.165	A28	33.4	43.9	21.9	0.791	0.0545
A13	76.1	3.52	12.7	2.10	4.03	A29	84.0	7.42	7.03	1.20	0.0704
A14	14.9	3.37	63.0	5.95	5.25	A30	12.1	37.7	38.1	6.72	3.57
A15	49.4	7.74	30.7	1.10	2.82	A31	85.0	2.43	10.5	0.552	0.994

6.24

6.24

PERCENTAGE DISTRIBUTION OF ENERGY IN EACH HARMONIC

FIGURE 6.19

harmonic content and the MTF.

The relative harmonic content versus MTF suggests little correlation (see Figs. 6.20 to 6.22). It is obvious that there may be other factors which need to be considered.

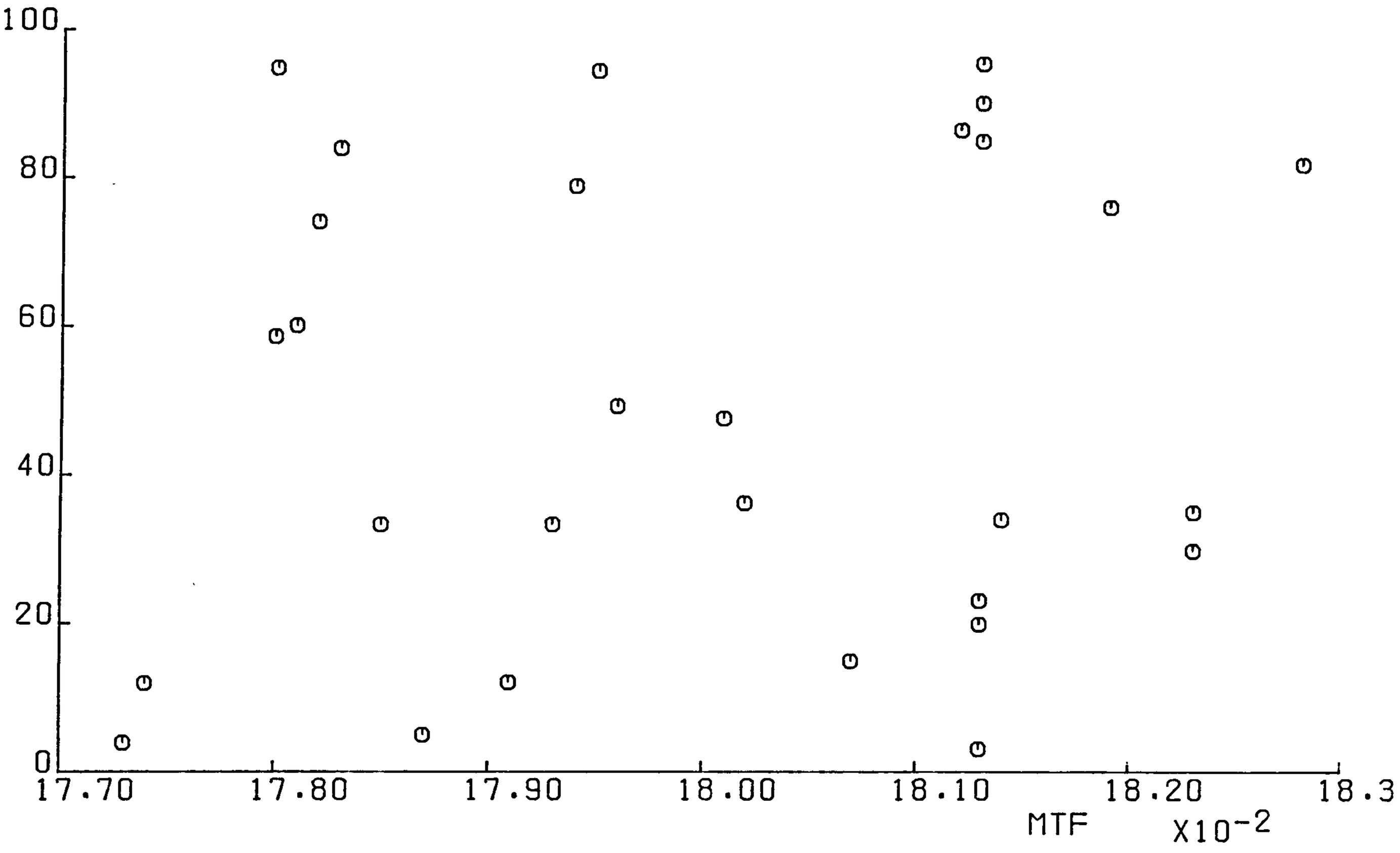

Energy in 1st harmonic against MTF
Correlation = 0.1097

FIGURE 6.20

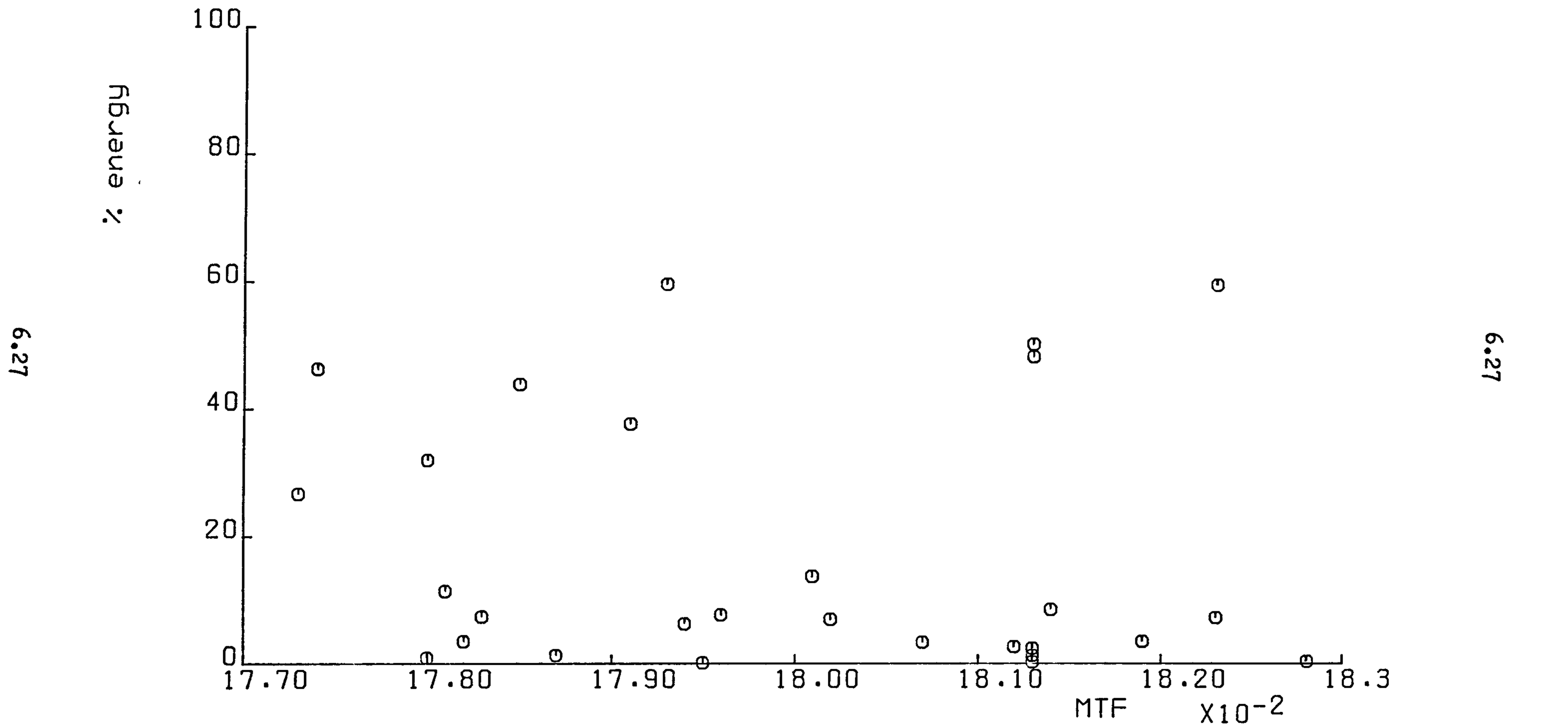

Energy in 2nd harmonic against MTF
correlation = -0.1453

FIGURE 6.21

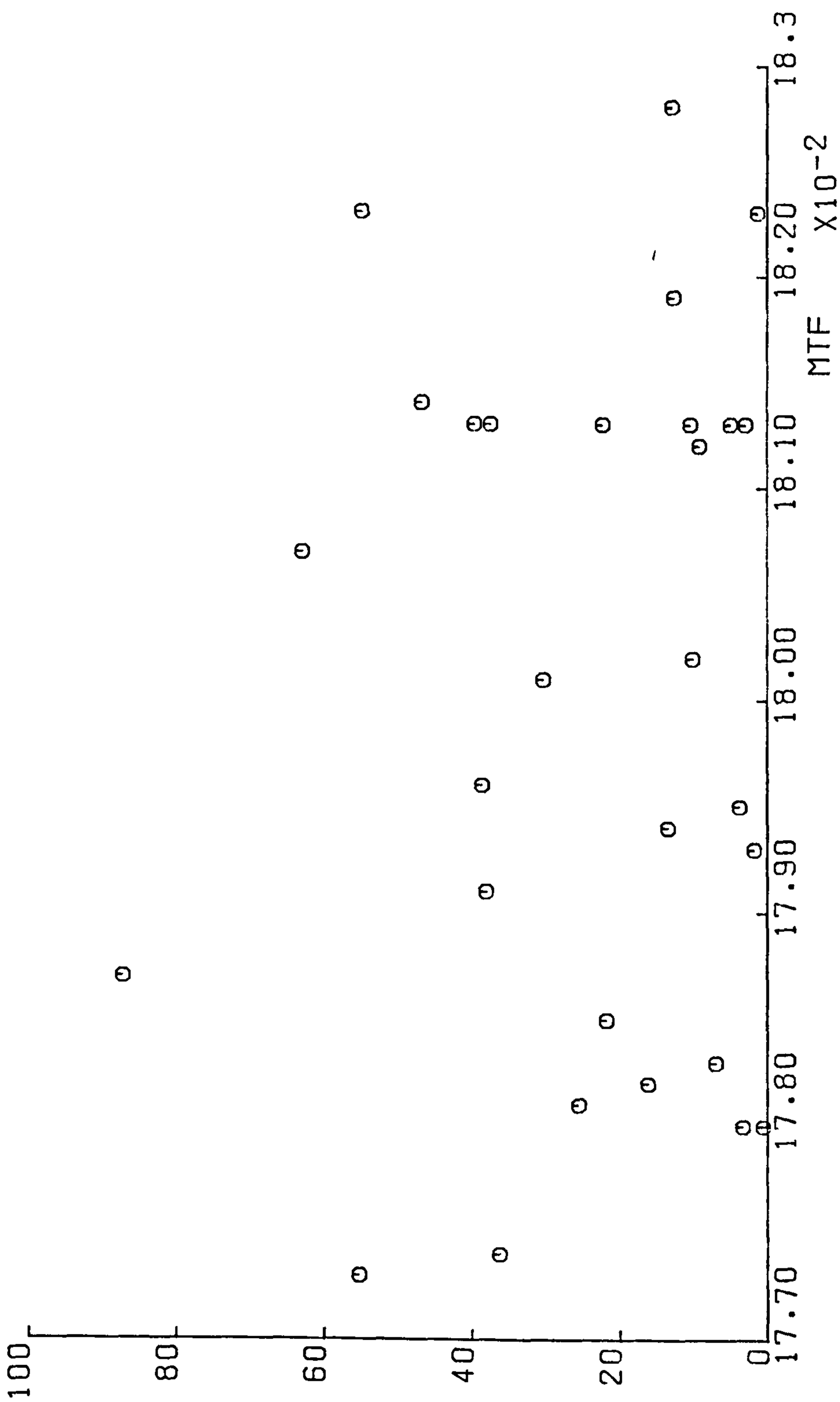
Energy in 3rd harmonic against MTF
correlation = -0.0816
% energy
MTF
X10-2
17.70
17.80
17.90
18.00
18.10
18.20
18.3
0
20
40
60
80
100

FIGURE 6.22

C H A P T E R V I I

RADIUS WEIGHTED PARAMETER

CHAPTER VII

RADIUS WEIGHTED PARAMETER

In light of the work already performed, a more searching look at the error profiles was needed.

7.1

Wavefront Error

One of the primary functions of a lens is to to convert plane waves into spherical wavefronts (see Fig. 7.1). Any error on the surface of the lens can therefore be expected to be present in the output wavefront. In other words the error profile is the wavefront error. In this respect there are two points of interest:

(a) A special case of such error might be small deviations in the radius of curvature of the lens profile. The effect of this error is merely to shift the focus point, as illustrated in Fig. 7.2. Provided this error is relatively small, it can be corrected simply by adjusting the lens position for best possible focus. This would correspond to maximum intensity (and hence energy) at the focus point. The MTF would therefore be independent of such an error. A mean line can hence be fitted to the data of interest (-7 mm to +7 mm). The effective error at any point on the lens can then be computed, as shown in Fig. 7.3.

(b) The energy transmitted by the lens is not uniform across

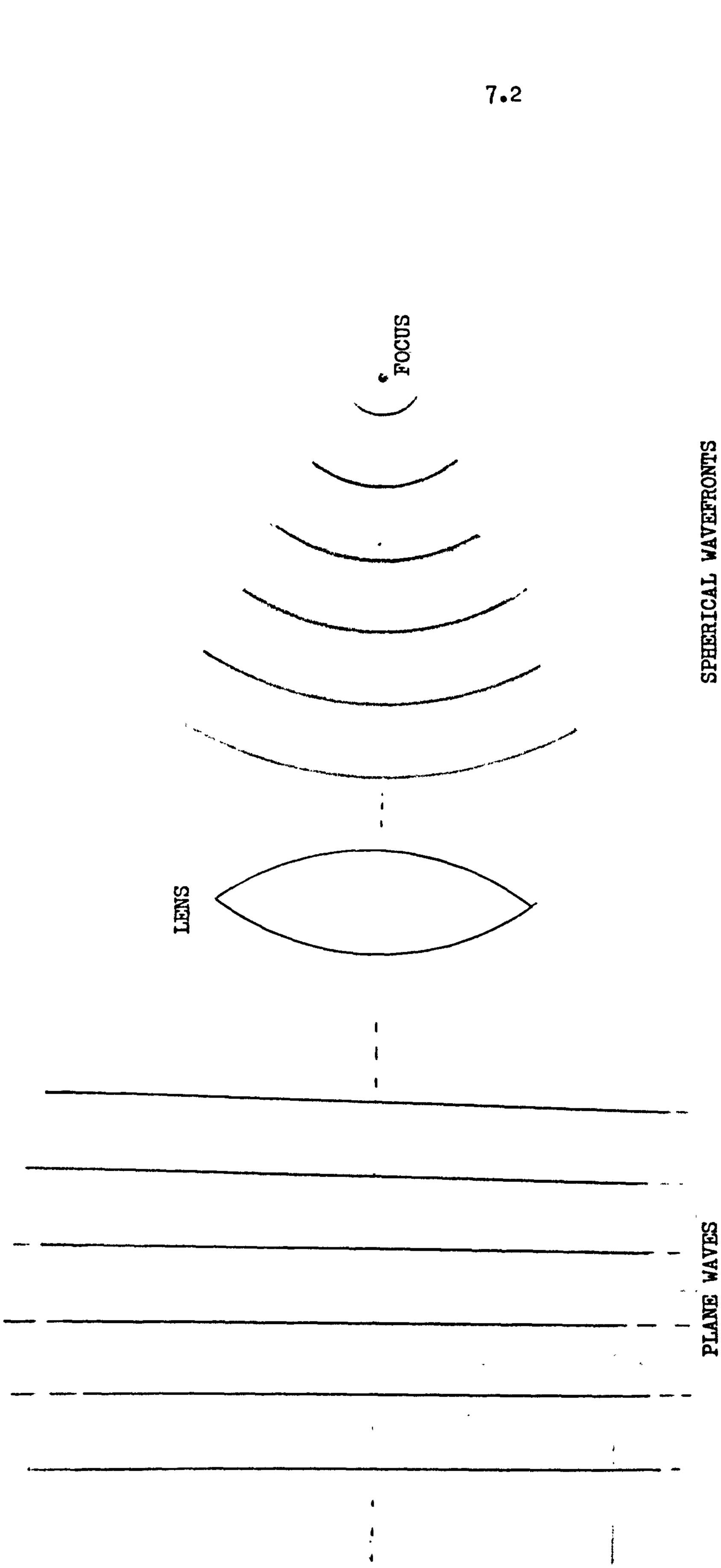

CONVERSION OF PLANE WAVES INTO SPHERICAL WAVES

FIGURE 7.1

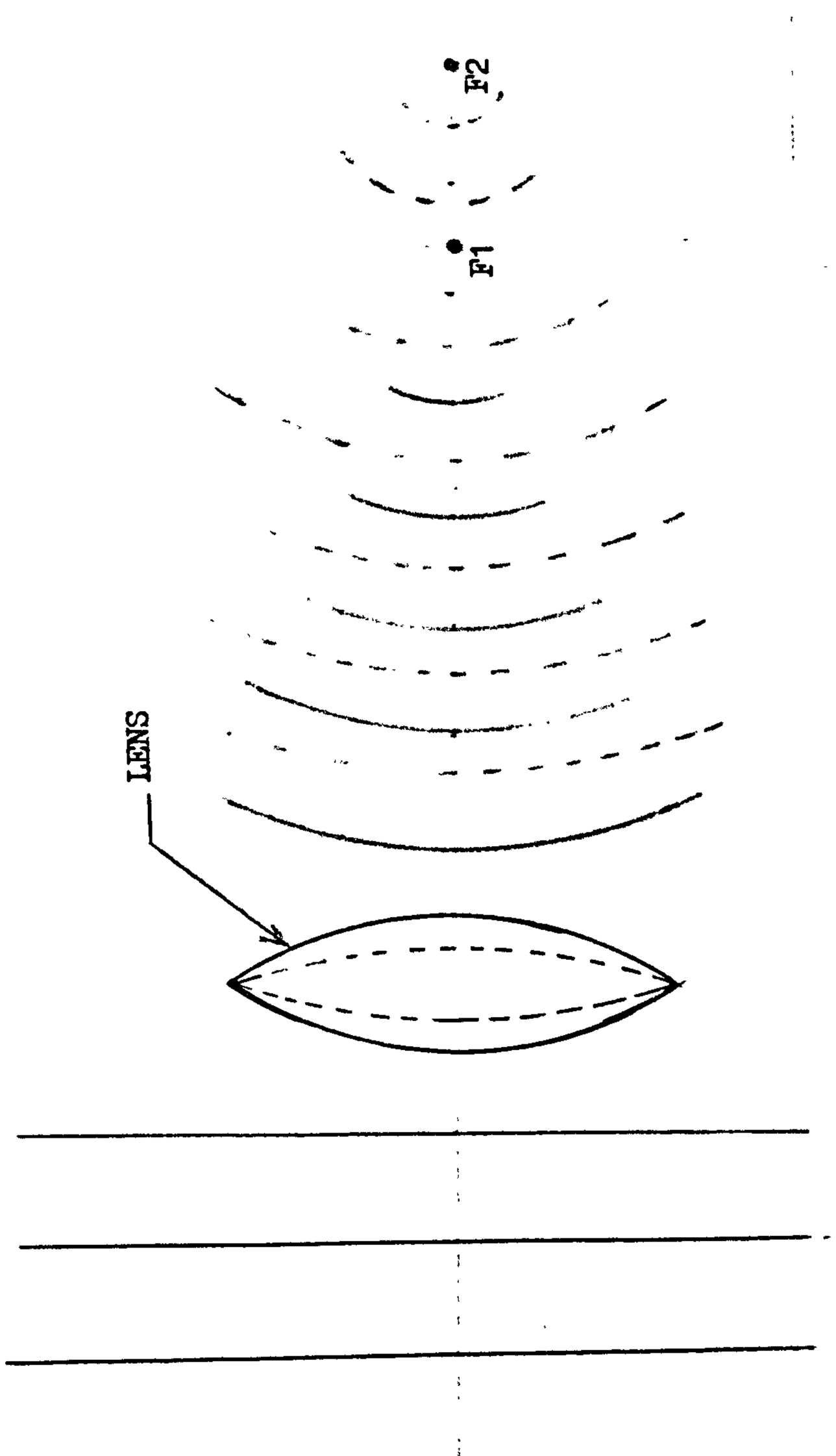

SHIFT OF FOCUS POINT

FIGURE 7.2

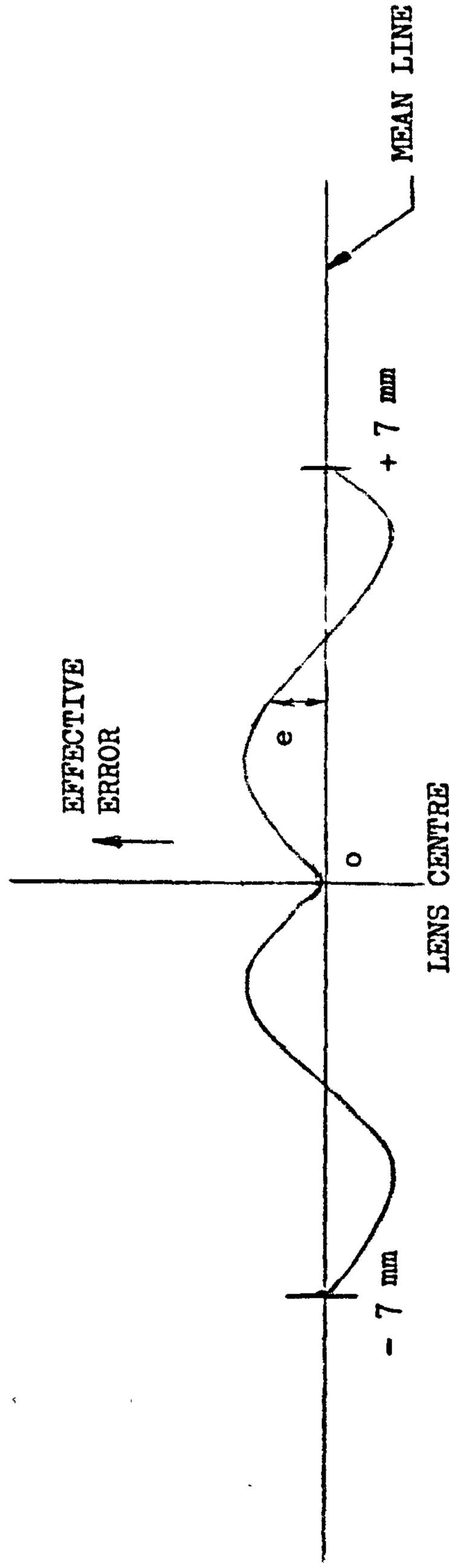
EFFECTIVE ERROR
MEAN LINE
+ 7 mm
e
EFFECTIVE ERROR
LENS CENTRE
o
- 7 mm

FIGURE 7.3

the surface of the lens (consider Fig. 7.4). Two elemental rings of thickness dr are shown at radial distance of R_1 and R_2 (note this radial distance is not radius of curvature mentioned earlier). The energies transmitted through these rings would be proportional to their respective areas A_1 and A_2. Since the area A of any such element ring at radial distance R

$$A = 2\Pi r\, dr$$

the corresponding energy $\propto$ R.

Hence, deformations of the lens profile at higher values of R must have a more serious effect on the MTF than deformations at lower values of R. Any mechanical parameter derived from the profile must therefore take this fact into account.

Such a parameter ought to show correlation with the MTF. A straight forward method would be to derive a radius weighted mean error.

7.2

Radius Weighting

A parameter named - radius weighted wavefront error (RWWE) was derived in the following way:

A straight line was fitted to the composite profile. The radius weighted wavefront error was then derived by weighting each

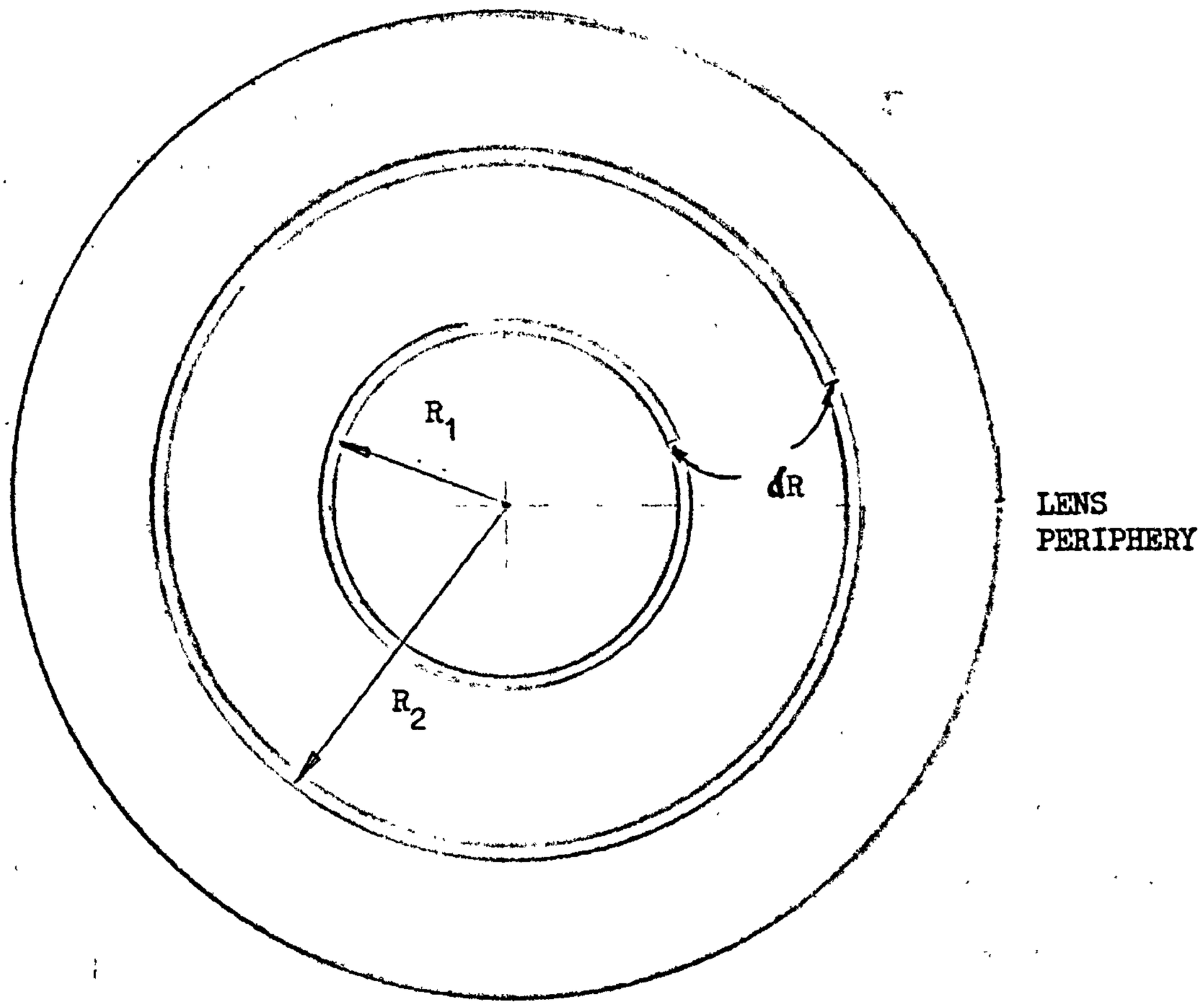

RADIAL DISTANCE ON LENS SURFACE

FIGURE 7.4

error value by its corresponding radial distance from the centre.

Thus RWWE $= \frac{1}{N} \sum_{n=1}^{n=N} \left| R_n x \; e_n \right|$ where N is the total number of error values considered. The radius weighted wavefront error (RWWE) for each lens together with MTF (energy) is shown in a tabular form in Fig. 7.5. A corresponding spot diagram is shown in Fig. 7.6. The inspection of the spot diagram suggests a rather general reduction of MTF with increasing RWWE. This observation at least points towards the right direction as far as the relation between RWWE and MTF is concerned.

However, the correlation between RWWE and the MTF figure turned out to be rather low - -0.17. Since the underlying trend appeared to be as expected, it was concluded that there has to be some secondary effect which the parameter such as RWWE has failed to take into account. It was hence decided to fit a suitable function to the spot diagram, with a view to make a more detailed study of this aspect. Perhaps a straight line fit might be suitable. It is, however, highly unlikely that in a practical situation the value of RWWE would become 0. At the same time it is highly unlikely that the MTF value would be 0, even for worst of the lenses. A search, therefore, was made for a suitable type of function.

LENS No.	MTF (ENERGY)	RWWE
3	0.1793	0.402E-03
4	0.1823	0.270E-03
5	0.1780	0.350E-03
6	0.1773	0.164E-03
7	0.1828	0.284E-03
9	0.1782	0.246E-03
10	o.1813	0.414E-03
11	0.1795	0.393E-03
12	0.1802	0.121E-03
13	0.1819	0.290E-03
14	0.1807	0.147E-03
15	0.1796	0.257E-03
16	0.1801	0.203E-03
17	0.1813	0.148E-03
18	0.1780	0.811E-03
19	0.1812	0.367E-03
20	0.1813	0.122E-03
22	0.1781	0.249E-03
23	0.1813	0.147E-03
25	0.1814	0.152E-03
26	0.1823	0.144E-03
27	0.1787	0.177E-03
28	0.1785	0.601E-03
29	0.1783	0.436E-03
30	0.1791	0.184E-03
31	0.1813	0.504E-03
32	0.1794	0.509E-03
33	0.1813	0.896E-03
34	0.1774	0.331E-03

MTF (ENERGY) AND CORRESPONDING RWWE

FIGURE 7.5

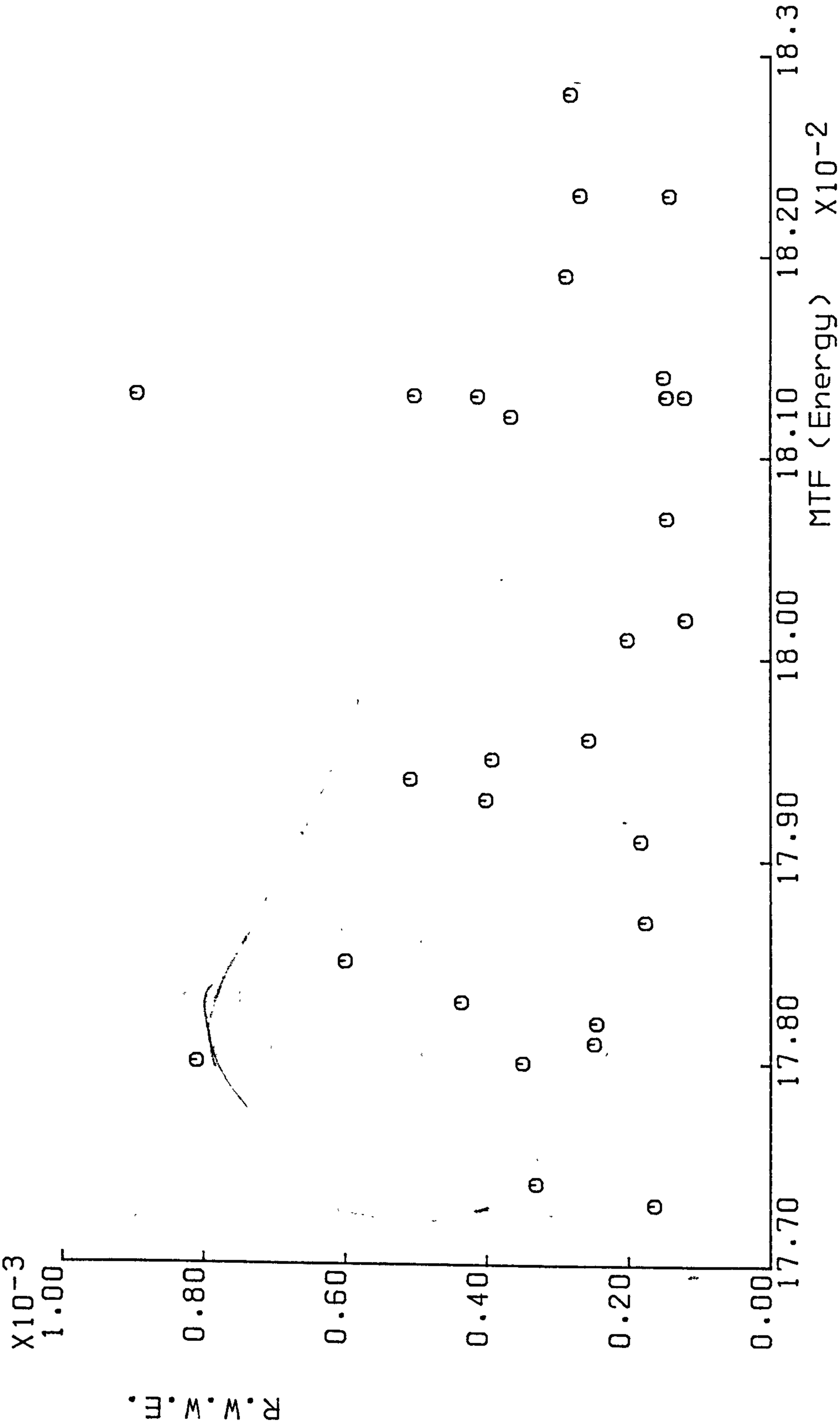
Spot Diagram RWE Vs MTF
R.W.W.E.
X10-3
1.00
0.80
0.60
0.40
0.20
0.00
17.70
17.80
17.90
18.00
18.10
18.3
X10-2
MTF (Energy)

FIGURE 7.6

7.3

Fitting a function

Several different types of functions were fitted to the data, and the least square error computed in each case. A function with least square error was chosen. The Table in Fig. 7.7 shows the type of function chosen and the corresponding value of the least square error. The function of the type $y = A + B/_X$ was hence fitted to the data as shown in Fig. 7.8.

7.4

Turning Points

An initial pilot study with a limited number of lenses suggested some relation of the MTF with the number of turning points in the error profile (see Appendix C). While the magnitude of the error is reflected in the parameter RWWE, the number of turning points would not be accounted for.

Suitable polynomials had already been fitted to the error profiles (Chapter VI). In order to find the number of turning points for any profile, the corresponding polynomial is differentiated twice to yield the first and second slope. The point at which the first differential is 0 marks the turning point. The number of such points in any given profile can be counted.

If we assume that the poor correlation of RWWE with MTF is

FUNCTION TYPE	LEAST SQUARE ERROR
$y = Ax$	0.109 E - 5
$y = A + Bx$	0.107 E - 5
$y = Ax^B$	0.113 E - 5
$y = A + B/x$	0.105 E - 5
$y = 1/(A + Bx)$	0.125 E - 5
$y = \frac{x}{(A + Bx)}$	0.126 E - 5

BEST FIT FOR RWWE VERSUS MTF

FIGURE 7.7

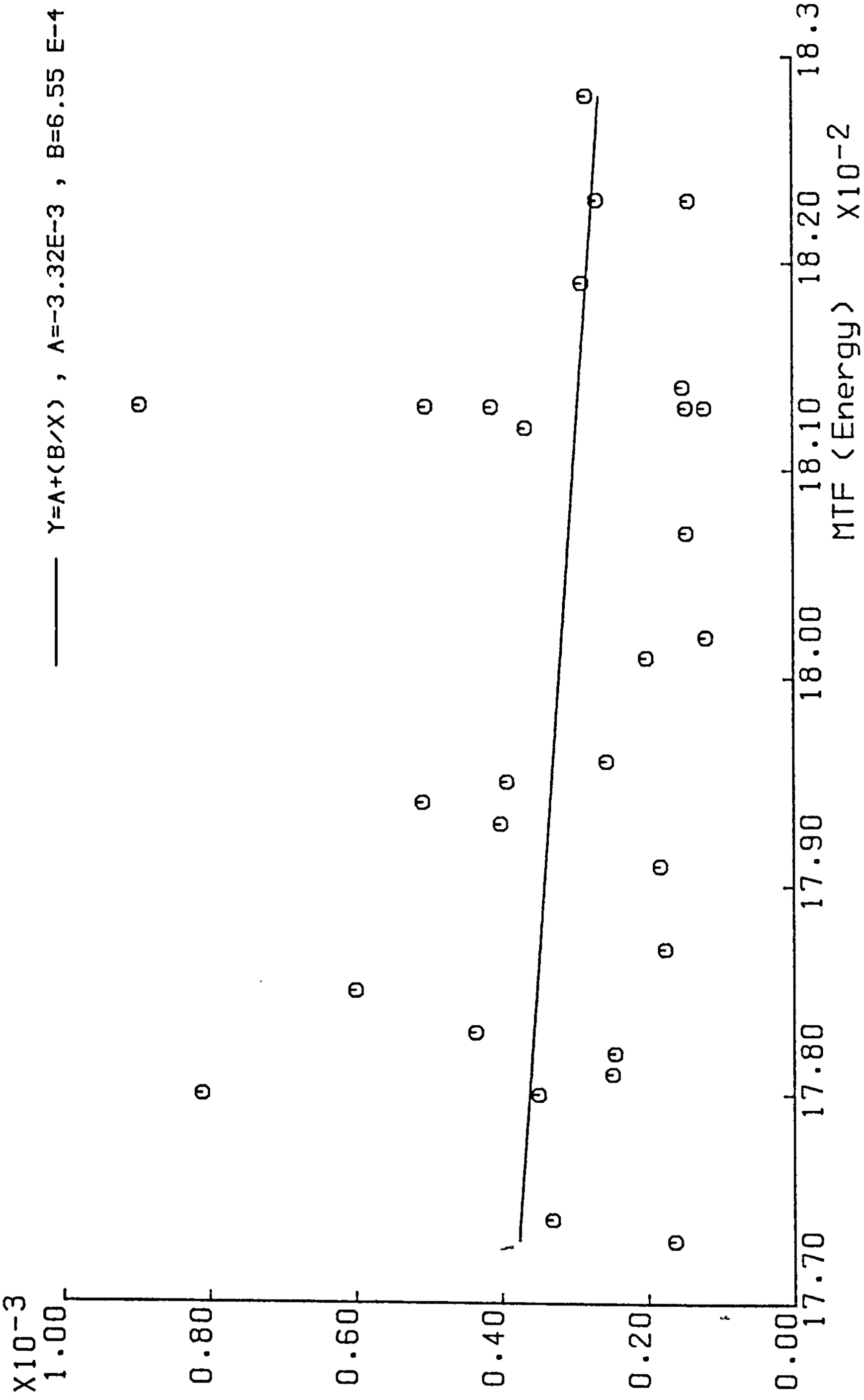

The Function Y=A+B/X Fitted to the data

FIGURE 7.8

related in some way to the turning points, we need an quantitative estimate which may be used to modify the RWWE.

The first step in this connection was to establish a deviation of RWWE from its expected value, for each lens. This deviation was expressed as a percentage of the origianl RWWE. Thus each lens can be associated with a percentage which represents the difference between the actual RWWE and the expected RWWE. This percentage figure has been called residual error (See Fig. 7.9).

In order to relate this residual error to the number of turning points, a table of the residual errors together with corresponding number of turning points is derived. This information is shown in Fig. 7.10. (Note. Since the error profile is regarded as symmetrical, only half the total number of turning points were used in each case). Most lenses with 2 or more turning points have a positive sign for the residual error while lenses with fewer turning points have a negative residual error. This observation when referred to the original RWWE versus MTF curve shows broadly 2 classes of lenses - one with higher number of turning points below the fitted curve, while the others above the fitted curve, as shown in Fig. 7.11.

This leads to an inference: that where there are relatively large number of turning points, the RWWE has been underestimated,

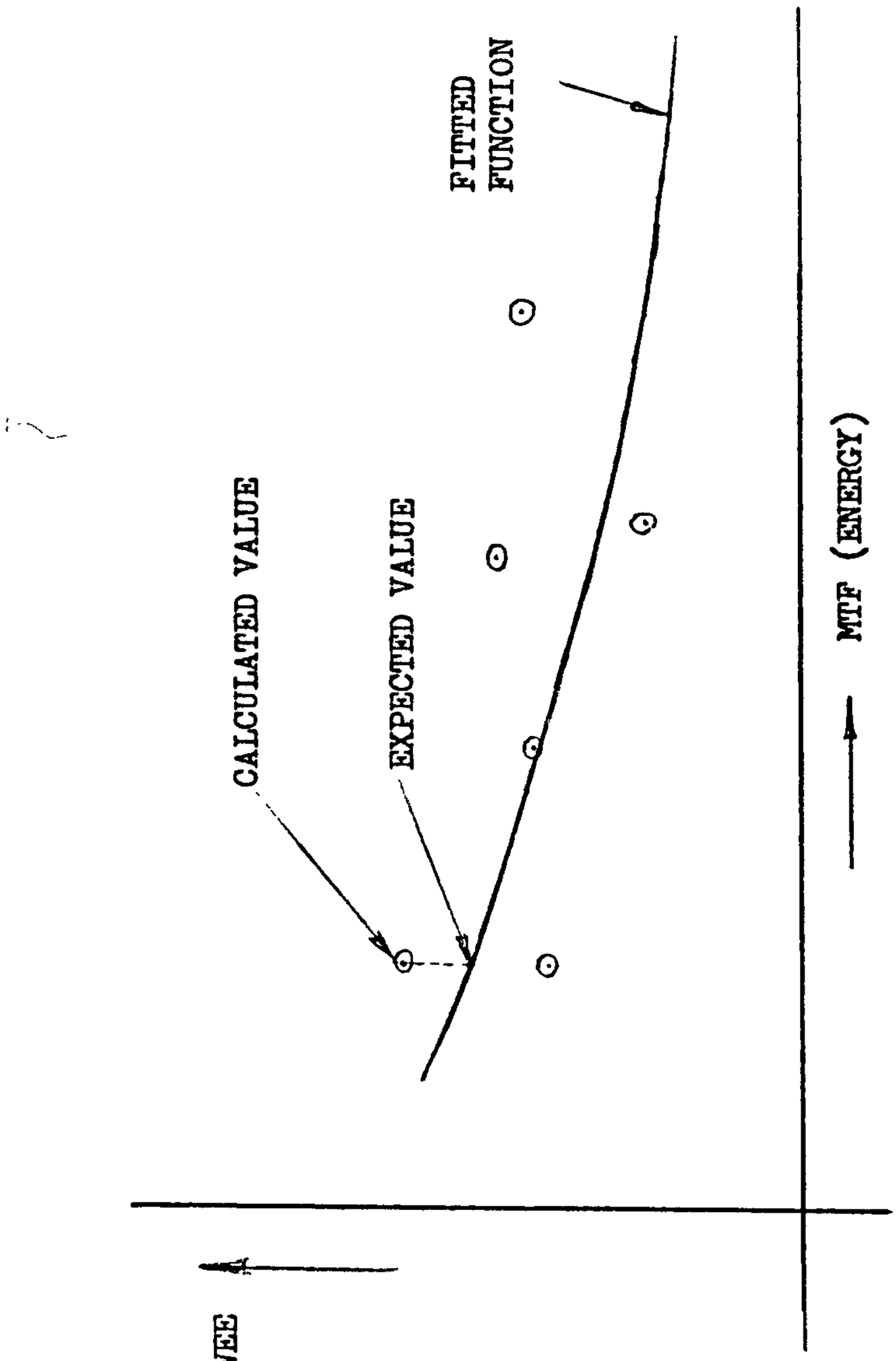

DERIVATION OF RESIDUAL ERROR

FIGURE 7.9

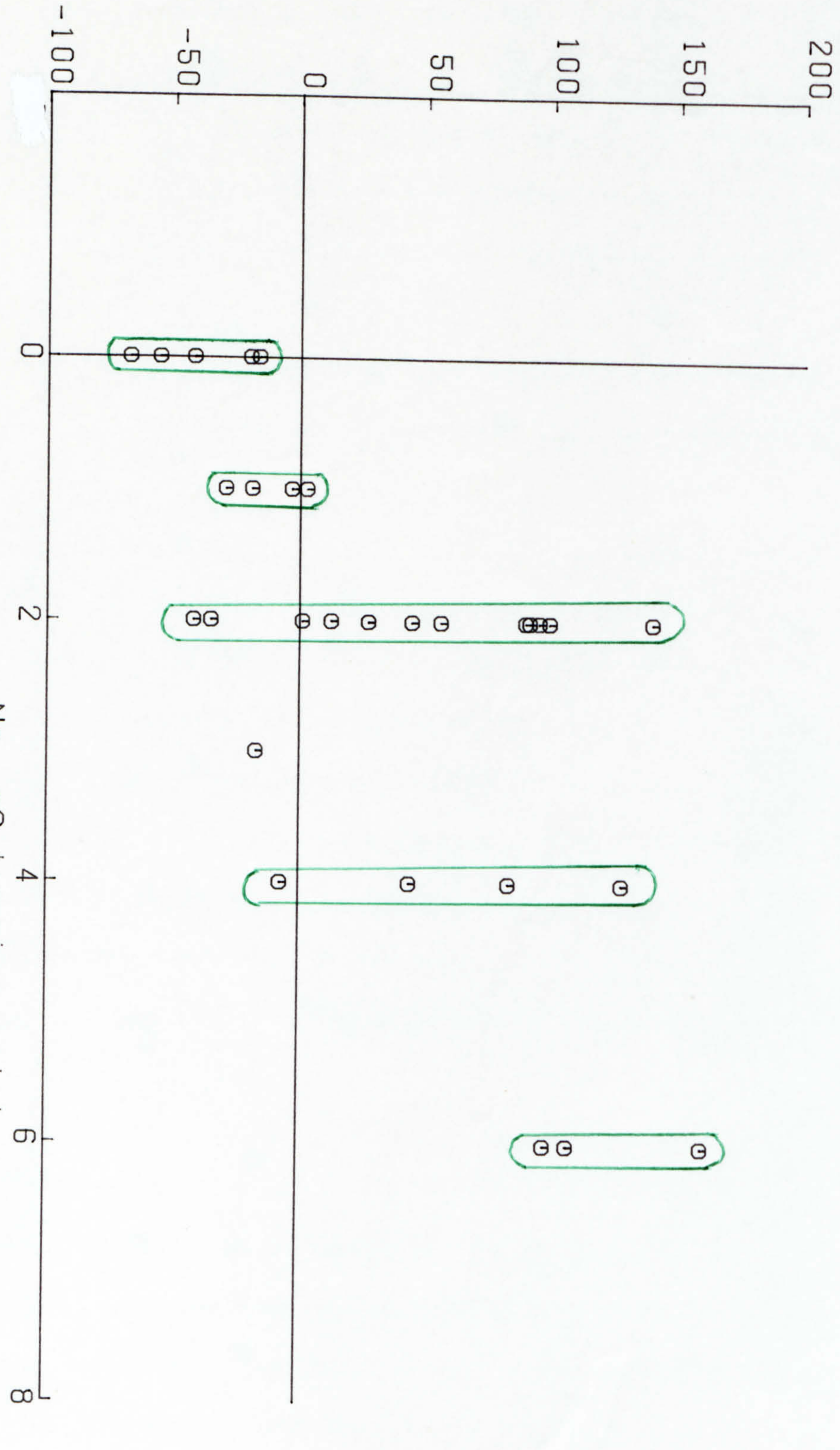
% Residual Error
-100
-50
0
50
100
150
200
No. of Turning Points
0
2
4
6
8
Clustering according to Turning points

FIGURE 7.10

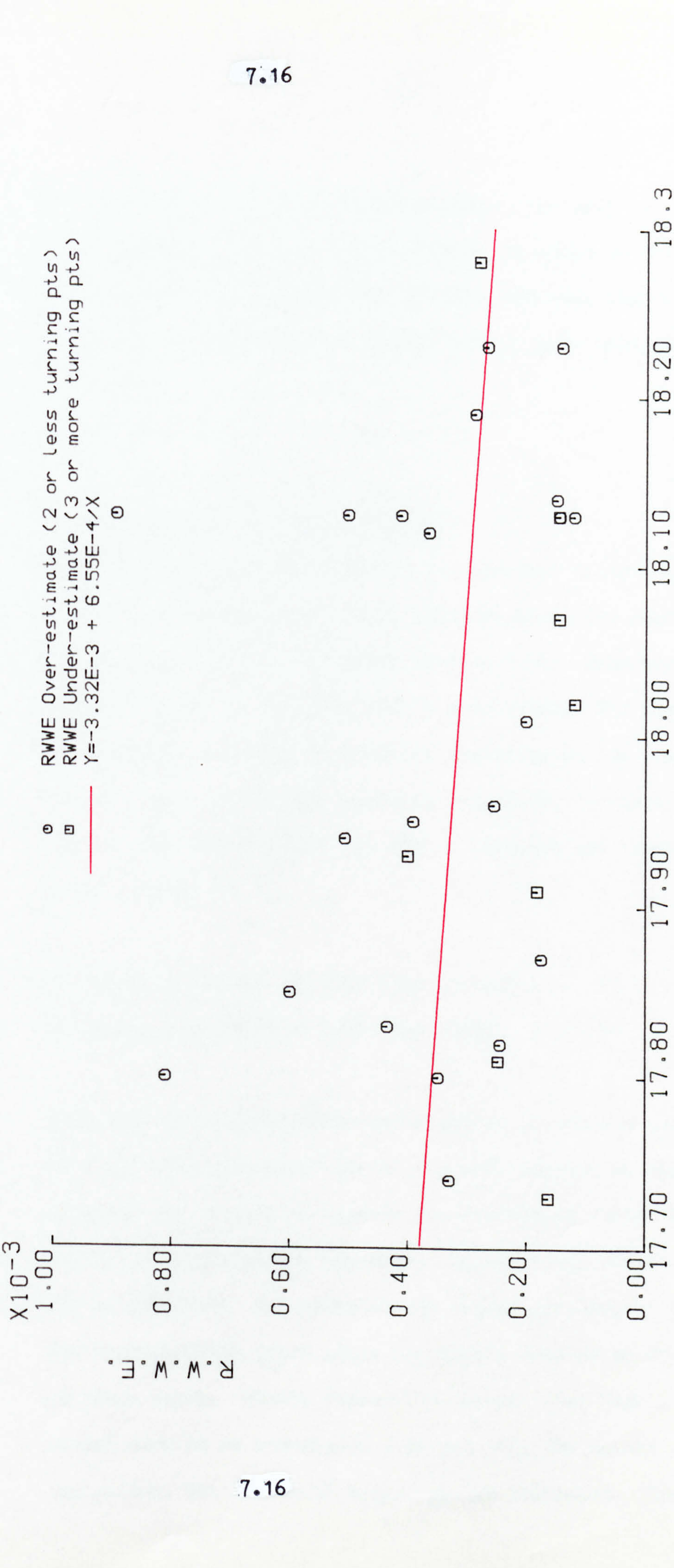

Classification of errors according to the Number of Turning Points

FIGURE 7.11

and where there are fewer turning points, the RWWE has been over-estimated. Even on this evidence, it would be fair to say that a lens displaying largish RWWE and more than a usual number of turning points is likely to be a poor lens with lower MTF.

7.5

Correction Based on Turning Points

One very simple way to implement a correction factor, is to compute an average (or typical) residual error for each of the clusters shown in the graph of Fig. 7.10. Thus each cluster (class) is assigned with a mean value. The RWWE for each lens can then be modified according ot its respective cluster. The results are shown in Fig. 7.12. A correlation between modified RWWE and the MTF is computed and turns out to be - 0.30.

The correlation MTF and RWWE (unmodified) = - .17

The correlation MTF and RWWE (modified) = - .30

While the correlation after modification is still a low figure at - .3, the improvement due to the modification is almost 100%. Attempts can be made to improve the correction factor by utilising more rigorous approach. In addition, other features may be examined. For example, the radial distance at which the turning point takes place may have a bearing on the residual error. Simple inspection reveals that high residual errors seem to be associated with not only the number of turning points, but also with bigger radial distances. This line

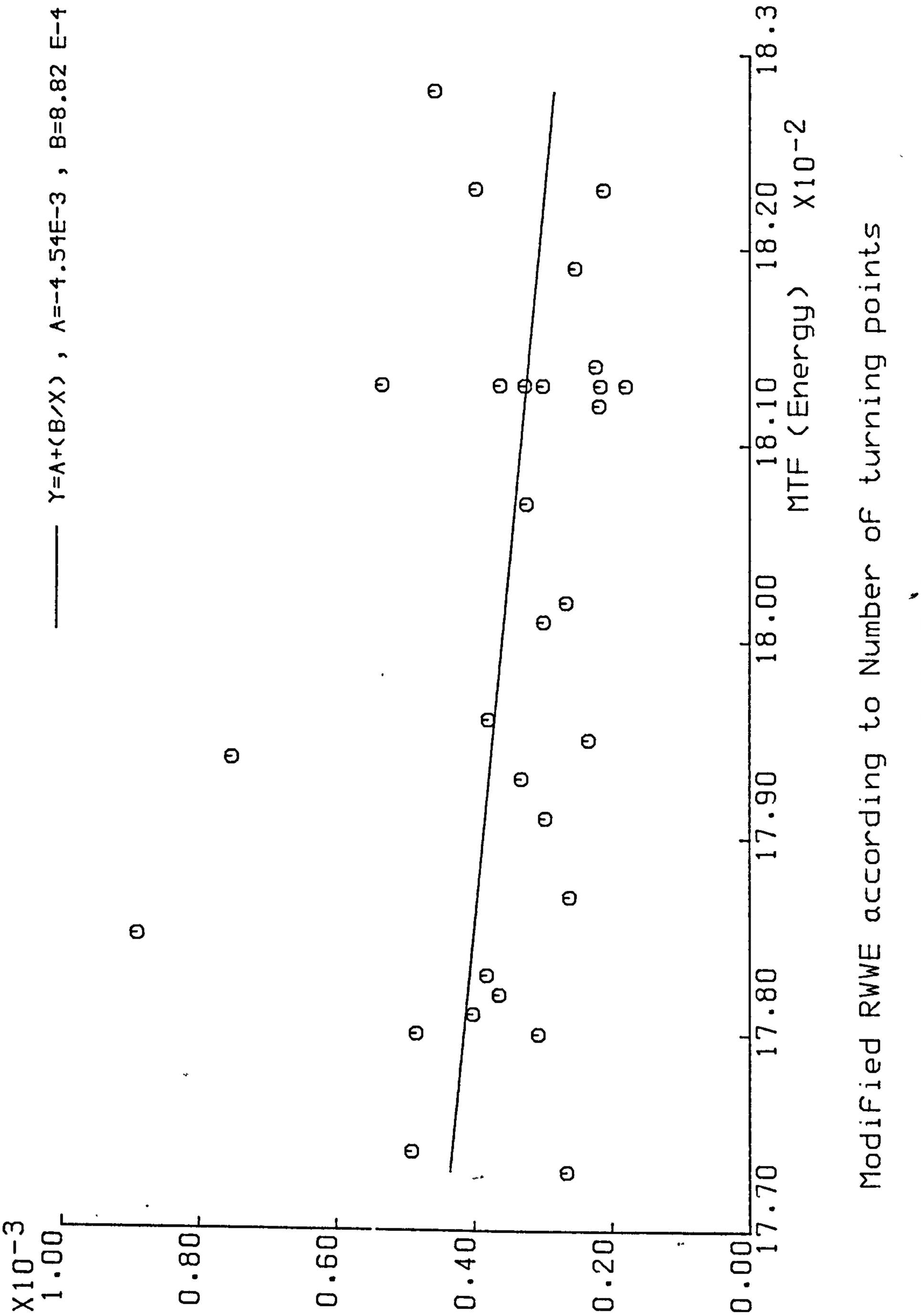
—— Y=A+(B/X) , A=-4.54E-3 , B=8.82 E-4
Modified RWE according to Number of turning points
MTF (Energy)
X10-2
18.3
18.20
18.10
18.00
17.90
17.80
17.70
X10-3
1.00
0.80
0.60
0.40
0.20
0.00
Modified R.W.E.

FIGURE 7.12

of enquiry, seemingly reasonable, introduces other ambiguities. For example, there may be turning points which appear much more "severe" while others appear to be "mild", as shown in Fig. 7.13. The exact effect of this feature would have to be studied.

Nevertheless, the RWWE is a simple, yet unique parameter. Further, a correction factor based on the number of turning points also covers new ground.

A more coherent and rigorous approach is the subject of the next chapter.

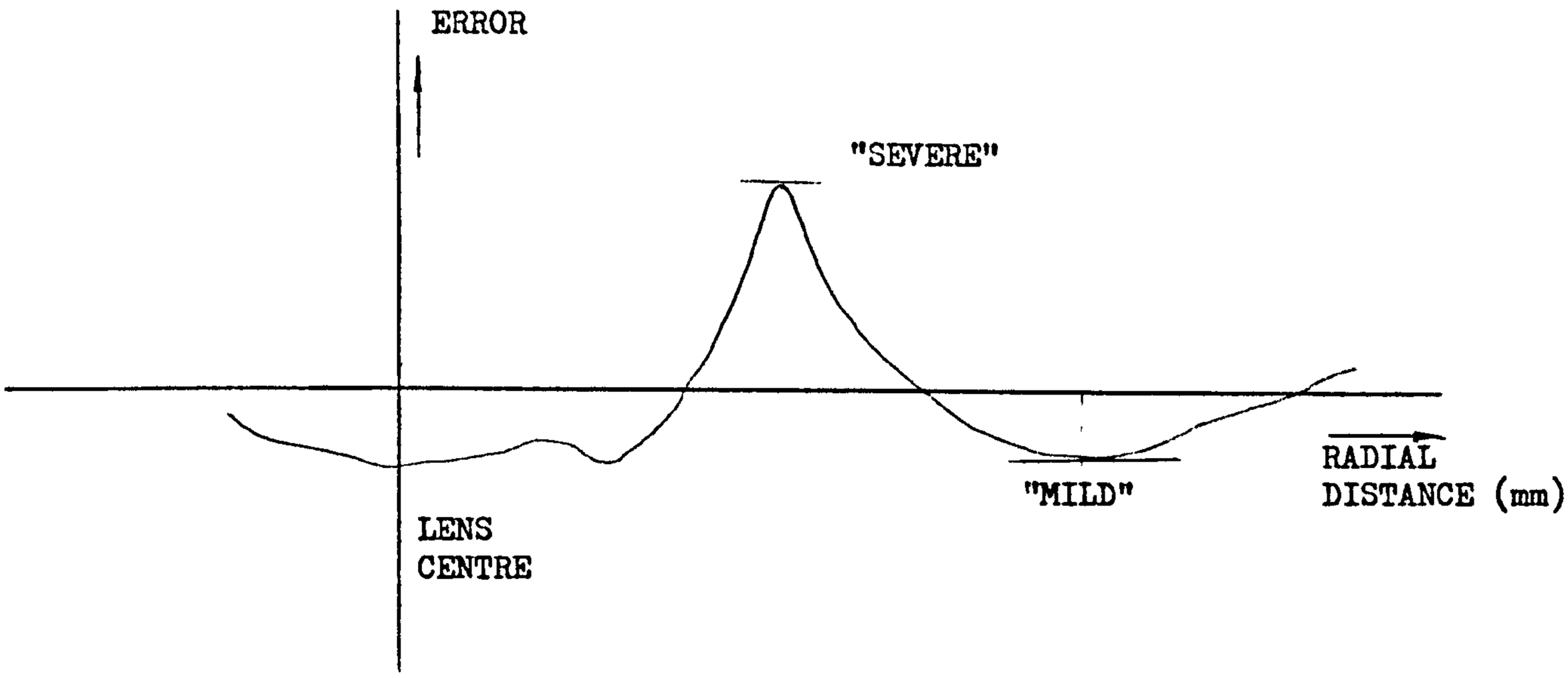

TURNING POINTS OF AN ERROR PROFILE

FIGURE 7.13

C H A P T E R V I I I

ENERGY IN LOWER HARMONICS AND RESIDUAL ERROR

CHAPTER VIII

ENERGY IN LOWER HARMONICS AND RESIDUAL ERROR

The discussion in the final stage of the last Chapter was mainly confined to the number of turning points in a given error profile. However, the number of turning points in any error profile must be related to the harmonic content of that signal. It therefore follows, that some correlation should exist between the harmonic content of the profiles and the corresponding residual errors.

8.1

Energy in the First Harmonic

Since the maximum energy is expected to be in the lowest of the harmonics, the lenses were sorted according to the energy in the first harmonic, as shown in the Table of Fig. 8.1. The residual error was then plotted against the energy in the first harmonic (see Fig. 8.2). The corresponding value of the correlation between the residual error and energy in the first harmonic is: - .7704. This value of correlation is obviously a great improvement over previous such figures. This suggests that as the energy moves from the first harmonic to higher harmonics the residual error increases.

The value of correlation of - .7704 although respectable, is not high enough for practical purposes. A correlation of some .8 to .9 could perhaps be a more appropriate figure.

LENS	ENERGY % 1st HARMONIC
A33	95.4
A18	94.8
A11	94.5
A10	90.1
A19	86.5
A31	85.0
A29	84.0
A 7	81.8
A32	78.9
A13	76.1
A 9	74.1
A22	60.1
A 5	58.7
A15	49.4
A16	47.7
A12	36.3
A 4	35.0
A25	34.0
A 3	33.4
A28	33.4
A26	29.8
A17	23.2
A23	19.9
A14	14.9
A30	12.1
A34	12.0
A27	4.99
A 6	3.95
A20	3.08

LENS SORTED ACCORDING TO
ENERGY IN 1st HARMONIC

FIGURE 8.1

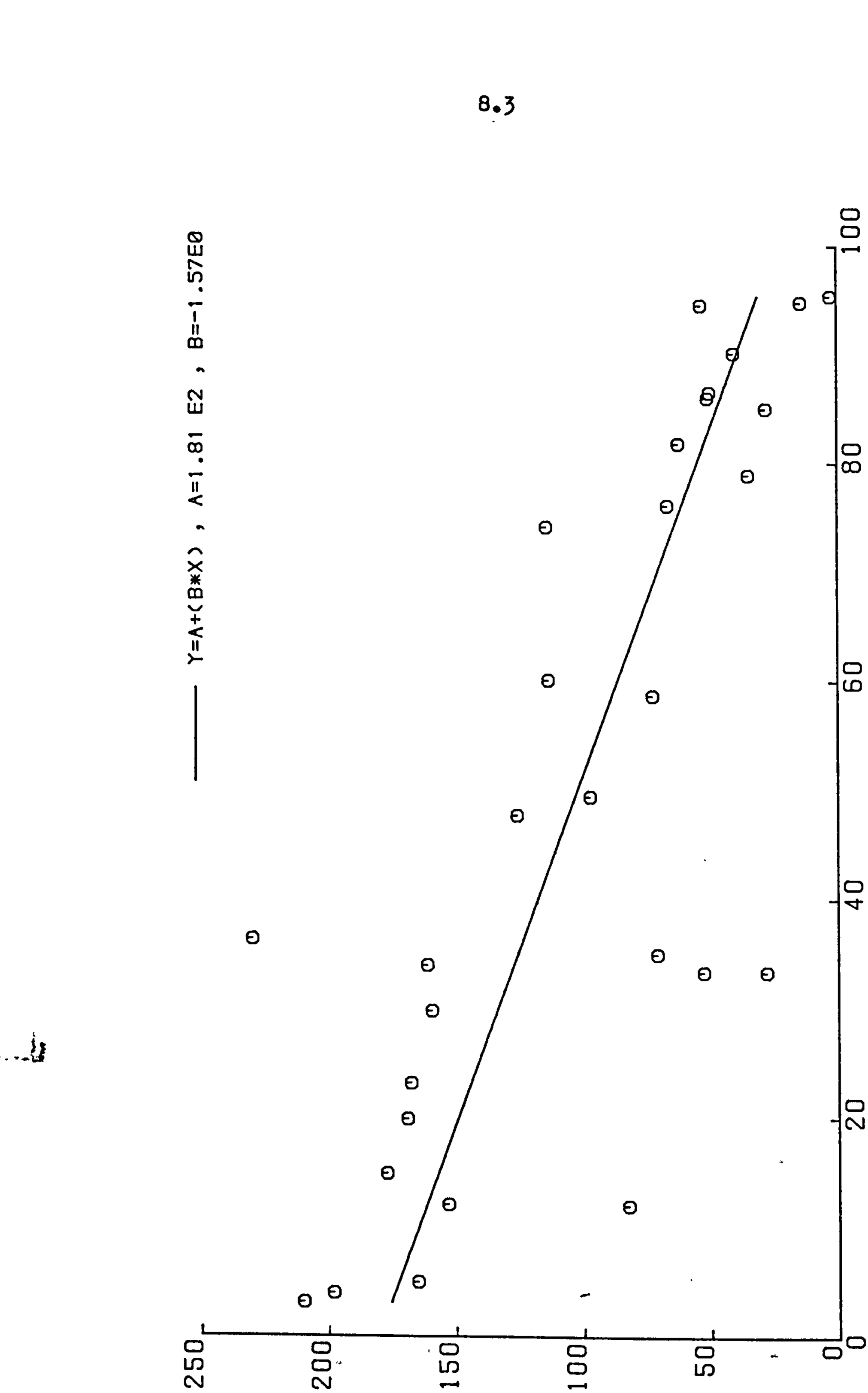
Y=A+(B*X) , A=1.81 E2 , B=-1.57E0
% Residual Error
% Energy in 1st harmonic
Correlation = -0.7704
250
200
150
100
50
0
20
40
60
80
100

FIGURE 8.2

8.2

Improvement of Correlation

A closer inspection of the graph of Fig. 8.2 shown previously, reveals that while a majority of results hug the straight line, in a fairly typical manner, there exists a set of some half a dozen results which seem to be far removed from the straight line. Had it not been for this set, the correlation figure would be much higher. Indeed, by omitting the particularly offending cases, a correlation of .96 was obtained. It is unlikely that this deviation is due to noise only. In order to study the pattern of behaviour of these lenses, the table of Fig. 8.3 may be useful. The "untypical" cases as previously observed on the graph of Fig. 8.2 are highlighted, in the Table of Fig. 8.3. Two observations can be made in this connection:

(a) In general, the highlighted results display the content of energy in first harmonic as being well below the mean value ($\approx$50%).

(b) The highlighted results display the content of energy in the second harmonic as being well above the mean value ($\approx$17%).

8.3

Algorithm to Improve Correlation

These two observations when considered simultaneously can certainly provide a means to classify the so called un-typical results. Indeed in many cases an above average energy

ENERGY % IN HARMONICS

LENS	1st	2nd	3rd	4th	5th
A33	95.4	0.266	3.02	0.403	0.609
A18	94.8	0.918	3.34	0.328	0.437
A11	94.5	0.133	3.79	0.275	0.660
A10	90.1	2.41	5.06	0.813	0.334
A19	86.5	2.69	9.27	0.336	0.922
A31	85.0	2.43	10.5	0.552	0.994
A29	84.0	7.42	7.03	1.20	0.0704
A 7	81.8	0.379	13.0	0.792	2.95
A32	78.9	6.27	13.6	0.545	0.347
A13	76.1	3.52	12.7	2.10	4.03
A 9	74.1	3.50	16.3	1.02	3.76
A22	60.1	11.4	25.6	0.959	1.06
A 5	58.7	32.0	0.597	1.52	5.27
A15	49.4	7.74	30.7	1.0	2.82
A16	47.7	13.8	30.4	1.78	3.76
A12	36.3	7.04	10.2	29.6	0.165
A 4	35.0	59.4	1.39	0.849	1.77
A25	34.0	8.57	46.8	6.56	2.86
A 3	33.4	59.6	1.79	2.91	0.477
A28	33.4	43.9	21.9	0.791	0.0545
A26	29.8	7.26	54.9	1.19	4.15
A17	23.2	1.29	39.7	12.0	11.5
A23	19.9	50.1	22.4	1.72	3.01
A14	14.9	3.37	63.0	5.95	5.25
A30	12.1	37.7	38.1	6.72	3.57
A34	12.0	46.3	36.3	3.75	0.956
A27	4.99	1.33	87.3	2.98	1.37
A 6	3.95	26.7	55.3	4.06	6.35
A20	3.08	48.2	37.5	0.531	5.84
AVERAGE ENERGY	50.1	17.0	24.2	3.21	2.59

DISTRIBUTION OF RELATIVE ENERGIES IN THE LOWER HARMONICS

FIGURE 8.3

in second harmonic is accompanied with an above average energy in third harmonic also. Hence some form of correction to the value of the first harmonic energy would undoubtedly improve the results. Since the energies of second and third harmonics appear to be well above average, a straight forward linear correction based on the difference between expected and actual energies might be used. A flow diagram illustrating this strategy is shown in Fig. 8.4. After the application of this correction, the graphical output i.e. energy in first harmonic versus residual error is shown in Fig. 8.5. The corresponding correlation = - 0.85. This value of correlation when compared to - .77 is readily acceptable. Using this in formation a corrected set of RWWE can be derived and a better RWWE versus MTF curve may be derived (see Fig. 8.6).

Without making any further amends, a method is now needed which predicts the value of the MTF from the profile measurement. This is discussed in the next chapter.

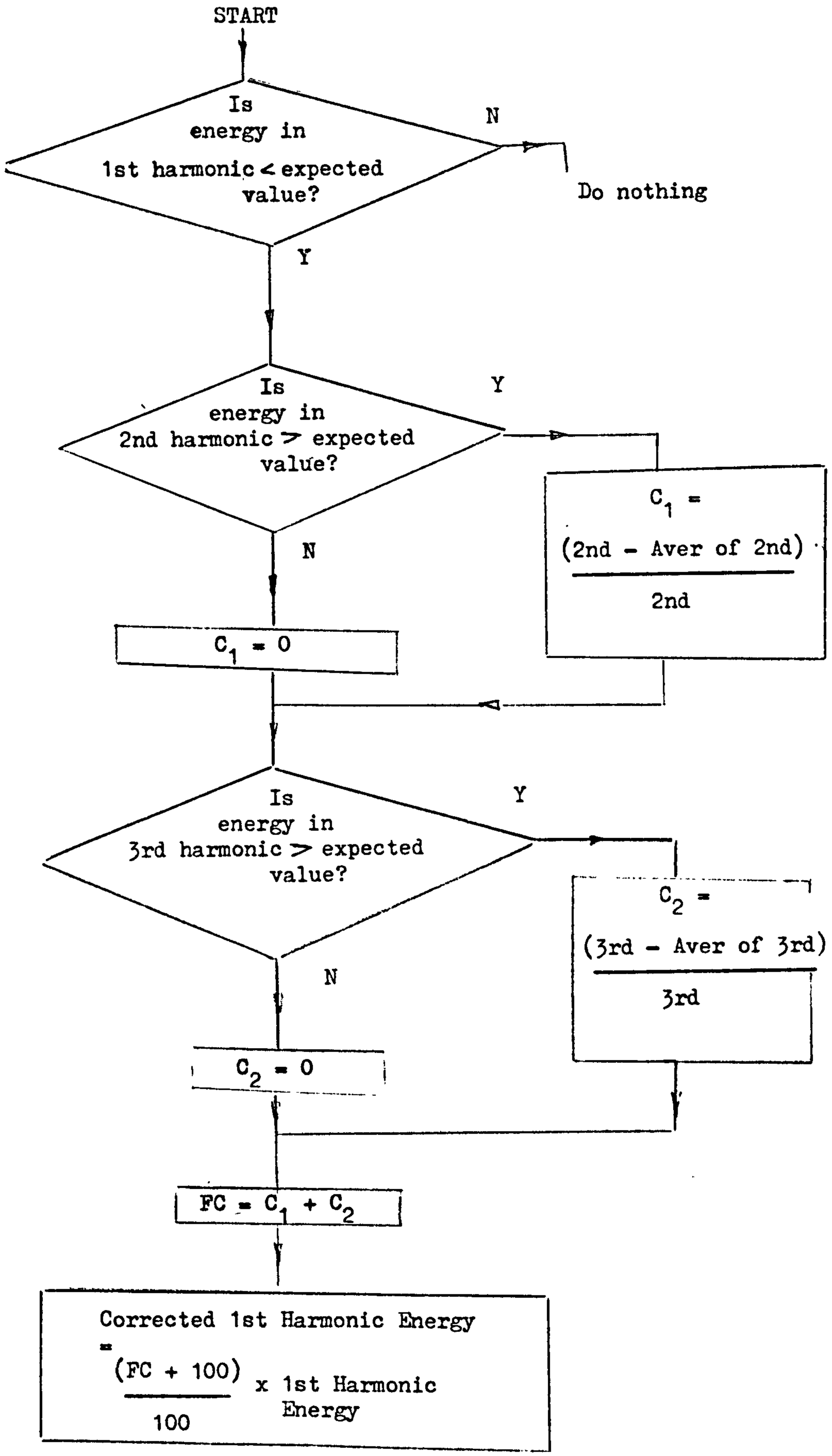

DERIVATION OF CORRECTION FACTOR FOR
1st HARMONIC ENERGY

FIGURE 8.4

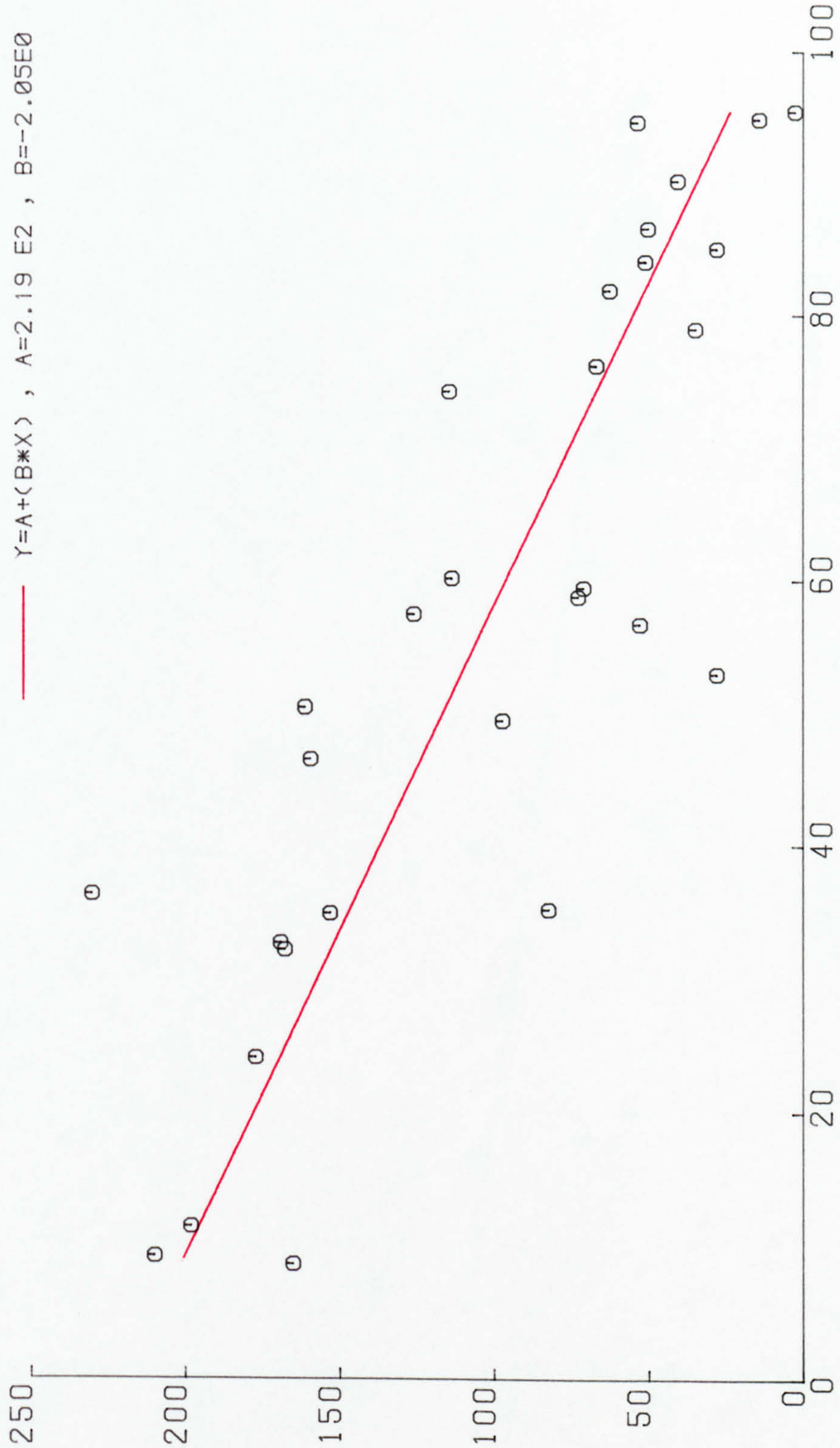
Y=A+(B*X) , A=2.19 E2 , B=-2.05E0
% Residual Error
250
200
150
100
50
0
0
20
40
60
80
100
% Energy in adjusted 1st harmonic
Correlation = -0.8462

FIGURE 8.5

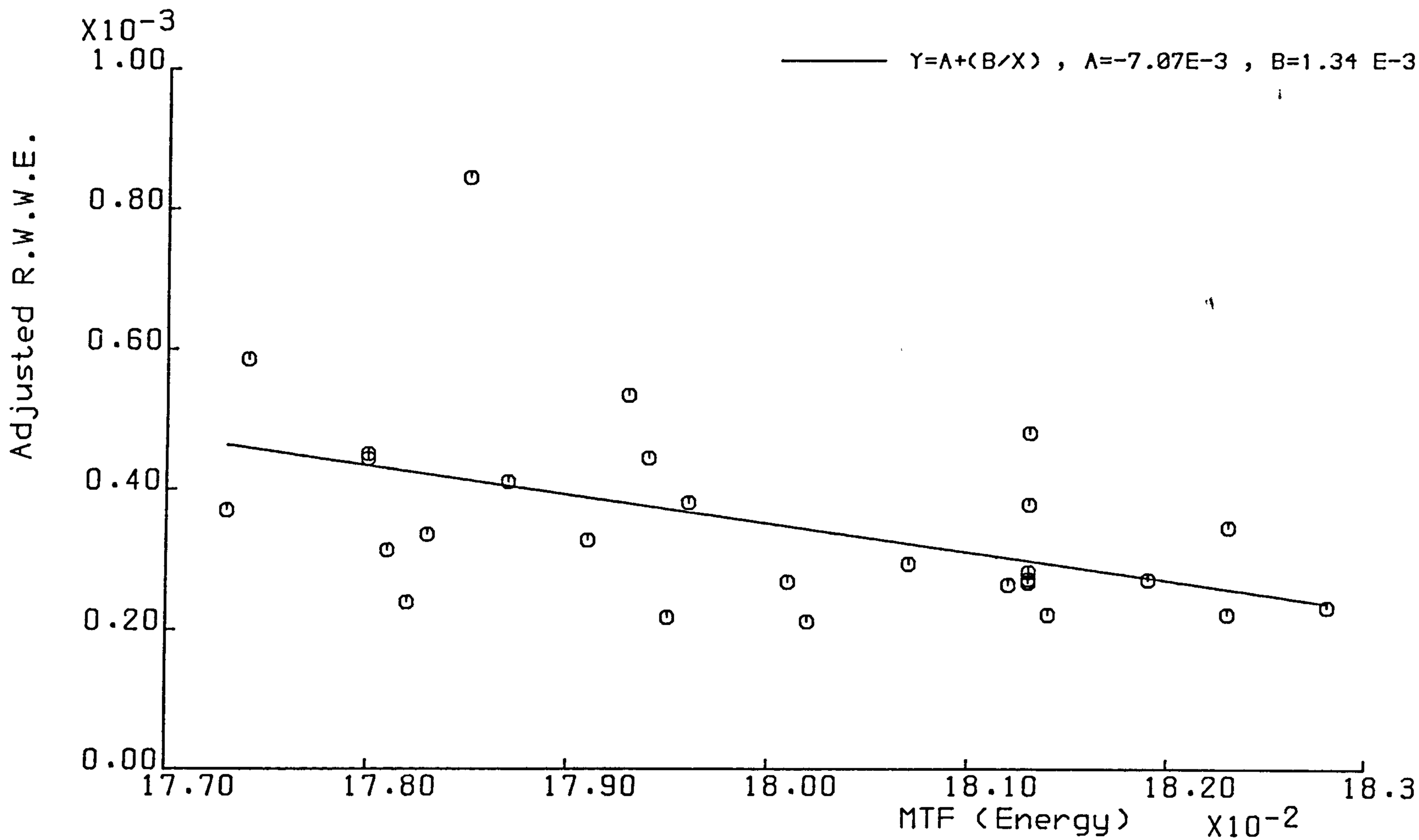

Modified Function Y = A + B/X Fitted after adjusting the Radius Weighted Wave-Front Error according to Energy in 1st Harmonic

FIGURE 8.6

C H A P T E R I X

PREDICTION OF MTF

CHAPTER IX

PREDICTION OF MTF

Once a quantity of lenses have been manufactured, the first quality control operation might be to obtain an error profile by using Form Talysurf style instrument, the operation of which has been described in Chapter V. Given the error profile of a particular lens, a predictor is required to provide the corresponding value of MTF.

From the work conducted in this research, mainly two functions are available:

(a) $RWWE = \frac{B}{MTF} + A$ $\quad (y = A + B/_x)$ See Chapter VIII

(b) Residual error = m. (energy in first harmonic) + c

$(y = mx + c)$ See Chapter VIII

9.1

MTF Prediction

The steps involved in arriving at a prediction from the error profile are shown in the flow diagrams of Fig. 9.1 and Fig. 9.2. The very first estimate of the goodness of the lens could be the RWWE. Exceptionally high values of RWWE are likely to correspond to low MTFs.

START

OPERATOR MEASUREMENT
USING FORM TALYSURF

ERROR PROFILE

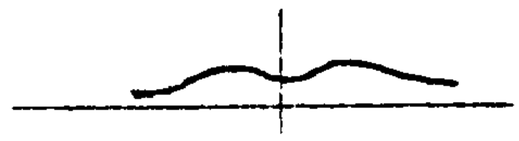

FIT STRAIGHT LINE

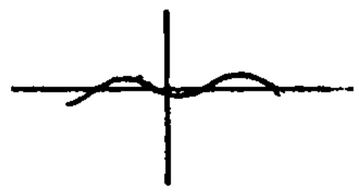

GENERATE
RWWE

FIRST
ORDER
CHECK
OF
QUALITY

SEE NEXT PAGE **

FIND FFT

FIND ENERGY

FIND TOTAL
ENERGY

1-10 HARMONICS

SEE NEXT PAGE *

FIGURE 9.1

FULL PROCEDURE FOR MTF PREDICTION

..../continued

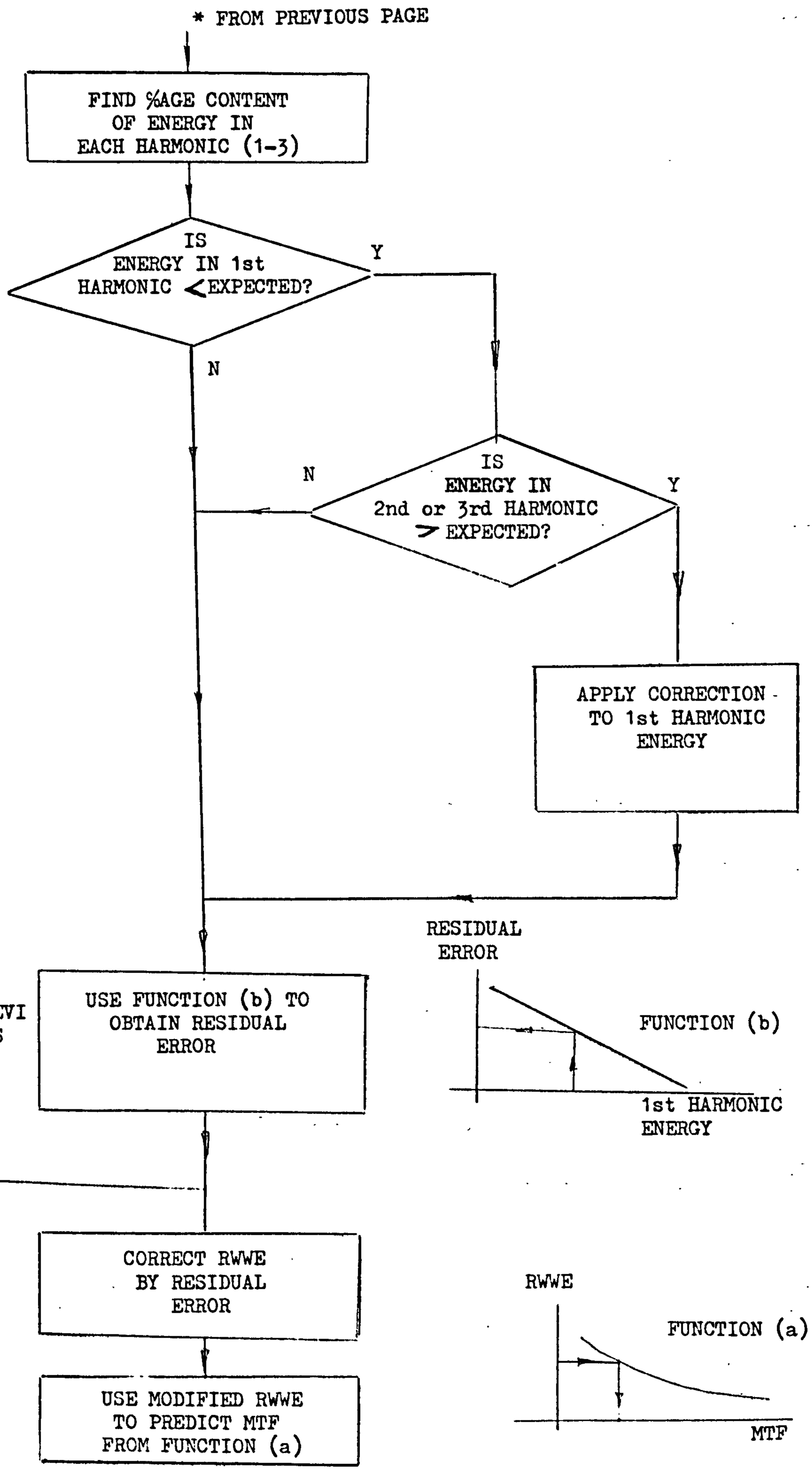

FULL PROCEDURE FOR MTF PREDICTION

FIGURE 9.2

However, the modification of the measured RWWE in the manner prescribed would lead to a better estimate. This claim can readily be put to test, since some 29 error profiles together with 29 MTF values are available.

The table of Fig. 9.3 shows a set of results which include the predicted MTFs and the measured MTFs.

9.2

Accuracy of Prediction

The average prediction error $\approx$0.36% seems to be a very low figure. However, remembering that the total variation in the data = 3%, a prediction accuracy of some 10% or 20% is achieved. In the absence of any other estimate of prediction, these figures are welcome. Never-the-less, higher accuracy is always desirable.

9.3

Future Work

Clearly, the correlation between energy in lower harmonics and the residual error is a major component in the design of the predictor. The correction algorithm applied earlier, improved the correlation from - .77 to - .85. There might be a scope of improvement in this direction. The manner in which the energy is distributed in the harmonics needs to be studied in a greater detail. However, since a batch of 29

LENS	MEASURED MTF (ENERGY)	PREDICTED MTF (ENERGY)	PERCENTAGE ERROR
A 3	0.1793	0.1762	-1.712
A 4	0.1823	0.1808	-0.8498
A 5	0.1780	0.1782	0.1032
A 6	0.1773	0.1801	1.583
A 7	0.1828	0.1835	0.4040
A 9	0.1782	0.1833	2.884
A10	0.1813	0.1827	0.7481
A11	0.1795	0.1839	2.442
A12	0.1802	0.1840	2.128
A13	0.1819	0.1826	0.3679
A14	0.1807	0.1820	0.7089
A15	0.1796	0.1799	0.1525
A16	0.1801	0.1826	1.414
A17	0.1813	0.1825	0.6844
A18	0.1780	0.1784	0.1969
A19	0.1812	0.1827	0.8468
A20	0.1813	0.1823	0.5475
A22	0.1781	0.1815	1.905
A23	0.1813	0.1826	0.7302
A25	0.1814	0.1838	1.311
A26	0.1823	0.1838	0.8123
A27	0.1787	0.1792	0.2550
A28	0.1785	0.1693	-5.137
A29	0.1783	0.1810	1.493
A30	0.1791	0.1812	1.154
A31	0.1813	0.1799	-0.7476
A32	0.1794	0.1783	-0.5960
A33	0.1813	0.1775	-2.089
A34	0.1774	0.1750	-1.330

Average Error 0.359%

PREDICTED MTF

FIGURE 9.3

lenses may have a subset of only 6 or 7 lenses displaying a particular trait, a reliable analysis may not be possible. Indeed, the procedure of manufacture/measurement is subject to noise at almost every stage. It would hence be desirable to deal with a much bigger batch of some 100-150 lenses. Such a study could form an extention to this research.

In addition, the algorithm to correct the energy in the 1st harmonic could benefit from a more generalised approach. For example, it may be possible to deduce a generalised formula which could be applied to all the lenses, thus making the procedure simpler.

Other ideas for future work are discussed in the next chapter.

CHAPTER X

GENERAL DISCUSSION AND SUGGESTIONS FOR FUTURE WORK

CHAPTER X

GENERAL DISCUSSION AND SUGGESTIONS FOR FUTURE WORK

In a real production situation, several batches of 25-40 lenses would be manufactured. Each lens has to be optically tested, by measuring MTF.

If the results of this research were to be practically implemented, the need to optically test each and every lens could be curtailed. Initially, a small batch of say some 10-12 lenses could be manufactured and MTFs predicted. If the predicted MTFs were within the expected range, the production could continue with a further set of lens elements. An abnormality in the production process could hence be detected at an early stage (see flow diagram of Fig. 10.1).

10.1

Saving in Resources

At this stage, by examining the error profiles, it might be possible to re-machine certain lens elements. Any marginal cases can be rejected or accepted by measuring the MTF at a later stage. Assuming that the production process is in check, most of the lens elements are likely to display satisfactory predictions. Thus actual MTFs need to be measured only on randomly selected lens elements. Indeed, a profile measuring instrument could become an integrated part of the production cycle. If large production quantities are envisaged then a

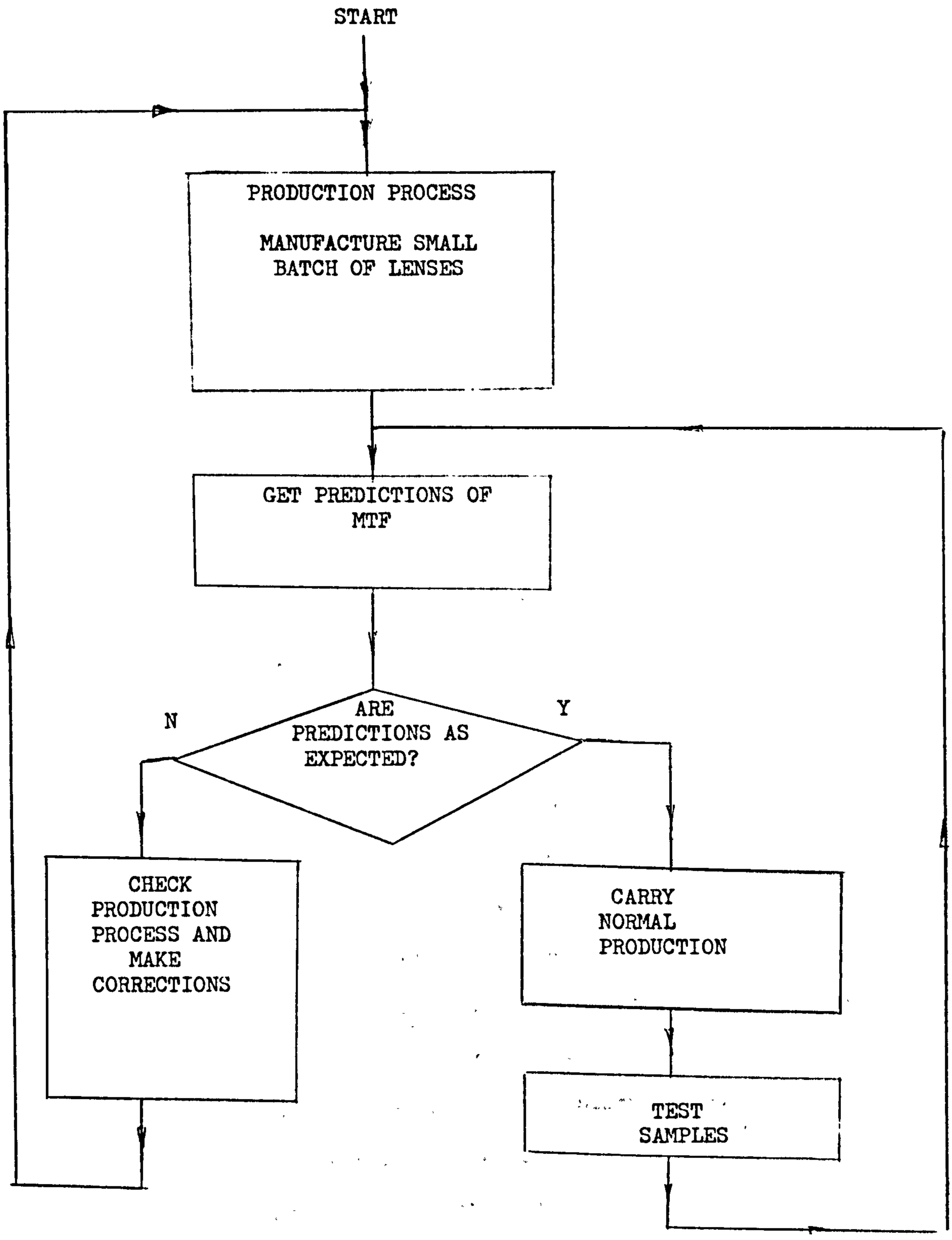

QUALITY CONTROL IN PRODUCTION

FIGURE 10.1

specially designed jig or fixture could be used to facilitate the loading of the lenses on to the measurement instrument. Since the machine possess a fair amount of computational power, implementation of FFT algorithm might be possible. In any case, addition of suitable hardware/software might be a more acceptable solution.

10.2

Machining Faults

An early warning about faulty production process is extremely useful. However, an indication of the faulty aspect of the machining process would be of much greater value. The manufacturing diameter of the lens is about 20 mm (although the optically used part is only 14 mm). The machining time taken for a tool to traverse the whole radius is almost half an hour. A slow unwanted variation in the tool position is likely due to wear in the slides and drift resulting from temperature changes. Such deviation would show up as a first harmonic in the corresponding error profile. If such an error was dominant then, the energy in the first harmonic would reflect this. As an example see Fig. 10.2 of lens A 11 and the corresponding energy in first harmonic = 94.5%. As already demonstrated, such lenses will display lower residual errors. In addition, if the amplitude of the error is low, RWWE will also be low, leading to higher values of MTF. This observation certainly confirms the very original rule of thumb

F1 - Analysis
F2 - Graph
F3 - Dump
F4 - Display Run 1
F5 - Display Both

Mode	Traverse Length	Reference	Ignore
UNFILTERED	20.0 mm	ASPHERIC	2 %
Aspheric 11 Trace 1			

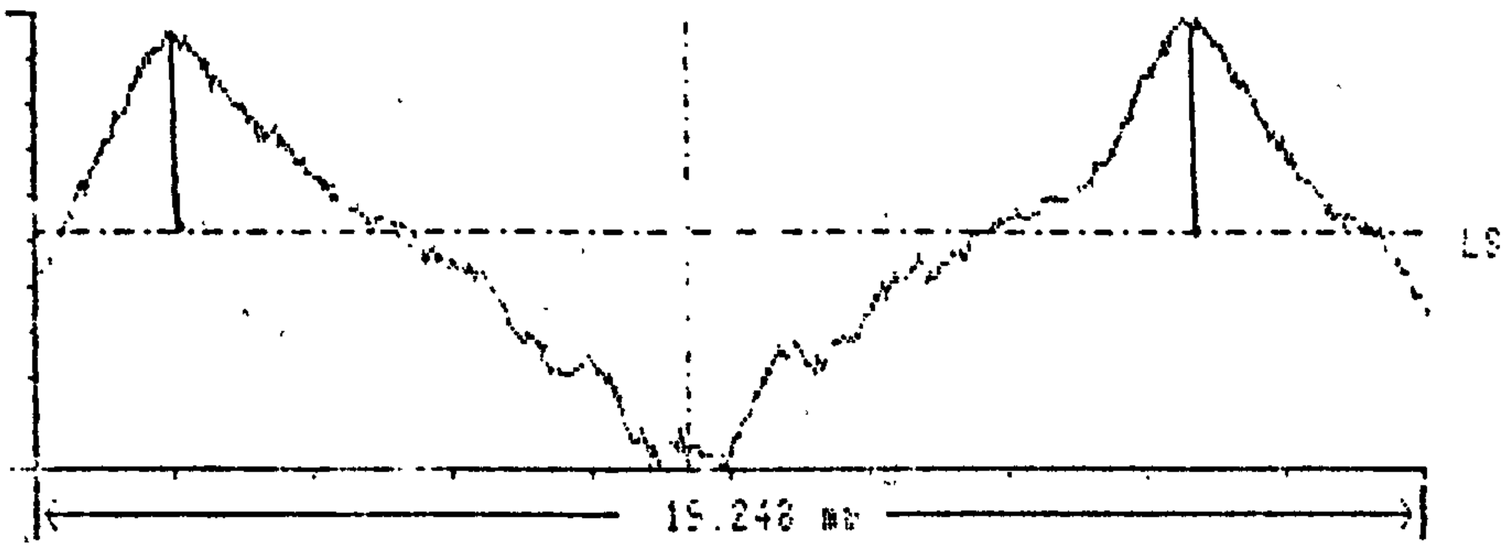

	FIGURE	AVERAGE ACCURACY	SMOOTHNESS Average	SMOOTHNESS Maximum	TILT
#1 #2	- 262 um	117 um	- 00 Deg	.03 Deg	.02 Deg

TIME: 0:22 Peak To Valley = 558 um
DATE 18-JAN-86

Taylor-Hobson

F1 - Analysis
F2 - Graph
F3 - Dump
F4 - Display Run 1
F5 - Display Both

Mode	Traverse Length	Reference	Ignore
UNFILTERED	20.0 mm	ASPHERIC	2 %
Aspheric 11 Trace 2			

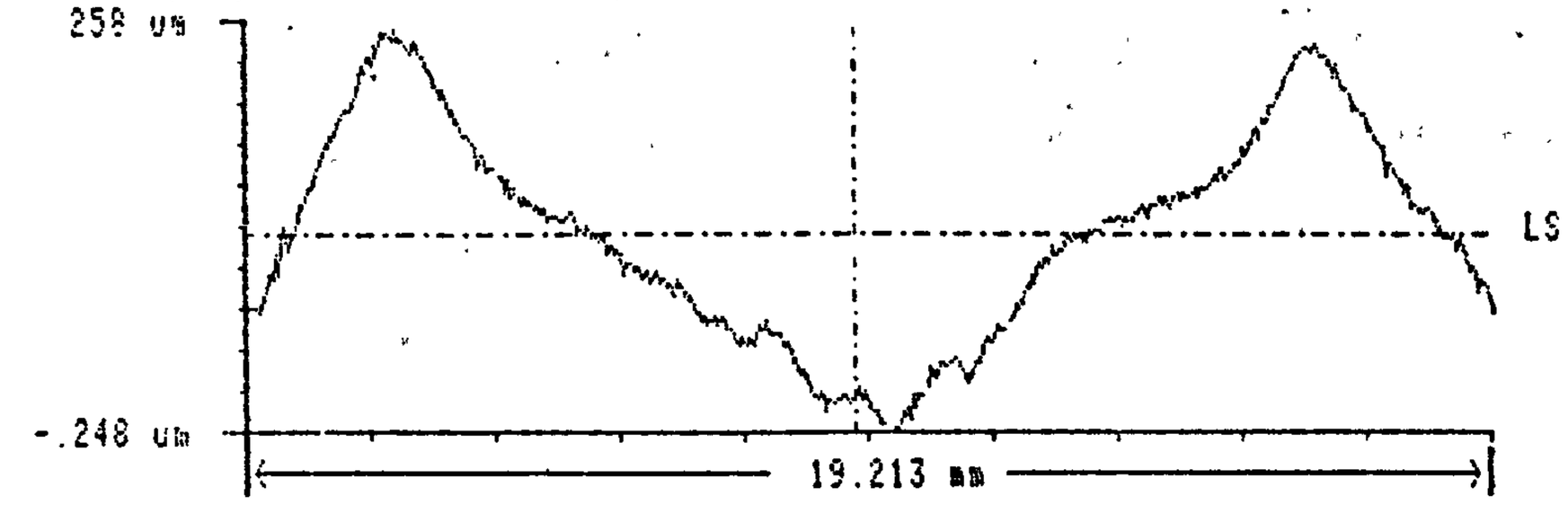

	FIGURE	AVERAGE ACCURACY	SMOOTHNESS Average	SMOOTHNESS Maximum	TILT
#1 #2	-.187 um	.104 um	.00 Deg	.00 Deg	.15 Deg

TIME: 0:23 Peak To Valley = .506 um
DATE: 18-JAN-86

Taylor-Hobson

FIGURE 10.2

used by the machine shop personnel:

"a single "bow" displayed in the error profile is tolerable provided the amplitude is not too big . . ." (see Appendix A). Large errors towards the periphery of the lens could be related to the chucking process particularly when the lenses are relatively thin. The parameter RWWE is hence quite appropriate for this requirement.

However, there are other features on the error profiles which need to be linked to the machining process. The dominance of any particular physical feature is bound to be reflected in the energy content of one or more harmonics. Since relatively high energy in the first harmonic suggests low variations in the machining process, it could be fruitful to examine the higher harmonics in a similar way. The Fig. 10.3 shows groups of lenses with energies above the mean value for a given harmonic.

For example, if all the error profiles in the third group (i.e. lenses where the energy in third harmonic > its average value) are inspected, it is found that the profiles are similar in character. A typical example of lens A 15 is shown in Fig. 10.4. Since this type of error is repeated in some 14 lenses, it is very unlikely to be random. Remembering that each lens takes about half an hour to machine, this problem is not drift related either. It is worthwhile noting that

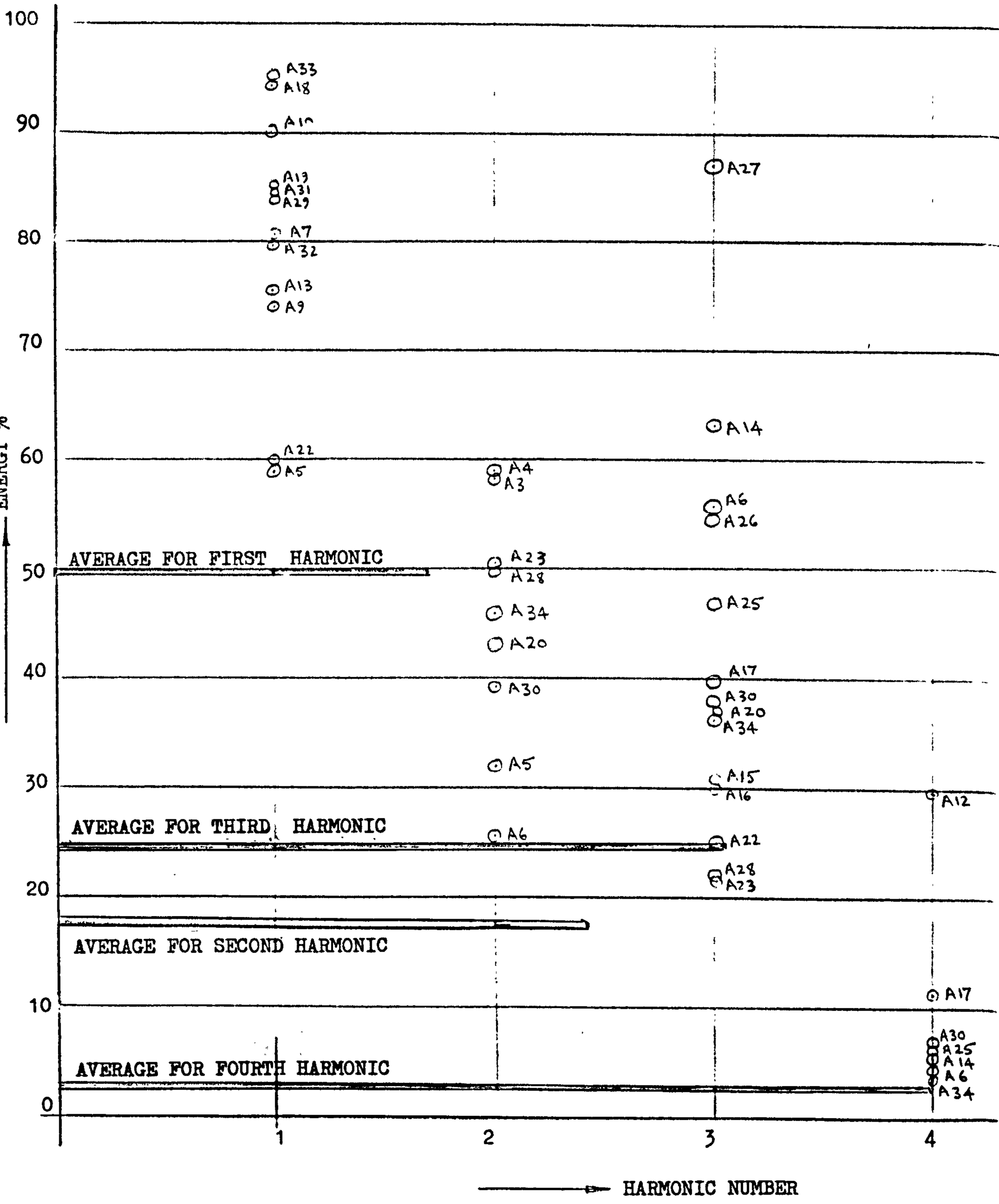

RELATIVE DISTRIBUTION OF ENERGY (ABOVE AVERAGE) IN HARMONICS

FIGURE 10.3

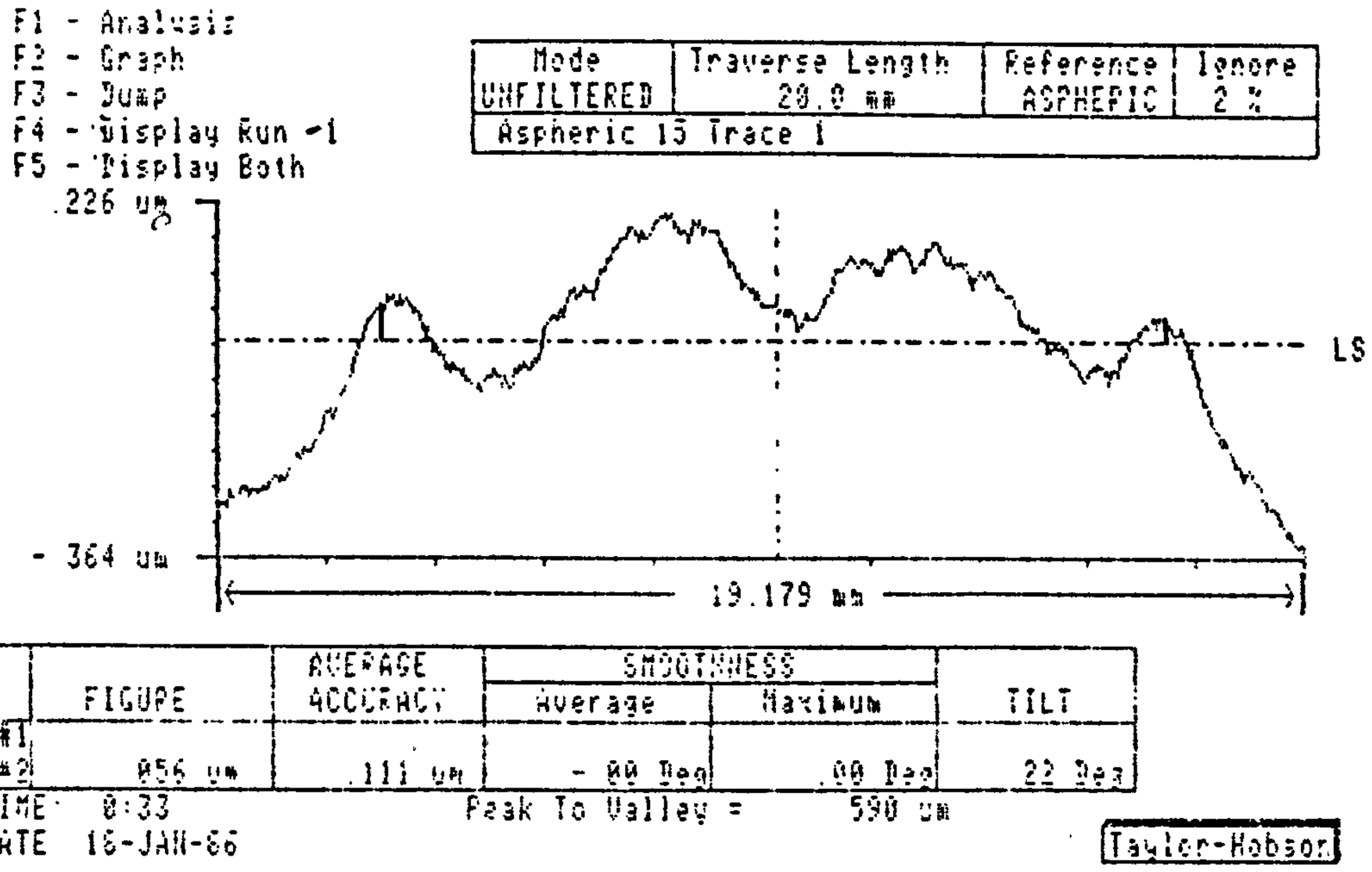
F1 - Analysis
F2 - Graph
F3 - Dump
F4 - Display Run -1
F5 - Display Both
Mode UNFILTERED
Traverse Length 20.0 mm
Reference ASPHERIC
Ignore 2 %
Aspheric 15 Trace 1
.226 um
- 364 um
LS
19.179 mm
FIGURE
AVERAGE ACCURACY
SMOOTHNESS
Average
Maximum
TILT
#1
#2
.856 um
.111 um
- 00 Deg
.00 Deg
22 Deg
TIME 8:33
DATE 16-JAN-86
Peak To Valley = 590 um
Taylor-Hobson

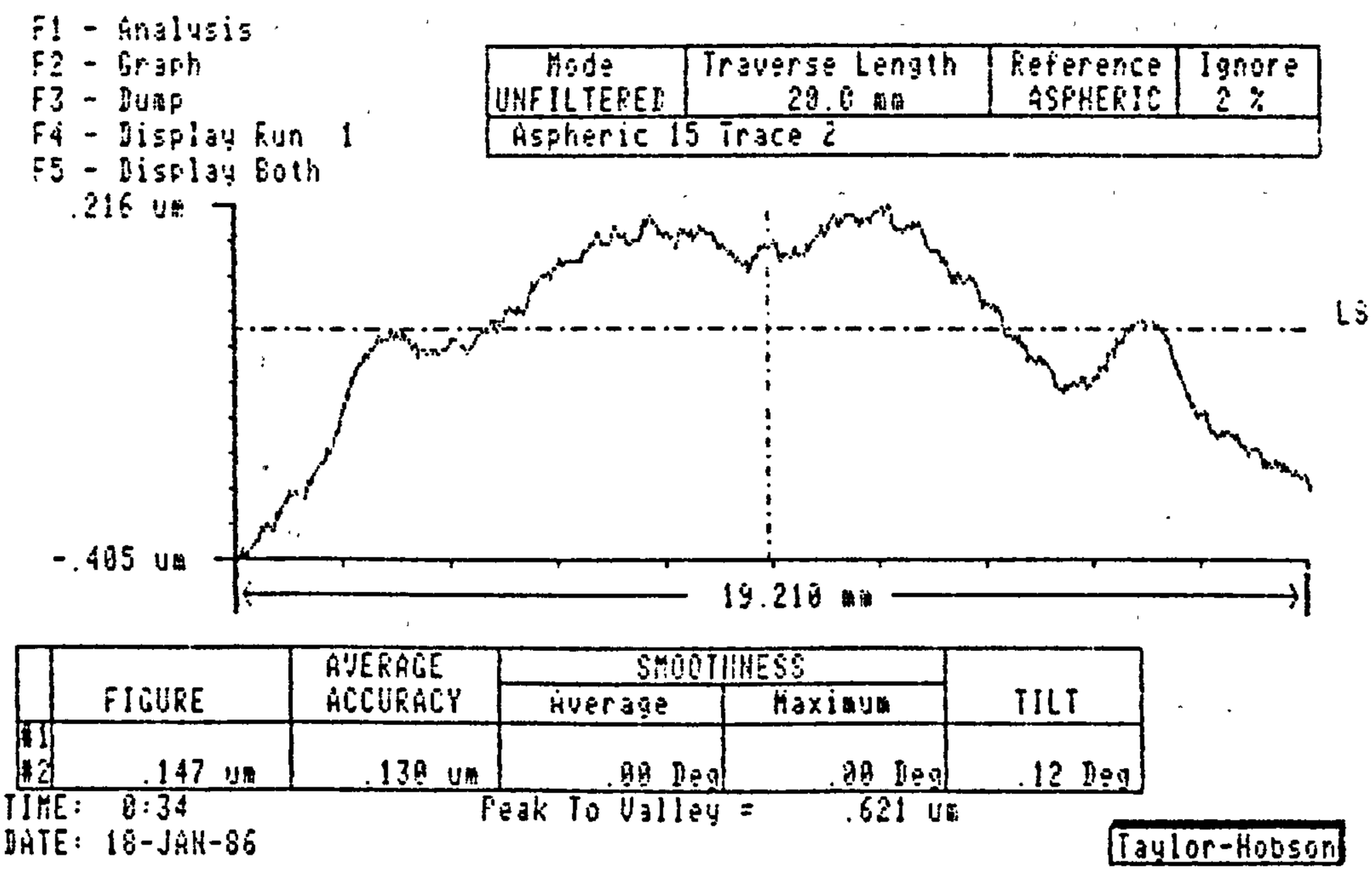
F1 - Analysis
F2 - Graph
F3 - Dump
F4 - Display Run 1
F5 - Display Both
Mode UNFILTERED
Traverse Length 20.0 mm
Reference ASPHERIC
Ignore 2 %
Aspheric 15 Trace 2
.216 um
-.405 um
LS
19.210 mm
FIGURE
AVERAGE ACCURACY
SMOOTHNESS
Average
Maximum
TILT
#1
#2
.147 um
.130 um
.00 Deg
.00 Deg
.12 Deg
TIME: 8:34
DATE: 18-JAN-86
Peak To Valley = .621 um
Taylor-Hobson

FIGURE 10.4

the maximum error deviation is of the order of 0.3 um. In normal machining terms, this can be regarded as fairly high standard of accuracy.

10.3

Cyclic Errors

Never-the-less, if the physical distances between the successive peaks is measured, it turns out to be a constant $\approx$2 mm, as shown in Fig. 10.5. The cyclic nature of this fault is hence confirmed. One source of such error could be small inaccuracies in the turntable spindle and/or associated tool post assembly as shown in Fig. 10.6. In making a traverse from one end of the lens to the centre, the turntable turns through an angle of about 14^{o}. The accuracy of the spindle of the turntable appears to be a contributary factor here. The need to study the geometry of the toolpost and the turntable hence arises. Suitable efforts may be fruitfully directed in this area in the future.

10.4

Tool Wear

The radius of the tool is some 2 mm. Any wear in the tool is hence likely to be represented as fractions of a mm. The energy in higher harmonics viz fifth harmonic is likely to be due to tool wear/and or vibration.

TYPICAL ERROR PROFILE

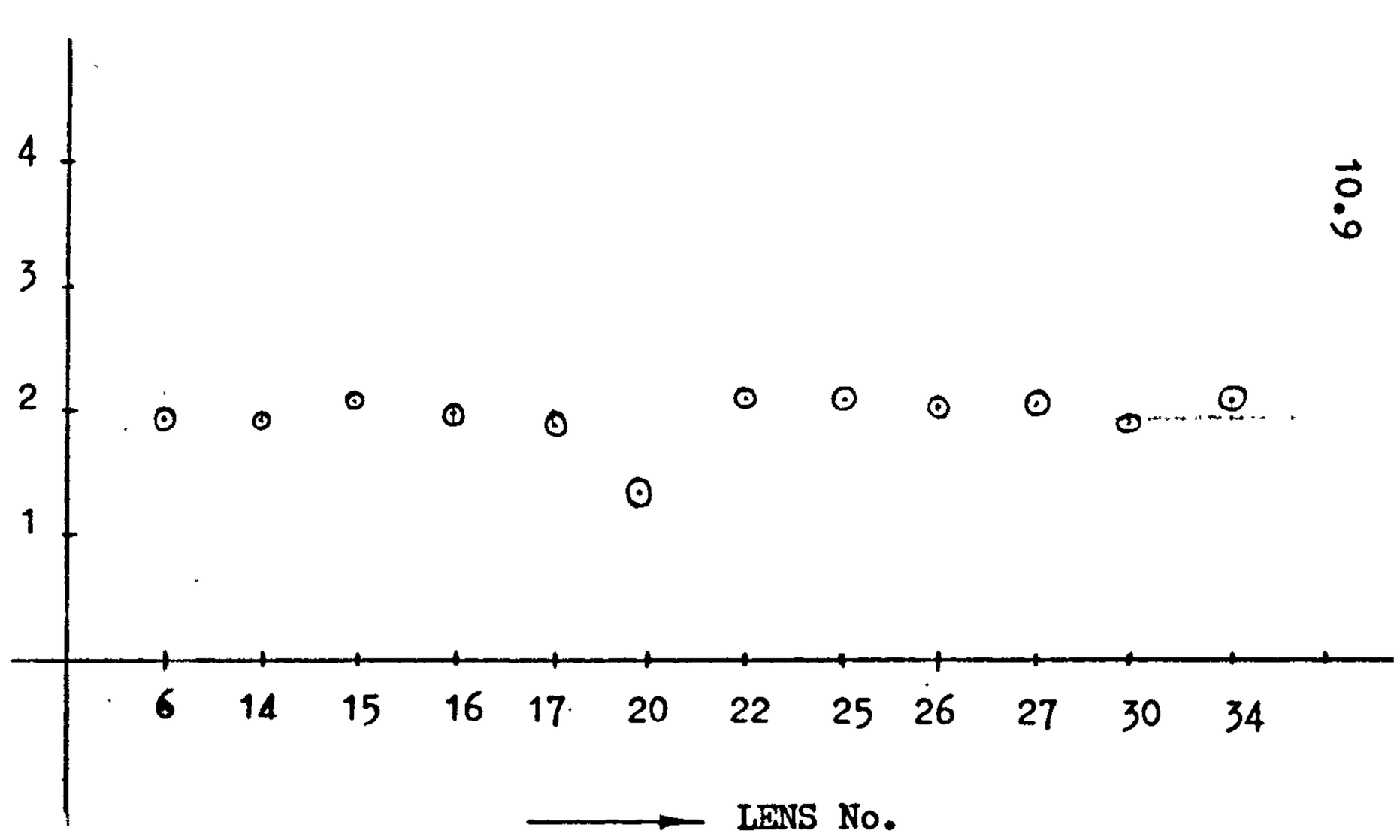

LENSES DISPLAYING CYCLIC ERROR

FIGURE 10.5

10.9

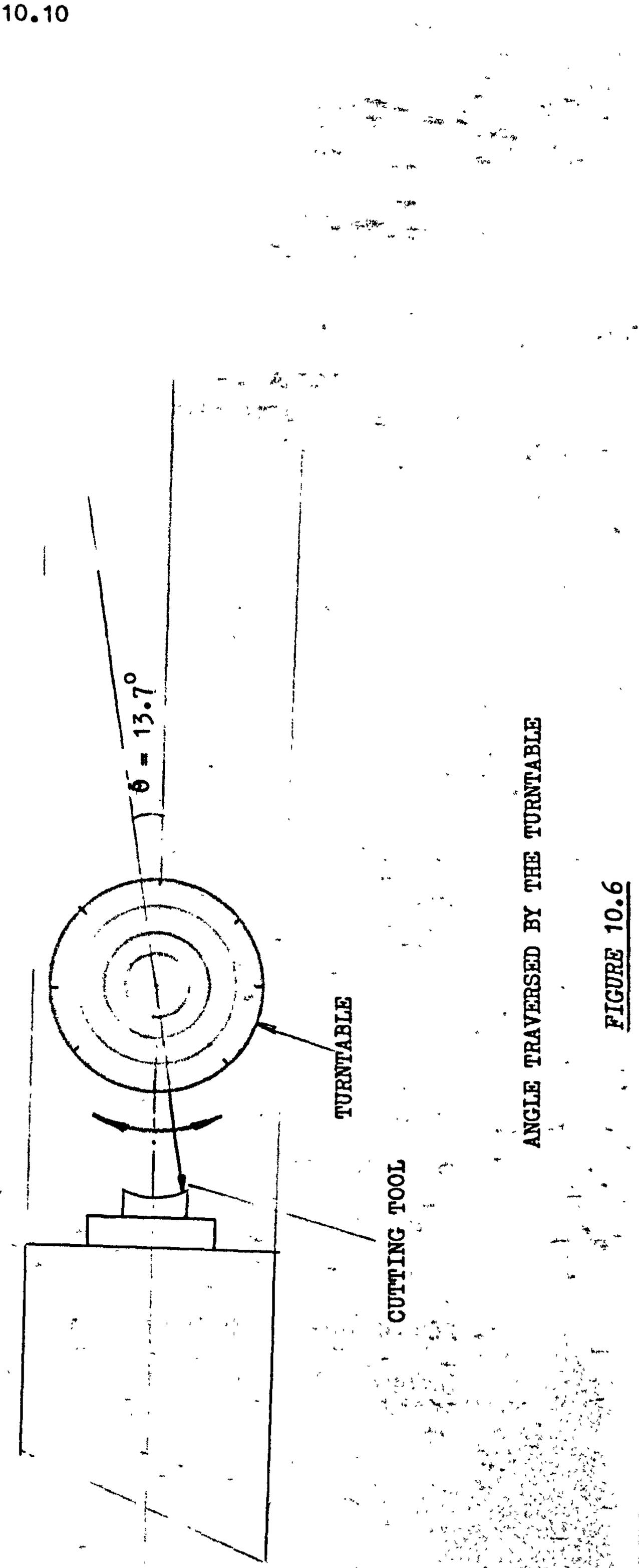

ANGLE TRAVERSED BY THE TURNTABLE

FIGURE 10.6

To Summarise:

Harmonic With Above Average Energy	Associated Machine Error
First Harmonic/Second Harmonic	Mainly drift or set-up and wear in slides, etc.
Third Harmonic	Cyclic error due to turntable/load, etc.
Fourth - Higher Harmonic	Tool wear, vibration, etc.
High RWWE	Faulty chucking

10.5

Future Work in General

The current work provides some limited guide in connection with machine faults. The provision of explicit parameters which estimate any particular faulty aspect with greater accuracy, requires not only a detailed knowledge of the production process, but also the precise conditions under which the production takes place. These could include measurement of temperature, vibration, tool wear, etc. during the production of a typical batch of lenses.

10.6

General Conclusions

It may be concluded that the main objectives of the research have been achieved.

To Summarise:

The optical performance as characterised by the area under the MTF curve is related to two parameters which can be measured at the manufacturing stage:

(a) Radius weighted wave front error (RWWE)

(b) The residual error

A combination of these two effects can be utilised to predict the MTF of a given lens at an early stage in the production cycle, thus saving vital resources.

REFERENCES

REFERENCES

1. Fukunaga
Introduction to stastical pattern recognition
1972

2. Reason
Report on measurement of roundness
Rank Taylor Hobson, 1966

3. Siddall
Roundness and relativity
Quality Assurance, Vol.2, Dec 1976

4. Dagnall
Let us talk roundness
Rank Taylor Hobson, 1976

5. H C Sharma
M Sc Thesis
Rank Taylor Hobson, 1977

6. Siddall and Player
Centring of a limited arc
Rank Taylor Hobson Internal Report, Aug 1974

7. Whitehouse
A best fit ref line for use in partial arcs
Scientific Instruments, Vol.6, March 1973

8. R E Reason
The measurement of surface texture
Rank Taylor Hobson, 1970

9. F Twyman, FRS
Prism and lens making
Hilger & Watts Limited, 1952

10. David Casasent
Pattern recognition: a review
Data Processing IEEE Spectrum, March 1981

11. Lendaris and Stanley
Diffraction-pattern sampling for automatic pattern
Proc IEEE, Feb 1970

12. G F Doughty, et al
Aspheric Geodesic lenses in an integrated optics spectrum analyser
SPIE, Vol.235, Aspheric Optics, 1980

13. Nicholas and Boon
Production of an aspheric surface for an f/1 focusing lens by a CNC Machine
SPIE, Vol.235, Aspheric Optics, 1980

14. Tom G Gijsbers
Colath - The two axis computer numerical controlled (CNC)/interferometer controlled diamond turning capability of Philips Research
APIE, Vol.235, Aspheric Optics, 1980

15. Buttery
    Leicester Polytechnic
    Discussion

16. Dave Kinsey
    Rank Taylor Hobson
    Discussion

17. G Gale and Stedman
    Non spherical mirror in x-ray optics
    SPIE, Vol.235, Aspheric Optics, Oct 1980

18. Television programme on badgers

19. Colin Lewis, et al
    Optical requirements for thermal imaging lenses
    SPIE, Vol.163, Advances in Optical Production Technology, April, 1979

20. Worrall
    Infra red transmitting glass
    SPIE, Vol.163, Advances in Optical Production Technology, April, 1979

21. Paul Kuttner
    Optical systems with aspheric surfaces for the correction of spherical aberration as main error in the infra red and visible spectral regions
    SPIE, Vol.235, Aspheric Optics, 1980

22. R Little
Rank Taylor Hobson
Discussion

23. R C Spragg
Latest techniques for contact measurement of surface finish and the latest means of characterizing surfaces
SPIE, Vol.235, Aspheric Optics, 1980

24. Alan Ashton
Internal Report
Rank Taylor Hobson, May 1980

25. ARTHUR COX
PHOTOGRAPHIC OPTICS 1971
FOCAL PRESS LTD.

A C K N O W L E D G E M E N T S

I would like to thank the Directors of Rank Taylor Hobson for the permission to publish this research work. In particular, Mr John Adams helped to co-ordinate various requirements very efficiently. Mr Ray Frampton helped with technical advice and played a major role in securing the most important lens data. Numerous members of staff at Rank Taylor Hobson helped, but some of the names that immediately come to mind are, Messers Dave Stevens, Nick Dunnington, Eric Nightingale, John Garrat, Alan Ashton, John Farnsworth, Dave Warner, Tom Hall, Paul Scott, etc.

Here, at the Leicester Polytechnic, I am grateful to Dr Abdullah Hashim for providing not only technical advice but also moral support. I have been most impressed by the service provided by all the members of the Computer Centre. In particular, I would like to record my thanks to Mr Dave Bradley whose active help in software support was a major component in the progress of the research.

Finally, I am thankful to my wife, for not only patiently typing all the work, but also for the support she gave me throughout the research work.

If through oversight I have failed to acknowledge any individual's effort, I seek apology.

A P P E N D I X A

APPENDIX A

MEASUREMENT ON PRODUCTION MACHINE

In general, the machined component is checked for departures from the desired profile. In an ideal condition, the result on the Talysurf graph would be a straight line. After polishing, if the same test is repeated a straight line may not be produced. A general rule is to examine the graph for the number of "bows" from the centre of the lens to the edge. A single bow may not be too objectionable. Two "bows" may need closer examination. Any more than two bows, almost certainly would need some re- machining. The maximum peak to peak amplitude of the bows has to be no more than 1 μm. Implicit within this "number of bows" is the number of times the slope changes sign. This situation is depicted in Fig. A1. The partial graphs of a component which "passed" this criterion are shown in Figs. A2A to A2C. Figure A2A merely represents the aspheric relative to a sphere. This graph obtained at low magnification, shows how the aspheric departs from a sphere. It does not therefore show any error. Figure A2B represents the departure from the required profile i.e. it is an "error graph" and in an ideal case should be a straight line. One small division represents 0.5 μm.

Figure A2C represents the same component after polishing. In this instance the shape is preserved, and hence the component is passed as satisfactory.

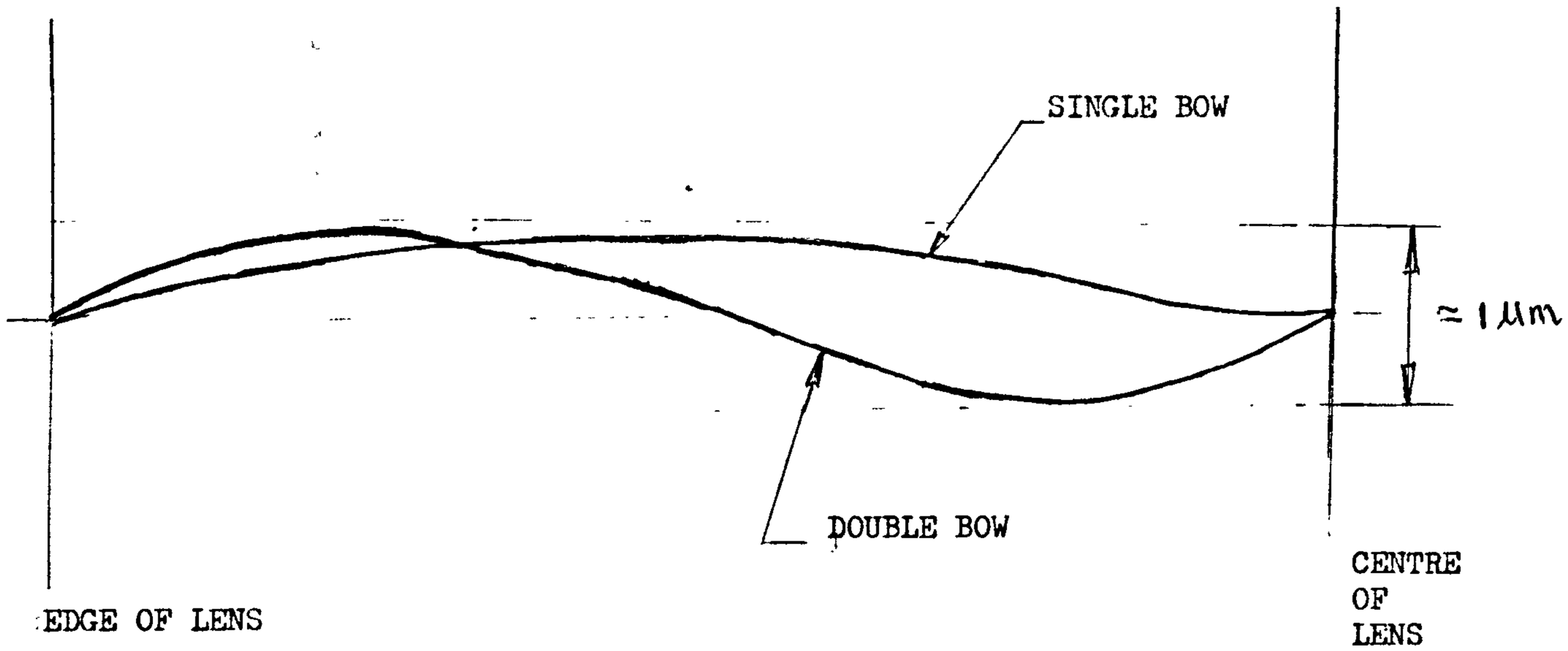

SINGLE AND DOUBLE BOW ERROR

FIGURE A1

A.3

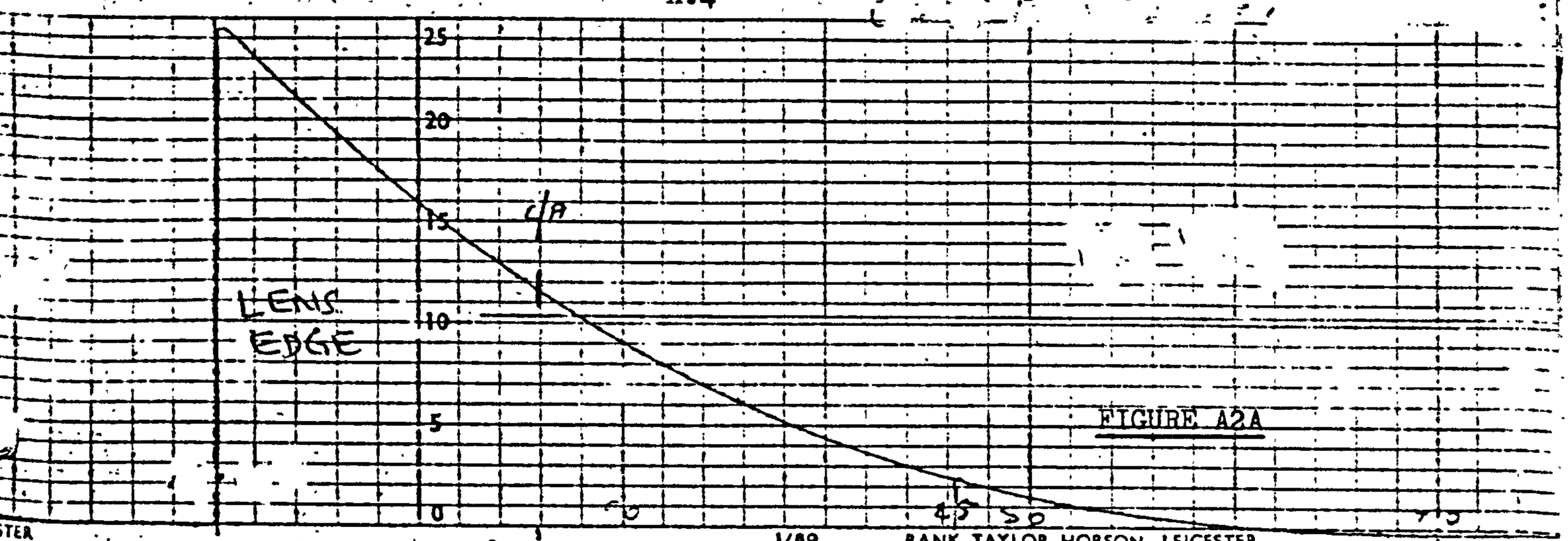

FIGURE A2A

A112/1211.E MADE IN ENGLAND A112/1211.E

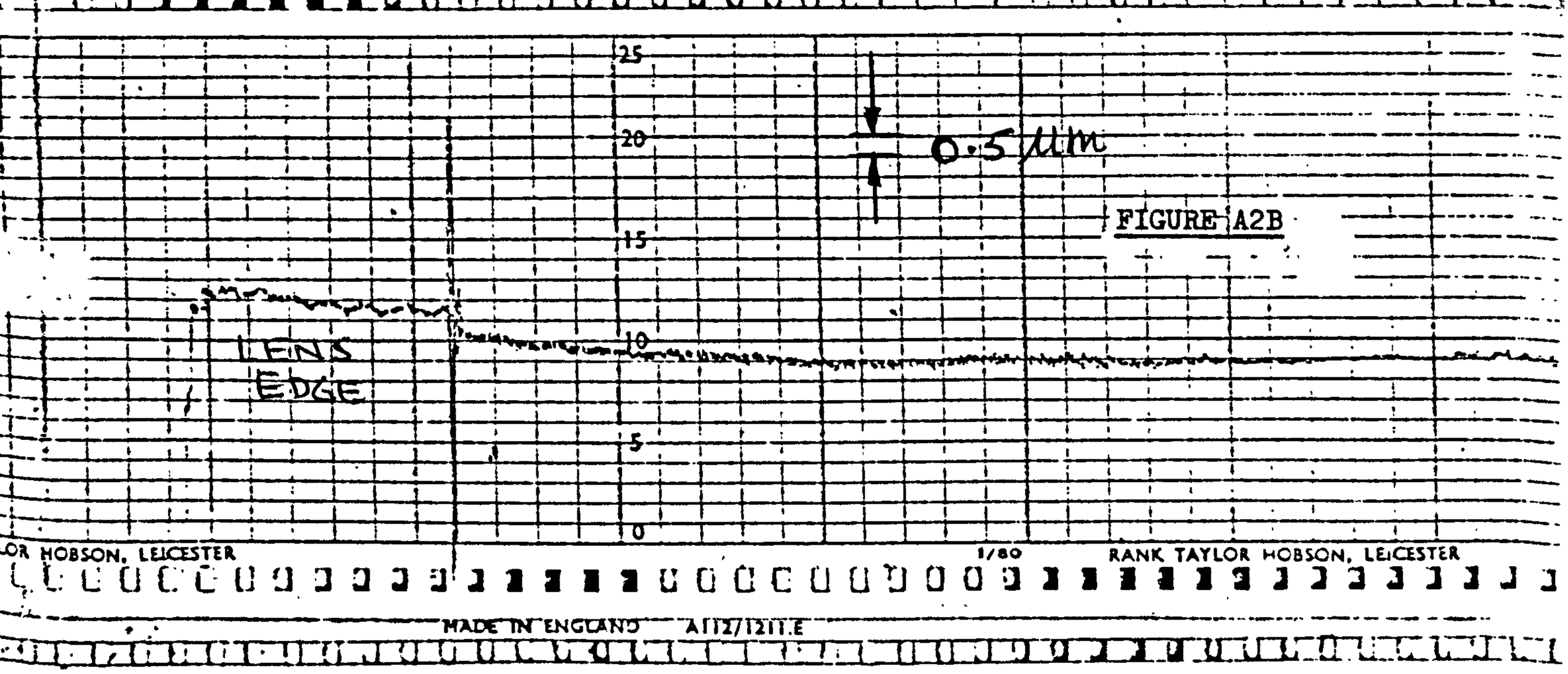

FIGURE A2B

MADE IN ENGLAND A112/1211.E

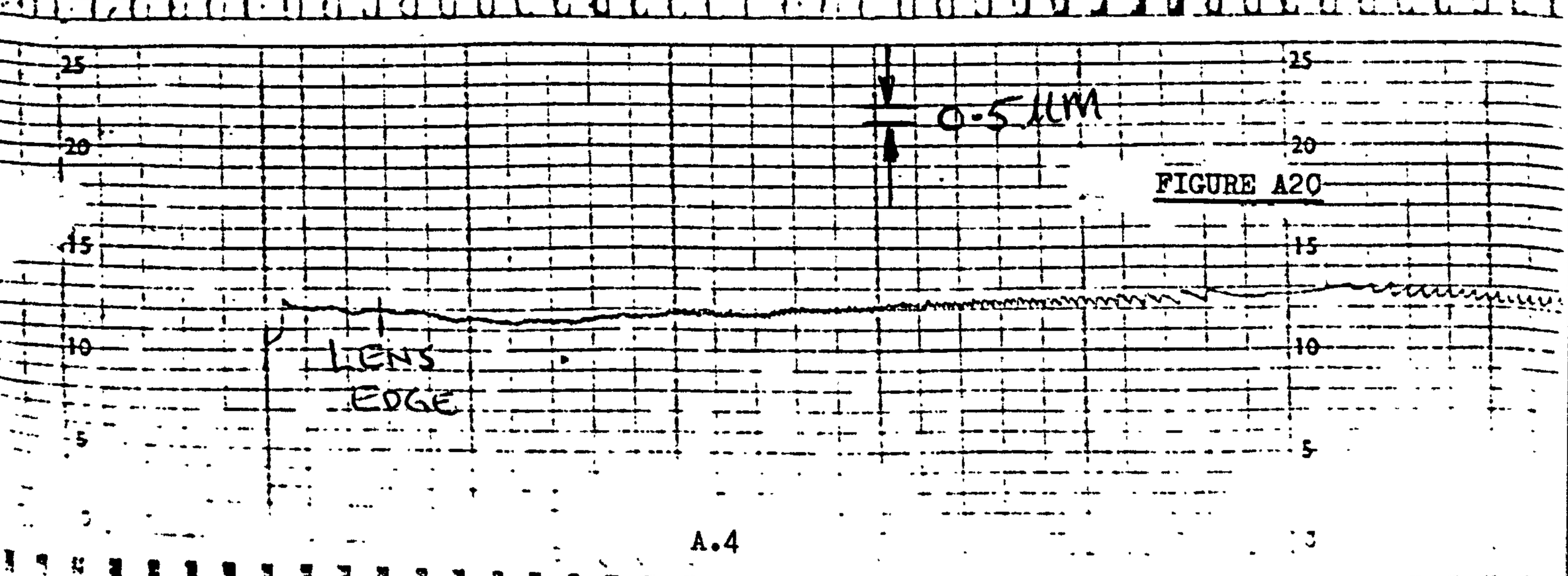

FIGURE A2C

A P P E N D I X B

APPENDIX B

MEASUREMENT OF ALUMINIUM PARABOLA ON SIRA MACHINE

The operation of the Sira instrument relies on a precision spindle. The measurement is made by a probe, which is sensitive to radial displacements (see Fig. B1). The spin table is driven at a constant rate, as the arm tracks across the test surface. Thus an effective fine spiral scan of the test surface is performed. This, coupled with the angular information about the spindle and the arm allows various forms of display to be made.

An extremely useful analysis of these measurements have been reported (24). Figure B2 shows the measured form of the aluminium parabola relative to a base radius of 452.365 mm. If the measured form is subtracted from the specified or true parabola, a plot of the "error form" is obtained. It is demonstrated that this is a combined effect of an error which linearly increases with radius (coning error) and a parabolic component. The largest form errors, hence encountered are of the order of 30 μm. If these form errors are corrected then the residual error is 2-3 μm.

An important observation reported in connection with the parabola is that the aluminium parabola with a large coning error has a much poorer image quality than a parabola with no coning error (24).

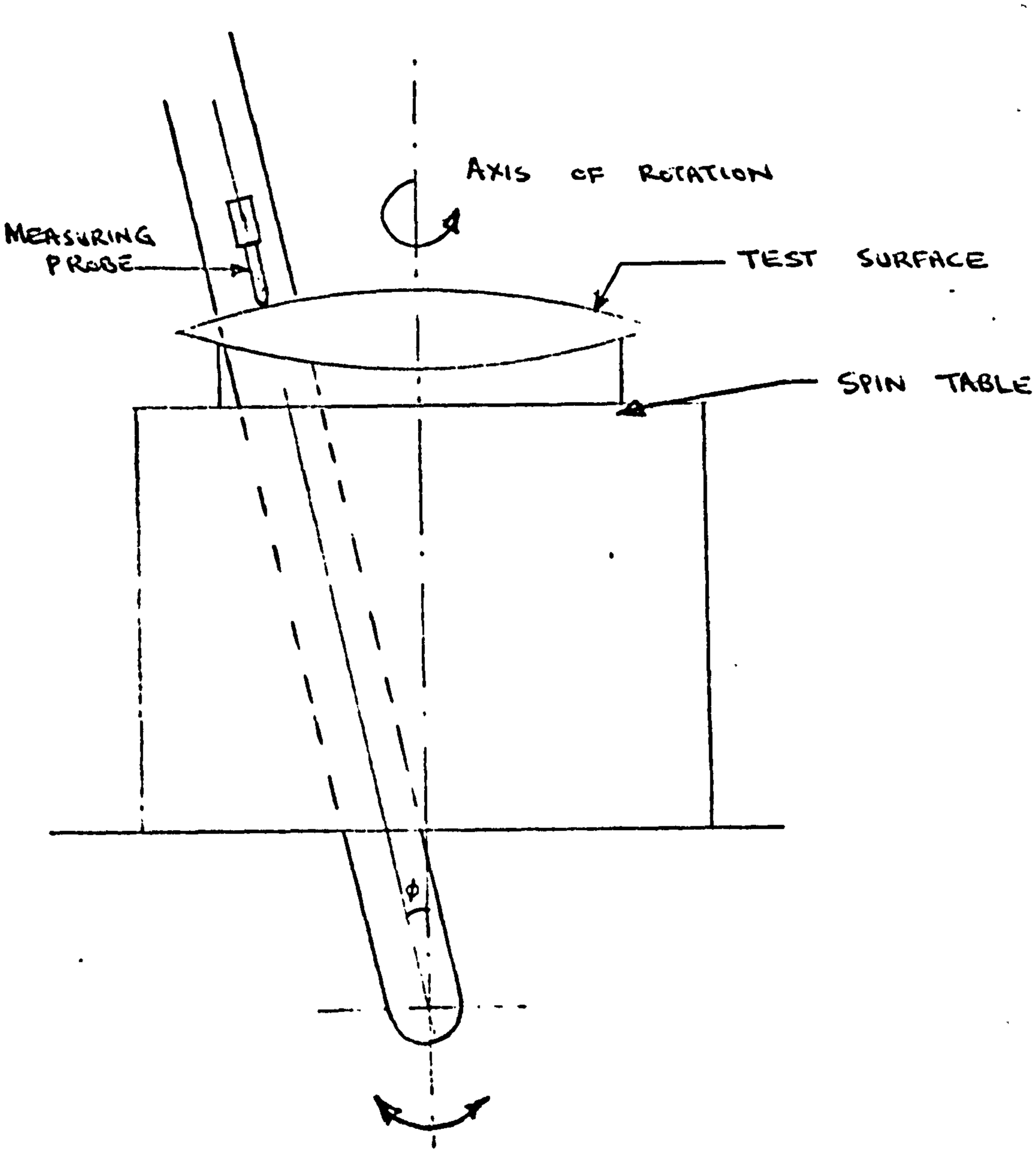

SIRA PROFILE MEASURING EQUIPMENT

FIGURE B1

PARABOLA ... MSG 325 test piece.

FCI Al. Alloy.

RTH 1 Sira form instrument 30.4.80.

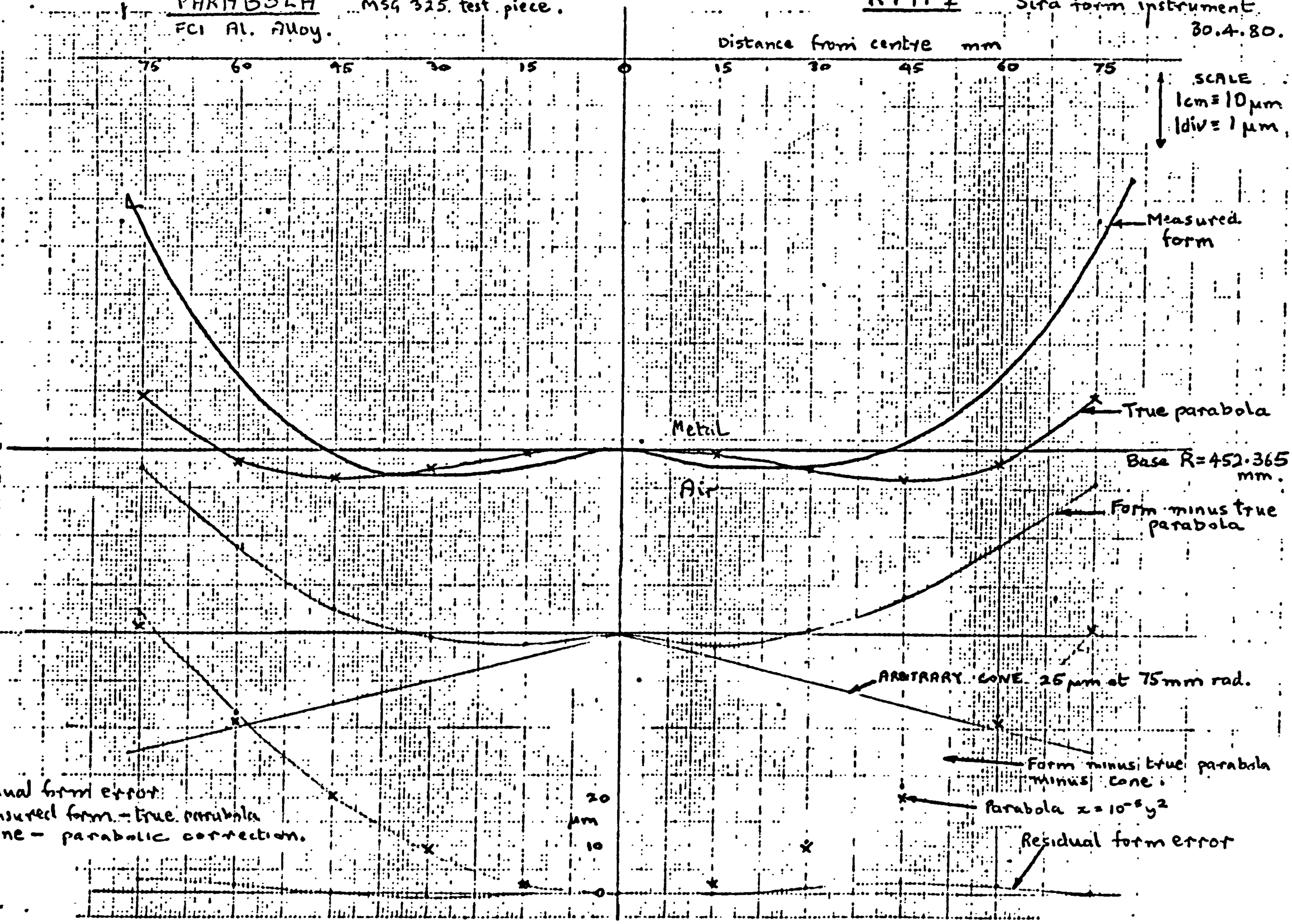

FIGURE B.3 B2

A P P E N D I X C

APPENDIX C

A PILOT STUDY WITH 6 LENS ELEMENTS

In the early part of the research, the Form Talysurf instrument as described in Appendix B was still under development. In addition a reasonable sized batch of suitable germanium lenses was not readily available. Hence only 6 lenses were measured on the development instrument. Fig. C1 shows two of the error profiles. Several parameters such as average slope, radius weighted average slope, etc. were generated. An attempt was made to correlate these parameters to mid values of MTF for each lens. The correlations were poor and improved slightly when radius weightings were introduced.

However, when the number of turning points and their radial position was taken into account the correlation improved by a relatively large amount. The introduction of the radial terms was accompanied by the choice of constants which were mainly obtained by trial and error. With many uncertanties about the instrumentation and with such a small data set, no further work was possible.

Although no conclusions were really possible, the relationship between MTF and the turning points was a clue which became useful in later part of this research.

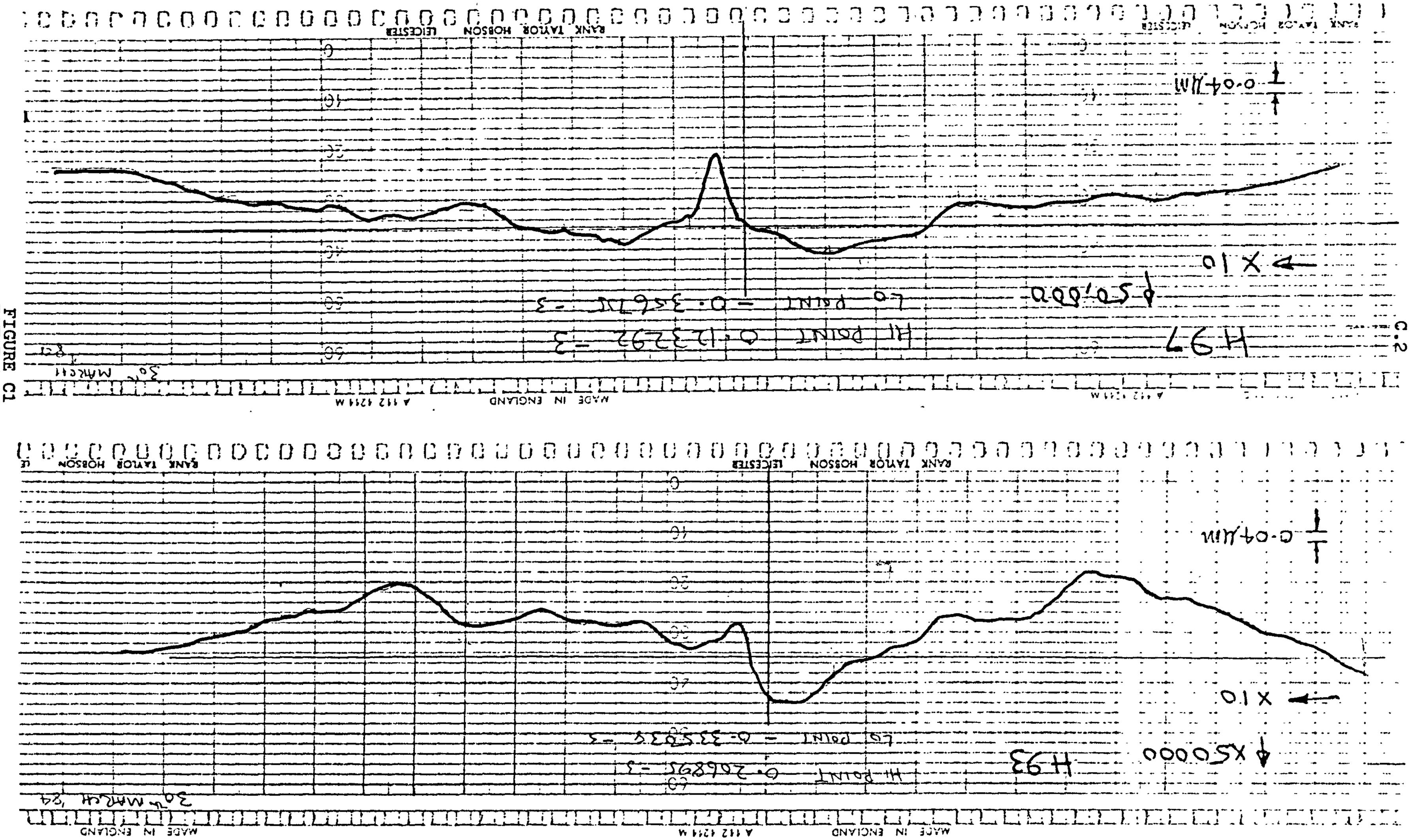

FIGURE C1.2 C.2

APPENDIX D

FORM TALYSURF

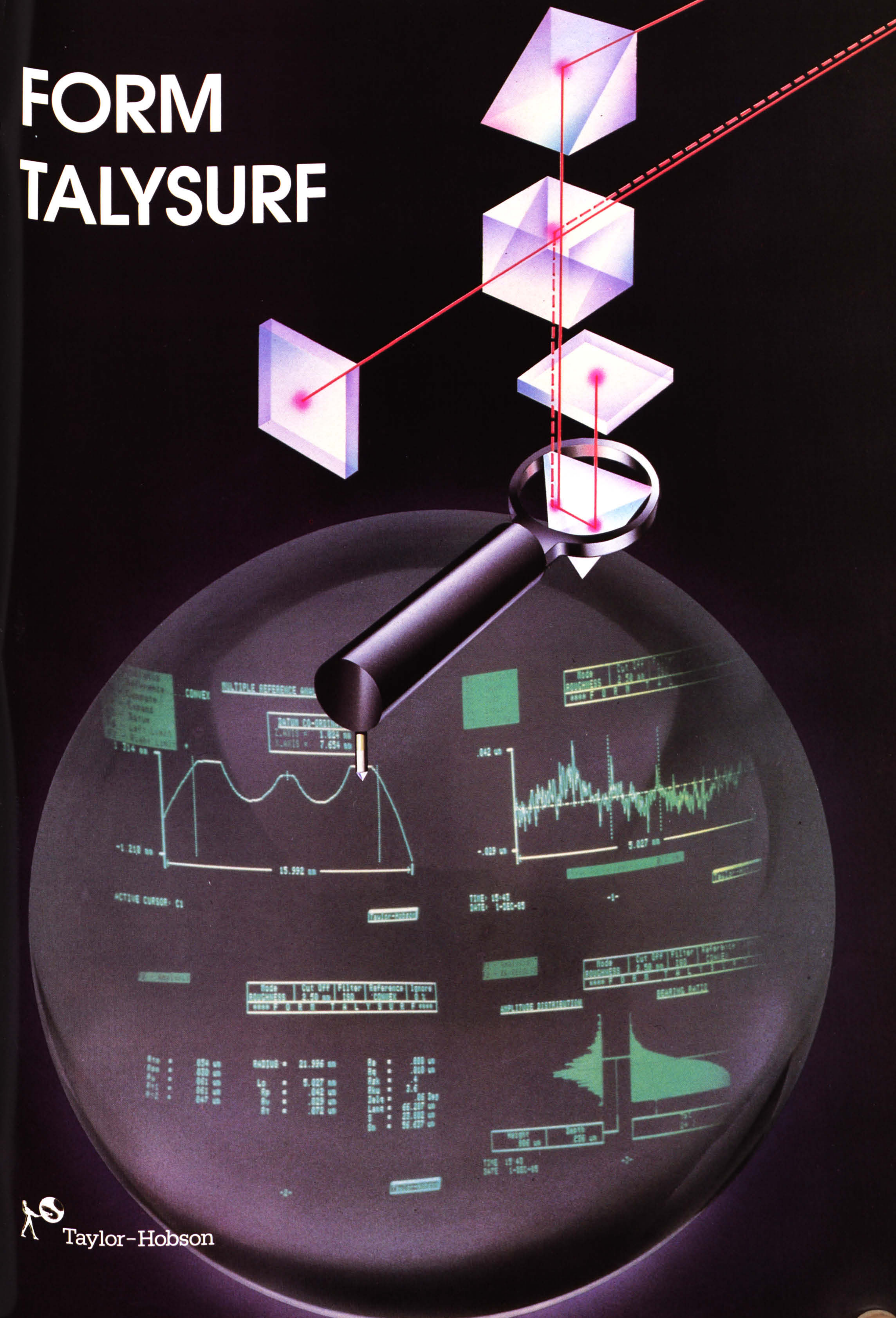

Taylor-Hobson

FORM TALYSURF — Versatile, precise

THE MOST DIFFICULT ASSESSMENT TO MAKE WITH FORM TALYSURF IS ITS OWN POTENTIAL

Form Talysurf is the first measuring system, which, in a single traverse over a workpiece surface will provide precise analyses of:-

- Surface texture
- Form error
- Radius
- Angle of surface inclination
- Dimensions

In addition, Form Talysurf will perform more complex functions such as aspheric and conic analysis, and also provide statistical analyses.

Such a searching investigation of a component's physical features would normally require two or more measuring instruments. In Form Talysurf it is achieved quickly and simply, and with outstanding resolution.

Form Talysurf's versatility has enabled many users, particularly in the automotive industry to significantly expand their capabilities for the inspection of complex components. Designers can now specify optimum data for the manufacture of parts which previously would have been extremely difficult, if not impossible to measure by other means.

Form Talysurf with computer equipment on optional desk.

Range and resolution

Form Talysurf is a stylus instrument with a wide dynamic measuring range. The range is achieved by using a laser interferometric transducer, the signals from which are transmitted to a microcomputer for detailed processing.

When fitted with the 60mm (2·36in) diamond tipped stylus arm for surface texture or form measurement, the vertical range is 4mm (0·16in) with a resolution of 10nm (0·4μin), or approximately 1/64 of the wavelength of helium neon laser light. Using the standard 120mm (4·72in) ball ended stylus (for form measurement only), the transducer vertical range is increased to 8mm (0·32in), with a resolution of 20nm (0·8μin).

Measuring versatility

In one traverse (with a diamond tipped stylus), Form Talysurf will provide precise measurement of workpiece form, surface texture, radius and angle of surface inclination.

Microcomputer processing separates texture and form by fitting a reference profile to the measured profile. This reference can be either a best fit straight line, a best fit concave or convex circular or conical arc, or by using the multiple reference feature various combinations of these forms can be measured. Measurement of aspheric surfaces can also be made with Form Talysurf.

Fast, simple operation

Simple and tolerant setting-up procedures combined with microcomputer analysis and display of results reduce workpiece assessment time to an absolute minimum. A complete measurement sequence can be performed in less than 1 minute by relatively inexperienced personnel. Because of the power and flexibility of the system, the position of the surface to be measured is not critical, provided it is within the 4mm (0·16in) range of the standard stylus.

Every function in a measurement cycle is controlled from the keyboard, the operator being guided step by step from options and instructions displayed on the screen of a visual display unit (VDU). Screen dialogue is selectable from English, German, French and Italian languages.

Permanent records of input data and results can be obtained from a dot matrix printer, and data may be stored for later retrieval.

Automatic calibration

The complete system is calibrated by measuring a calibration standard of known dimensions.

A system set-up dynamic graphic scale allows the crest of the calibration standard to be quickly found with the stylus tip after which the calibration is carried out automatically. Calibration constants can be retained in computer memory and applied to subsequent measurements with the same stylus.

A new stylus instrument with a wide dynamic range for use in surface metrology

J.D. Garratt*

An instrument has been developed which can measure not only radius of curvature but also form deviation and surface texture at the same time. A computer is used to mathematically separate the form from the texture. The technique can be applied to the measurement of cross track curvature of bearing raceways and to other precision components whose form is defined as a circular arc, or a straight line, in which case angle will be measured instead of radius. The measurement of other forms such as parabolic, elliptical, hyperbolic and aspheric are the subject of continuing development. The instrument provides a distinctive and useful advance in measurement by the stylus method, offering possible solutions to many obdurate problems in the field of surface metrology

Keywords: surface roughness measurement, form tolerances, curved, transducers

In modern technologies, the assessment of performance of a component in respect of its various physical specifications[1] is often dependent on a comprehensive measurement of component surface topography. Two essential aspects of this are its form and texture which hitherto have required separate assessments, often with interdependent error.

Conventional surface finish instruments have a measuring range of typically 0.1 mm, but are adapted to the measurement of texture of a curved component by matching a curved datum to that component. The method is tedious and time consuming and never gives the exactitude derived by a comprehensive assessment supported by the analysis of a digital computer.

In order to acquire the data for this comprehensive analysis, a pick-up with a wide dynamic range is essential because of the disparate amplitudes of form and texture. This type of comprehensive assessment is now feasible by a new stylus instrument which incorporates a digital transducer with a wide dynamic range.

Setting up to measure a curved component is considerably simplified, reducing the complete measurement cycle time to typically less than one minute. Component form is separated from the surface texture mathematically in the calculation of its various dimensional parameters which describe the form.

Applications include the measurement of circular formed components such as ball bearings, bearing raceways, diamond turned mirrors and diamond turning tools.

Pick-up

To measure the form, surface texture and radius of the component depicted in Fig 1 in a single traverse, a pick-up is needed which can measure in the y direction with a range of at least h and a resolution high enough to detect the surface texture detail. Accurate measurement of the pick-up traverse, in the x direction, is essential.

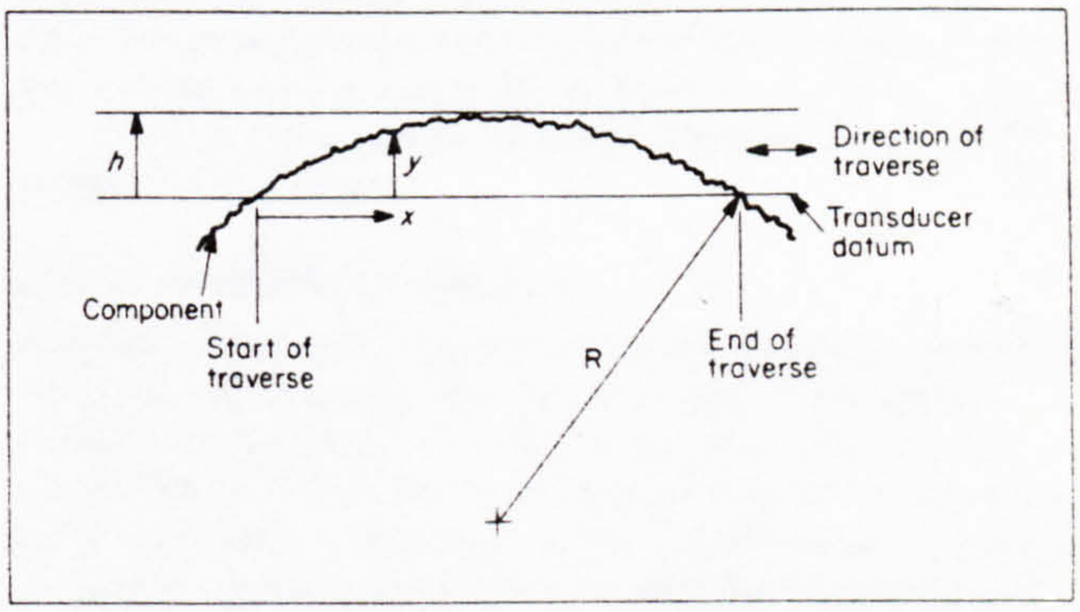

Fig 1 Co-ordinate system used in the assessment of both form and texture of a curved surface

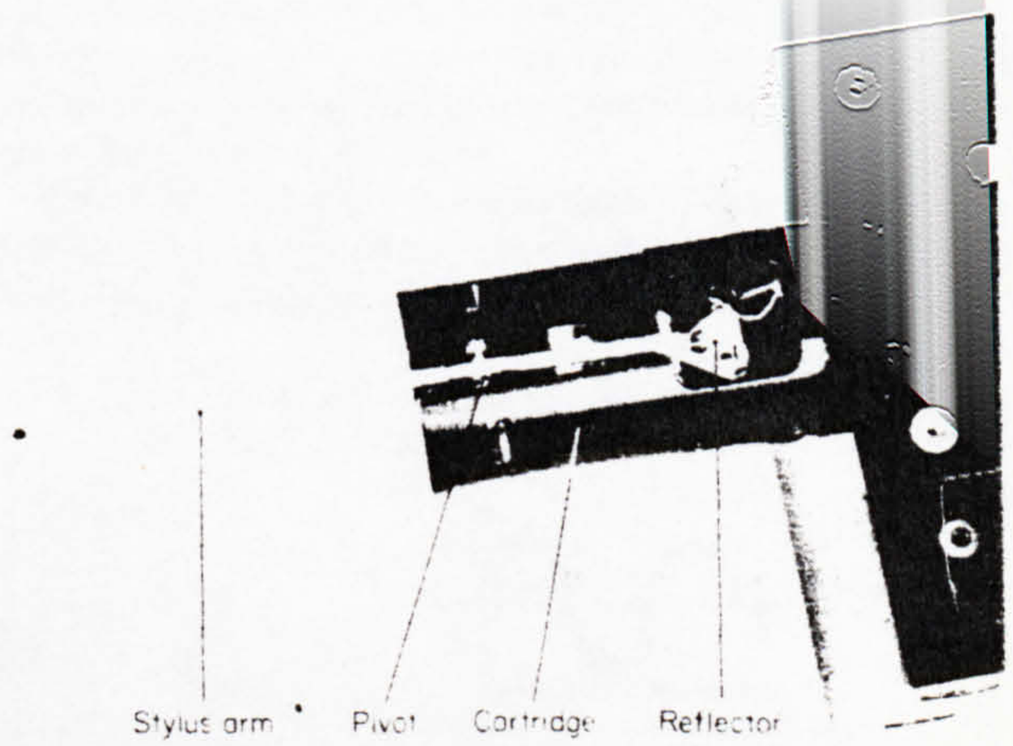

Fig 2 Pick-up cartridge of the new instrument

The pick-up comprises a pivoted lever, on one end of which is the stylus which contacts the surface to be measured, and on the other end is a reflector. This acts as the measurement arm of an interferometric transducer[2] to give a direct digital output with a measuring range presently of 2 mm, a resolution of 5 nm and a frequency response of about 300 Hz. The interferometer and stylus arm are housed in a 30 mm diameter cartridge (Fig 2).

The light source for the Michelson type interferometer is a commercially available helium-neon laser of 1 mW output and wavelength λ. The output beam from the interferometer, derived from both measurement and reference arms, is split into four, enabling four photodiodes to detect the fringe pattern. These signals, indicating the stylus displacement y, are fed into a preamplifier board producing the conventional quadrature signals which enable bidirectional counting and interpolation to $\lambda/128$[3]. This gives a range to resolution ratio of 5×10^5, ie equivalent to 19 bits.

Rank Taylor Hobson Limited, PO Box 36, Guthlaxton Street, Leicester, UK, LE2 0SL

Fig 3 shows the transducer and a traversing unit which provides the accurate x axis traverse.

Certain factors must be taken into account when using a transducer with these capabilities, described as follows.

Transducer linearity

The stylus arm pivot has a precise axis of rotation which introduces minimal friction and allows for the wide measuring range. The variation in static stylus force over this range is also minimal. These constraints help to ensure that the stylus arm moves accurately over the wide range. However, the normal assumption of linearity of stylus movements will no longer apply in either the y or the x directions, and a small correction is made by the computer for the cross axis relationship of the pick-up geometry.

The corrected $y \simeq Ay + By^2$, where A is nominally 1 and $B = a/2b^2$ and horizontal stylus movement $x \simeq Cy - Dy^2$, where $C = a/b$ and $D = 1/2b$, and where a is the distance from the stylus tip to the stylus arm and b is the distance from the stylus to the pivot.

Stylus arm vibration and sampling interval

Any unwanted resonance in the stylus arm of an analogue transducer is usually controlled in design to be well outside the frequency range of the instrument; it is therefore 'lost' before digitising. This is not so for the case of a digital transducer and its effect must be 'lost' by digital filtering.

To satisfy the Nyquist criterion, the sampling interval must be less than half the shortest wavelength present in the signal, otherwise aliassing will occur. The arm resonance in this instrument design is to be at 350 Hz. The traversing table holding the workpiece has a velocity of 1 mm/s, giving the resonance a wavelength of 2.85 μm. This may be assumed to be the shortest wavelength of interest, in which case a data sampling interval of 1.4 μm or less is required.

The stylus tube is constructed from aluminium alloy for lightness, but this material has a low damping ratio. Hooker[6] states a value as low as 0.0001, which would give a sustained amplitude of vibration when excited. This has been increased to about 0.1 in this instrument, by the application of a visco-elastic damping material[6].

This damping helped to reduce the vibration amplitude which was further reduced by the use of a digital notch filter, the characteristics of which give zero transmission at a wavelength of 3 μm and 70% at 6 μm.

The use of a carbon fibre stylus arm is considered valuable in this context.

Digital sampling of the data

The sampling of data in a digital system may be controlled temporally or spatially. The use of temporal sampling to measure the x direction in Fig 1 is not advisable, as any speed fluctuations in the traverse give related errors E in the sampling distance. Referring to Fig 1, if the best fit arc was calculated using temporal sampling and then subtracted from the data, the resulting surface detail would show this error with amplitude $e = E \tan a$, where a is the angle at which the stylus is traversing (ie the tilt of the component being measured) relative to the true datum of the instrument. To avoid this, spatial sampling is employed which is more reliable, though less convenient.

The motion of the traversing table (Fig 3) is measured by a Michelson interferometer. A 1 mW laser unstabilised in frequency, is attached to the rear of the traversing table,

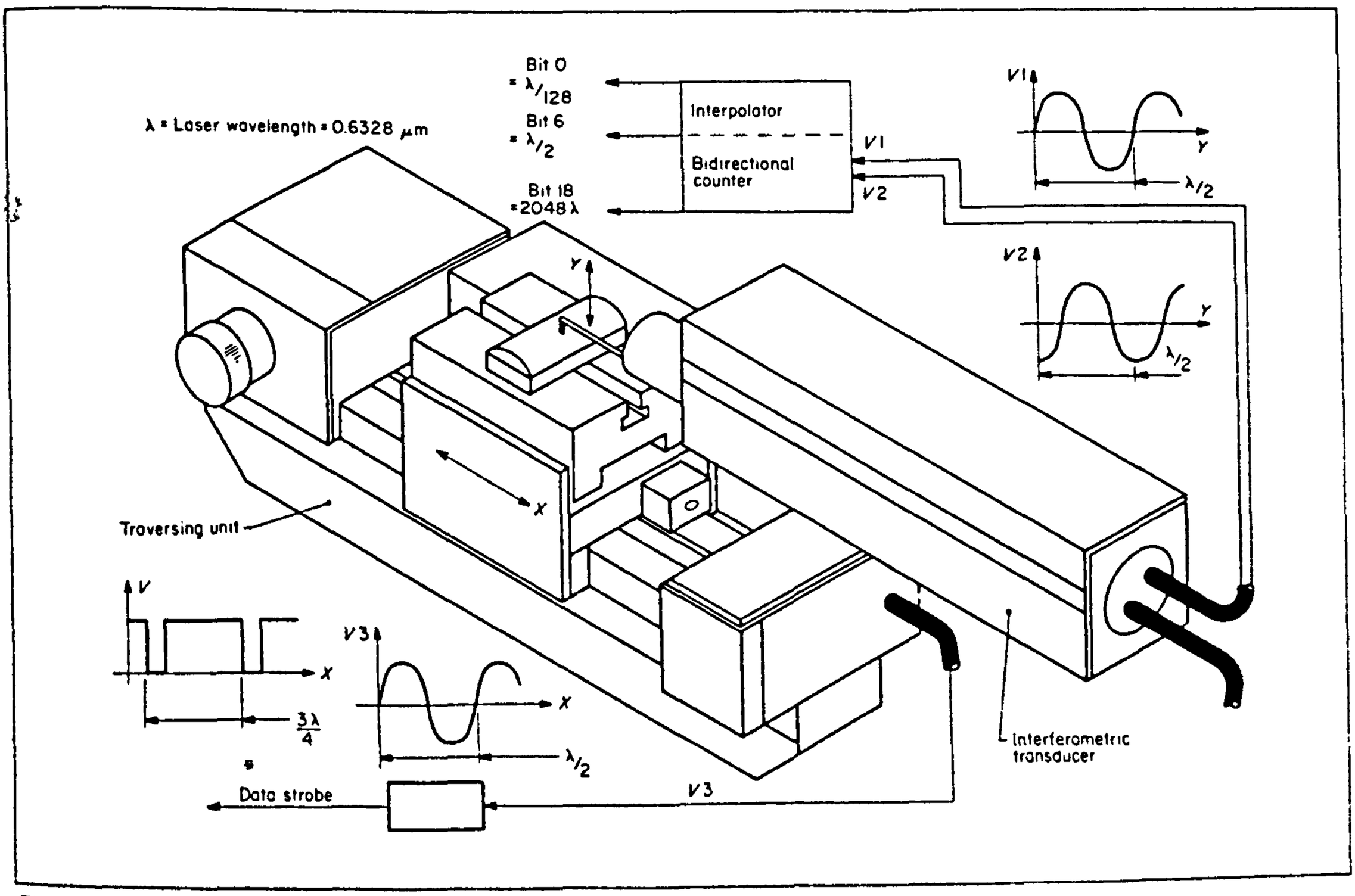

Fig 3 New instrument

Table 1 Comparison between a stylus instrument incorporating a conventional analogue transducer and one incorporating the new digital transducer

Digital transducer		Analogue transducer
2.59 mm	Range	0.1 mm
5 nm	Resolution	5 nm
5×10^5 (19 bits)	Usable range/ resolution ratio	10^3 (10 bits)
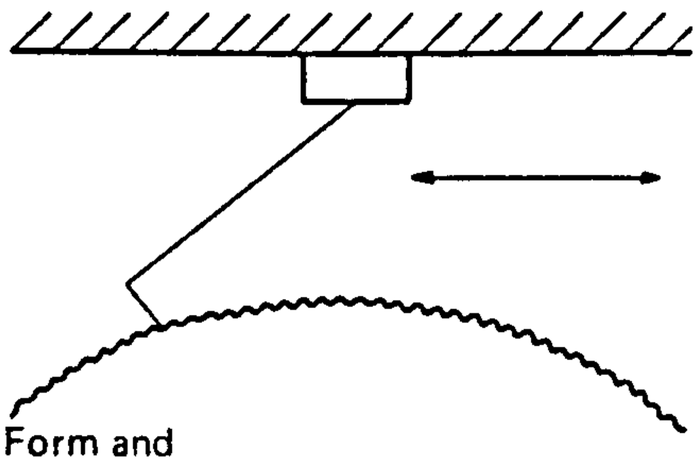 Form and texture	Curve measurement	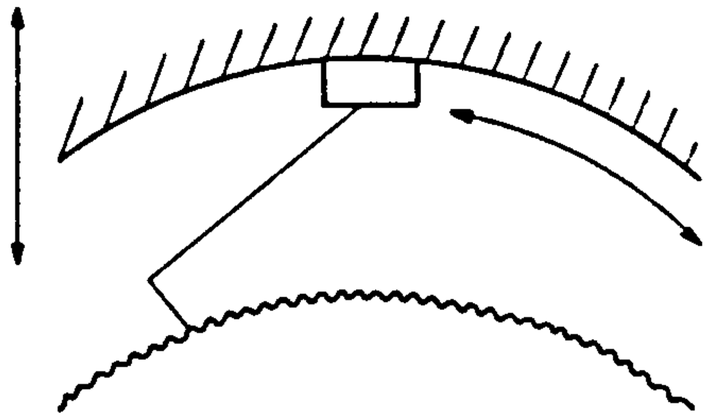 Form or texture
$y' = Ay + By^2$ $\Delta x = Cy + Dy^2$	Calibration 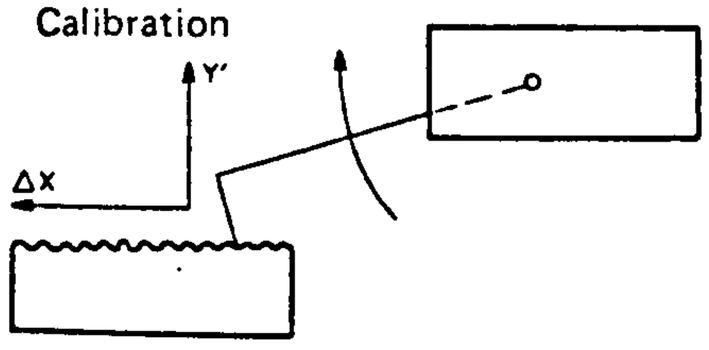	$y' = Ay$
Wavelength = 2.85 μm Data sampling ⩽ 1.4 μm Damping Digital filtering	Stylus arm vibration 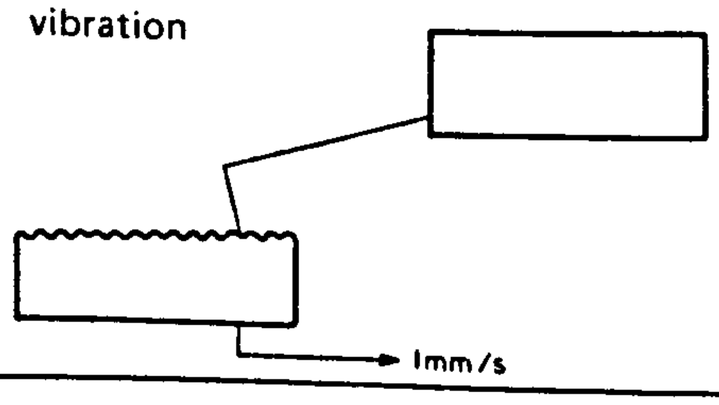	Beyond frequency range of instrument

providing the light source for the interferometer which is positioned in the lower end block. The mirror for the measurement arm is attached to the carriage table, as near as possible to the vertical measuring plane of the interferometric transducer to reduce offset error in accordance with the Abbe principle.

With a traverse length of 150 mm, the coherence length of the laser is adequate because the position for zero path difference occurs when the table is at its mid-traverse. Two photodiodes detect the fringe pattern, and hence the movement of the table. The resultant signals are fed to a preamplifier and signal conditioner located near to the interferometer, to produce a data sampling pulse every 0.4746 μm, which satisfies the Nyquist criterion.

Comparison of digital and analogue transducer characteristics

A comparison between a stylus instrument system incorporating a conventional analogue transducer and the one incorporating the new digital transducer which has been described above, is summarised in Table 1.

The instrument system

Fig 4 shows a view of the system with a schematic layout in Fig 5. This is built around a standard Rank Taylor Hobson product, Talydata, embodying a Data General microNova computer. Nineteen of the logic inputs are used for the data of the interferometric transducer. The dac provides an analogue signal to the recorder. Instrument operation is controlled by the handheld console, responding to 'menu' messages displayed on the vdu.

Reference lines and calibration

Considering the component in Fig 1, to accurately fit a reference line conforming to a best fit circular arc[4,5] to the data collected by the transducer, a calibration routine is required in respect of constants of the individual geometry of the pick-up. It is not sufficient to use calibration standards of the step height or average (R_a) type. A round, smooth, ball of known radius is traversed under the stylus. After the best fit arc has been calculated and subtracted

from the data, the modified data should show minimum form error and the calculated radius should agree with the true radius of the ball, enabling the calibration referred to under 'Transducer linearity' above to be achieved.

This calibration is absolute and will be true for other measurements whether the reference line is a circular arc, a straight line, or any other curve. The accuracy in radius measurement or parameter of any curve depends mainly on the calibration accuracy, traverse length chosen, and the surface texture present.

The stylus tip has the form of a truncated pyramid and has a finite dimension (about 2 μm); its value has to be taken into account as it passes the valley on a concave component, or the peak on a convex component.

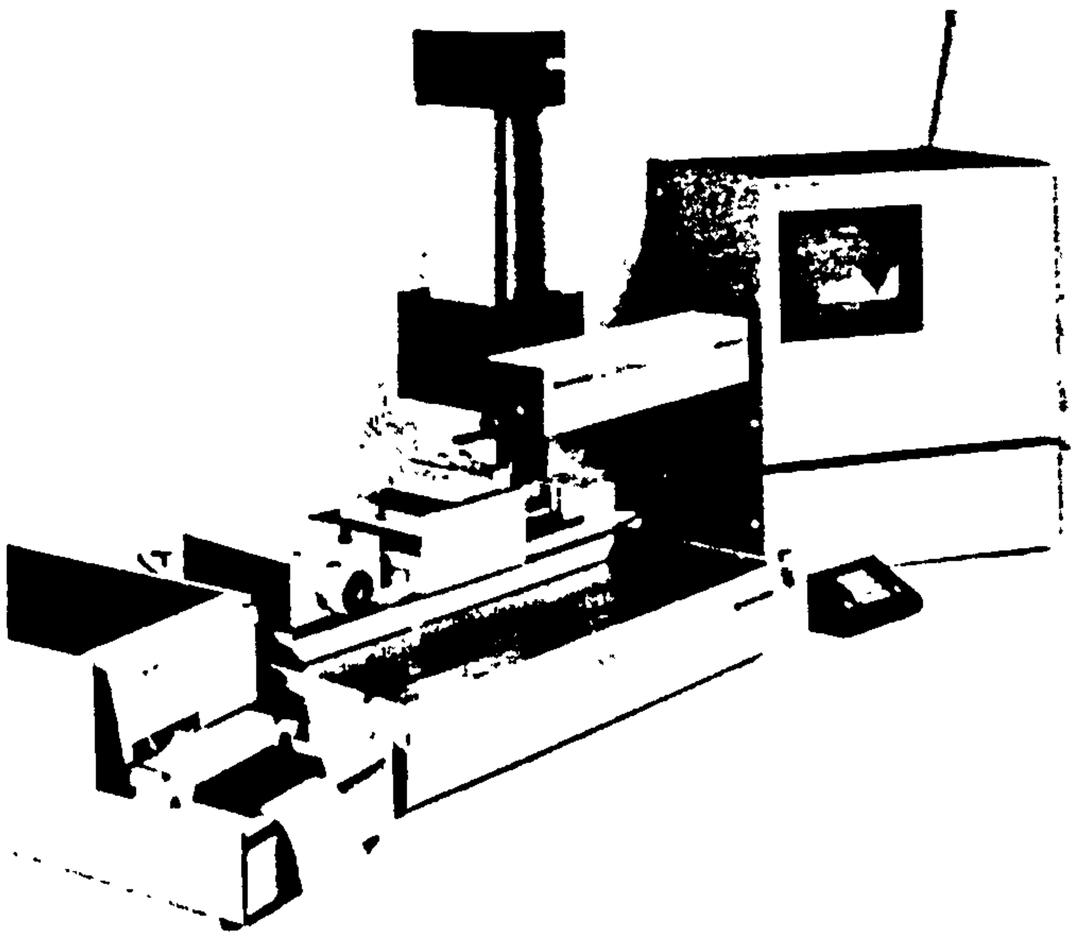

Fig 4 Complete system

The stylus is not always normal to the surface being measured; the inclination has to be compensated to give valid form error and surface finish height information. The stylus included angle is 90°, therefore, if the contact angle between stylus and surface approaches 45°, measurements will become inaccurate.

When the best fit is calculated, the ordinate spacing is based on the chord of the arc; after the arc has been subtracted, the residual data are referred to the arc itself, to give valid form error and surface finish wavelength information.

Similar corrections are necessary if a straight line reference is used to remove large angles of tilt when measuring a flat component. The accuracy of the measured angle of tilt of the straight line reference again depends on the calibration accuracy, traverse length chosen and the surface texture present.

Surface texture measurement

Surface texture comparisons were made between a Taylor-Hobson Talysurf 4 instrument and the new instrument, by measuring a fine turned surface with a high harmonic content.

For each measurement, three traverses were taken over similar sections of the component and the results averaged. Each traverse yielded 1000 ordinates at 2 μm spacing. A best fit least squares straight line was subtracted from the sets of data and further modified by a standard 2CR high pass filter with a 0.25 mm cut-off to obtain the surface texture parameters and power spectrum shown in Fig 6.

The new instrument has a low wavelength limit, but as this is very near to the stylus tip size, it will have a minimal effect on measurements taken over general engineering surfaces. Good correlation is indicated between the

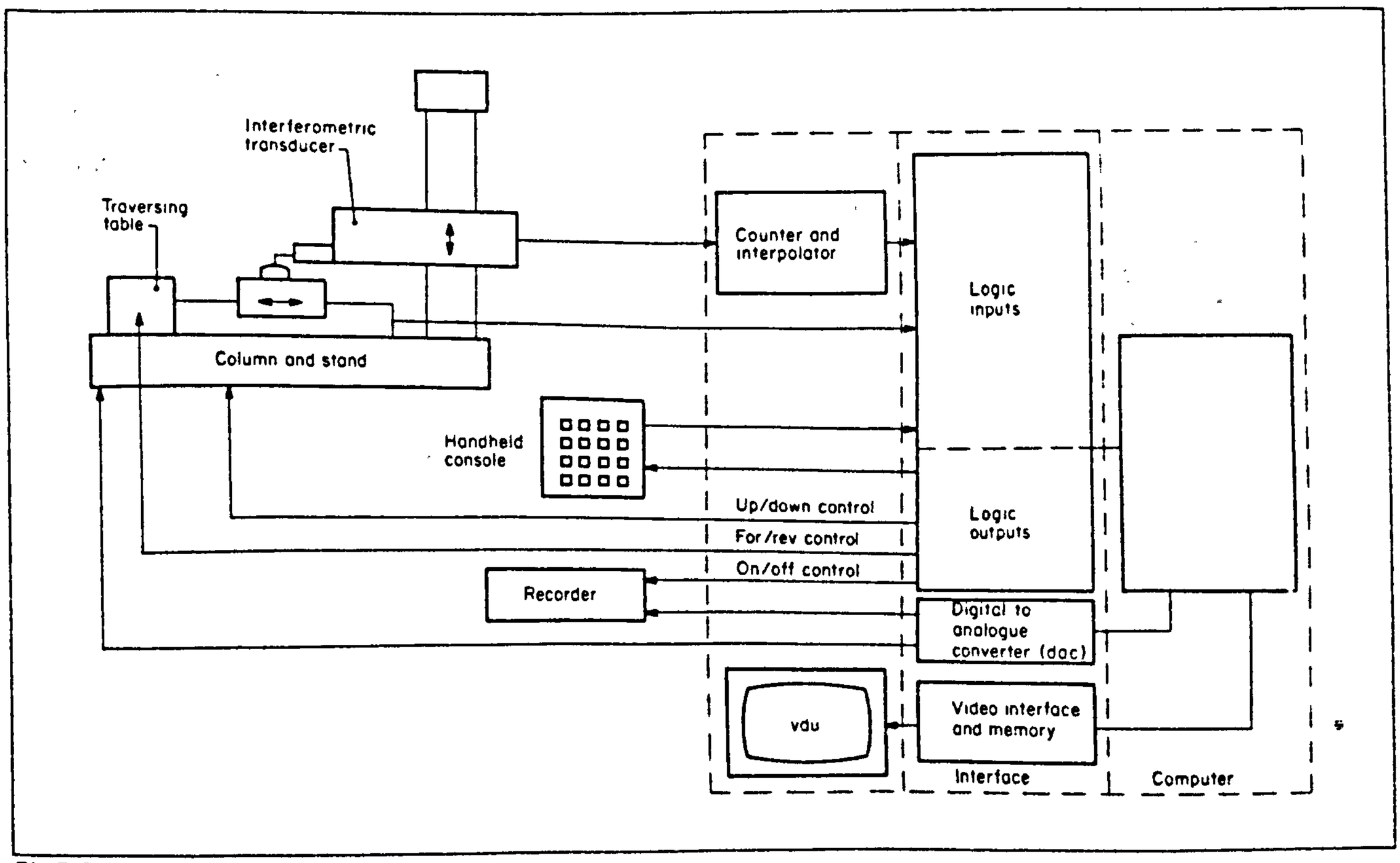

Fig 5 Complete system

Turned surface				
0.25 mm ISO filter cut-off				
Instrument	Talysurf		New	
Tilt, °	0.01	0.1	19	32
Power spectrum				
R_t, μm	1.45	1.54	1.62	1.49
R_a, μm	0.262	0.262	0.260	0.263
Δ_a, °	3.12	3.02	3.03	3.12
λ_a, μm	30.2	31.2	30.9	29.9

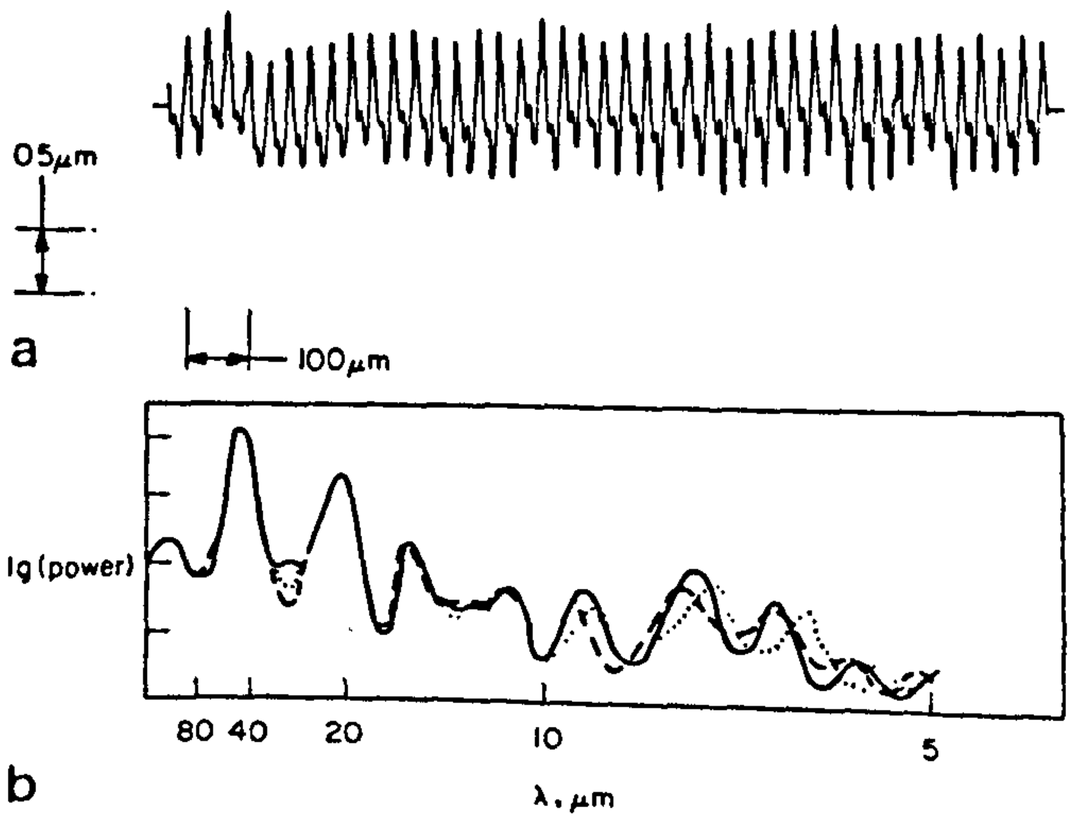

Fig 6 Comparison between Talysurf and new stylus instruments on surface measurements (a) filtered profile and (b) power spectrum

measurement from both instruments, even when the component surface has a large tilt, relative to the instrument's datum. Four filtered profile traces could not be distinguished.

Applications

Fig 7 shows a measurement over a ϕ25.4 mm ball. The profile contains the form errors and texture after the best fit arc has been subtracted from the data. The peak to valley (P-V) is taken over the assessment length L (P-V) and the R_a and R_q values are taken over $L(R_a)$, the difference in these lengths being the settling distance for the filter, typically twice the cut-off.

The ball was used to calibrate the instrument, and all applications described in this section were taken with respect to this one calibration.

Ball bearings

An important application is the measurement of cross track curvature of bearing raceways. One traditional method of measuring the radius is to project the arc onto the screen of an optical comparator at an appropriate magnification and compare it to arcs drawn on a template. This method has a number of disadvantages, one being that the measurement is subjective and depends on operator interpretation.

Fig 8 shows results of a bearing raceway measurement; Fig 8(a) shows the whole cross-section including lands, after the best fit line has been subtracted. The same data are used for obtaining the results shown in Fig 8(b), where a

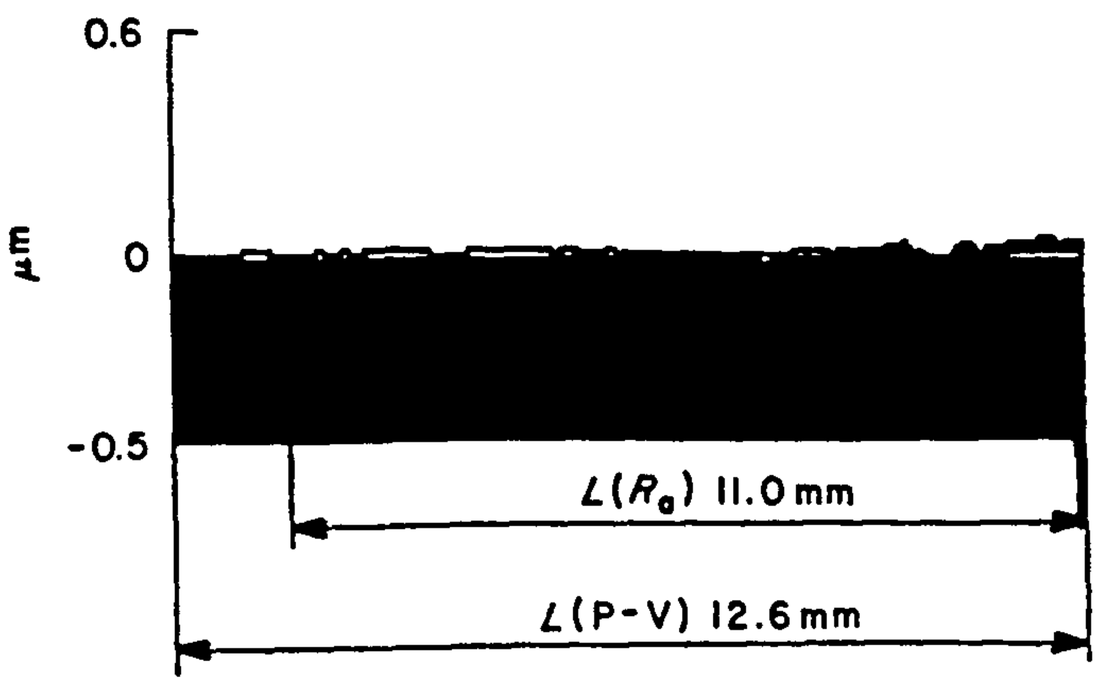

Fig 7 Measurement of ϕ25.4 mm ball

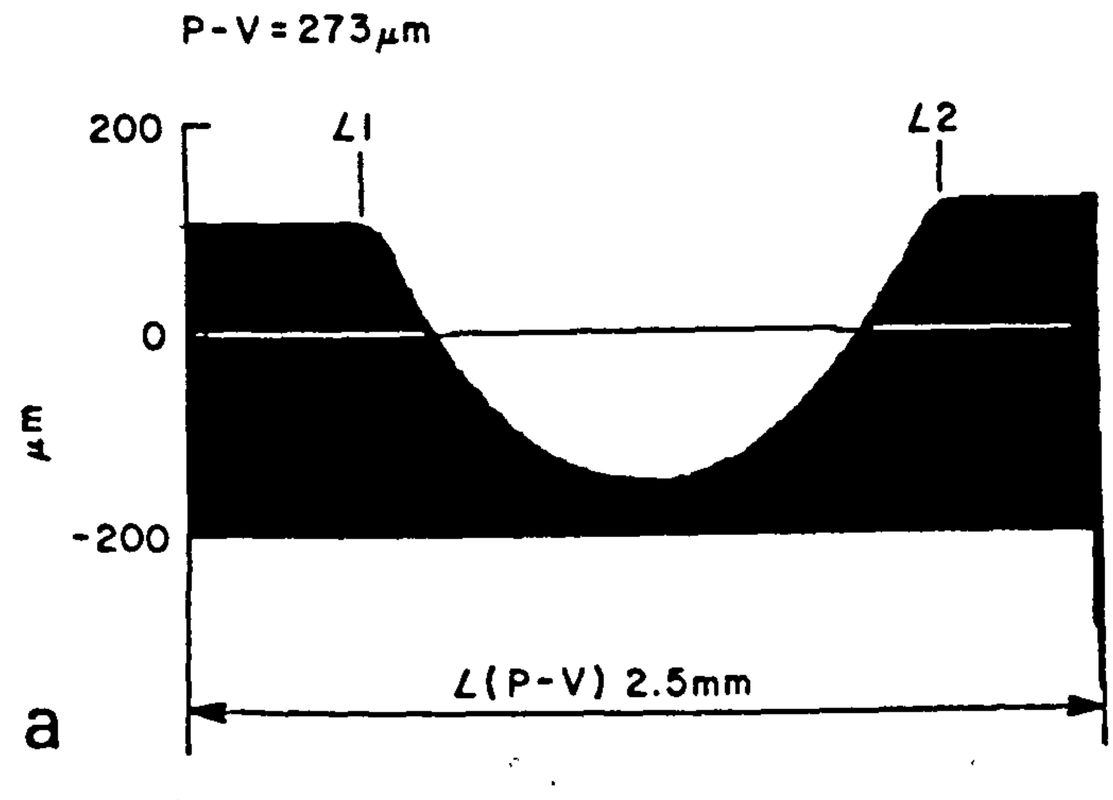

Fig 8 Measurement of cross track curvature on bearing races (a) with best fit line subtracted and (b) with best fit arc subtracted

best fit arc is subtracted from the circular part of the raceway to display the form errors and surface texture.

The range of radii of interest is usually between 0.4 mm and 20 mm. The measurement accuracy on radius has been found in practice to be generally better than 3 μm for this range.

Further applications include the measurement of the balls (Fig 7) and rollers that make up the rest of the bearing.

Optical components

Diamond turning is becoming highly important in the manufacture of mirrors and some lenses. The traditional method of measurement is by interferometry, with problems of interpretation and setting-up. This technique cannot be used for many modern types of infra red lenses.

Fig 9 shows the measurement of a diamond turned mirror with a hole through its centre. Figs 9(b) and 9(c) show measurements taken over assessment lengths *L*1 and *L*2 respectively. There is a harmonic error in the machining process which is clearly shown in the measurement. Also note the expected relationship between form errors of the left and right hand traces. The radii of interest are usually between 20 mm and 600 mm with a measurement accuracy of radius better than 0.1% of the nominal value.

The diamond tools that are used to generate these surfaces can have an arcuate cutting surface. Fig 10 shows a measurement of such a tool after the best fit arc has been subtracted. Fig 10(a) is the tool as new, whereas Fig 10(b) is the same tool after many cuts have been taken, hence the slight wear on one side of the cutting edge, shown encircled in Fig 10(b).

Fig 11 shows measurements of both a concave and convex glass gauge of the same radius after the best fit arc has been subtracted. The difference in measured radii could be accountable to the stylus size and shape, but the measurement is still within the specification of the instrument. Many optical components are highly polished and have R_a values better than 0.008 μm, which is approaching the noise level of conventional instruments. Fig 11(a) shows an R_a value of 0.003 μm for the concave glass gauge, which demonstrates the low noise limit of the instrument.

Aspheric mirrors and lenses could also be measured. With the best fit arc subtracted, the resulting asphericity will be displayed. Where the asphericity is large, it will not be easy to measure small asphericity deviations unless reference is made to the aspheric form. However, if this deviation is not of interest, high pass filtering will enable the surface finish detail to be obtained.

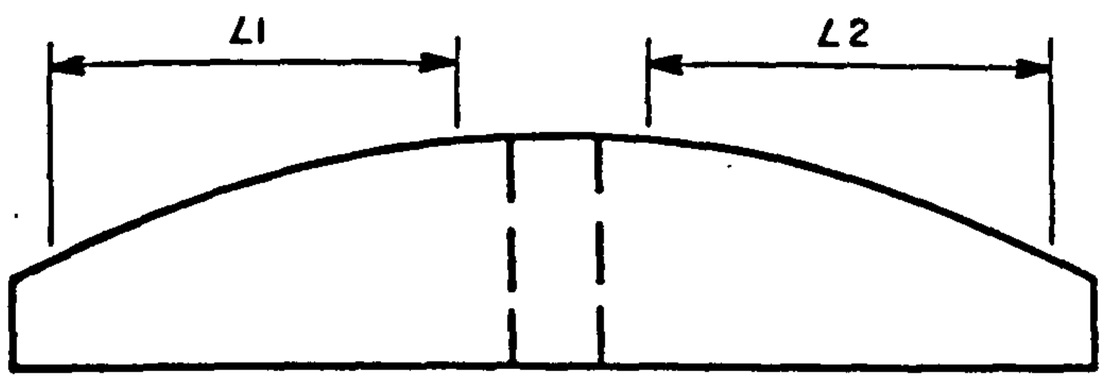

Fig 9 Measurements of a diamond turned mirror (a) cross-sectional view, (b) form and texture over L1 and (c) form and texture over L2

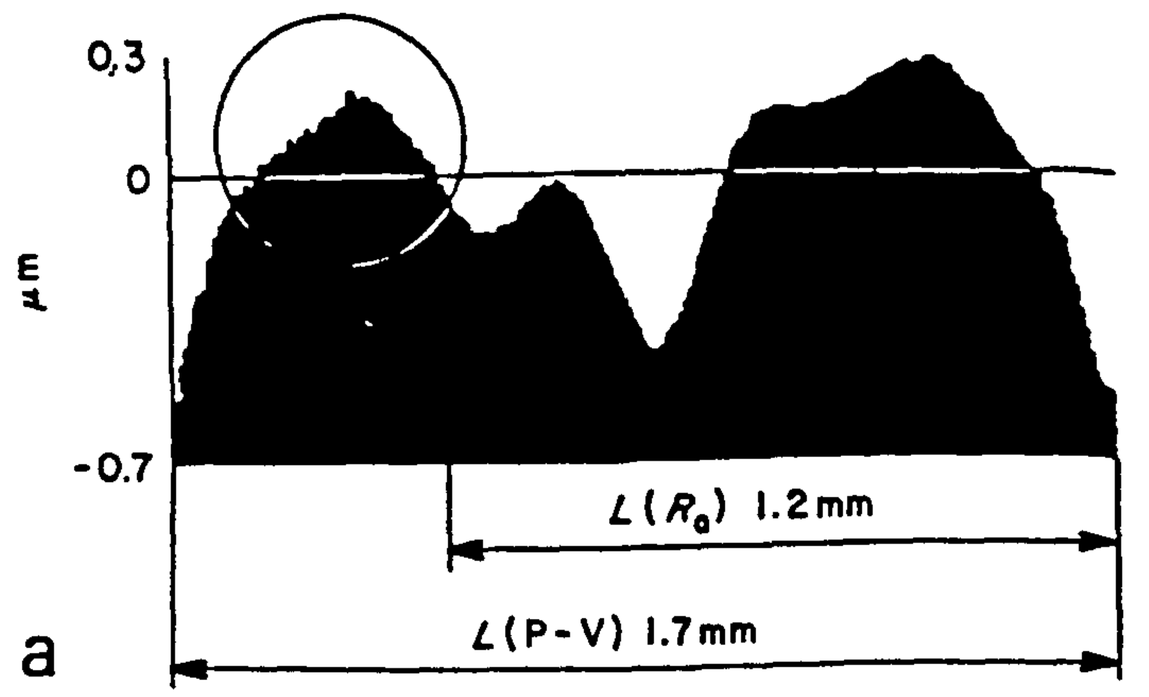

Fig 10 Measurement of a diamond turning tool, (a) new tool and (b) tool, showing wear

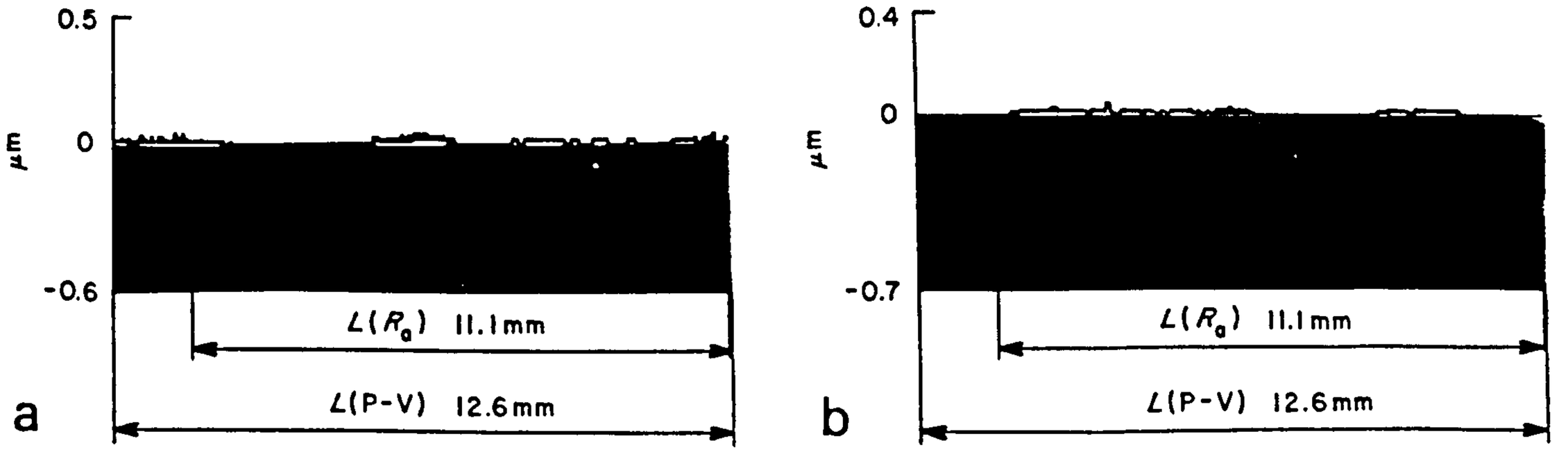

Fig 11 Measurement of glass gauges of radius 12.116 mm. (a) Concave gauge and (b) convex gauge

Acknowledgements

The author thanks Mr P.R. Bellwood for his valuable advice and the directors of Rank Taylor Hobson Limited for permission to publish.

References

1. **Whitehouse D.J.** The Measurement and Analysis of Surfaces. *Tribology International, December 1974, 7(6), 249–259*
2. **Garratt J.D.** An Interferometric Transducer for Surface Metrology. *M.Sc. Thesis, University of Aberdeen, 1977*
3. **Duffin F.** Electronic Interference Fringe Counter and Divider. *M.Sc. Thesis, University of Aberdeen, 1974*
4. **Whitehouse D.J.** Computational Replacement of Curved Datum and the Measurement of Radius on Talysurf 5. *RTH Technical Note T52, 1974*
5. **Scott P.J.** Statistic Analysis of Circular Profiles. *M.Sc. and DIC Report, Imperial College, London, September 1980*
6. **Hooker R.J.** Noise and Vibration Control by Visco-Elastic Damping. *Journal of The Institute of Engineers, Australia, March 1972*